A new standard in testing mattresses for use in x-ray imaging: Developing, validating and using a novel method to test x-ray mattresses for pressure ulcer development, radiation dosimetry and image quality

Nadi Milhan T Alresheedi

School of Health and Society
University of Salford

Submitted in Partial Fulfilment of the Requirements of the
Degree of Doctor of Philosophy (PhD)

.

26th Aug 2020

Table of Contents

List of Figures

List of Tables

Research Supervisors

Prof. Peter Hogg (main supervisor)

Health and Society School Executive Office
Allerton building, Frederick Road Campus,
University of Salford, Manchester M6 6PU
Email: P.Hogg@Salford.ac.uk

Dr. Andrew K. Tootell (co-supervisor)

Directorate of Radiography
Allerton Building, Frederick Road Campus,
University of Salford, Manchester M6 6PU
Email: A.K.Tootell@salford.ac.uk

Dr. Lucy Walton – Co-Supervisor

Directorate of Radiography
Allerton Building, Frederick Road Campus,
University of Salford, Manchester M6 6PU
Email: L.A.Walton@salford.ac.uk

Dr. Webb Jo-Anne (co-supervisor)

Directorate of Radiography
Allerton Building, Frederick Road Campus,
University of Salford, Manchester M6 6PU
Email: J.Webb@salford.ac.uk

List of Publications and Presentations

Date	Title	Type	State
July 2019	A method for investigating the influence of X-ray mattress on ulcers development potential problems	Conference poster (SPARC)	Presented
July 2019	A method for investigating the influence of X-ray mattress on ulcers development potential problems	Conference presentation (SPARC)	Presented
March 2020	A method for investigating the influence of X-ray mattress on ulcers development potential problems	Seminar presentation	Presented
July 2020	A novel method to investigate the influence of X-ray table mattresses on pressure ulcer development	Conference poster (European Congress of Radiology (ECR)	Presented
July 2020	Impact of using X-ray table mattress on ulcers development potential problems	Conference poster (ECR)	Presented

July 2020	Analysis of seven clinical X-ray table mattress for their impact on image quality and radiation dose	Conference poster (ECR)	Presented
January 2020	Breast Dose from shoulder Imaging	Conference poster	Presented
May 2020	A phantom-based method to assess X-ray table mattress interface pressures	Journal of Medical Imaging and Radiation Sciences	Published
November 2020	Evaluation of X-ray table mattresses for radiation attenuation and image quality	Radiography Journal	Published
December 2020	Pressure Distribution Analysis of X-Ray Table Mattresses	Journal of Medical Imaging and Radiation Sciences	Published

Training Sessions Attended During the Study

Date	Sessions name	Hours
2017/2018	Postgraduate Research Induction Week	20
2017/2018	Completing a Learning Agreement & the PhD Progression Points	2
2017/2018	Completing a Literature Review	2
2018/2019	Excel: The Basic Excel: Formulas and Functions	8
2018/2019	Thermoluminescent Dosimeters (TLDs) training	12
2018/2019	Intro to Endnote X7	4
2018/2019	Seminar on undertaking Research	2
2018/2019	Power point Academic poster	2
2018/2019	Get more out of your reading	6
2018/2019	Electronic Resources for researchers	2
2018/2019	Google Scholar for research	1.5
2018/2019	Time Management and Procrastination	2
2018/2019	Writing a Research Methodology	4
2018/2019	Referencing & Information Ethics for Research	2
2018/2019	Excel-Analysing data	2
2018/2019	Referencing your work APA (Harvard) style	2
2018/2019	Seminar (Writing for Publication)	2
2018/2019	PGR writing workshop on undertaking Research	2
2018/2019	Writing an argument (PGR Writing workshop)	3
2018/2019	PGR writing workshop on undertaking Research	2
2018/2019	Introduction to 3D Printing Models	1

2018/2019	PGR writing workshop on undertaking Research	2
2018/2019	Researcher Development Day - Writing for your IA and IE.	2
2018/2019	Researcher Development Day: - Proofreading, and How to write an abstract	4
2018/2019	Researcher Development Day: - Designing and presenting a poster - Giving confident presentations with impact	6
2018/2019	Seminar of Postgraduate Research	2
2018/2019	Critical and Analytical Skills	2
2018/2019	Search the academic way	1
2018/2019	Completing a Learning Agreement & the PhD Progression Points	2
2018/2019	Analysis of 1,000 words from your thesis or IA/IE report.	2
2018/2019	Introduction to SPSS	3
2018/2019	T-TEST, ANOVA and repeated measures	2
2018/2019	Organizing and synthesising your work	2
2018/2019	Seminar of Postgraduate Research	2
2018/2019	Seminar of Postgraduate Research	2
2018/2019	Saudi Student Conference in London, UK	10
2018/2019	Writing for publication - PGR seminar	2
2018/2019	Private Training – TLD and MOSFETs training course – Day 1	6
2018/2019	Private Training- CT, X-ray rooms' training course – Day 2	6
2018/2019	Presentation Skills	2
2018/2019	Proof reading, editing and letting go	2
2018/2019	PGR Presentation Practise Session	2
2018/2019	Critical Thinking and Critical Writing at Doctoral Level	6

2018/2019	Seminar of Postgraduate Research	2
2018/2019	SPARC Conference 2019	1
2018/2019	Private SPSS training	2
2018/2019	Pressure Ulcers, a joint research seminar	2
2018/2019	Endnote Basics for Researchers	2
2018/2019	How to write an abstract Researcher	2
2018/2019	Defending your thesis	2
2018/2019	Writing argument - PGR writing workshop	2
2018/2019	Larger group and small group teaching.	2
2018/2019	Developing Critical Writing for PhD Science Students (Discussion)	2
2018/2019	Developing Critical Writing for PhD Science Students (Conclusions)	2
2018/2019	Abstract writing - PGR writing workshop	2
2018/2019	Peer review and feedback - PGR writing workshop	2
2018/2019	Peer review and feedback - PGR writing workshop	2
2019/2020	Getting ready for the viva	2

Acknowledgements

I would like to express my deepest appreciation to my lead supervisor Professor Peter Hogg for his immense contribution towards the successful completion of this thesis. I am grateful to you for your advice, feedback, and constructive criticism. You are a great academic and a wonderful person. Thank you very much for those little 'are you okay Nadi?' emails. These came during some of the most difficult times of my PhD journey. Words would not be enough to express my feelings for your tremendous help and support. Thank you.

I am also grateful to Dr. Andrew Tootell, Dr. Lucy Walton, and Mrs Jo-Anne Webb for their consistent support and guidance during the running of this research project. Furthermore, I would like to thank Chris Beaumont for his huge help in helping to construct the [3D] phantom and for his advice.

Finally, I would like to take the opportunity to thank my mother and father for their support, encouragement, and attention. Also, I am also grateful to my wife for her support, kindness, and patience as she accompanied me along this PhD journey. In addition, I would like to thank my brothers, sisters and friends for their support throughout all my PhD studies. I would also like to express my utmost gratitude to all who supported me to complete my PhD thesis.

List of Abbreviations

Acronym	Definition
3D	Three-dimensional
Al	Aluminium
AP	Antero-posterior
APD	A Priori difference of the mean
ANOVA	Analysis of variance
BMI	Body Mass Index
CNR	Contrast to Noise Ratio
DICOM	Digital Imaging and Communications in Medicine
kV	kilo-Voltage
LNT	Linear No Threshold Model
mAs	Tube current (milliamperes) multiplied by exposure time
MOSFET	Metal Oxide Semiconductor Field Effect Transistors (seconds).
MTF	MTF Modulation Transfer Function
mGy	Milligray
nC	Nanocoulomb
SD	Standard Deviation
SID	Source to Image Receptor Distance
SNR	Signal to Noise Ratio
PMMA	Poly (Methyl Methacrylate)
QC	Quality Control
TLD	Thermoluminescent dosimeter
UK	United Kingdom

VGA	Visual Grading Analysis
VCFs	Vertebral Compression Fractures
PPI	Peak Pressure Index
IP	Interface Pressure

Abstract

Background

In hospitals, patients often undergo X-ray imaging while lying on a mattress. Therefore, mattresses must have low X-ray attenuation properties to minimise radiation dose to the patient. Mattresses should create no artifacts within the X-ray image, as this may compromise image quality and diagnosis. Finally, mattresses should be constructed in such a way that interface pressure (IP) is minimized, limiting the chance of pressure ulcer formation.

Aim

For evaluating X-ray imaging table mattresses, this thesis has three aims (1). to develop and validate an anthropomorphic-phantom-based method of assessing X-ray table mattress IP as an index of mattress performance; (2) to assess X-ray table mattress pressure redistribution properties; and (3) to evaluate mattress radiation attenuation characteristics and their impacts on image quality.

Methods and Materials

An anthropomorphic phantom, simulating adult head, pelvis, and heels, was 3D-printed from X-ray computed tomography (CT) image data. Dry sand was added to represent 5 human weights and XSensor technology was used to assess pressure distribution. Phantom mattress IP characteristics were compared for the 5 weights against 27 sets of human mattress IP data to achieve phantom validation.

Twenty-four X-ray table mattresses, 21 thinner and 3 thicker were assessed. Anthropomorphic phantom and Xsensor mattress interface pressure measurements were conducted for head, pelvis and heels, with and without X-ray table mattresses. Image quality and radiation attenuation were also assessed. Incident air kerma (IAK) was measured, with and without mattress, over a range of exposure factors using a digital dosimeter. Inverse image Quality Factor (IQF_{inv}) was calculated to assess image quality using a commercially available phantom (CDRAD).

Results

The anthropomorphic phantom proved suitable for use in this thesis - based on correlation coefficient R values, there was a good correlation for the 5 phantom weights between the phantom and human pressure data. (R values: head =0.993, pelvis =0.997, and heels =0.996). There were statistically significant differences ($p<0.05$) between peak pressure values with and without X-ray table mattress for head, pelvis and heels. Additionally, there were statistically significant differences ($p<0.05$) between the IP ratio values with and without X-ray table mattresses. The type and age of the mattresses also had an impact on peak pressure values and IP ratios.

IAK and image quality measures were impacted by mattress addition. IAK values decreased because of attenuation, with IQF_{inv} having worse image quality. There was a negative correlation between mattress age and IAK, meaning that older mattresses had higher attenuation properties. The clinical impact of this finding, for the potential for radiation increase, was insignificant. No correlation was found between image quality and age.

Conclusion

A novel method for testing X-ray mattress IP was established and validated in this thesis. This method could be valuable for aiding mattress design and development and subsequent testing when in clinical use. For new mattresses, peak pressure values and IP ratios were greatly reduced, compared with older ones. The impact mattresses had on radiation attenuation and image quality are clinically insignificant.

Chapter One: Introduction to the Dissertation

This chapter introduces the study and explains its rationale and aims/objectives; Chapter Two reviews the relevant literature and discusses the research background; Chapter Three outlines the study methodology; Chapter Four presents the results of the study; and Chapter Five, Six and Seven discuss the study's results and present the conclusion and recommendations, respectively.

1.1 Background of and Rationale for the Research

This study considered X-ray table mattresses from three perspectives: pressure redistribution, X-ray attenuation/transmission and the impact of these two factors on medical image quality. In this section, the concepts of image quality and radiation dose are introduced before their relation to the imposition of a mattress is briefly explored. Next, pressure ulcers are introduced and the roles that mattresses play in the development and minimisation of pressure ulcers are outlined. These are then contextualised with respect to X-ray mattresses.

Medical imaging is a valuable and powerful diagnostic tool. Consequently, its use has increased extensively over the past few decades (Mineyuki, 2014; Tan et al., 2014; Smith et al., 2010). In 2015, however, The Royal College of Radiologists (RCR) outlined the side effects of diagnostic X-ray examinations, raising concerns about the potential detriment caused by exposure to ionising radiation. The most serious of these is the associated risk of developing cancer. Considering the adverse effects of exposure to ionising radiation, it is important to minimise its dosage to the lowest extent possible. To this end, the risks posed by diagnostic imaging procedures should be balanced against their potential benefits. The risk of radiation can be reduced by decreasing the radiation dose administered to the patient. However, such a reduction may also lower the quality of the X-ray image, potentially reducing its value. Achieving dose reduction while maintaining or improving image quality is therefore paramount

and is referred to as optimisation (Uffmann & Schaefer-Prokop, 2009). Ultimately, optimised images should have adequate acceptable diagnostic quality so that the radiation dose administered to the patient is not higher than suggested levels (ICRP, 2006).

There are factors that can confound image optimisation. Some of these can be isolated once identified and strategies can be put in place to address them. Other factors, however, cannot be isolated and addressed. Their impact must therefore be minimised. An example of a factor that can interfere with image optimisation but cannot be isolated and addressed is patient obesity. Here, the exposure factor selection must minimise the patient's radiation dose while ensuring that the resulting X-ray image is of an acceptable quality. Another example would be the introduction of an attenuating material between the X-ray source and the detector, such as the X-ray table and the mattress upon it. A strategy that is currently employed to minimise the impact of X-ray tables and mattresses as potential attenuating materials for the patient's radiation dose and on the X-ray image quality is to ensure that they are fit for the purpose. This means that they will need to meet adequate strength and comfort standards whilst also having an acceptable radiolucency level. Their design characteristics must therefore be carefully considered to meet the competing demands of strength/comfort and dose/image quality.

Image optimisation has several aspects, and the quality of a radiographic image must always be at the required level (or higher). A confident diagnosis must be attained from an image, and the selection of appropriate X-ray acquisition parameters for image production is paramount. These parameters should be carefully selected, taking into consideration radiation dose reduction where it is possible and appropriate. The parameters include source-to-image distance (SID), beam collimation, beam filtration, selection of kVp and mAs, and, where appropriate, the use of automatic exposure control (AEC) (Martin, 2007). Acquisition parameter selection is extremely important, as an unsuitable exposure can easily result in inadequate image quality. This can in turn cause a missed pathology and/or the delivery of an

excessively high radiation dose (Walker et al., 2011). For this reason, it is necessary for the radiographer to have a comprehensive understanding of how these parameters affect both the patient's radiation dose and the X-ray image quality.

While cancer (and cataract) can be induced by exposure to ionising radiation, which drives the need for X-ray image optimisation, pressure ulcers are caused by high/prolonged pressure (Brienza, 2007). Pressure ulcers pose a serious and significant threat to patients - particularly to those suffering from movement restrictions perhaps due to advancing age and/or chronic diseases (Gomez-Batiste et al., 2014; Pieper, 2012; Anton, 2006). While efforts have been made to reduce the incidence and seriousness of pressure ulcers, the occurrence of pressure ulcers acquired in hospitals is increasing. Furthermore, pressure ulcers can be an important cause of further medical complications and even death. As a result, recent studies have recommended more research on pressure ulcers to reduce their occurrence and to help identify better ways of reducing their impact on patients and on the healthcare system (e.g. easing their financial burden) (Brennan et al., 2014; Stoelting et al., 2007; Stotts et al., 2013; Goodell and Moskovitz, 2013).

A range of products have been developed to counteract the development of pressure ulcers and to manage those who have them. Such products include appropriately designed mattresses (ArjoHuntleighs, 2010). For many years 'regular bed' mattresses have been designed simply for comfort. However, unlike bed mattresses, X-ray table mattresses have not been featured in the evaluative literature in relation to their pressure redistribution characteristics and no national or international guidelines exist about their construction, testing or replacement frequency.

A gap in the literature exists regarding the potential negative impacts of radiography procedures employing X-ray table mattresses, such as their contribution towards pressure ulcer formation, radiation cancer induction (i.e. increased radiation doses to counteract the impact of

a mattress) and image quality degradation (due the inclusion of the mattress). No industry standard exists for assessing X-ray table mattresses for these three characteristics and almost nothing has been reported in the literature.

Many X-ray imaging examinations are short, and it is presumed that their potential to induce pressure ulcers is limited. However, some radiological procedures can be lengthy, and the patients may have to lie in a single position on the X-ray table/mattress for 2 hours or more. This can heighten the risk of pressure ulcer formation. Additionally, certain radiological studies occur within operating theatres, and the patient may lie on the X-ray/operating table for several hours. Such radiological procedures have the potential to induce pressure ulcers in patients due to the length of time that they must remain motionless (Pope, 1999a; Scott, 1998). Another scenario in which a patient may lie on an X-ray table mattress for a prolonged period would be in the emergency department. In this case, it would be on trolleys that have been modified to allow for X-ray imaging to be done on an image receptor tray beneath the bed (Donnelly & Sawer, 2014).

A key demand for X-ray table mattresses is that they be constructed not only to minimise radiation attenuation while preserving X-ray image quality, but also to reduce the risk of pressure ulcer formation. The National Institute for Health and Care Excellence (NICE; 2011) has considered the impact of X-ray table mattresses on X-ray image quality and radiation dose and proposed some recommendations. After performing comparative analyses of mattresses with low X-ray attenuation, NICE (2011) suggested that ‘warming mattresses’ negatively impacts X-ray image quality and radiation dose. The comparison was made based on the transmission capabilities of the mattresses (Vennart, 1997).

The physical methods of assessment identify the objective technical performance through repeatable and reproducible means. These include the contrast-to-noise ratio (CNR), sharpness, quantum efficiency and modulation transfer function. Another method is computerised

modelling, in which a Monte Carlo computer software calculates a stimulation of the imaging process. The observer performance methods include contrast detail (CD) visualisation, lesion detection through an eye-tracking methodology, and visualisation of anatomical structures. All of these methods are valuable to an accurate analysis, which is important for the optimisation of the X-ray image quality and for clinical practice (Vldimirov, 2010; Lyra et al., 2010).

Within the existing literature, there is a dearth of information about the assessment of X-ray table mattresses for their radiation attenuation and image quality characteristics, or their pressure redistribution characteristics. This is particularly true for methodologies that could be used for carrying out such assessments. This PhD thesis attempted to address this gap by developing and validating a valid and reliable method for assessing X-ray table mattresses for all the three aforementioned factors (i.e. radiation attenuation, X-ray image quality and pressure redistribution) and, by applying the new method, assess mattress performance. It is anticipated that the results of this thesis will inform international guidelines on how X-ray table mattresses should be tested and what performance data about them should be provided by the vendors to help guide clinicians in purchasing them.

1.2 Research Question

The following is the research question, an answer for which was sought within this thesis:

This thesis will investigate how much X-ray table mattresses vary in their pressure redistribution, image quality and radiation dose attenuation properties

1.3 Aims of the Research

The following are the aims of this research: (1) to develop and validate a new method of evaluating X-ray table mattresses for their pressure distribution, radiation dose attenuation and image quality properties; and (2), to use the developed method to evaluate a range of commercially available and currently-in-clinical-use X-ray table mattresses.

1.4 Objectives of the Research

The objectives of this research were divided into two phases, each of which related to one of the aims. The thesis considered the development and validation of a method using three mattress characteristics: pressure redistribution, radiation attenuation and image quality. Each of these characteristics was addressed separately, as outlined below. Phase one consisted of the development of the method while phase two involved the use of the method.

1.5 Phase One

1.5.1 Pressure Distribution

- Develop and validate a method for objectively assessing the pressure redistribution properties of X-ray table mattresses
- Use the developed method on a sample of X-ray table mattresses for the three main pressure ulcer jeopardy areas (posterior of the head, sacrum and heels) and assess the average and peak IP
- Identify how the overall efficiency of a mattress's pressure redistribution can be portrayed to allow an easy comparison of mattresses

1.5.2 Radiation Attenuation

- Develop and validate a method of assessing the radiation attenuation properties of X-ray mattresses

1.5.3 Image Quality

- Develop and validate a method of determining if a defined X-ray table mattress negatively impacts image quality

1.6 Phase Two (Commercially Available Mattresses)

- Evaluate commercially available mattresses for pressure redistribution, radiation attenuation and image quality.

Chapter Two: Pressure Ulcer Formation Research Background, Radiation Dose, and Image Quality

2.1 Overview

In this chapter, the results of a literature search on the history and origins of pressure ulcers will be presented, including their definition, aetiology, prevention and treatment, as well as the design of general mattresses intended to minimise pressure ulcers and the various types of general mattresses and X-ray table mattresses. The chapter will also include a discussion on radiation dose measurements and instrumentation, as well as the methods for image quality assessment when utilising X-ray table mattresses. There is a gap in the radiographic literature on the pressure distribution, image quality and radiation dose of X-ray table mattresses, which explains the rationale for this study.

2.1. Search Strategy Used in the Literature Review

For the literature related directly to this thesis, a comprehensive literature search of online catalogues was conducted use the following search engines: Google Scholar, Ovid-Medline, AMED and Pub-med. There are many available search engines, but these were used as they were deemed to be the most relevant to the field of research to which this thesis belongs. Furthermore, relevant magazines, leaflets, and books (particularly relating to pressure ulcers and mattresses) were also researched.

Literature relevant to the aetiology and risk features for pressure ulcers, radiation-induced biological effects, radiation measurements, image quality assessment, physical and visual measurements, the low-CD CDRAD 2.0 phantom (Artinis Medical System, The Netherlands), the features of CDRAD and the analysis of CDRAD data was researched. The following keywords were used for this: decubitus ulcers or pressure sores, decubitus ulcers or pressure

injury, pressure ulcer formation, radiation attenuation and image quality preservation. These were combined with the following keywords: aetiology, risks factors, epidemiology, skin damage, shear, IP, tissue viability, pressure-induced skin damage, biological effects of ionising radiation (stochastic and deterministic), X-ray mattress, general bed mattress, construction of X-ray mattresses, radiation measurement, dosimetry detectors and disadvantages and advantages of dosimetry.

There was no time limit for the search. The literature review was limited to English-language journals and texts. The search operators (NOT, OR, AND) were also used.

2.2 Pressure Ulcers in Clinical Practice

2.3.1 Definition of Pressure Ulcers

Pressure is defined as the force exerted on a surface per unit area. The standard unit for pressure is Pascal (Pa), as shown in the following equation:

$$P = F/A \tag{1}$$

where F is a force and A is the area it acts upon.

2.3.2 Complications and Types of Diseases Caused by Pressure

Pressure ulcers, also known as bedsores and decubitus ulcers, are injuries that occur on the subcutaneous layer of the skin and the underlying tissue. They can occur because of prolonged pressure imposed on the skin (Moore & Cowman, 2013, 2014, 2015). Pressure ulcers develop gradually and can worsen quickly. They are also known to heal quickly with treatment, although some never heal completely. Pressure ulcers are most often seen to develop on the skin that surrounds the bony areas of the body, such as the heels, ankles, hips and sacrum ((Mcinnes et al., 2015; Norman et al., 2016). People who are more likely to suffer from the

occurrence of a pressure ulcer are those with physiological conditions that restrict their mobility, so spend most of their time in bed or on a chair (Mert et al., 2004).

Many researchers have stated that before the onset of a pressure ulcer, there are certain signs and symptoms that appear. These are appropriately referred to as warning signals that the individual is likely going to suffer from pressure ulcers on the specified area (Mcinnes et al., 2015). These warning signals include unusual changes in skin colour or texture, swelling or inflammation, pus-like drainage from the specified area, an area on the skin that feels cooler or warmer to the touch compared to the other surrounding areas, and tenderized spots on the skin. According to Swisher et al. (2015), pressure ulcers have been categorised into certain stages or classes depending on their depth, severity and other features (Bishop & Droste, 2014). The extent of skin or tissue damage ranges from reddening unbroken skin to deep-tissue injuries involving the muscle and the bone (Tubaishat et al., 2016, 2018).

The most common sites where pressure sores occur in patients who spend most of their time on a wheelchair are those against which these patients rest. They include the skin over the sacrum or buttocks, the spine and shoulder blades, and the backside of the arms and legs. For those who spend most of their time in bed, the most common sites where pressure ulcers develop are the back or sides of the head, the shoulder blades, the hips, the lower back or tailbone and the heels, ankles and skin behind the knees (Mcinnes et al., 2015; Norman et al., 2016).

There are many factors that cause pressure ulcers to develop. Among these are immobilisation and reduced blood circulation in the veins and skin due to the pressure exerted on the skin. The three primary contributing factors to the occurrence of pressure ulcers are as follows (Dumville et al., 2015, 2015; Mcinnes et al., 2015; Norman et al., 2016):

- **Pressure:** Continuous pressure on any part of the body can restrict blood circulation to the tissue. Blood circulation is essential for the transmission of oxygen and other

nutrients to the tissue, and the absence of these can cause damage to the skin and the nearby tissues which can in turn lead to necrosis. According to another study, for people suffering from restricted mobility pressure ulcers are seen to occur in the areas that are less padded with muscle or fat lying over the bone, such as the spine, tailbone, shoulder blades, hips, heels and elbows (Banks et al., 2013; Bauer, 2012; Edsberg et al., 2016; National Pressure Ulcer Advisory Panel [NPUAP], 2016).

- **Friction:** Friction on the skin is induced when any part of the body is rubbed against a hard or rugged surface, thereby making the fragile skin more vulnerable to injury - especially if the skin area is moist.
- **Shear:** Shear stress occurs when two surfaces move against each other, such as when a patient slides down the bed after the bed is elevated. Moreover, when the sacrum moves downward, the skin above the bone may stay in place, thereby inducing stress in the opposite direction (Aziz & Bell-Syer, 2015).

There are various complications associated with pressure ulcers, some of which can be lethal. These include cellulitis, which is an infection of the skin and the connective soft tissues. This can lead to oedema, erythema and raised temperature in the affected area. People suffering from abnormalities in motor neuron response often do not feel any pain. Additionally, infections on account of pressure ulcers can spread to the joints and bones as well. Joint infections like septic arthritis can damage the tissue and cartilage (Chopra et al., 2017; The Joint Commission, 2017). In addition, bone infections like osteomyelitis can reduce the functionality of the limbs and joints. Long-term unhealed wounds, such as in the case of Marjolin's ulcers, can develop into lethal stages of squamous cell carcinoma. It has also been seen that skin ulcers can even develop and progress into sepsis.

Pressure ulcers were defined by Black et al. (2007) as a form of skin injury that stems from increased pressure or friction and causes tissue damage (Black et al., 2007). Additionally,

these forms of skin injury, as noted by Maklebust (1997), often cause a patient to feel distinct pain and discomfort. Bennett et al. (2004) stated that pressure ulcers could also impose economic burdens on the country's taxpayers, wherein health care is funded by taxation. Four grades of pressure ulcers have been described by the European Pressure Ulcer Advisory Panel (EPUAP; 1999), and are as follows:

- Grade 1: Skin tissue discolouration together with oedema (common in darker-skinned individuals)
- Grade 2: Partial superficial skin loss, wherein an abrasion presents itself clinically
- Grade 3: Subcutaneous tissue loss, commonly extending downwards although not profound enough to penetrate the tissue underneath
- Grade 4: Excessive tissue destruction, possibly including muscle and/or supporting structural damage which may occur with or without extreme skin tissue damage and loss (EPUAP & NPUAP, 2014, 2009)

The US has a 15.5% pressure ulcer prevalence rate among healthcare facilities, with between 28 and 17.2% of the pressure ulcers occurring at the sacrum and buttocks, respectively (Vangilder et al., 2009, 2008). In the UK, the pressure ulcer incidence rate among older adults is 4.7% according to the U.K. General Practitioner Research Database (Dealey, 2012). In comparison, Europe has an 18.1% pressure ulcer prevalence rate (Vanderwee et al., 2007). However, these figures vary from one country to the other and in terms of the degree of the injury. Superficial and deep pressure ulcers have a different aetiology and different characteristics from the other types (Bouten et al., 2003). For instance, prolonged pressure causes Grade 3-4 pressure ulcers, and these normally start to develop close to distinctly bony surfaces due to the higher IP (Brienza, 2007). Superficial ulcers, on the other hand, can be caused by skin shears or tears (Gould et al., 2000).

Interestingly, the U.K. Department of Health (2011) noted that the prevalence of pressure ulcers could accurately indicate the levels of care quality within healthcare settings. On the other hand, Moore (2013) mentioned that this could not be used in isolation without the aid of other factors, such as the population's risk status and the different types of cases. In particular, imminent death is commonly related to tissue tolerance reduction levels, which increase the probability of pressure ulcer occurrence (Moore & Cowman, 2013).

2.3.3 Effect and Classification of Pressure Ulcers

There has been sufficient classification of pressure ulcers, making it easier for physicians to treat pressure ulcers depending on their severity and propensity level inside the body. Although most pressure ulcers fall within the six well-known categories, some researchers have argued that there are some pressure ulcers that present characteristics of more than one stage and hence can be difficult to categorise (Boyko et al., 2018). Pressure ulcer classification determines the treatment and management pathway that a patient suffering from pressure ulcers is recommended to receive (Boyko et al., 2018). Based on the recommendations of international organisations like NPUAP of the UK, EPUAP, and Pan Pacific Pressure Injury Alliance (PPPIA), which formulate policies on pressure ulcers, there are six main groups of pressure ulcer, as outlined below.

Group 1 pressure ulcers

The first category of pressure ulcers consists of pressure ulcers with symptoms associated to non-blanchable erythematous progressions on the skin, wherein the skin continues to change. Pressure ulcers falling within this category are difficult to identify, especially in patients with a darker complexion. The affected area becomes painful with oedematous progression and heat generation from underneath the skin. This is due to the secretion of pyrogens through the

synthesis of interleukins by the surrounding T-cells in the necrotic area (Engels et al., 2016). This type of bedsore may take up to 28 days to heel and looks somewhat like hyperaemia, thereby making it difficult to distinguish from it, although they are different from moisture lesions.

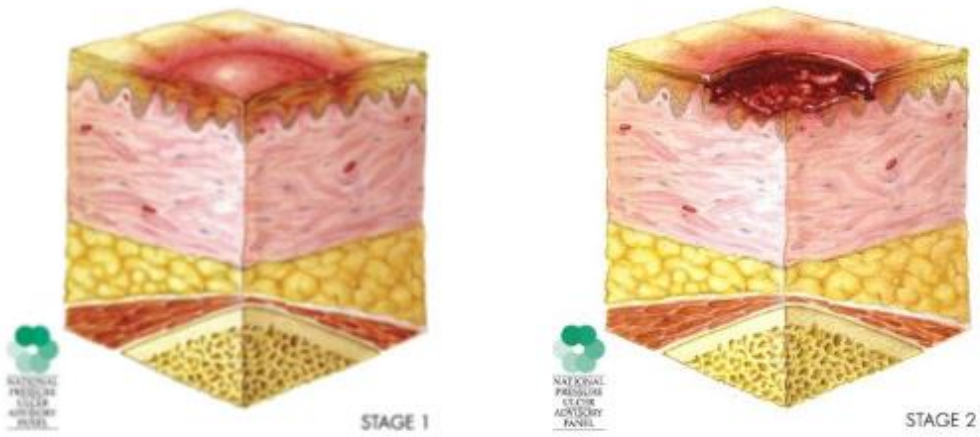

Figure 2.1: Staging Image of Pressure Injuries for Group 1 and 2 Pressure Ulcers (Source: NPUAP, 2014).

Group 2 pressure ulcers

In this category of pressure ulcers there is clinical superficial thickness of intact skin and skin loss with respect to epidermal association, dermis or both in certain circumstances. These pressure ulcers also appear on the skin in the form of an abrasion or a blister, with an average healing time of about 94 days (Fletcher, 2015). This category of pressure ulcers is completely different from that of moist lesions.

Group 3 pressure ulcers

For the third category of pressure ulcers, the pressure ulcer formation is associated with the occurrence of necrosis of the underlying skin tissues, especially the subcutaneous tissues, thereby resulting in the formation of a tiny clatter fascia (Yusuf et al., 2015). This phenomenon is also referred to as a loss of full-thickness skin. The average healing time of this type of pressure ulcer is approximately 127 days after the introduction of medication (Bennett et al., 2004).

Group 4 pressure ulcers

For the fourth category of pressure ulcers, the pressure ulcer that develops is defined as a chronic form of necrosis that eventually leads to excessive destruction of the bone tissues and muscles. This type of pressure ulcer may be cured in almost 155 days from the onset of medication (Akins et al., 2011, Bennett et al., 2004).

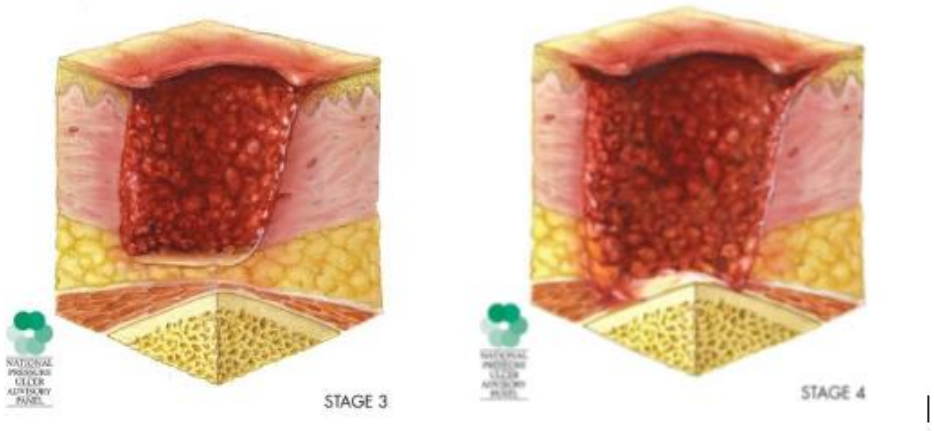

Figure 2.2: Staging Images of Group 3 and 4 Pressure Ulcers (NPUAP, 2014).

Group 5 pressure ulcers

This category of pressure ulcer involves full-thickness tissue damage. The extent of tissue loss may not be fully determined due to the presence of slough and eschar on the area. To determine the actual deepness of the wounds, the slough or eschar would need to be removed. The pressure ulcers within this category may be wrongly assessed as belonging to the third or fourth category. These ulcers are maroon and purple in colour and are found in localised skin areas. The soft tissues underneath that are damaged due to pressure and shear cause redness and swelling. The result is that the area gets warmer or cooler and painful compared to normal skin. This is often difficult to locate in patients with a darker skin tone.

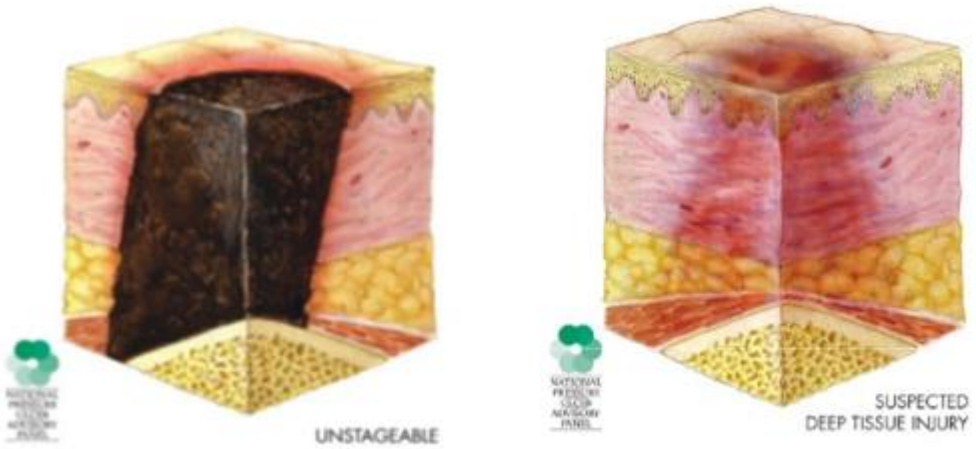

Figure 2.3: Staging Image of an Unstageable Pressure Ulcer and a Suspected Deep-Tissue Injury (NPUAP, 2014).

2.3.4 Tissue Breakdown Due to Pressure

It has been stated that the areas in the body that are less commonly affected by excessive pressure leading to tissue breakdown are the knees, scapulae, earlobes, and elbows. However, tissue breakdown may occur at any part of the body when excessive pressure is imposed upon it. It has also been indicated that tissue breakdown occurs more frequently over bony surfaces,

such as the ischial tuberosities, while the position of a patient, together with her or his level of immobility, often determines where the damage occurs. For instance, in the supine position, the sacrum, buttocks, coccyx and heels are the areas in the body that are most vulnerable to tissue breakdown as they are more likely to remain in contact with the mattress (Engels et al., 2016; Santamaria et al., 2015).

2.3.4.1. Risk factors of tissue breakdown

The risk factors of tissue damage leading to pressure ulcer formation can be related to intrinsic or extrinsic factors, or to both. These include poor nutrition, immobilisation, chronic diseases, cognitive deficit, steroid use, pressure, friction, shear force or humidity (Qaseem et al., 2015).

2.3.4.1.1. Intrinsic factors

Intrinsic factors relate to a patient's physical health status. For example, ageing skin is associated with slower epidermal development, decreased vascularity, and decreased subcutaneous adipose tissue, together with decreased collagen and elastin (Raju et al., 2015; Swafford et al., 2016). As a result, the skin becomes susceptible to tissue breakdown, injury and infection, and the immune system response to any inflammation is also reduced.

2.3.4.1.2. Extrinsic factors

Research states that the common extrinsic factors related to tissue pathogenesis are friction, pressure, moisture, and shearing. The normal arteriole, capillary and venule pressure values are 12, 20 and 32 mmHg, respectively. 300 mmHg pressure can be generated under the ischial tuberosities when an individual is seated, while 100-150 mmHg sacral pressure can be generated when a person is lying on a standard hospital mattress (Black et al., 2007).

2.4 Development of high risk areas (Jeopardy Areas) Predisposed towards Pressure Ulcer Formation

Pressure ulcers can often be caused by high IP, which is the level of pressure between the body and the surface supporting it. High IP occurs when body tissues are compressed together. This is prominent over bony surfaces, where soft tissue is not as present and the compressive forces pressing upon the skin are thus higher and harder to tolerate. Research has demonstrated that blood circulation is likely to be compromised by an IP that is higher than the capillary closing pressure (CCP; 32-47 mmHg) for any duration in excess of 2 hours. This may result in tissue anoxia and cell death (Defloor, 1999; Maklebust & Sieggreen, 2001). CCP is defined by McGinnis and Stubbs (2014) and Messer (2012) as the pressure required to occlude the blood flow within the capillaries (completely or partially). Furthermore, the at-risk areas, defined in this thesis as the head, sacrum and heels, are the most common locations of pressure ulcers due to their higher bony prominence. This has been demonstrated by a variety of research studies relating to pressure ulcer aetiology, incidence, prevention and treatment (Casey & Gittins, 2013; Peterson et al., 2010; Regan et al., 2009; Sayar et al., 2009; Edwards, 2006; Kernozek et al., 2002).

2.5 Policies and Guidelines for Minimising the Development of Pressure Ulcers

Various policies and guidelines have shown how vital pressure ulcer prevention is. These helps define clinical practice. Two examples of such guidelines can be seen in the Benchmarks for the Fundamental Aspects of Nursing Care (Department of Health [DOH], 2011) and in Essence of Care (2010). Pressure ulcer prevention and treatment are of utmost importance in health care. For example, in Sweden, pressure ulcer prevention, management and treatment are a quality indicator of patient care in nursing (Ek et al., 1997). Even though considerable time, finance and human resources are spent planning pressure ulcer preventive strategies, Moore

(2004) reported that the incidence or prevalence of pressure ulcers is not decreasing. In 2009, NPUAP and EPUAP developed pressure ulcer prevention guidelines recommending that the nutritional status of all patients at risk of developing pressure ulcers be assessed. Studies have also shown that there is a direct link between a patient's risk of developing pressure ulcers and malnutrition (NPUAP, 2014; Samuriwo, 2012).

2.6 Causative Factors of Pressure Ulcers

Pressure intensity directly relates to the hardness levels of the surfaces supporting the body, as stated by Defloor (1999). Accordingly, Pope (1999a) noted that the external pressure applied to the skin on the muscle/bone interfaces can be three to five times higher than that applied to other skin surfaces. Simpson et al. (1996) indicated that a high IP is generated by most standard hospital mattresses.

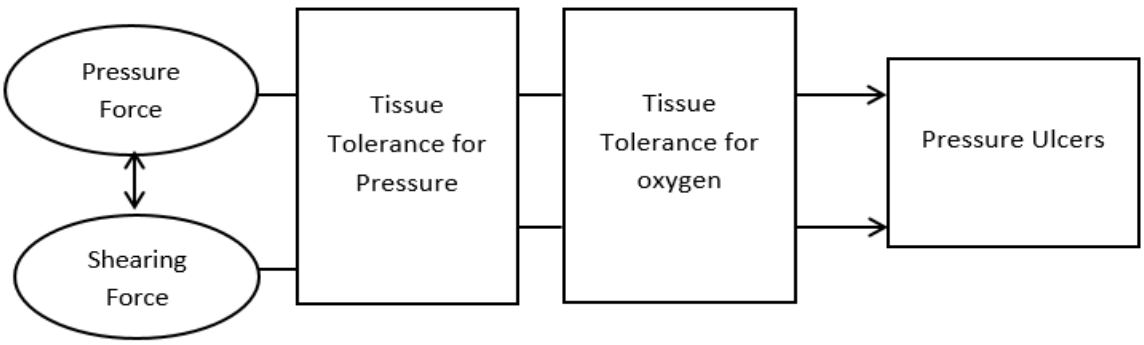

Figure 2.4: Defloor's Conceptual Scheme.

According to Defloor's (1999) argument, the progress of pressure ulcers is intermediary, and affected more by tissue tolerance rather than actual contributors. In other words, the risk of tissue damage depends on the capability of the patient's skin tissues to endure pressure. The main causative factors of tissue damage are the intensity of the pressure applied and the time

duration of the pressure application. However, these may vary in value from one patient to another depending on the patient's ability to withstand pressure.

2.6.1 Effects of Pressure

Pressure is the vertical weight-force exerted on a specific part of the skin (Agrawal & Chauhan, 2012; Messer, 2012). It is a primary causative factor of pressure ulcer development as it significantly affects an individual's blood flow and can cause partial or even complete blood vessel occlusion (Demarre et al., 2012).

2.6.2 Effects of Skin Shear

The following equation mathematically describes shear:

$$\tau = \frac{\mathrm{F}}{\mathrm{A}} \tag{2}$$

where τ is the shear stress, F is the force applied, and A is the cross-sectional area of the material within an area parallel to the applied force vector.

Skin shear occurs due to force and friction directed parallel to an individual's skin. This commonly occurs when forces bear down on a body together with the friction caused by the body-surface resistance (Messer, 2012; Pieper, 2012). Consequently, stretching and tearing occur due to the shear while the blood flow and stasis in the subcutaneous tissues are reduced. This can result in distortion and/or blood and lymph vessel damage (Byrant, 2012).

2.7. Complications Caused by Pressure Ulcers

According to Brienza (2007), IP measurement is used as a vital tool for assessing the risk of developing pressure ulcers. Gomez-Batiste et al. (2014) and Pieper (2012) stated that within the healthcare setting, patient health is frequently threatened by pressure ulcers. This is particularly true for elderly or partially/fully immobile individuals, or for individuals suffering

from chronic diseases. Unfortunately, cases of hospital-acquired (nosocomial) pressure ulcers have continued to increase despite significant attention that has been directed to their reduction on a global scale. Unfortunately, pressure ulcers can still result in adverse complications and death (Stotts et al., 2013; Brennan et al., 2014). The Health and Social Care Information Centre (HSCIC; 2014) in the UK has shown that the total prevalence rate of pressure ulcers within a variety of healthcare settings, including nursing and care homes, as well as hospitals and private care providers, is 4.7%.

2.8 Anatomy of the Jeopardy Areas

The body can develop pressure ulcers in different areas, and pressure ulcers can develop at different rates. The pelvic region, for instance, is more susceptible to pressure ulcers. Pressure points or zones can be distinguished and identified in many areas of the body in different situations. For this reason, the focus of this thesis was body parts that are most ‘at risk’ for the development of pressure ulcers (head, pelvis and heels), as shown in Figure 2.5.

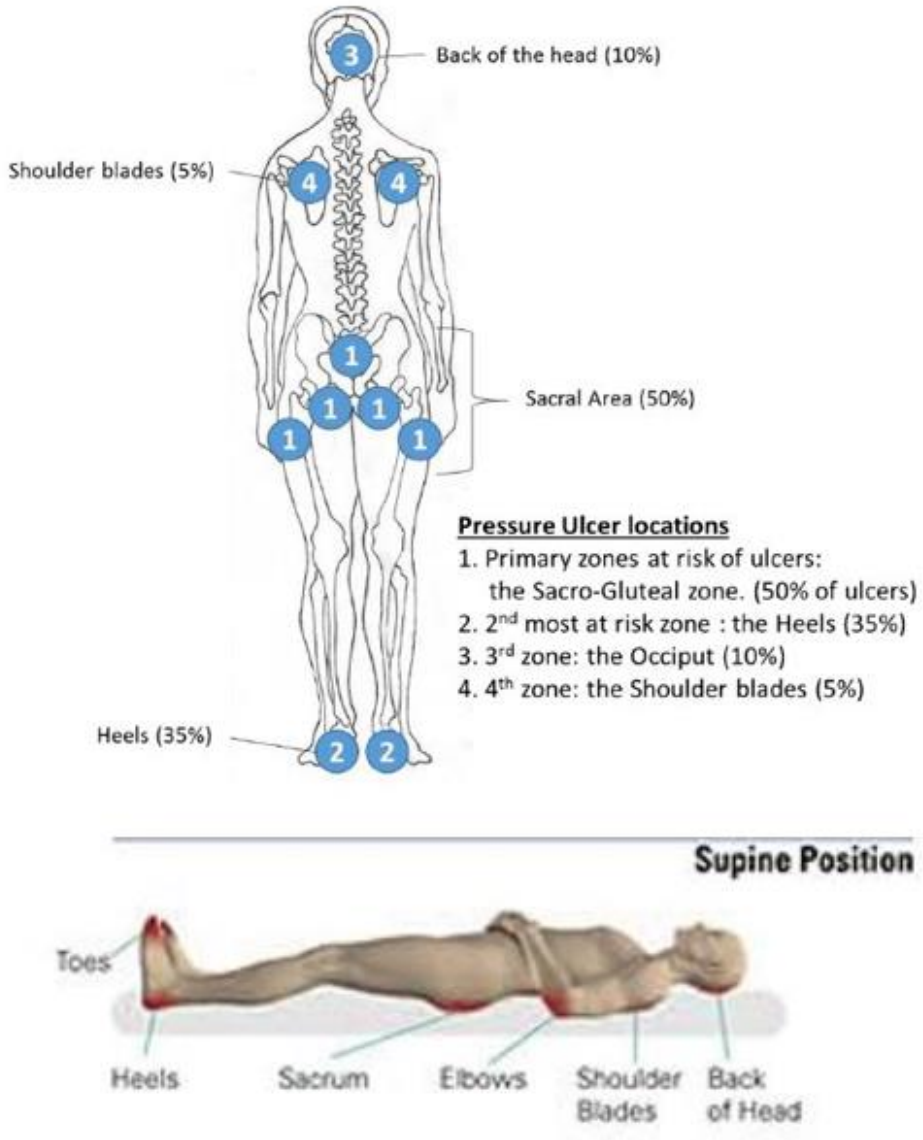

Figure 2.5: Common Pressure Sore Sites on the Human Body and Areas of Pressure Ulcers in the Supine Position (Medical Education, Inc., 2017; SORE, 2017).

2.9 General Bed and X-Ray Table Mattress Properties

It is important to understand the properties of general mattresses before considering those of X-ray table mattresses. Presenting the similarities and differences between the two mattress types will give a better insight into properties of X-ray table mattresses. For instance, X-ray table mattresses are thinner (typically 2.5 or 5 cm thick) than normal mattresses and must be

adequately radiolucent. Thus, given that X-ray table mattresses are thinner than general bed mattresses, they have a poorer pressure redistribution performance compared to general bed mattresses (Pessanha et al., 2014). Furthermore, the two types of mattress have specific advantages and disadvantages. In a study conducted by Chen (2015), normal bed mattresses were shown to have a good level of serviceability and softness, therefore providing more comfort compared. However, most normal mattresses are less manoeuvrable due to their weight (Doxastakis et al., 2015). Meanwhile, X-ray table mattresses are purposefully thinner than normal bed mattresses and are intended to be highly radiolucent (Pessanha et al., 2014). X-ray table mattresses therefore tend not to be as soft as general bed mattresses and may provide less comfort than general bed mattresses. Table 2.1 shows the main differences between general bed and X-ray table mattresses.

Table 2.1: Differences between General Bed and X-Ray Table Mattresses

Features	**General bed mattresses**	**X-ray table mattresses**
Thickness	10-25 cm	2.5-5 cm
Radiolucent	They do not need to be tested for radiolucency as this is not a mandatory characteristic of these mattresses.	Yes
Level of serviceability	The vendor literature contains information regarding their softness/ firmness, comfort and value rather than their level of	Little to nothing is reported in the literature about their comfort levels.

	serviceability considering their intended purpose.	
Material components	Consist of several materials (foam, mantel, etc.) often promoted as good materials for getting a comfortable night's sleep	Usually consist of only one material (foam), but some newer X-ray table mattresses are starting to use two materials in combination

2.10 X-ray Table and Normal Bed Mattress Design

In both hospital and community settings, an alternating pressure (AP) pad can be fitted underneath the patient and on top of the general bed mattress to mechanically reduce the duration of pressure application on a patient's skin, with a view to reduce pressure ulcer incidence and/or help with the healing process. An AP pad is a support surface that generates varied low to high IP values between itself and the body (Angmorterh et al., 2019; Bordier et al., 2014; Tugwell et al., 2017). The utilisation of AP pads helps maintain higher levels of perfusion in the deep and superficial tissues that the body weight causes compression to. This is a result of the redistribution of the IP from the skin (Marchesini et al., 2008; Stock, 2008). Another study conducted by Chai and Bader (2013) mentioned that the air-filled cells in AP pads are cyclically inflated and deflated, resulting in IP redistribution. However, the sustained IP effects are lowered on the soft tissues overlying the parts of the body with a bony prominence, such as the head (Chai & Bader, 2013).

AP pads need to be inflated correctly, as specified by the manufacturer. Moreover, the user/patient's weight should define the proportional air cell pressure for the pad (Chai & Bader, 2013). Accordingly, the AP pad becomes too hard when the air cell pressure is too high,

producing elevated IP values and augmenting the risk of pressure ulcer development (Chai & Bader, 2013; Chai et al., 2017). Comparatively, the air cell pressure of the AP pad normally decreases excessively under the weight of its user. As Demarré et al. (2012) noted, the inflation and deflation rates of the air cells in the AP pad must therefore be identical for effective IP redistribution. Additionally, the air cells' inflation-deflation cycle duration period is generally 10-12 minutes (Demarré et al., 2012). To accurately measure the air cells' pressure during both the inflation and deflation stages, Demarré et al. (2012) stated that a sensor must be connected to the AP pad (Demarré et al., 2012).

Whist the above sheds light on the current design of general bed mattresses, the design features that have been highlighted cannot be used in the design of X-ray table mattresses because such features will undoubtedly result in image artefacts. This will likely increase the radiation dose administered to the patient because of the additional attenuation that will arise from the mattress design itself and/or the mattress's mechanics.

2.10.1 Types of X-Ray Table Mattresses in Hospitals

Over the last two decades, many innovative products and processes have been developed to benefit humanity. For instance, memory foam mattresses have transformed mattress design and have become popular and affordable. These are good alternatives to the ubiquitous spring beds and have been made possible by technological advancement with the needs of the consumers or users in mind (Denk et al., 2017).

Visco memory foam is an innovation in general bed mattress design that was originally developed in 1966. As noted by Siddharth and Deshpande (2016), Visco memory foam is now being used in the medical field to protect and provide comfort to patients in intensive care units and to patients in wheelchairs. The pressure-relieving benefits of these memory foam mattresses have been used extensively to prevent the formation of pressure ulcers and to

minimise the pain in sensitive areas of the body (Siddharth & Deshpande, 2016). Mattress covers have also evolved and have become vapour-permeable, capable of reducing heat and moisture build-up and also minimise the risk of shear and friction (Siddharth & Deshpande, 2016). Another benefit of memory foam mattresses is that they yield and adjust to the patient's body shape. Unlike springs and other materials used in conventional mattresses, memory foam does not 'push back' or impose added upward pressure on the user.

The different types of hospital mattresses in use cause different stages of pressure ulcers (Table 2.2) based on the quality of the mattress and its characteristics. X-ray table mattresses pose a risk of inducing pressure ulcers, but the coloured circles in Table 2.2 shows a low risk of pressure ulcer formation from the use of different types of X-ray table mattresses. It has also been noted that pressure ulcers occur more frequently at some levels of immobility than at others and this often determines where the damage occurs. This is typically in the areas of the body that are most vulnerable to tissue breakdown, which are those that are more likely to remain in contact with the mattress for an extended period.

Table 2.2: Different Types of Hospital Mattress (Sidhil Ltd., 2013)				
Mattress name	**Mattress characteristics**	**Mattress weight**	**Mattress dimensions**	**Mattress-caused pressure ulcer** High risk Low risk
Acclaim VE	A specially designed castellated foam that can be moulded to a specific shape to provide support and comfort to the patient by facilitating pressure reduction, providing additional strength and stability to support patient transfer via the constructed walls in the 'U' foam and serving as a vapour-permeable cover, a user-friendly zip cover,	15 kg	Height: 15.2 cm Width: 86.4 cm Length: 199 cm	

	a multi-stretch waterproof material and a heavy-duty anti-slip nylon material at the base ○ Reliable for high-risk practice and can carry a maximum weight of 254 kg (40 st)			
Acclaim Profiler	A foam designed to provide comfort to the patient and to keep the patient firmly in place • A cover with a back-and-forth stretch and an impermeable/vapour-sensitive porous material • Distinctive user-friendly zip cover • Heavy anti-slip material at the base • The specially engineered U-shaped foam provides force and stiffness for safe patient transfer. • Extensions available for a reliable mattress • Maximum weight-carrying capacity: 254 kg (40 st)	14 kg	Height: 15.2 cm Width: 86.4 cm Length: 199 cm	

Acclaim **Bariatric VE**	A static Visco elastic layered foam with an extra supportive material at the base • Two-way cover with an impermeable/porous material • The heavy anti-slip material at the base of the 'U' foam construction provides added strength and stability and supports patient transfer.	20 kg	Height: 16.5 cm Width: 116.8 cm Length: 203.2 cm	
Softrest VE	• Castellated top layer with a supportive base • Optimum pressure reduction zone, provides maximum comfort to the patient • Waterproof, two-way-stretch cover • Porous material permitting vapours, and colourless bottom • Exceptional zipper position	12 kg	Height: 15.2 cm Width: 86.4 cm Length: 199 cm	

Softrest Contour	A Visco elastic layered foam with optimal pressure decrease, preferably designed to provide comfort and to keep the patient in place • Porous material permitting vapours, and colourless bottom • Covered zip	14 kg	Height: 15.2 cm Width: 86.4 cm Length: 199 cm	
Softrest Foam Mattress	Designed to provide maximum support to the patient as well as maximum comfort through pressure reduction • Two-way-stretch, vapour-impermeable cover and porous, colourless base • Covered zip • Exceptional zip set display	12 kg	Height: 15.2 cm Width: 86.4 cm Length: 199 cm	
Essentials Contour Mattress	High-density mattress • Mattress supported by a four-way junction	10 kg	Height: 12.5 cm Width: 86.4 cm Length: 199 cm	

	• Two-way-stretch, vapour-impermeable cover and porous, colourless base			
Essentials Foam Mattress	• Castellated, swirl-gel profiling support foam mattress • Mattress supported by a four-way junction • Two-way-stretch, vapour-impermeable cover, and porous, colourless base	10 kg	Height: 12.5 cm Width: 86.4 cm Length: 199 cm	

2.10.2 X-Ray Tables and Radiolucent Mattresses for Use in X-Ray Imaging

A standard poly foam radiolucent mattress provides relief and good support to patients. The radiolucent materials that are used in medical imaging are thermoplastic resin combined with carbon fibre (Kwong et al., 2018). These materials must be radio-translucent for X-rays.

Radiolucent X-ray table mattresses have been synthesised to provide core benefits to patients with serious injuries. Novel materials and features can be utilised to further the development and innovation required in the medical industry (Fogel et al., 2008). The addition of radiolucent materials in X-ray technologies meets the current need for them.

There are two significant radiolucent composite materials: a thermoplastic resin matrix and carbon fibre. Both are used according to their manufacturing process, category and orientation (Trzeciak & Rivers, 2003). For medical imaging, the most used resins are thermoplastics. The selection of materials depends on the performance priority and the X-ray imaging application the mattress is to be used for. However, there are certain criteria that are critical, such as chemical, temperature and impact resistance; tensile strength; elasticity; hardness; dimensional strength; transparency; and biocompatibility (Davis & Affatato, 2006; Orlinsky & Bright, 2006). Fabricating thermoplastic resin in such a way as to make it compatible with its desired applications can be quite challenging.

2.11 Radiation Dose Assessments

The increased radiation dose that is required because of the modification of thermoplastic resin to make it compatible with its desired applications can cause damage to the cells. While most individual cells can repair the damage, such repairs can result in mutations (Alpen, 1998). This is because the changes in cells can result in deterministic or stochastic effects. Deterministic effects occur if the ionising radiation reaches a specific threshold, with the severity of the effect increasing as the dose increases. The radiation doses associated with Alpen's study (1998) (AP

pelvis on a trolley), however, were primarily concerned with protection against radiation-induced cancer and hereditary diseases, known as the stochastic effect. Chan and Fung (2014) expressed concerns about this stochastic effect when imaging the pelvis in trauma situations, as multiple follow-up examinations may be required. As such, the pelvic organs, including the gonads, may be exposed to a high cumulative radiation dose. It is essential for the radiation dose administered to a patient to be measured or estimated to check it against the standards of good practice and also to estimate the risk associated with the radiation dose absorbed by the patient's organs and tissues (Wall et al., 2011). In radiology, radiation dose estimation is important for several reasons. Firstly, because standards of good practice must be set and checked, and compliance with the regulatory requirements must be ensured. In this way, the recorded doses can be used for identification of the radiation dose delivered to the patient and for the evaluation of different techniques or equipment (RCR, 2008). Secondly, because it enables the determination of the risk associated with radiation exposure (Wall et al., 2006). The ionising radiation's interaction with living cells causes chemical-bond modification and splitting.

2.11.1 Radiation Dose Measurement and the Risk from Low Radiation Doses

Epidemiologists state that radiation risk refers to data from incidences of cancer and radiation exposure in two distinct styles: relative risk, which is the cancer incidence rate in comparison between an exposed population and an unexposed population; and absolute risk, which is a particular population's simple rate of cancer incidences (NAS, 2006). Various methods for showing radiation lifetime risk can be used, as outlined in Table 2.3.

Table 2.3: Some Methods that Can Be Used to Show Radiation Lifetime Risk.	
1 - Excess lifetime risk (ELR)	Comparing the mortality or cancer incidence rate in two different groups of the same population: one group theoretically exposed to radiation and the other unexposed to radiation
2 - Risk of exposure-induced death (REID)	Comparing the rates of death from specific causes in two groups of people of a certain age and gender: one group exposed to radiation and the other group theoretically unexposed to radiation
3 - Loss of life expectancy (LLE)	The period of life lost under the impression of being due to radiation exposure
4 - Lifetime-attributable risk (LAR)	Gives the excess mortality or cancer incidence rate over a study period in a (theoretically) unexposed population (ICRP, 2007)

Statkiewicz-Sherer et al. (2010) stated that radiation risk refers to the potential for ionising radiation to damage the tissues exposed to it as a result of tissue energy deposition, which occurs when the photons pass close to an orbital electron and create enough energy for the electron's liberation. There are several factors that affect the risk induced by radiation exposure, including radiation dose, the form of the radiation, internal or external damage, exposure duration, distribution of the radiation, the form of the tissue exposed and the age and gender of the individual exposed (HPA, 2011). Balonov and Shrimpton (2012) noted that males have a lower risk of developing cancer than females do, while the risk decreases for older patients and the degree of radiosensitivity of children is three to four times that of adults. For

instance, Lin (2010) demonstrated that 20-year-old patients are 50% more likely to be at risk from radiation damage compared to those twice their age, and that 40-year-old patients are 50% more likely to be at risk from radiation damage compared to 60-year-old patients.

The radiation energy deposited into DNA can result in molecular structural alterations, whereas radiation energy in indirect interaction is absorbed by water molecules which create free radicals and can consequently also damage the DNA molecules. Suzuki and Yamashita (2012) reported that the DNA damage from 100 mGy X-ray exposure, which is caused by direct interaction, accounts for 30-40% of radiation damage, while 60-70% of it is caused by indirect interaction. Radiation has two distinct detrimental health effects: deterministic effects, which follow high radiation doses and produce an immediate (in minutes, hours or days) tissue reactions or damage that is relatively predictable, and stochastic effects from low radiation doses, which may cause cancer (ICRP, 2007). Lin (2010) added that the stochastic effects could take effect after 5, 10 or even 20 years.

Regarding stochastic effects, they generally occur randomly because of DNA mutations and increase as the radiation dose increases. Dose-response curves (linear and linear-quadratic) present the probability of the occurrence of stochastic effects with radiation doses. However, the resultant disease level is unrelated to the radiation dose, as cancer can be induced by 2Sv radiation and gets no more severe than when produced at this level. Furthermore, Statkiewicz-Sherer et al. (2010) illustrated that stochastic effects are seen in reproductive-cell damage and radiation-induced cancer, which can cause defects in offspring due to the affected sperm and ova. Additionally, Brenner (2014) reported that the results of life span studies (LSSs) on atomic-bomb survivors showed that radiation-induced cancer is clearly related to radiation exposure level. Nonetheless, no clear evidence has been found for the correlation between radiation-induced cancer risks and low radiation doses (5-100 mSV), as more than 60% of the LSS-analysed individuals to date have received low radiation doses.

Dobrzynski, Fornalski and Feinendegen (2015) analysed data on radiation-induced cancer and its links to childhood fatalities from individuals living in areas with higher natural background radiation. They found that the risk level of radiation-induced cancer from small radiation doses is lower than the level anticipated by the linear no-threshold (LNT) model, which the adaptive physiological-tissue mechanisms help to explain. Thus, the LNT model seems to commonly exaggerate the risk of radiation-induced cancer (Dobrzynski et al., 2015). Meanwhile, Suzuki and Yamashita (2012) found that a LSS cohort data analysis of their study participants who had received 0-150 mSv radiation doses highlighted how radiation-induced solid cancer risk is linear, while incidences of cancer are statistically irrelevant when radiation doses below 100 mSv are received.

In general, the present limited data regarding the risks posed by exposure to low radiation doses (i.e. from conventional radiography) have produced even greater uncertainty of the complete effects of exposure to low radiation doses (De González & Darby, 2004; Brenner, 2014). The risk of developing radiation-induced cancer from exposure to low radiation doses has been shown to be minimal, but not nil (Wall et al., 2006).

For determining the correlation between exposure to a low radiation dose and solid cancer incidences, it may be valuable to use the LNT model (NAS, 2006; ICRP, 2007; Little et al., 2009). However, Dobrzynski et al. (2015) and Wall et al. (2006) recommended that low-radiation-dose-induced cancer be classified into four groups to overcome the uncertainty regarding the LNT model (Table 2.4).

Table 2.4: X-Ray Examinations Divided into the Four Low-Radiation-Dose Risk Groups Defined by Wall et al. (2006).		
Risk category	**Typical type of X-ray examination**	**Risk range (cases/10^6)**
Negligible risk	Chest, limbs, and teeth X-ray	Less than 1
Minimal risk	Head, neck, and joints X-ray	1-10
Very low risk	Spine, abdomen, and pelvis X-ray	More than 10-100
Low risk	Interventional radiology, angiography, biliary contrast studies of the alimentary and urinary tracts, and CT	More than 100-1,000

2.11.2 Radiation Dose Measurement

According to Hine and Brownell (2013), for patients exposed to ionising radiation, it is necessary to determine their absorbed radiation doses from diagnostic radiology. Accordingly, using software simulations, diagnostic imaging anatomical phantoms are commonly utilised for both direct and indirect absorbed-radiation-dose measurements. In addition, for patients undergoing radiological examinations or nuclear medicine procedures, in-vivo dose estimations are made (i.e. either absorbed- or effective-radiation-dose estimations). The absorbed-radiation-dose estimation method utilises dosimeters (e.g. thermoluminescent detectors [TLDs] or metal-oxide-semiconductor field effect transistors [MOSFETs]) and is referred to as the direct measurement method, while the effective-radiation-dose estimation

method utilises computer-based simulations and is referred to as the mathematical or Monte Carlo method.

Indirect measurement of radiation

Indirect measurement of radiation involves the measurement of specific factors at certain locations. This helps in estimating the dose at these locations. For example, the measurement of reference air kerma presents the direct measurement at specific reference points through the dose-area product (DAP) as the X-ray tube is corrected for distance measurements. However, DAP is not obtained through direct measurement because its calculated value is based on the evaluation of system parameter tables.

Direct measurement of radiation

The principal detectors utilised in clinical dosimetry to provide direct absorbed-radiation-dose measurements using a physical phantom are ionisation chambers, semiconductors and TLDs. Moreover, measurements of the radiation doses provided from the relevant organs or tissues in physical phantoms are conducted using TLDs or MOSFETs. Hashemi-Malayeri and Williams (2003) stated that the essential required time can also be reduced by switching to a near-real-time MOSFET-based dosimetry system instead of using TLDs. Specifically, TLD and MOSFET dosimeters are directly relevant to the current report. As such, further details of these methods are outlined below.

2.11.3 Radiation Dose Measurement Instrumentation

In some countries, absorbed radiation doses are required by law in various situations within the air kerma measurement in diagnostic radiology. They are also required for obtaining better-quality images along with minimising patient radiation dose (Hourdakis, 2014). Moreover,

various radiation dosimeters exist, and most of these come in the form of either an ionisation chamber or a solid-state detector. Bushong (2013) mentioned that the process of developing dosimeters considers the optically stimulated luminance (OSL) and includes a TLD alongside a semiconductor. Meanwhile, Lemoigne and Caner (2011) indicated that specific clinical situations and the selection process determine the type of dosimeter to be used. For instance, as Hendee and Ritenour (2002) and Hobbie and Roth (2007) showed, the measurement instruments should have the same properties as the medium used to measure the radiation doses. Table 2.5 highlights the advantages and disadvantages of the different types of dosimeter.

Table 2.5: Some Advantages and Disadvantages of Different Dosimeters.

Serial no.	Dosimeter	Advantages	Disadvantages
1	**Electronic personal dosimeter**	• Directly reads the dose and the dose rate • Sounds an alarm when the dose exceeds the threshold level • Can withstand a drop from a 1.5 m height • Accuracy not dependent on the dose rate • Immune to an external magnetic field • Portable (Xavier Ortega, 2000)	• Can underestimate the dose value • Can sound an alarm when the threshold value is not exceeded • Has poor energy response • Can lose data when the power is turned off • Can show wrong readings and spurious signals (Xavier Ortega, 2000)
2	**MOSFET dosimeter**	• Provides instantaneous readouts • Has permanent dose storage • Waterproof • Efficient and easy to use (Scalchi, 2009)	• Depends on the temperature • Has a limited life • Sensitivity affected with an accumulated dose for unbiased MOSFETs

			• Dependent on energy
3	**Film badge dosimeter**	• Has a permanent record • Can distinguish between energies of photons • Measures radiation exposure accurately (Anon., 2017)	• Time-consuming • Heat exposure can deteriorate the film (Anon., 2017) • Requires processing facilities • Processing difficult to control • Needs proper calibration • Dependent on energy • Cannot be used for beam calibration • Cannot accurately measure less than 20 millirem radiation dose exposure (Anon., 2017)
4	**Thermoluminescent dosimeter (TLD)**	• Wearable • Can measure as low as 1 millirem radiation dose exposure	• Has no permanent record • Immediate readout not possible • No re-readability

		• High-precision • Responds linearly to dose • Not dependent on energy • Sensitive to low radiation doses • Reusable (Anon., 2017)	• Has memory effects • More expensive than other personal devices
5	**Optical fibre dosimeter**	• Has high sensitivity • Has good linearity (up to seven orders of magnitude) • Reusable • Low-energy-dependent • Low-fading • Reproducible (Ristic, 2017)	• Response can be saturated • Cannot be used in real time • Can heat up
6	**Silicon diode dosimeter**	• Has higher relative sensitivity • Quick-response • More mechanically stable • Does not require external biasing	• Depends on the temperature, energy and radiation dose rate • Needs an electrical connection in irradiation

		• Small • Less energy-dependent (Zhu, 2009)	• Needs special care (Rajan, 2017) • Varied calibration (Rajan, 2017)
7	**Diamond dosimeter**	• Responds linearly • Has an excellent resolution • Has flat energy response • Small • Has negligible directional dependence • Waterproof • Temperature-independent (Rajan, 2017)	• Stabilisation needed • Depends on the radiation dose rate • Expensive
8	**Ionisation chamber dosimetry system**	• Measures radiation dose exposure accurately • Recommended for beam calibration • Precise • Has known necessary corrections • Provides instant readouts (Rajan, 2017)	• Requires cables for connection • Requires a high voltage supply • Requires many corrections for high-energy dosimetry

9	**Self-reading dosimeter**	• Portable • Responds linearly • Provides immediate reading • Reusable (Anon., 2017)	• Has a limited range • Cannot provide a permanent record • May suffer loss of reading • Easily discharges
10	**Photographic film dosimeter**	• Provides permanent records • Energy and nature of exposure • Cheaper compared to other dosimeters (Rajan, 2017)	• Energy-dependent • Fades • Small • Difficult to process • Cannot be used for beam calibration
11	**pMOS dosimeter**	• Provides immediate readouts • Has permanent storage • Has an extensive radiation dose range • Has very low power consumption (Ristic, 2017) • Compatible with microprocessors • Has a competitive price	• Needs calibration • Low-resolution • Non-reusable

2.11.3.1 Thermoluminescent detectors

As indicated in the literature, TLDs are commonly utilised in various applications of medical dosimetry and personal monitoring due to their suitable dosimetric characteristics, reliability, small size, tissue equivalence as well as their accuracy and precision (Rivera, 2012; Mukundan et al., 2007; Yoshizumi et al., 2007). The use of TLDs, however, is particularly labour-intensive and time-consuming. Routine dosimetry typically takes around 7 hours, as annealing requires further stages as well as readouts in order to generate accurate results for one exposure to a fully-TLD-loaded adult dosimetry phantom (Knežević et al., 2013; Vokhmintsev et al., 2013; Zaman et al., 2011).

2.11.3.2 MOSFET theory

As has been reported by various researchers, a different measurement device is the MOSFET. This has value in the diagnostic radiation field, particularly in dosimetry (Arora, 2007; Lundstrom, 1997; "Power MOSFETs: theory and applications," 1990). MOSFET dosimeters have several advantages, including their small size, provision of instant readouts, increased levels of sensitivity and ease of use (Siebel et al., 2015). The first applications of MOSFET dosimeters in the field of radiotherapy were in the late 1990s, and since then, they have been used for various medical applications, including diagnostic X-ray procedures and dose verification in radiotherapy (Wang et al., 2005). The basic MOSFET structure is shown in Figure 2.6.

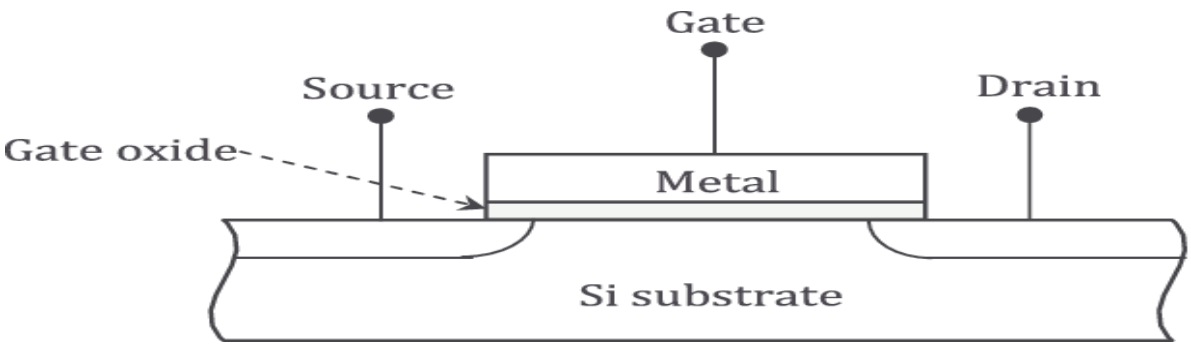

Figure 2.6: Basic Diagram of the Main Components of the MOSFET Detector.

The literature review showed that TLDs, MOSFETs, and Unfors have been empirically tested to decide among them should be used for radiation experiments. Dong et al. (2002) showed higher levels of sensitivity for MOSFET sensors at low radiation dose levels (approximately below 5 mGy) compared to TLD-100H chips, which demonstrated a less than 3% variation regarding the same range of radiation doses. This suggests that it may be better to use TLDs when the radiation dose is very low. Consequently, TLDs are generally used in conventional radiography experiments and dosimetry work, however they need to be tested empirically to verify if they are better for low radiation doses.

2.11.4 Effective Risk of Radiation Dose

As shown by Brenner (2008), the effective risk relates to the consideration of the lifetime risk of cancer caused by exposure to cancer-inducing radiation doses. The use of effective-risk levels replaces the utilisation of factors relating to radiation-induced cancer risks, which are organ-specific with tissue weighing. The Nuclear and Radiation Studies Board and Wall et al. (2011) published these findings. From organ radiation dose data, which can be measured by a MOSFET or TLD, it is possible to calculate the lifetime risk as informed by epidemiological studies. Tootell et al. (2014) noted that the direct radiation dose measurement approach minimises the bias stemming from the committee-generated weighting factors used in Monte

Carlo simulations. The effective-risk level used as a radiation dose quantity at low doses is also more likely to be understood by patients, healthcare workers and the public, making it possible for them to calculate the risks posed by radiation exposure themselves.

2.11.5. Dose Detector Type Used in This Thesis

2.11.5.1. RaySafe X2 dosimeter (Unfors)

As noted in the methods section (Page 105), a commercially available solid-state dosimeter (RaySafe X2, Unfors RaySafe AB, Billdal, Sweden; Figure 2.7) was used to measure the IAK (μGy) on the surface of the phantoms (the point of entry of the X-ray beam central ray). The RaySafe X2 dosimeter was used to ensure the precise measurement of the radiation dose that was received. The RaySafe X2 has a 40-150 kVp working range and can detect radiation doses within a wide range (from 1 nGy to 9,999 Gy). According to the manufacturer, RaySafe X2's accuracy is within ±5% of the calibrated values. Unlike TLD, RaySafe X2 directly measures the radiation dose received which minimises the errors that can result from the TLD calibration process. Furthermore, while TLD is time-consuming, the RaySafe X2 provides instant measurement readouts. Even though TLDs have high sensitivity to low radiation levels (e.g. scatter radiation), this was not an issue in this thesis because the radiation dose received was measured within the primary radiation field.

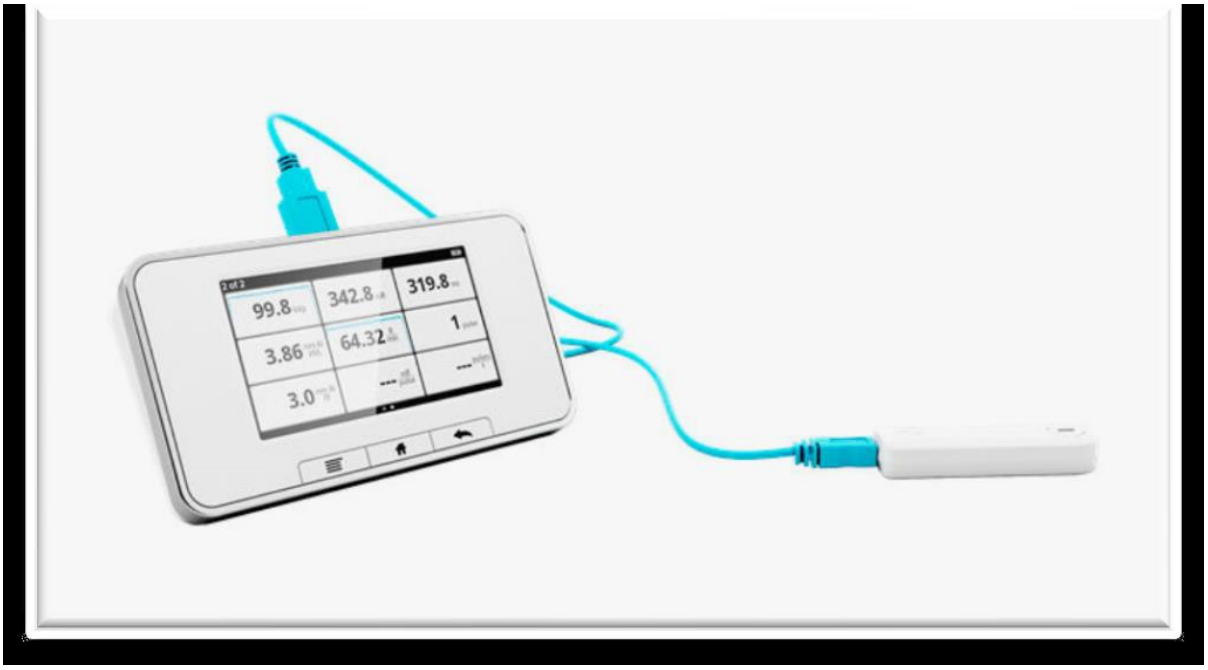

Figure 2.7: RaySafe X2 Dosimeter (RaySafe X2, 2016).

2.11.5.2 Comparison of TLD, MOSFET and Unfors

Unfors is preferred to TLD because it directly measures the radiation dose received which minimises the risk of measurement errors, whereas TLD requires calibration. Unfors is an instant measurement technique available when using the RaySafe X2. TLD can be time-consuming but is more sensitive to low radiation doses (i.e. scatter radiation). The sensitivity issue was eliminated in the current report, however, because the radiation dose received was measured within the primary radiation field.

Following this review and critique of the different dosimeters or detectors, the biological effects of radiation exposure and a detailed description of the two types of radiation dosimeters, the next section reviews various aspects of image quality measurement. It considers some methods for assessing image quality (physical and visual) whilst also discussing the benefits and limitations of each method.

2.12 Image Quality Assessment

The quality of a medical image is often evaluated using an imaging process or is based on the admissible features of the imaging equipment and the imaging variables selected by the operator. Image quality is not normally assessed by a single parameter, but consists of at least five factors (i.e. contrast, noise, blur, distortion and artefacts) and of the interconnection between these factors. The imaging system variables are extremely important for facilitating the best image quality (Suetens, 2017).

2.12.1 Definition of Image Quality

In the process of controlling the imaging instrumentation quality, data quality analysis (e.g. CNR or MTF) is commonly used as it instils a greater level of objectivity in the measurement of image quality with minimal bias (Roth et al., 2016). Nonetheless, data quality analysis is restrictive as it only measures specific individual device performance characteristics. Image quality analysis, on the other hand, often utilises human observers to analyse the patterns in the test images and is more subjective as the observers assess the [visual] displayed data. This can ultimately present a more varied set of clinical perspectives. However, human observers can be inconsistent which can cause both intra- and inter-variability to occur (i.e. multiple observers or re-testing one observer; Gissibl et al., 2016). As a result, it is difficult to obtain reliable data. Therefore, it is necessary to evaluate the different physical measurement methods utilised in image quality assessment as well as the alternative observer methods. The next section considers the physical and visual measurement methods that are used to assess image quality as well as observer methods used for the same purpose (Eskicioglu & Fisher, 1995; Kriete, 1998; Sheikh & Bovik, 2006; Wang et al., 2004).

2.12.2 Visual Measurements

Diagnostic performance analysis can be based on image quality assessments (or pathology detection) by observers. Moreover, as noted by West et al. (2017), the interpretation of image quality is connected to the quality of medical images which requires human participants to judge the visibility (and possibly the importance) of the features in the images. It is imperative to optimise the radiation dose within the practice of medical imaging while simultaneously maintaining an acceptable level of image quality for diagnostic purposes (Jung et al., 2019). Overall, various visual/cognitive evaluation methods exist in image quality assessment and adhere to certain criteria the most common of which are the receiver operating characteristic (ROC) and visual grading analysis (VGA).

2.12.2.1.Visual grading analysis (VGA)

VGA is utilised by observers in the assessment of a structures' visualisation, where they are asked to provide a rating of the anatomical reproduction in terms of its visual quality. Indeed, VGA is known to be quite relevant to clinical practice and is preferred by many researchers for assessing image quality (Liu et al., 2015). Furthermore, there have been studies on the value of VGA in detecting pathologies and these have shown a strong association between normal-anatomy visibility and the detectability of pathological structures on images (Gutjahr et al., 2016). Two types of VGA are the most common and can be utilised in the assessment of structures' visualisation: absolute VGA and relative VGA. In absolute VGA, the observers have no reference image, and thus the analysed images are shown individually. In relative VGA, the observers rank image quality compared to the quality of reference images.

2.12.3 Physical Measurements of Image Quality

To achieve the optimisation of an imaging technique it is necessary to determine and measure the quality of the resultant images and evaluate if they are fit for diagnostic purposes. However, image quality (IQ) is a broad term, and it is difficult integrate into the specified goals for improving medical imaging, or to set metrics through which it can be measured or compared. The meaning of image quality is likely to differ from one person to another and there is no specific or widely accepted definition of image quality (Shet et al., 2011; Singh & Pradhan, 2015). In medical imaging, there is no viable subjective or objective definition of image quality that can allow for the identification of a typical or perfect image. The reason for this is that medical images are acquired for different clinical indications, and this tends to fix the observers concentration on specific features within a given image. Consequently, an image that is perfect or acceptable for one purpose may not be acceptable for another. This causes enormous variation in the evaluation of acceptable image quality values and results in difficulties in determining optimum imaging protocols and radiation exposure. For instance, the optimum imaging protocol and its resultant radiation dose for determining the position of a nasogastric tube would be very different from those needed for the detection of a subtle lung lesion, pneumothorax or a rib fracture in the chest (Shet et al., 2011). Therefore, image quality is determined by the observer's ability to utilise the image for a specific diagnostic problem (Burgess, 1995). With this in mind, the general definition of image quality could be 'a measure of how well an image demonstrates the physiology and/or anatomy of a person, as well as any alterations to an anatomical structure as a result of an abnormality' (Bourne & Kagadis, 2010). On the other hand, the utility of radiologic images and the precision of diagnosis rely on two factors: the quality of the radiologic images and the performance of the observers. Images with a good quality can improve the task-related performance, but they are not sufficient for obtaining a precise and correct diagnosis (Barrett et al., 2004; Mansson, 2000; Tapiovaara,

2008). For instance, a missed lesion may be related to an observer's incorrect decision, rather than the lesion's limited detectability (Manning et al., 2004). A moderate or low image quality may be seen by an observer as sufficient for a given clinical task, while an image with good image quality may require technical modifications (Kundel, 1979).

2.12.3.1. Types of physical image quality assessment methods

There are several medical imaging methods through which image quality and the performance of imaging systems can be evaluated. Physical image quality assessment methods are designed for assessing the 'total' X-ray imaging system performance and also for evaluating the performance of individual components. These methods form the basis of acceptance testing prior to commissioning a new piece of equipment in clinical practice. They also form the basis for the decisions made for assessing equipment performance over time (Vennart, 1997). Such methods have the advantage of being repeatable means of evaluating image quality, and, unlike visual image quality measurement, they yield objective rather than subjective results if carried out consistently (Morrell, 2006). Physical image quality assessment methods permit the characterisation of an imaging system's performance by measuring specific physical parameters and compiling the measurement data obtained according to the demands of a specific imaging task. Parameters like detective quantum efficiency (DQE; this refers to the efficiency of a detector's conversion of the inputted X-ray energy into a useful image output, which depends on the number of detected photons), signal-to-noise ratio (SNR), contrast-to-noise ratio (CNR) and low contrast detail (LCD) detectability are considered to be physical measures of image quality. These are routinely used for quality assurance measurement to ensure that the performance of an imaging system is both accurate and consistent (Vennart, 1997). Physical image quality measures have also been widely used for evaluating image quality and in optimisation studies (Ekpo et al., 2014; Samei et al., 2005; Smans et al., 2010).

They have high reliability (Krupinski, 2010), but as are limited in that they consider only one or two aspects of image quality.

Consequently, questions have arisen regarding the extent to which physical measures of image quality are valid in radiography. Such measures are specified by a single factor of image quality (e.g. noise only or contrast only) and do not include a combination of essential factors. Linking these physical measures of image quality to the diagnostic performance of radiography would be very beneficial to optimisation studies, routine quality control and evaluation of the general performance of imaging systems.

2.12.3.2. Measurement of the physical parameters of image quality evaluation

The resolution of the imaging system is described by the modulation transfer function (MTF), which indicates the percentage of an object's contrast that is recorded by the imaging system as a function of the object's size. In medical imaging, information on patients and their possible abnormalities is transmitted to the radiologist in two steps: (1) image formation and data acquisition; and (2) processing and display. The first step depends on the technical and physical characteristics of the equipment, while the second largely depends on the radiologist's performance.

There are several methods that can be used to evaluate image quality in diagnostic imaging according to level of evaluation required. At the lowest evaluation level, image quality can be investigated through the radiographic technique, considering the equipment characteristics, and measuring exposure parameters. At the highest evaluation level, patient images are investigated with techniques like the ROC analysis and VGA (Tingberg & Sjostrom, 2005). Physical measurements characterize digital imaging systems' primary physical characteristics and overall performance. These include the MTF, SNR, noise power spectrum (NPS) and DQE. The measurement of SNR in digital imaging systems can be

executed more directly, without going through function analysis. This is done by estimating the expected signal based on the difference between the average signal and the signals of the background images. However, it is more difficult to detect details in patients' radiographic backgrounds than to detect the details in the uniform background of homogenous phantoms (Birkfellner, 2016).

2.12.3.3. Association between physical and clinical assessments for diagnostic performance in radiography

Several studies have examined image quality assessment and its methods in the medical or clinical sciences. Sandborg et al. (2001) studied the correlations between the image criteria-based visual evaluation of radiographs and the measures of physical image quality in chest and spine film screen-based radiography, and in digital pelvis and chest radiography. Their findings showed a significant correlation between blood vessel contrast and visual evaluation in film screen-based chest imaging. The correlation between the physical measure of SNR and the subjective visual evaluation of noise, however, was lower. Their study suggested that clinical image quality in film screen-based chest radiography is more limited by contrast than by noise. While in film screen-based lumbar spine imaging, the predictors of clinical image quality are the contrast and SNRs of the small soft-tissue cavities in the bone.

When physical image quality improves, important radiological patterns become more recognizable and diagnostic performance can improve. Beyond a certain level of physical image quality, wherein all the important features are visible and no additional clinical image information can be displayed, diagnostic performance can be maximised.

Digital images can be altered easily, and as such NPS and MTF are not equally important, unlike in film-based imaging. They are combined to express imaging quality. This combination is based on the statistical decision theory (SDT; Beautel et al., 2000; Mayers, 2000; Barret &

Mayers, 2004), wherein image quality is evaluated through an observer's performance in a specified imaging task. Many published papers have discussed human performance in detecting a known signal embedded in noise. Often, clinical image quality is a subjective judgment of the quality of the radiograph. The effects-based assessment does not necessarily relate to clinical utility, and its utility has been questioned (Barrett & Myers, 2004).

The assessment of a digital system's image quality is often undertaken using physical quality metrics like NPS, MTF, DQE, CNR and threshold contrast measurement (Dobbins et al., 1992; Samei, 2003). These parameters describe the inherent performance of the image detector well, despite it being difficult to link this to clinical image quality (Mansson, 2000). The measurement and theory of effective DQE (eDQE), effective noise equivalent quanta (eNEQ) and effective dose efficiency (eDE) have been comprehensively described in the literature (Samei et al., 2008).

These objective physical measures are essential tools for assessing and describing imaging system performance in terms of image quality, but they do not take into account all the components of the imaging chain. The image quality assessment tools for digital radiography optimisation consist of physical measures and observational performance methods such as the visual grading of normal anatomy, as well as various ROC methods (Toennies, 2017).

2.12.3.4. Overview of physical image quality

As mentioned earlier, the physical measurement methods of image quality apply to the use of digital imaging systems for primary medical interventions as well as to the overall performance of imaging systems. These methods eventually determine the MTF, SNR, NPS and DQE (Zhou et al., 2017). The measurement of SNR with respect to digital imaging systems can be done more directly, without conducting functional analysis, by estimating the expected signal based

on the difference between the average signal and the signals of the backgrounds of the images. It is more difficult to detect the details in patients' radiographic backgrounds than to detect the details in the uniform background of homogeneous phantom images (Birkfellner, 2016).

As per the study of Badano et al. (2015), the objective of the physical measurement of image quality is essential. Furthermore, the utility of the measurement tools for determining imaging system performance (in terms of image quality) is required, however complete relativity has not been found with respect to all components of the imaging chain. The image quality assessment tools for digital radiography optimisation consist of the aforementioned physical measurement tools and observational performance methodologies, such as the visual grading of the normal anatomy and the various ROC methods (Toennies, 2017). In digital radiography, the European Guidelines on Quality Criteria for Diagnostic Radiographic Images has become a tool, and it suggests optimisation through the use of VGA is valid (Commission of the European Communities [CEC], 1996a). This requires the observer to evaluate image quality depending on her or his opinion of the reproducibility of the defined anatomical structures and their visualisation through either absolute evaluation or a rating scale (Chen et al., 2017).

CD analysis has been widely used for the evaluation of the image quality of diagnostic imaging systems. It includes the routine evaluation of equipment performance, and relevant optimisation studies (Jin et al., 2017). It has been seen that evaluation of CD images consists of human observers' visual detection of the threshold contrast combination in the image. According to Papp (2018), digital imaging technologies have been commonly utilised in medical imaging departments. The routine assessments and control of the image quality in both the clinical and technical aspects have been fundamentally associated with good practice. In image quality assessment, the human decision criterion is considered a fundamental element for inclusion within the imaging chain. It plays a crucial role in the medical diagnostic process

(Russ, 2016). Image quality assessment that relies on the objective measurement of image data is not affected by human perception because human subjects do not get bothered by variation that is aligned with the evaluation parameters. Thus, it is potentially more reliable and reproducible (Viergever et al., 2016).

The evaluation of a physical image is reliant on the visual observation of the images by the test subjects, such as the LCDs or the CD phantoms. Clinical image quality refers to a subjective judgment of the quality of a clinical radiograph or fluoroscopic image (Sato et al., 2019). The best-defined pathway for the assessment of image quality is the measurement of clinical performance through a quantitative method such as ROC analysis. As this is not a practical alternative for determining whether clinical images are used for image quality evaluation or are not, the scenario could be more comprehensive with the addition of subjective opinion-based assessments (Benner et al., 2019).

2.12.3.4. CDRAD phantom description and its use in image quality assessment

The CDRAD 2.0 phantom is a physical instrument for obtaining radiographic images. It is designed to determine the difference in threshold detectability. In general, for radiographic systems, it also evaluates the minimum threshold for visualising objects of different sizes above the noise threshold. Dobbins et al. (1992) and Funama et al. (2005) stated that the output obtained from the CDRAD phantom is more medically beneficial than that obtained from other tools due to its minimum contrast detectability. However, this is still a challenge for radiographic systems. The CDRAD phantom is composed of a 10-mm-thick square acrylic plastic plate (265×265 mm^2) along with flat drilled holes with variable diameters and depths, and a Pb grid composed of different line patterns equally distributed into rows and columns (15,15) to form a total of 255 squares. The diameters and depths of the drilled holes in each column and row change logarithmically from 0.3 to 0.8 mm.

One or two visible holes are present in each square. The first three rows consist of a visible hole in the centre of each square. Each of the remaining rows from the 4th to the 15th has two identical holes (one in the centre of the square and the other in one of the four corners). Figure 2.8 and 2.9 show the CDRAD phantom and its resultant radiographic image, respectively (Thijssen et al., 1988). The CDRD phantom has five different versions in various locations.

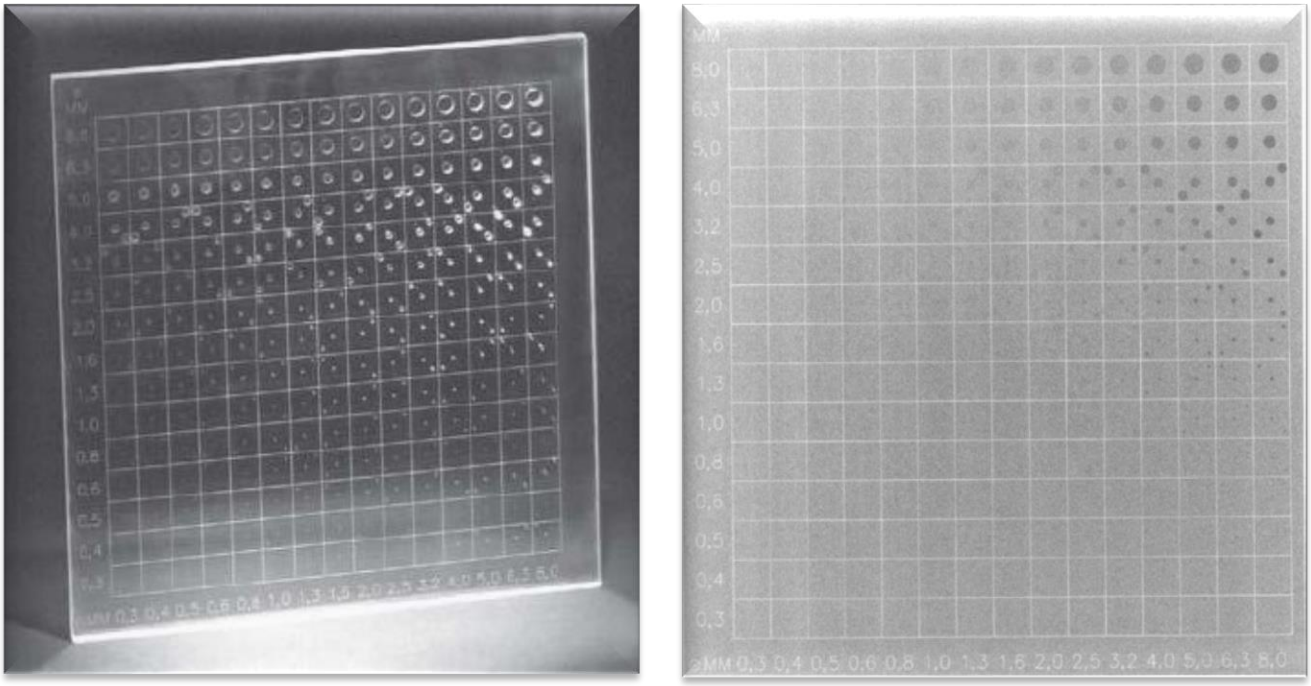

Figure 2.8: CDRAD Phantom Consisting of Holes in Four Corners to Reduce the Familiarity in Sites (Thijssen & Bijkerk, 1988).

There are two factors that determine the low contrast threshold detail: the size of an object and the noise of the imaging system. Further, Rose (1974) explained that tiny objects' details need a high contrast while large objects' details require a low contrast. This relation is expressed by the following equation:

$$C.\,D = k \tag{3}$$

where *C* is the contrast detail (CD), *D* is the size detail, and *K* is the constant signifying the threshold of the detail visibility.

Thijssen and Bijkerk (1988) proposed a method of measuring LCD detectability through the calculation of the CD curve or the IQF. For the CDs, a graphical demonstration of LCD detectability was undertaken. This demonstration consisted of a combination of the smallest depths or contrasts of the visible holes in each column (diameter) of an image (Thijssen et al., 1988, 1989). Figure 2.9 shows a better LCD performance when the CD curve is near the origin. The CD curve is difficult to form and compare with those of .0020d images. The numerical value of the CD curve is the IQF. The various parts of the CD curve utilised as an indicator of LCD detectability are outlined herein. IQF's ease of use is beneficial comparing the properties of images with various acquisition parameters obtained through diagnostic imaging systems. IQF is calculated from the sum of the lowest-diameter products from each of the 15 columns, and its use has enabled the correct detection of objects and intrinsic depths (Aichinger et al., 2004). This is summarised in the following equation:

$$IQF = \sum_{i=1}^{15} c_i \times d(i, th) \tag{4}$$

where *d (i, th)* is the lowest diameter (threshold diameter) in the column, *(i)* is the correctly detected visible hole, and *ci* is the depth value (contrast) of the object (visible hole) in a column (i).

IQF has an inverse relation with image quality. When the IQF values are lowered, the image quality becomes higher. The smallest size that can be seen with the lower contrast lesions and can be obtained by taking the inverse of IQF in equation (4). IQF_{inv}, on the other hand, has a direct relationship with image quality. When its value is increased, the image quality becomes higher.

$$IQFinv = \sum_{i=1}^{15} \frac{1}{ci \times d(i,th)} \tag{5}$$

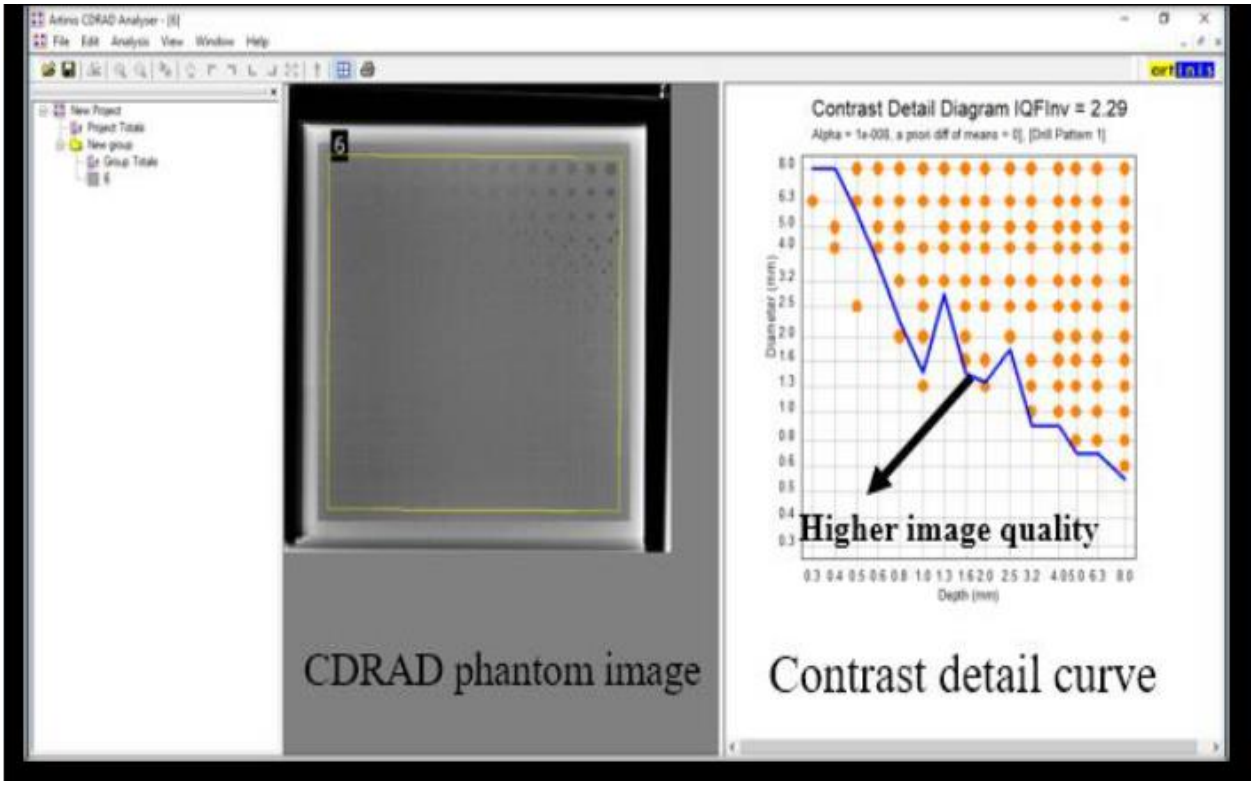

Figure 2.9: CDRAD Phantom Radiograph and Calculation of the CD Curve (Al-Murshedi et al., 2018).

One of the main purposes of the CDRAD phantom is quality control in diagnostic imaging. According to the CDRAD phantom manual (Thijssen & Bijkerk, 1988), it has various applications, as shown below:

- Comparison of image qualities by the diagnostic imaging screen system
- Determination of the optimal density of the background with varying density
- Determination of the optimal exposure system utilising parameter settings like the tube potential
- Simulation of the difference in object thickness through the polymethyl-methacrylate (PMMA) slabs
- Performance of image quality comparison at a constant density for various object thicknesses

- Investigation of the filtration impacts on the alteration of the thicknesses of the additional filters

2.12.3.5. Physical assessment method using the CDRAD software analyser

The CDRAD software is used to analyse images, and its results are displayed as a CD curve and as IQF_{inv}. This software identifies a visible hole in each square cell of a phantom image and locates the centre of the noticeable peripheral hole. Consequently, a statistical approach is used to determine the presence of an object. The two factors of standard deviation and mean pixel signal for the object and its background are used in this statistical method. Another statistical model used by Welch (student t-test) checks if the average signal altitude is higher than the background signal. This is possible because a difference exists between the background and object signals (Thijssen & Bijkerk, 1988). The CDRAD software uses an algorithm that determines the positions of the visible holes in an image and then the position of a visible spot on a square. The algorithm has three stages, as shown below.

(1) Examination of the borders of the CDRAD phantom images

The border of the phantom image and the lead grid's outline is determined by the software by its recognising that a phantom is illuminated with a black background. The lead outline is analysed by a search algorithm and four phantom corners whose locations are illustrated in Figure 2.10.

(2) Identification of the centre square cells and visible spots of the CDRAD phantom image

The second step is to determine the four sides of each of the 255 square cells. The centre of each square cell is in the middle of the four sides which identify the centre of the visible spot in a cell. A peripheral visible spot is identified by the software via the four corners of the cell

through statistical computation based on an ideal observer model. The statistical computation involves the average maximum value (eccentric visible spot), which symbolises the object, and the mean pixel value of the four corners of a cell (Karssemeijer & Thijssen, 1996).

(3) Determination of the background and object signals

In this step, the object/visible spot and background signals are measured. Each square cell consists of two varied sites in the CDRAD image, shown by red and white spots, respectively. This can be seen in Figure 2.10. The background location depends on the white-spot location in the square cell and the four red and white regions of the background and image. This lowers the Hall effect. The red region has the average pixel value (μbackground) and the standard deviation of the background (σbackground). The same values are also calculated for the white region (μbackground, σbackground). The curve is obtained as a CD by the CDRAD software and is calculated from the phantom image through the interpolation scheme (Karssemeijer & Thijssen, 1996). The curve is obtained up to the 50% threshold of the correct response (Thijssen & Bijkerk, 1988).

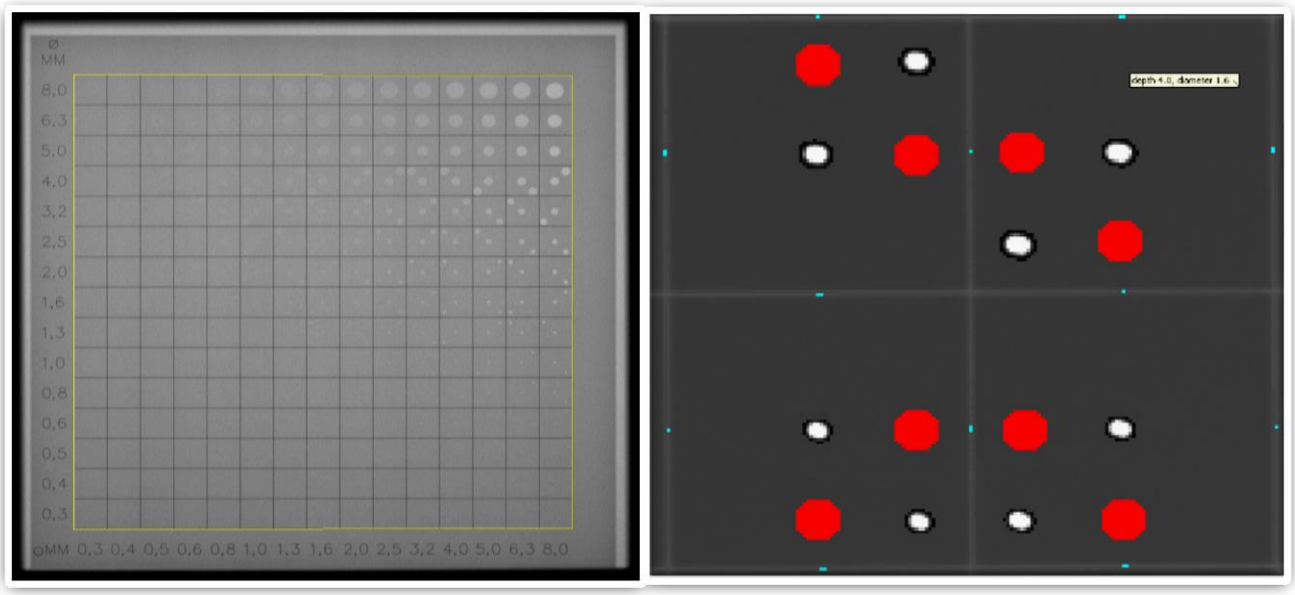

Figure 2.10: (a) Determination of the borders of the CDRAD 2.0 phantom images. (b) The background and visible spot signals are measured from two different locations in each square cell and are represented by the red and white regions, respectively (Burght et al., 2014).

Three sets of parameters in the software are considered before the analysis is conducted: the level of significance (alpha), difference in mean (APD) and source-to-image distance (SID).

Pascoal (2005) explained that the alpha-level statistical computation used in the phantom software has up to a 95% confidence level and a significance value ranging from 0 to 0.5 (Pascoal et al., 2005). He found that the significance of the alpha level on image quality assessment was equal to $1e^{-008}$. This was the value of the default CDRAD software that was proposed by Thijssen and Bijkerk (1988). The reason for this was to choose the best correlation of this value with the evaluated image quality (Pascoal et al., 2005; Spadavecchia et al., 2016; Brosi et al., 2011). An increase or decrease in the alpha value directly influences the image quality and results in an ascending or descending shift in CD. The CD detectability (IQF_{inv}) decreases with decreasing alpha value and increases as the alpha value increases. Thus, a low significance value and an increase in confidence level are correlated with the user image quality software used to analyse the detection details. A lower confidence level detects many details

due to a lower threshold value, which ultimately leads to higher-quality images (Norrman et al., 2005; Pascoal et al., 2005). Despite the different definitions of the term avalanche photodiode (APD), it is used as a scoring method for image bit depth and is set to 0 for various bit depths for valid comparisons between images (Brosi et al., 2011; Thijssen & Bijkerk, 1988).

2.12.3.6. Conclusion of physical image quality assessment

Most of the studies undertaken in medical imaging and practice, such as those by Ehman et al. (2017) and Pereira et al. (2016), have been related to clinical image quality estimation. Some of the studies, such as that of Matsumoto et al. (2015), showed that a meaningful method for evaluating clinical image quality is also a measurement of the importance of using the image for the intended diagnosis through ROC analysis or the multiple alternative forced choices (M-AFC) method.

Researchers like Zamani et al. (2016) have studied the correlations between image criteria-based approaches for the subjective visual assessment of radiographs. They also considered the measurement of physical image quality in chest and spine film screen-based radiography as well as in digitized pelvis and chest radiography. Their findings showed a significant correlation between blood vessel contrast and subjective evaluation in the case of the film screen-based chest-imaging platform. The correlation between the blood vessel SNR and its subjective assessment was found to be less considerable. Their study concluded that, in looking at film screen-based chest radiography in clinical image quality detection, one can expect to see a limited contrast compared to noise. In the case of film screen-based lumbar spine imaging, the predictors of clinical image quality have been found to be the contrast and SNR of the small soft-tissue cavities in the bone (Costa et al., 2018). Image quality is generally considered to be meaningfully defined only when the measurement is associated with the clinical purpose of the image and its estimation of the parameters (Chen et al., 2017). Thus,

according to the study conducted by Huang et al. (2018), the best alternative for evaluating image quality in the medical imaging department is measuring clinical performance through a quantitative method, such as ROC analysis.

As the physical imaging quality improves, the importance of radiological patterns becomes recognisable and the performance diagnostics improve subtly. Beyond a certain level of physical image quality, wherein all the associated components are visible, the radiologist is free to adjust the image saturation (Yu et al., 2017). Clinical performance does not necessarily improve the physical image quality, as the operational point becomes the saturated region of the curve. Jardini et al. (2016) also examined optimisation strategies for digital X-ray imaging. They found that digital imaging provides a new platform for optimising image contrast and image exposure and helped in suggesting imaging optimisation methods. These included: (1), the anatomical background during the optimisation; (2), performance at the constant effective dose; and (3), the separation of the image quality display stage from the image collection stage.

Alteration of digital images has been found to be easy, and thus the NPS and MTF parameters are not equally important. This is because they are associated with film-based imaging. They have been corroborated to express the imaging quality, and this corroboration has been dependent on the statistical decision theory (SDT). Within this, the image quality is assessed through the performance of the observer in a specified imaging task. Many of the studies that have been undertaken in this field have discussed the interconnection between human performance and the ideal observer performance (Huang et al., 2015). In addition to this, the computer and observer properties have been mostly focused on for detecting known signals embedded in noise. It has also been found that clinical image quality is a subjective judgement of the image quality of a fluoroscopic image or a radiograph. Impression-based assessment does not necessarily relate to its clinical usefulness, and its validity has been questioned many times by researchers and practitioners alike.

2.13 Chapter Summary

The research background chapter presented the different properties and consequences of general bed and X-ray table mattresses and of the materials used in radiolucent mattresses. It also discussed the potential for patients to develop pressure ulcers due to the use of poorly constructed X-ray table mattresses. The process of tissue breakdown and potential effects of pressure ulcers were also considered. Subsequently, the existing policies and guidelines for reducing pressure ulcers were analysed following a literature review. An overview of the radiographic literature on pressure ulcers was presented, together with radiation dose measurement methods and instruments. These two separate factors (pressure ulcers and radiation potential) were shown to be measured in image quality assessment when utilising X-ray table mattresses. The following chapter proposes a method of evaluating X-ray table mattresses and their requirements.

Chapter Three: Literature Review and Relevant Previous Studies

3.1 Overview

This chapter discusses how mattresses influence pressure ulcer development and the impact of radiolucent mattresses (X-ray trolley and X-ray table mattresses) on radiation dose and image quality. For this dissertation, the literature review is presented in a critical review format arranged into two sections.

3.2 Influence of X-Ray Table Mattresses on Pressure Ulcer Development

Earlier studies show the impact of the materials used in mattresses on pressure ulcer development. Their impact can be both positive and negative. Mattresses are also used as preventive intervention instruments in patient ancillary services, including radiology and radiotherapy (Messer et al., 2012). Nevertheless, it is not easy to compare the results of the previous studies as various kinds of mattresses were investigated. Furthermore, these studies used different methods, including the contact pressure profile, actigraphy, polysomnography and questionnaires (Messer et al., 2012; Bennett et al., 2017). As aforementioned, the literature (Park et al., 2015, Sardo et al., 2015, Carreau et al., 2015, Wang et al., 2014) has suggested that although conventional imaging methods are easy to carry out, using a risk assessment instrument, such as a questionnaire, would be beneficial. However, radiographers cannot precisely assess a patient's risk of developing a pressure ulcer using a pressure ulcer development risk assessment questionnaire owing to the limited time provided to each patient. This is due to their heavy workload. Moreover, radiographers must have expertise and training in formulating and administering risk assessment questionnaires so that they can be used an acceptable way – i.e., to adequately investigate a patient's risk of developing pressure ulcers.

Angmorterh et al.2018, used a calibrated Xsensor mat to measure the IP in the jeopardy areas (i.e. head, sacrum, and heels) in bodies of healthy control participants. The measurement was performed on an X-ray table with no mattress, a CT table surface, and an X-ray table with a thin radiolucent mattress. The patients were then asked to fill out a pain and comfort questionnaire. The study participants included 26 females and 23 males with ages ranging from 18 to 59 years. It was found that the mean IP for the head, heels and sacrum was statistically significantly differences across the three medical imaging table surfaces. It was also found that the head IP value was highest on the X-ray table with no mattress. Moreover, about 70% of the study participants felt uncomfortable on the X-ray table with no mattress and 67% reported the highest pain response in their head in this position, whilst 81% felt some pain in this position. It was concluded that an X-ray table with no mattress increases the risk of pressure ulcer development in radiology procedures.

3.2.1 Comparison of the Mattresses Used on X-Ray Tables and X-Ray Trolley Mattresses

NICE (2011) compared the thickness of an X-ray trolley mattress with that of an X-ray table mattress and highlighted the differences in their composition and X-ray attenuation coefficients. The standard X-ray table mattresses had 0.2 mm aluminium contents, while the X-ray trolley mattresses had 1.0 mm aluminium. This difference in composition affects the attenuation properties of mattresses, which would then directly influence the amount of radiation needed to produce an image. Siemens and Philips launched a new X-ray room to demonstrate the quality of their X-ray table mattress products for use in imaging procedures. Everton et al. (2014a) stated that radiological surfaces introduced to mattresses could also increase the radiation dose to which the patient is exposed. Furthermore, Everton concluded that X-ray tables without a mattress are inconvenient for patients because of their hard surfaces.

As far as image quality and radiation dose are concerned, however, an image taken using an X-ray table without a mattress is likely to be more beneficial for the patient's diagnosis than one with a mattress.

X-ray trolley mattresses tend to be synthesised to achieve standard conditions regarding material durability, infection control, tissue viability, and patient comfort. They are thicker than X-ray table mattresses and display a range of linear attenuation coefficients (Dawkins, 2012). According to Donnelly and Sawer (2014), the number of patients using X-ray trolley mattresses in England has increased over the last few years. This was also highlighted by the Welsh Society (WS; 2015) in Wales, wherein an 89-year-old patient waited for 34 hours on an X-ray trolley mattress in A & E. Pressure ulcers present more challenges to elderly patients, and this subpopulation is more vulnerable to ulceration and complications arising from this, including inflammation (Haleem et al., 2008).

3.2.2 NICE Experiments on Mattresses

The potential impact of the mattresses used in imaging on X-ray image quality and radiation dose was considered by NICE (2011). NICE evaluated the potential impact of Inditherm warming mattresses on radiation dose and image quality (Campbell, 2013). Comparative analyses were performed for a range of imaging mattresses - all of which were deemed to be low-attenuating, low-energy X-ray table mattresses and X-ray trolleys. Aluminium equivalence is often used as a measure within diagnostic radiography to specify the X-ray beam transmission or attenuation that occurs within objects. The aluminium thickness required to produce the mattresses' equivalent X-ray transmission was calculated to determine the potential radiation transmission capabilities of the Inditherm warming mattresses (i.e. its aluminium equivalence). NICE (2011) stated that through the aluminium equivalence

estimation, the low-attenuating X-ray table mattresses were found to have had a 0.2 mm aluminium equivalence while the X-ray trolley mattresses were found to have had 1 mm. The latter were much thicker than those that were used on X-ray tabletops.

NICE, however, failed to specify the exact models of the mattresses that were used in their study, as well as their types or thicknesses. Although NICE's report (2011) demonstrates significant differences in the aluminium equivalence of X-ray table mattresses and X-ray trolley mattresses, further information would have been valuable. Consequently, it is challenging to generalise their results, as there are a variety of mattresses used on X-ray tabletops and trolleys that are readily available in the market. Moreover, the aluminium equivalence of mattresses is not always specified, and as such, the comparative estimations based on the NICE guidelines cannot be easily compared. Meanwhile, NICE stated that the Inditherm mattresses do not adversely affect the quality of X-ray images or the radiation dose to which the patients are exposed. However, this was confirmed only by the inability of the new mattresses to change the clinical practice as there is no empirical evidence to support this view. Additionally, regarding the Inditherm mattresses, NICE also stated that no literature search on them has been conducted due to the belief that no beneficial information would be obtained. Therefore, the published evidence on image quality and on the radiation dose administered to patients in relation to the use of X-ray table mattresses remains questionable.

3.3 Pressure ulcers and radiography and radiotherapy

The aetiology, treatment and prevention of pressure ulcers has been analysed in different studies (Yap et al., 2013; Garcia-Fernandez et al., 2014a). Nevertheless, there have been few published materials regarding radiography patients' risk of developing pressure ulcers and the consequential procedures. A mere six studies have been found (Messer, 2012; Justham &

Rolfe, 2002; Brown, 2002; Justham & Rolfe, 2001; Howatson-Jones, 2001; Justham et al., 1996) through a literature search to directly or indirectly evaluate the risk of developing pressure ulcers, their prevalence rates, together with the assessment tools used in the radiotherapy procedures (Messer, 2012; Brown, 2002). Consequently, there is a literature gap on this topic. Therefore, the impact of medical imaging and radiotherapy surfaces on patients undergoing radiography/therapy procedures needs to be investigated (Ahmed et al., 2012).

Some studies have shown that the use of imaging and radiotherapy tables without a mattress can increase patients' chances of developing pressure ulcers. They can also have detrimental impacts on radiotherapy patients due to their long radiation exposure times (Hendrichova et al., 2010). In Hendrichova et al.'s (2010) study, patients could not find any cushioning to lie on during the imaging procedures, especially when thin radiolucent mattresses were used. In such situations, the patients' pressure ulcer predisposition may have reached dangerous levels, heightening the risk of tissue damage (Mcginnis & Stubbs, 2014; Moore & Cowman, 2013).

The results of the published studies (Brenner et al., 2011, Cordell et al. 1995) show that X-ray tables without a mattress pose intense IP risks. In clinical assessments of patients, it can be clearly observed that patients who lie for a long time on hard surfaces are exposed to severe IP risks. This is especially true when their head is exposed to the surface. Moreover, in the study conducted by Hendrichova et al. (2010), researchers obtained volunteers' perceptions of how comfortable X-ray tables without a mattress were by having them lie on them for certain periods of time. 70% of the study volunteers who were made to lie on X-ray tables without a mattress for 26 minutes perceived the table surfaces to be the least comfortable. They also experienced severe pain (Hendrichova et al., 2010).

3.4 Impact of Radiolucent X-Ray Table and Trolley Mattresses on Radiation Dose and Image Quality

The aim of this thesis was to investigate the different materials of mattresses and their impact on human body parts and their impact on pressure redistribution, image quality and radiation dose attenuation properties. It has been ascertained that there is a need for advanced methods of assessing pressure distribution in different parts of the body. Pressure distribution in the head, heels and sacrum should be assessed, and these body parts should be protected from pressure. Through the development of an advanced diagnostic imaging method, a wide range of the radiation attenuation characteristics of X-ray table mattresses can be easily assessed. All mattress manufacturing should aim to provide comfort to high-pressure body parts and to maintain the pressure balance on lower-pressure body parts without adversely affecting the X-ray image quality or increasing the radiation dose to which a patient will be exposed. The findings of the current study will be useful in the selection of a comfortable material for mattresses used in clinics and hospitals, wherein many at-risk people/patients are likely to be present.

In medical imaging, it has been seen that images can be produced with a low radiation dose depending on the design, radiography equipment and radiographer (Ahmed et al., 2012; Whitley et al., 2005). Furthermore, thin radiolucent mattresses can be used for diagnostic purposes (Ball et al., 2008). Image magnification can be minimised by keeping body parts near the image receptor through the use of thinner radiolucent mattresses (Beck, 2012; Razi et al., 2009).

Thin X-ray table mattresses are also known to minimise negative impacts on X-ray image quality (Chida et al., 2013; Brenner & Huda, 2008). To minimise the problems that may arise, patients are transferred onto tables prior to treatment procedures and patients who have severe

pressure ulcers are admitted to the hospital on trolleys that can be fixed onto modern pressure-relieving mattresses. These mattresses should be made in such a way that they minimise damage to body tissues through proper pressure distribution for contact surfaces. Thus, they would reduce the chance of pressure ulcer development (Makhsous et al., 2007). However, thin radiolucent mattresses are commonly used in hospitals, while hard carbon fibre X-ray tables without a mattress are used for diagnostic radiography procedures in some countries (Whitley et al., 2005). Nevertheless, none of the studies attempted to combine the optimisation of pressure distribution, image quality and radiation dose for X-ray table mattresses.

3.4 Chapter Summary

The literature review chapter showed that X-ray trolleys and table mattresses can have a significant impact on IP, radiation dose and image quality. All of these are important considerations for pressure ulcer prevention methods for patients undergoing radiology/radiotherapy procedures. In this chapter, relevant previous studies were compared, wherein different kinds of mattresses were investigated. The studies illustrated different methods including contact pressure profiles, actigraphy, polysomnography and questionnaires. Initially, X-ray table and trolley mattresses were compared based on the results of the different studies. The NICE recommendations and guidelines on mattresses and their experiments on mattresses suggested how different mattress types affect X-ray image quality and the radiation dose administered to patients. Then, pressure ulcers were analysed through different studies, wherein the risks of pressure ulcers for patients who needed to undergo radiography and the consequential procedures were discussed. It was found through the literature review that X-ray tables without a mattress pose intense IP risks. Following this, studies concerning the impact of radiolucent X-ray tables and trolley mattresses on radiation dose and image quality were

investigated. The aim was to investigate the different materials of mattresses and their impact on the human body parts. Considering the pressure contact areas in several body positions, the pressure distribution in the body and the X-ray image quality outcome, there appears to be a need to introduce advanced methods of assessing pressure distribution in different parts of the body. Pressure distribution in the head, heels and sacrum should be assessed, and these body parts should be protected from pressure. Previous relevant studies showed that thin mattresses minimise the negative impact on image quality. The reproducibility of patient body posture and treatment planning were shown to be the main requirements for effective radiotherapy/radiography. In conclusion, none of the previous relevant studies attempted to combine the optimisation of pressure distribution, image quality and radiation dose for X-ray table mattresses.

Chapter Four: Methods

4.1. Overview

This chapter will develop and validate a method to measure and assess the range of requirements that X-ray mattresses should meet. These requirements include pressure redistribution, X-ray transmission/attenuation and image uniformity/low-contrast detail detection. A pilot study was conducted to assess the feasibility of this method.

Thomas (1997) claimed that the sacrum, coccyx, and heels (when a person is in the supine position) are the most common locations wherein tissue breakdown occurs. This thesis therefore performed a pressure analysis to assess the pressure redistribution properties of X-ray mattresses by evaluating the average and peak interface pressures for the three most common areas for pressure ulcers (PUs): the head, the sacrum, and the heels. Radiation attenuation was calculated to assess the overall efficiency of the mattresses across a range of X-ray energies (Kilovoltage peaks (kVps)) that are typically used in diagnostic imaging. Finally, the impact of each mattress on IQ was evaluated. This evaluation involved assessing IQ by analysing the results from the CDRAD 2.0 (Artinis Medical Systems, Elnst, Netherlands), which is used for conventional radiography.

XSensor technology (SUMED International UK, 2014) was used in this thesis to measure the pressure distribution of the most common PU jeopardy areas. XSensor is a pressure imaging device that is routinely used for assessing interface pressure between mattresses/seat cushions and those lying/sitting on them. To improve the experimental consistency of the interface pressure evaluation when comparing X-ray mattresses, a three-dimensional (3D) anthropomorphic phantom was created using a 3D printer. The phantom was based on computed tomography (CT) image data of a human anthropomorphic phantom. Using the

phantom negated the need for human participants and controlled the ‘input’, i.e. there was no variability in the object being used to test the mattresses.

To determine the mattresses’ impact on radiation attenuation, this thesis developed a dosimetry experiment to measure the kVp and mAs (milliampere per second) values based on clinical protocols. An experiment was also conducted to assess the impact a mattress may have on IQ by performing an IQ assessment using a CDRAD 2.0 phantom and slabs of polymethyl methacrylate (PMMA) (Burger and Burge, 2016). Image analysis was conducted using the CDRAD 2.0’s accompanying software.

A detailed description of the method is provided below and in figure 4.1, alongside a justification for achieving the aims and objectives of the thesis. Figure 4.1 illustrates an overview and validation of the method and the development of the phantom.

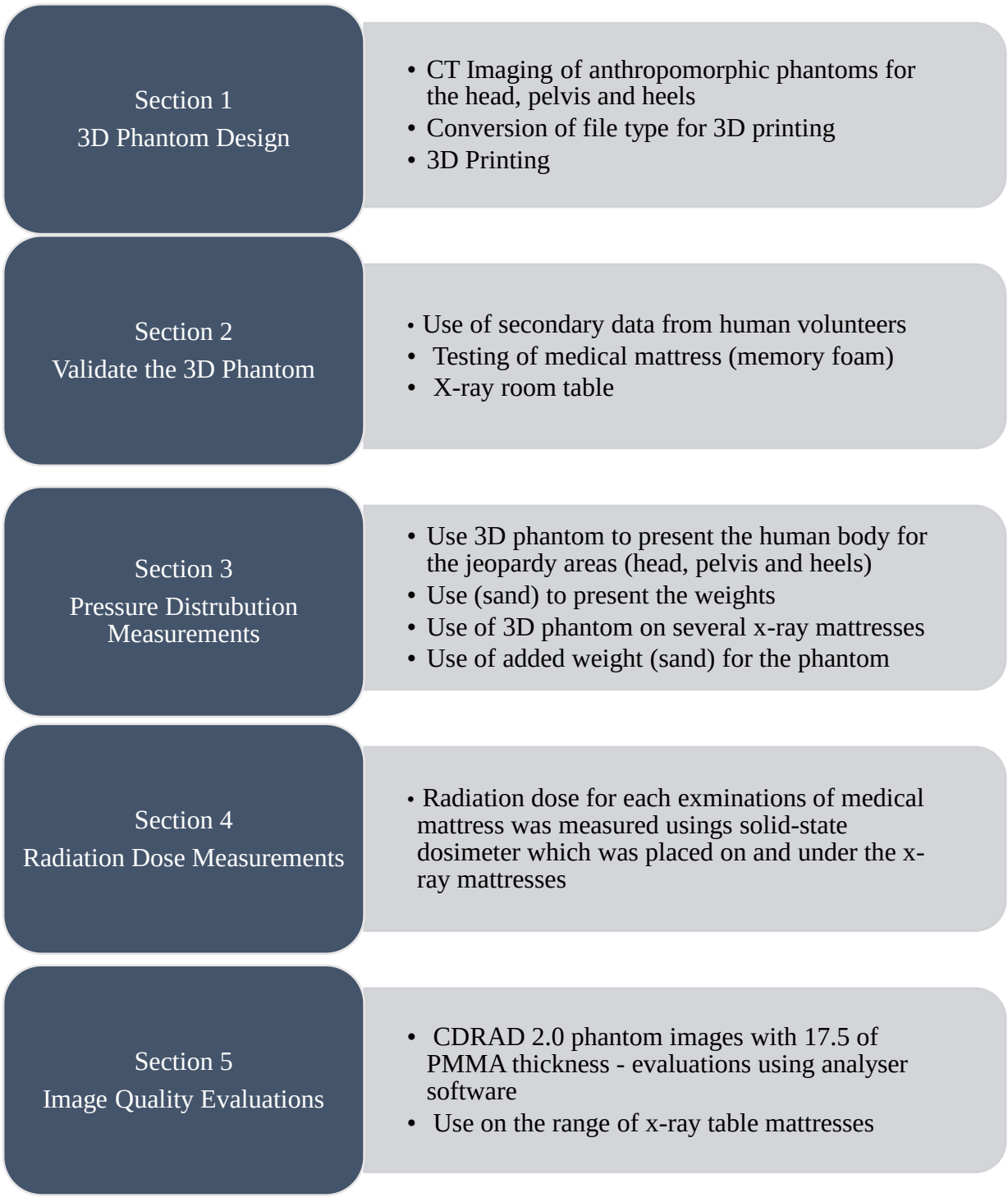

Figure 4.1: Flowchart of the methodology.

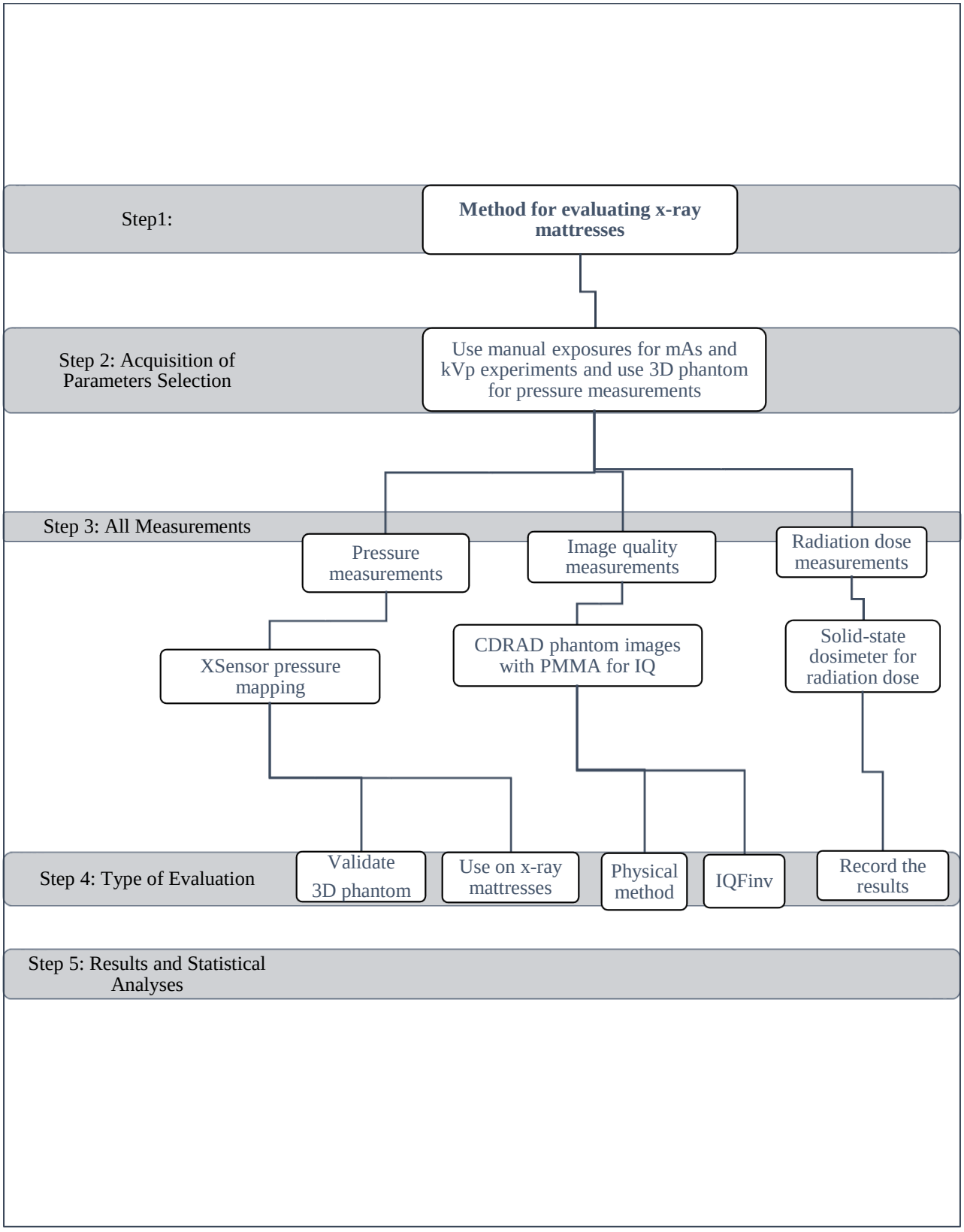

Figure 4.2: Methods used to evaluate the various X-ray mattresses.

4.2. Pressure redistribution

To assess the risk of PU formation, the pressure redistribution of the mattresses was considered at the pressure ‘jeopardy areas’ - the head, the sacrum, and the heels (Angmorterh, 2016). To perform the measurements, a 3D phantom which could represent different weights (from light to heavy) was created and its reliability for pressure imaging was tested. Finally, X-ray mattresses of different ages and thicknesses were assessed and evaluated to compare newer mattresses with those used in clinical practice.

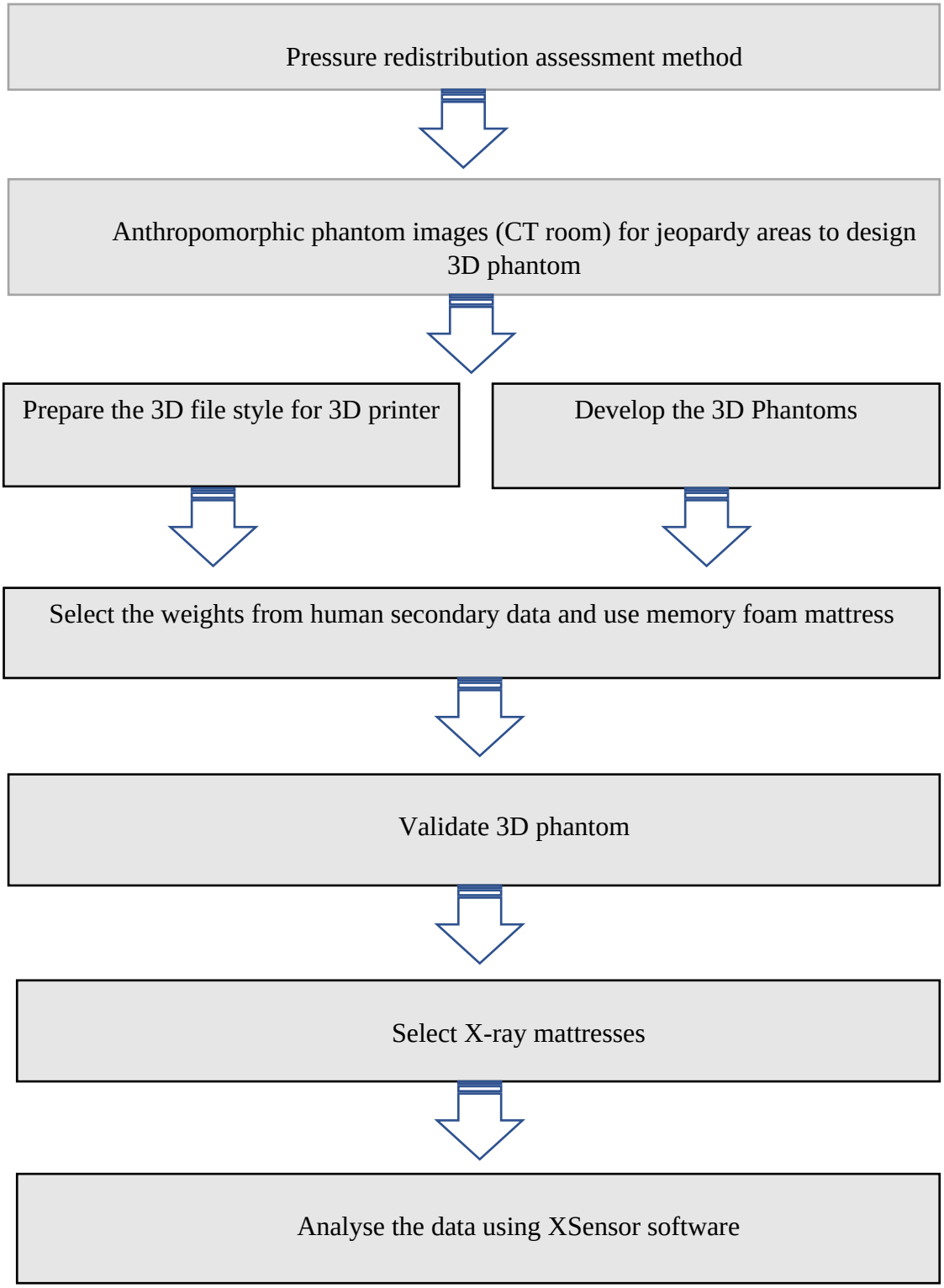

Figure 4.3*:* Method of pressure redistribution.

4.3. 3D Phantom Development

4.3.1. Rationale for using a physical 3D human anthropomorphic phantom

The reason for developing a 3D phantom rather than using humans in this thesis was to provide an objective and highly repeatable test. This cannot be achieved using humans. An objective and highly repeatable test were necessary to enable consistent testing for the evaluation of a range of mattresses. The use of a 3D phantom also enabled a range of weights to be added or subtracted to reflect a range of human weights.

4.3.2. Anthropomorphic X-ray phantom

Anthropomorphic phantoms are used in medical imaging and radiation therapy research as an alternative to using humans. Using humans can be unethical or even dangerous. In the context of medical imaging, these phantoms can be used to estimate doses administered to humans by proxy and to estimate IQ in radiography procedures. They can represent a range of human body parts and are constructed from tissue-equivalent materials with representative anatomical shapes. Their properties, such as density and attenuation coefficients, are comparable to human tissue. Thus, when imaged using X-ray techniques, their radiographic appearance can be similar to humans. Figure 4.5A shows examples of commercially available anthropomorphic X-ray phantoms (Martin et al., 2007). Commercially available X-ray phantoms can come in different statures, genders and ages (e.g. baby to adult).

The phantom development method is presented in two phases. Phase 1 outlines the development of the phantom and Phase 2 describes the steps taken to validate the phantom, which includes how the phantom pressure data were analysed and presented.

4.3.3. Rationale for selecting the Jeopardy Areas

The jeopardy areas are the common sites for PU development. Thomas (1997) claimed that this was the head, sacrum, coccyx, heels in the supine position, the hip and ankles when a person lies on their side, and the buttocks when a person is seated.

4.3.4. Phase 1: Phantom development

3D printing is a form of technology that produces physical models created from 3D computer images. This has been advanced to a point wherein 3D human datasets from CT and MRI scans can be printed using commercially available 3D printers. Figure 4.4 outlines the process adopted to create 3D prints from CT images of human anthropomorphic phantoms.

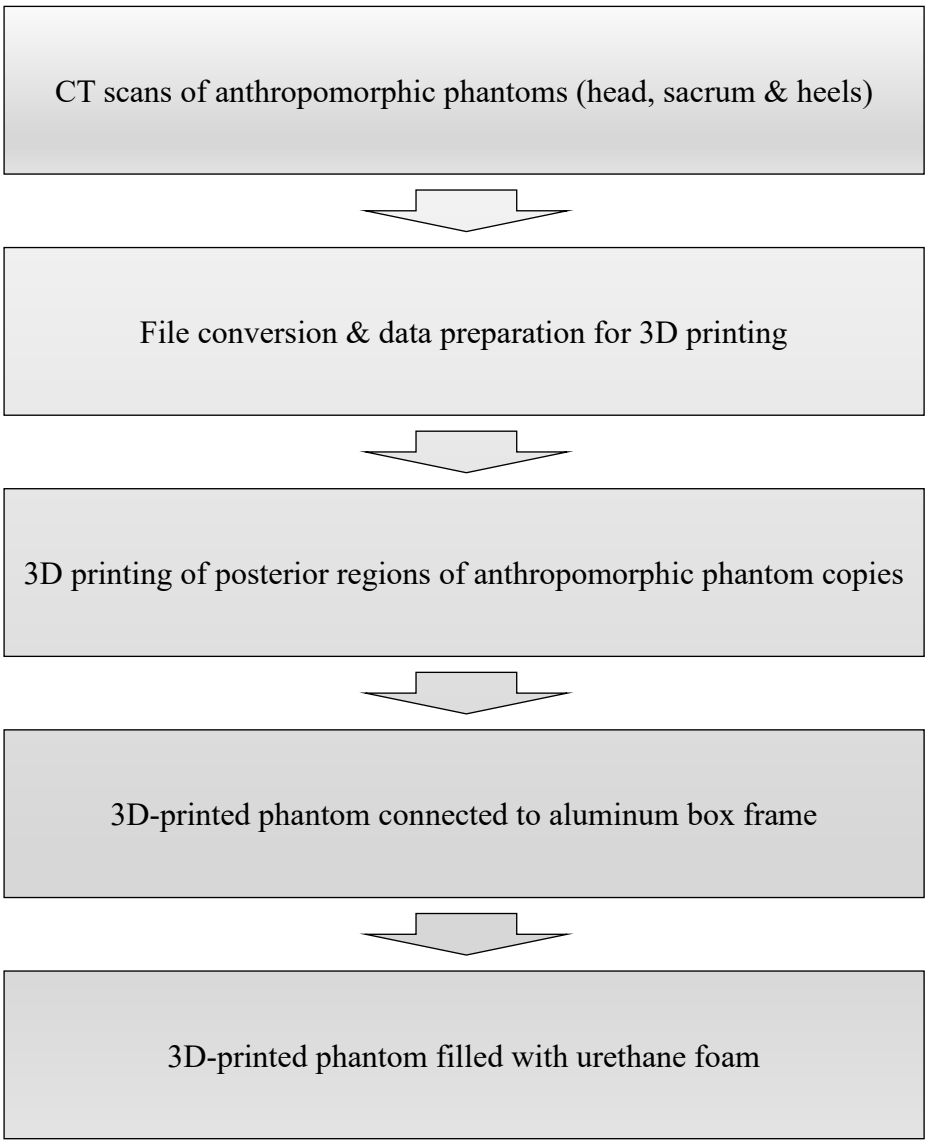

Figure 4.4: Flowchart displaying the development of the phantom.

4.3.4.1. Images of an anthropomorphic phantom in a CT scanner

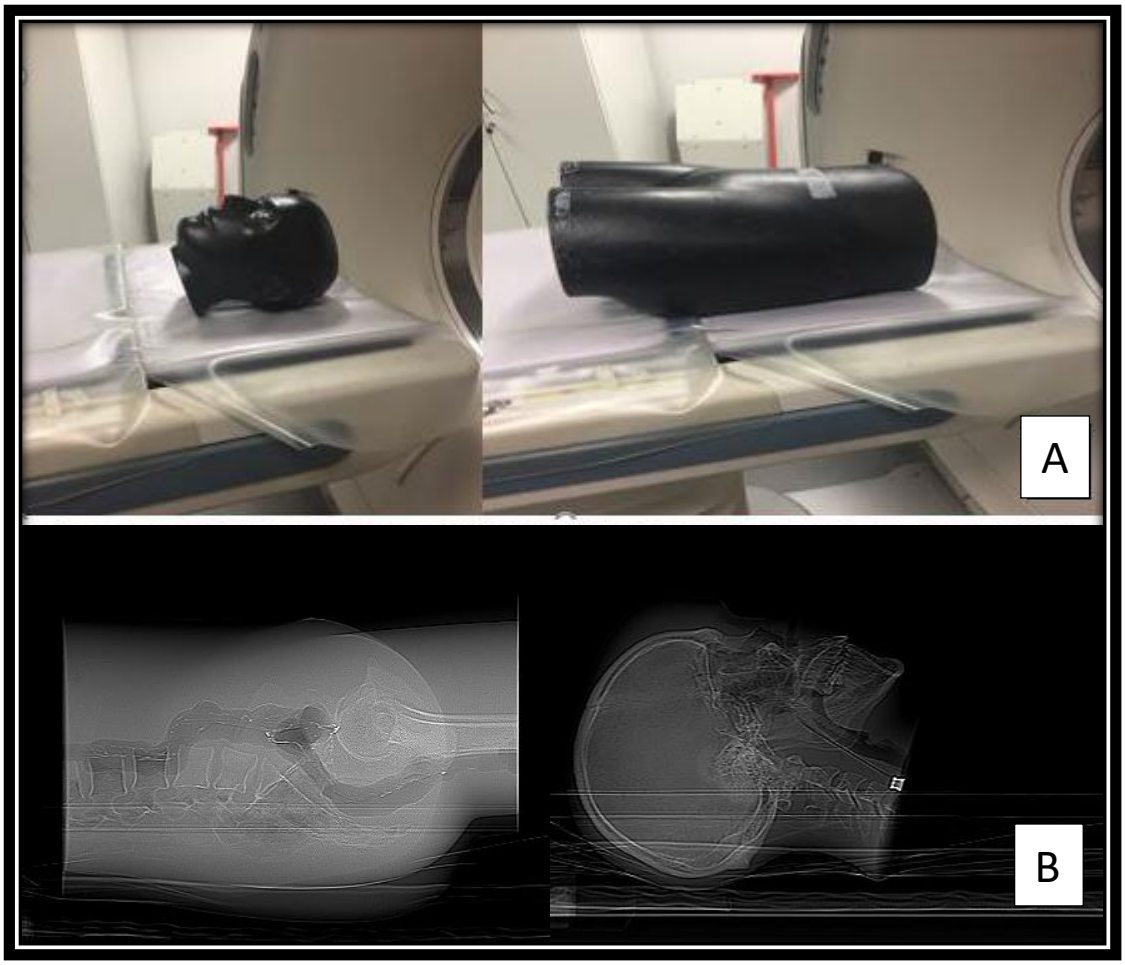

Figure 4.5: (A) Head and pelvis anthropomorphic phantoms used to acquire CT image data; (B) example CT images.

4.3.4.2. Steps taken to convert DICOM image data to an STL format for 3D printing

As shown in Figure 4.4, the process of creating a physical phantom using 3D printing involves several steps. In the first stage, several radiographic images of the anthropomorphic phantom need to be transformed into a standard surface description language (STL) format, before being loaded into the ReplicatorG software program (http://replicat.org/).

Stage 1: **Export CT images of anthropomorphic phantoms using DICOM format**

The anthropomorphic phantom (Rando SK250 sectional lower torso, SK150 head and heels)

was positioned on the CT table in the supine position and the CT images taken were exported using the DICOM format. The commercially available anthropomorphic X-ray phantoms (see Figure 4.5A) were positioned in the CT unit (Toshiba Medical Systems, Tokyo, Japan), which passed relevant quality performance tests before being used for imaging (Institute of Physics and Engineering in Medicine [IPEM] Report number 91; ICRP, 2007; Toshiba, 2014). CT data were captured using the following acquisition settings: 0 gantry tilt, 5 mm slice thickness, 1.5 pitch, field of view (FOV) ¼ 20.8 cm, grid 512x512, 120 kVp and 100/150 mA. Overall, 58 images with 5-mm thickness were acquired and saved using the DICOM file format. Figure 4.5B shows some example images of the acquired data. For 3D printer models, a radiologic image needs be changed into the STL arrangement to be uploaded to the ReplicatorG software to print. Image data were then always exported in the DICOM format.

Stage 2: **Convert DICOM files to an NRRD file using slicer software**.

In this step, the DICOM file was converted to an NRRD file using slicer software (https://www.slicer.org/) (version 4.1.1). This is a free, downloadable software platform that can be used to store image data for printing using a process known as segmentation. The segmented volume is changed to an NRRD and STL file format by utilising the default settings in ModelMaker, a specific module within the software.

Stage 3: **File conversion ready for 3D printing**.

The third stage consisted of uploading the NRRD file to the embodi3D.com website to convert the NRRD file to an STL file format. The files were then saved onto a USB or hard drive ready for uploading to a 3D printer. Appendix 2 provides detailed information about the file conversion.

Stage 4: Printing the 3D Models.

The STL data were processed using MeshLab (version 1.2.3-64) to correct any 3D surface anomalies. This software is also freely available as a download (http://meshlab.sourceforge.net). Four anthropomorphic phantoms for the head, pelvis, left heel and right heel were printed.

The 3D printer used for the larger prints (i.e. the pelvis and head) was the BigRep One (https://bigrep.com/bigrep-one/) and the printing material was MonsterFil 2.85 mm PLA in 2.26 kg spools (e.g. https://monsterfil.com/monsterfil-red-2-85mm-5-lbs-2-26-kg.html). The print files were prepared using the Simplify3D slicing software (https://www.simplify3d.com/). The 3D printer used for the smaller prints (the heels) was an Ultimaker 2 (https://ultimaker.com/3d-printers/ultimaker-2-plus) and the software used to prepare the files was Ultimaker Cura (https://ultimaker.com/software/ultimaker-cura).

4.3.4.3. Joining the 3D phantom together

Once printed, the four printed components were linked together to represent the human body (Figure 4.7A). To join the components together, a custom-made aluminium frame box, 25 mm x 25 mm x 1.5 mm and 175 cm long (the average height of a human), was used. The aluminium box was fixed together by plastic connectors to maintain rigidity, while the plastic connectors for the knee and elbow positions allowed the structure to bend to simulate potential human limb motion. This flexibility in the frame enabled the jeopardy areas of the head, sacrum, and heel areas to sink into the mattress when weight was added. Finally, urethane foam was used to fill the four 3D-printed components to give them adequate rigidity and to make them strong enough to withstand the weight applied during the experiments. Once assembled (see Figure 4.7B), the phantom could be placed on an X-ray table/mattress and different amounts of kiln-dried sand could be added to it to represent a range of human weights.

Figure 4.6: The XSensor Px100 system fixed on the X-ray table.

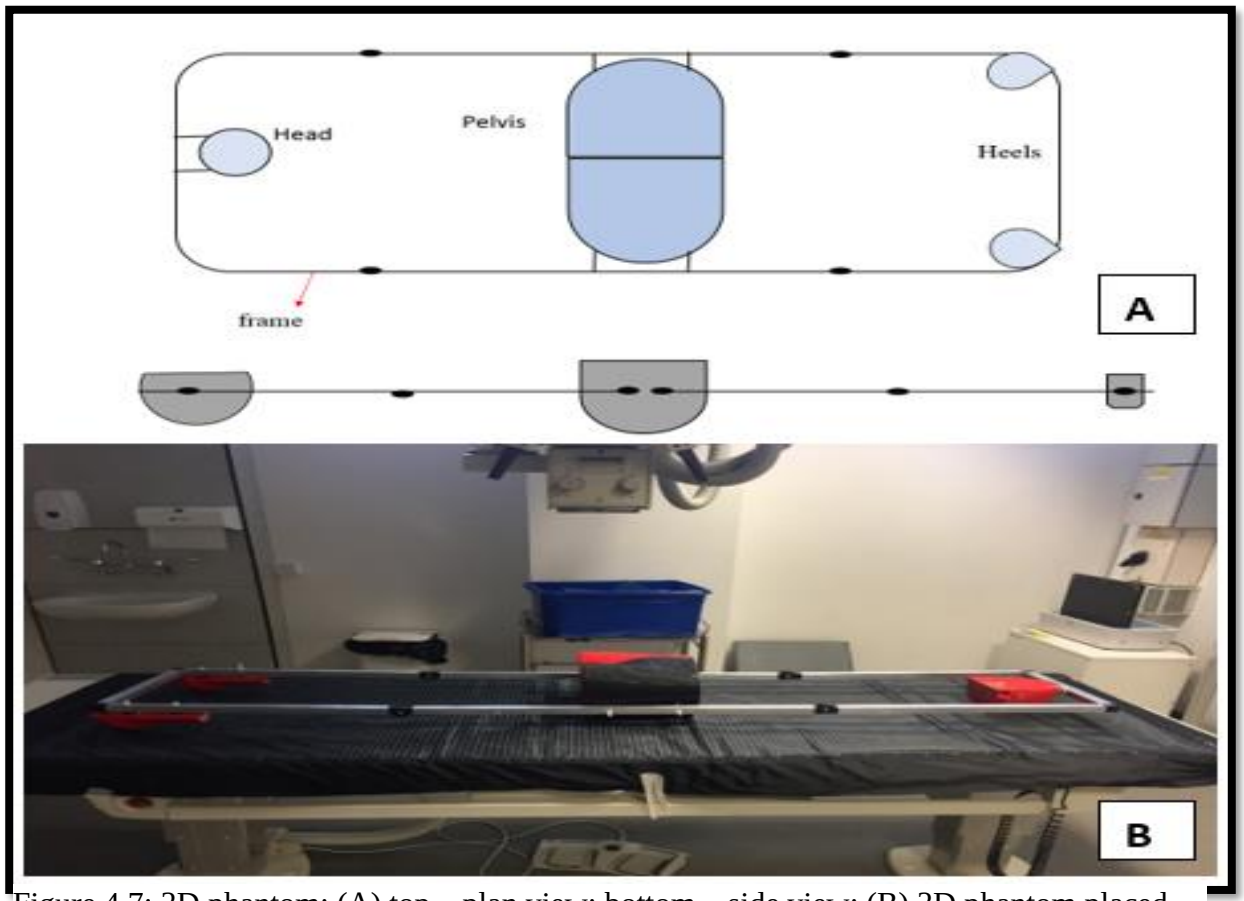

Figure 4.7: 3D phantom: (A) top – plan view; bottom – side view; (B) 3D phantom placed on an XSensor Px100 on an X-ray table mattress.

4.3.4.4. XSensor pressure imaging system

To obtain the interface pressure measurements of the 3D model phantoms, the XSensor pressure imaging system devised by Sumed International was utilised. This system is used in the pressure imaging of humans in clinical (Peterson et al., 2013) and academic studies (Trewartha and Stiller, 2011). According to Fader et al. (2004), XSensor pressure imaging systems are the most common technology used for human pressure imaging. The performance characteristics, which include precision and reliability, are defined in the literature provided with the product. This includes the pre-sales process, the manufacturer's calibration, and quality control (QC) data. QC and calibration should be carried out by the manufacturer every five years to maintain precision and reliability levels (Fader et al., 2004).

According to Sumed UK (2014), the XSensor pressure imaging system is flexible. In this thesis, the sensing area was 61 cm x 183 cm, with a 12.7 mm resolution of 6,912 sensing points. The pressure ranges were 5-50 mmHg and 10-200 mm/Hg, with a rate of accuracy of ±10 per cent for the calibrated values (Figure 4.6).

In its analysis, the individual pressure measurements are transmitted from the XSensor as a series of sensor values to a computer (Peterson et al., 2013). The XSensor is not the only technology that can be used for pressure mapping, although compared to other systems, such as Tekscan's F-Scan or Force Sensing Array (FSA), the XSensor is considered to be better and is also the industry standard (Mitchell et al., 2005). For example, in a comparison test against the other two systems, the XSensor was shown to be more accurate at measuring curved surfaces. Mitchell et al. (2005) showed that the radius of the curvature of anatomical areas is less affected by the XSensor. This helped in acting as a baseline experiment using the XSensor for this thesis. This is important, as this thesis aims to better understand IP values for body areas that consist of prominent bony structures and large curvatures (i.e. the head, sacrum and

heels). Mitchell et al. (2005) also showed that the XSensor has a higher level of accuracy, particularly for low-pressure readings, as it has more sensitive capacitance sensors.

4.3.3.5 Data Storage and data integrity/security

The XSensor has an in-built memory card for storing pressure measurements. The data were moved to a university hard drive, which was backed up and free from any computer viruses. The data were also stored on the researcher's computer and external hard drive as a backup.

The Xsensor pressure imaging system was used to obtain the measurement of interface pressure which occurred through the interaction of the mattress surface and the common pressure areas on the phantom. Sensors in a pressure mat (Figure 4.7B) interfaced with a computer provided a digital profile or map of the interface pressure.

To establish the weight of the sand required for the phantom to simulate a range of human weights, this thesis used data obtained from 27 human volunteers (Webb, 2018) . The average height of the participants was 164.63 cm (SD = 7.64), their average body mass index (BMI) was 28.18 (SD = 6.75), and their average weight was 77 kg (SD = 22.18), ranging from 50 kg to 148 kg. The 27 volunteers, comprising 24 females and 3 males, were grouped into five weight categories: maximum (148 kg), third quartile (84 kg), mean (76 kg), first quartile (64 kg) and minimum (50 kg).

To represent these five categories, the average weights for each category were calculated from the XSensor data to determine the amount of sand that needed to be added to the phantoms (Section 5.2.1.1, Page 132).

4.3.5. Phase 2: Application of XSensor technology and validation of phantom

For the pelvis, heels and head, the Peak Pressure Index (PPI) and interface pressure profiles were compared between the 3D phantom and a human volunteer body (Webb, 2018). The same mattress was used for the interface pressure data collection in both cases (Woodford, 2018).

XSensor technology was used to record the interface pressure readings of the mattress (Figure 8B). To minimise measurement error, the data for a human body should be acquired over 20 minutes, followed by a settling time of six minutes (Bader and Hawken 1986; Al-Eisa et al., 2000). As the 3D phantom does not contain soft tissue materials, only three minutes of settling time were required to achieve stabilised pressure readings and 15 minutes of data collection. A range of human equivalent weights were added to the phantom at the head, pelvis, and heels to minimise random error. The interface pressure measurements for each weight were taken three times, and the mean values were determined.

Before conducting the experiments with the phantoms, a QC step was implemented to determine whether weights placed on one body part had an impact on the XSensor interface pressure reading of another body part. That is, whether the weight placed on the pelvis impacted the readings taken at the heels and head. It was essential to ensure that this did not occur, as the weights added to the pelvis, head and heels had been calculated to mimic those that would be expected for each respective weight group. The QC experiment involved placing the maximum sand weights on the head, pelvis and heels one region at a time to determine whether a change in interface pressure at the other locations would occur (see Figures 4.8A, 4.8B and Table 3). The percentage difference in the weights was calculated using the following equation:

$$\text{Percentage difference} = \frac{V1 - V2}{\left\{\frac{V1 + V2}{2}\right\}} * 100 \qquad (6)$$

where V1 is the PPI without the weight, and V2 is the PPI after the weight was applied.

The results show that the percentage differences varied from 1.3% to 5.8%. The weight transference was quite small, suggesting minor errors were imposed.

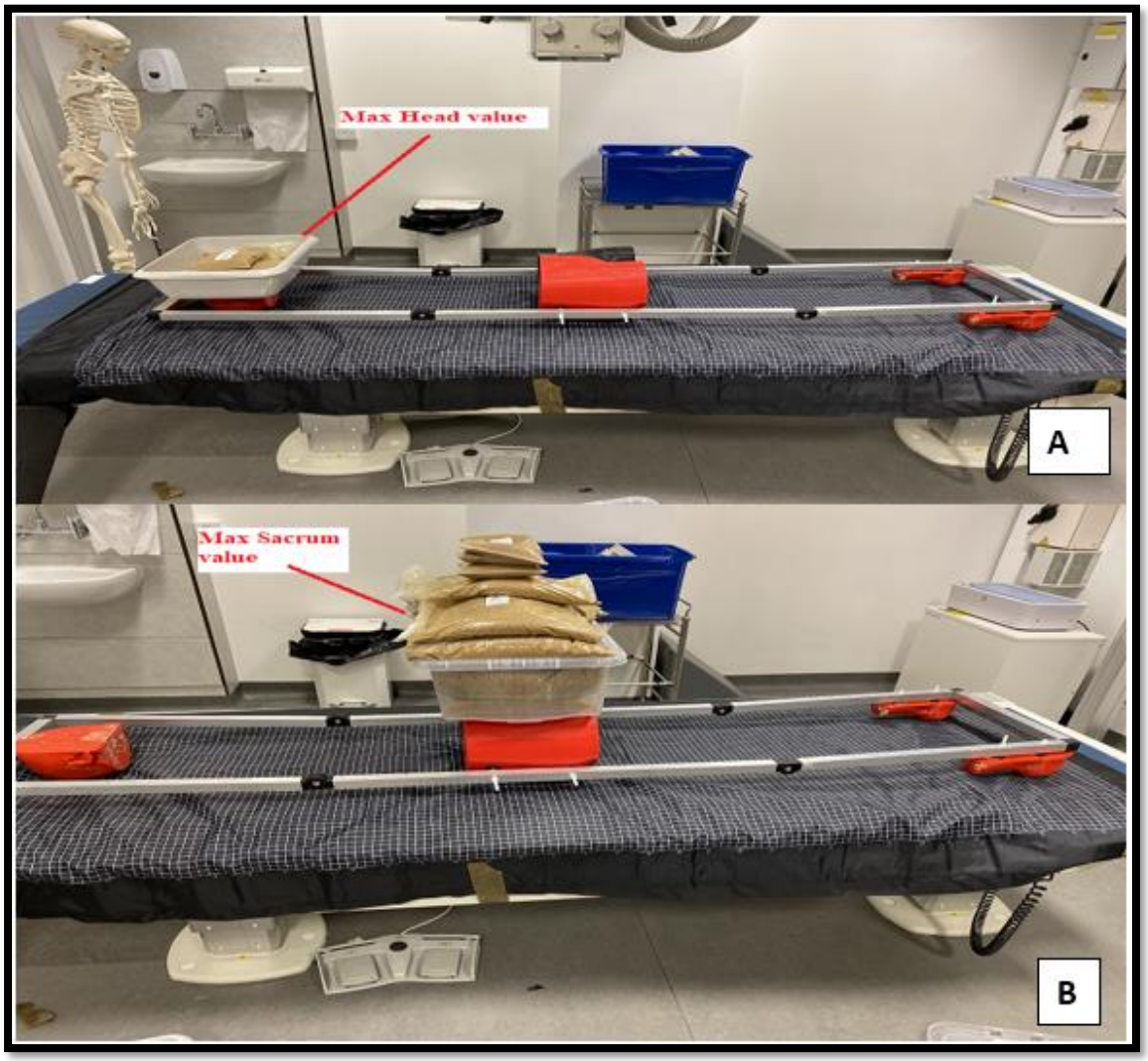

Figure 4.8: Maximum weight on the head (A) and maximum weight on the pelvis (B).

4.3.4.1 X-ray table surfaces and X-ray mattresses

Radiology departments use many types of X-ray tables, such as the Arco TN 0055 X-ray table. The tables and accessories, such as the mattresses, are often manufactured and supplied by different companies. In some instances, one company may manufacture the equipment while another company supplies the accessories for that piece of equipment.

Currently, radiographic procedures are conducted mainly on two table configurations: an X-ray table with a thin, radiolucent mattress, or an X-ray table with no mattress (such as the ones used in radiotherapy) (Whitley et al., 2005; Groheux et al., 2009; Suthar et al., 2015; Hawkes, 2015).

Advances in imaging equipment design have given rise to scanning modalities, such as Positron Emission Tomography CT (PET-CT) and Magnetic Resonance Imaging (MRI), which tend to have narrow, curved imaging surfaces for patients to lie on, as shown in Figure 4.9. Consequently, to understand the interface pressure on modern imaging and radiotherapy surfaces, it was important to use the latest pressure mapping equipment and/or technology. This helped to investigate the interface pressure on imaging and radiotherapy planning and treatment surfaces that are currently in use and provided an up-to-date objective measure of the interface pressure values on radiography and radiotherapy table surfaces.

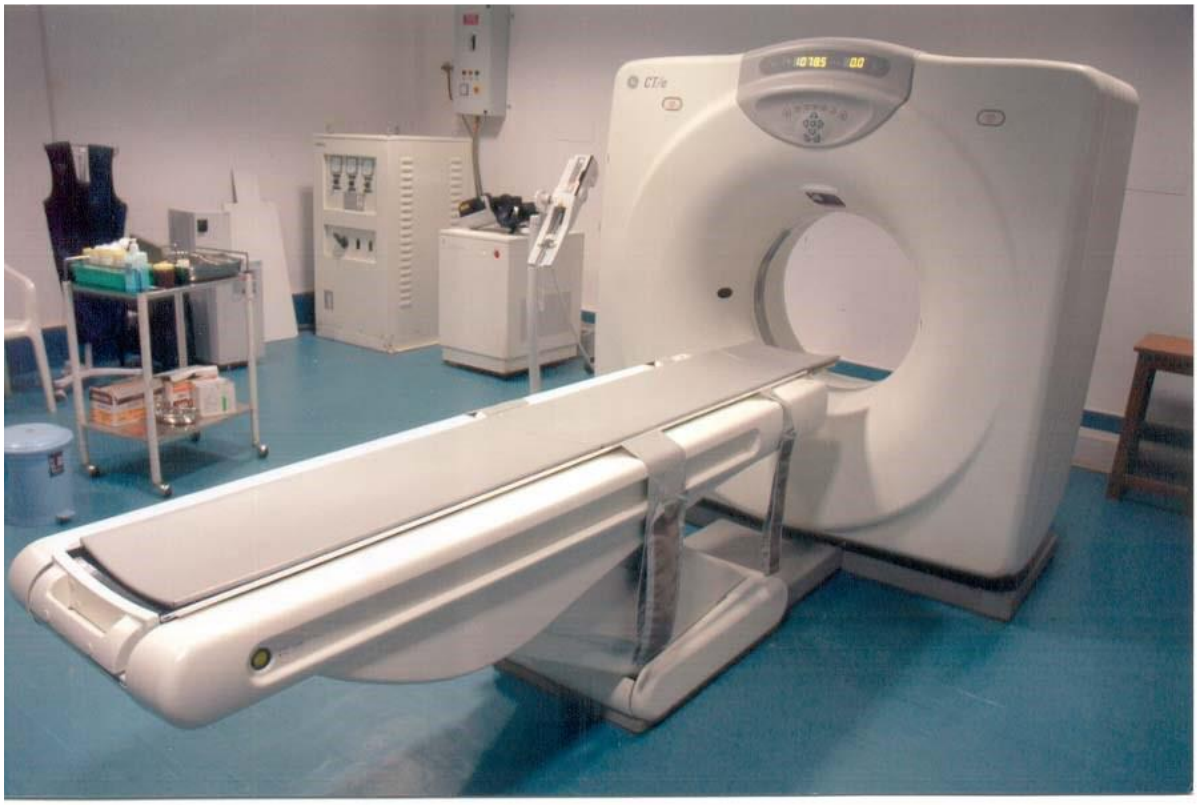

Figure 4.9: CT machine with a narrow, curved surface and a thin mattress.

This thesis used an Arco TN 0055 X-ray table with a thin radiolucent mattress (Figure 4.10), and an Arco TN 0055 X-ray table with no mattress (a hard surface such as those used in radiotherapy planning and treatment). The table is made from industrial-grade Rohacell carbon fibre, while its top is hard because it is made from closed rigid foam based polymethacrylimide (PMI) with 0.9 mm aluminium equivalence. The thin mattress is formed by the combustion polyurethane modified cellular foam. This type of X-ray table can cause medical device related (MDR) PUs (EPUAP et al., 2014). The tabletop has a weight limit of 250 kg and is 240 cm long, 85.3 cm wide, and 2.15 cm thick.

X-ray table mattresses are supplied by equipment manufacturers or sold separately by companies, such as WSR Medical Solutions Limited under the tradename of Rothband. Often, X-ray mattresses used in clinical practice are not accompanied by manufacturer information,

which was the case here. These X-ray table mattresses were purchased in 2009 and were offered by the X-ray equipment manufacturer at the point of sale. They are typical X-ray table mattresses for X-ray departments and are often used over long periods. Figure 4.10 shows the Arco TN 0055 X-ray table used in this thesis.

Figure 4.10: An Arco TN 0055 X-ray table with mattress.

4.3.4.2. Comparison of the pressure distribution 'shape' of a human and the 3D phantom

To verify the validity of the method, the pressure imprint shape of a human body was compared with that of the 3D phantom. The 3D design needed to be close to the shape of the patient's body to facilitate relevant results.

To compare the shapes, ImageJ software (ImageJ, 2014) was used. This is widely available and easily portable as an open-source image processing tool (Desai et al. (2010). It is often used for similar calculations, as shown by the National Institute of Health, Bethesda, MD. Sun et al. (2012) stated that ImageJ software establishes the mean pixel values of the region of interest (ROI) (i.e. signal) and the standard deviation (i.e. noise). Moreover, ImageJ provides a set of ready-made tools for the interactive manipulation and viewing of images in a tool called Line Profile, which is used to measure a range of pixels in a selected area on a line. This thesis used Line Profile to compare the line profile shape between a human volunteer and the 3D phantom for the three jeopardy areas: head, pelvis, and heels.

4.3.6. Pressure line profiles

To compare the interface pressure map images for a phantom and a human, profile lines (20 pixels wide) were created across the widest point of the head, pelvis and heels using ImageJ software (National Institute of Health, Maryland) for the five respective weight groups. Because the width of the profile lines differed between the phantom and the human, the data were dispersed, and linear interpolations were applied to enable easier visual comparison between samples with different widths (Section 5.2.2.1, Page 134).

4.3.4.3. Interface Pressure Ratio (IPR)

Using the 3D phantom and data obtained from the XSensor technology, a novel IPR was developed to indicate a mattress's interface pressure redistribution efficiency. The IPR served as a simple indicator to compare the pressure redistribution efficiency between different mattresses or in the same mattress over time. The IPR used phantom PPIs from the head, sacrum, and heels to compare the table with a mattress (experimental condition) to the table

with no mattress (control condition). This calculation was repeated for all five phantom weights so that for each mattress there were five IPR values for the head, pelvis and heels (where one average value for both heels was used). The formula for the IPR is as follows:

$$\frac{PPI\ when\ Mattress\ is\ used}{PPI\ for\ no\ mattress}$$

The IPR ranges between 0 and 1, wherein 1 implies that the mattress has the same interface pressure distribution properties as a hard surface (i.e. an X-ray table). As the ratio approaches 0, the IPR properties of the mattress are said to improve. To illustrate its use, Table 4.1 shows IPRs from a 15-year-old X-ray table mattress in current clinical use. For the five weight categories, the IPR indicates that the mattress IPR properties are similar to that of the X-ray table (i.e. approaching 1, which is very poor).

Table 4.1: IPR of a 15-year-old X-Ray Table Mattress and Corresponding PPIs for the Five Weight Categories

Weight category	**Peak Pressure Index (mmHg)**			**Interface Pressure Ratio**		
	Head	**Pelvis**	**Heels**	**Head**	**Pelvis**	**Heels**
Maximum (148 kg)	88.5	110.7	97.3	0.93	0.85	0.95
Third quartile (84 kg)	68.9	93.4	78.1	0.92	0.78	0.90
Mean (76 kg)	60.6	79.2	70.2	0.85	0.78	0.86
First quartile (64 kg)	55.4	62.5	53.9	0.84	0.70	0.94
Minimum (50 kg)	50.1	47.5	35.1	0.83	0.93	0.92

4.4. Method for Pressure Redistribution Assessment

4.4.1. Calculating and analysing the PPI

4.4.1.1. PPI

The PPI is the mean of the highest-pressure values within an area of 10-12 cm² (Davis and Sprigle, 2010; Hemmes et al., 2014a). According to Davis and Sprigle (2010), the number of data cells included in calculating the PPI depends on the spatial resolution of the pressure mat. Studies have shown that this area (10-12 cm²) is equivalent to a nine-cell matrix when using the XSensor pressure mat. PPI was used because it is a reliable parameter of predicting PU risks (Davis and Sprigle, 2010; Hemmes et al., 2014a). The values from the XSensor X3 medical software were inputted into SPSS version 22 (IBM Corp, Armonk, NY) for analysis.

The PPI data, recorded in mmHg and saved in the XSensor system, were transferred to a laptop for analysis using the XSensor software. The data were merged using the average peak pressures for all frames, and the ROIs were placed around the heels, the sacrum, and the head to calculate the highest PPI in the middle of the nine cells for each region. Once this was done, the mean of the three data PPIs collected for the jeopardy areas were calculated for each region (e.g. Everton et al., 2014).

4.4.1.2. The XSensor pressure imaging system

The XSensor pressure imaging system (supplied by Sumed International) was used to obtain the interface pressure measurements from the 3D phantom. The XSensor has been used to analyse PUs for individuals in clinical (Peterson et al., 2013) and academic settings (Trewartha and Stiller, 2011) (Figure 4.11).as mentioned in Section 4.3.4.4.

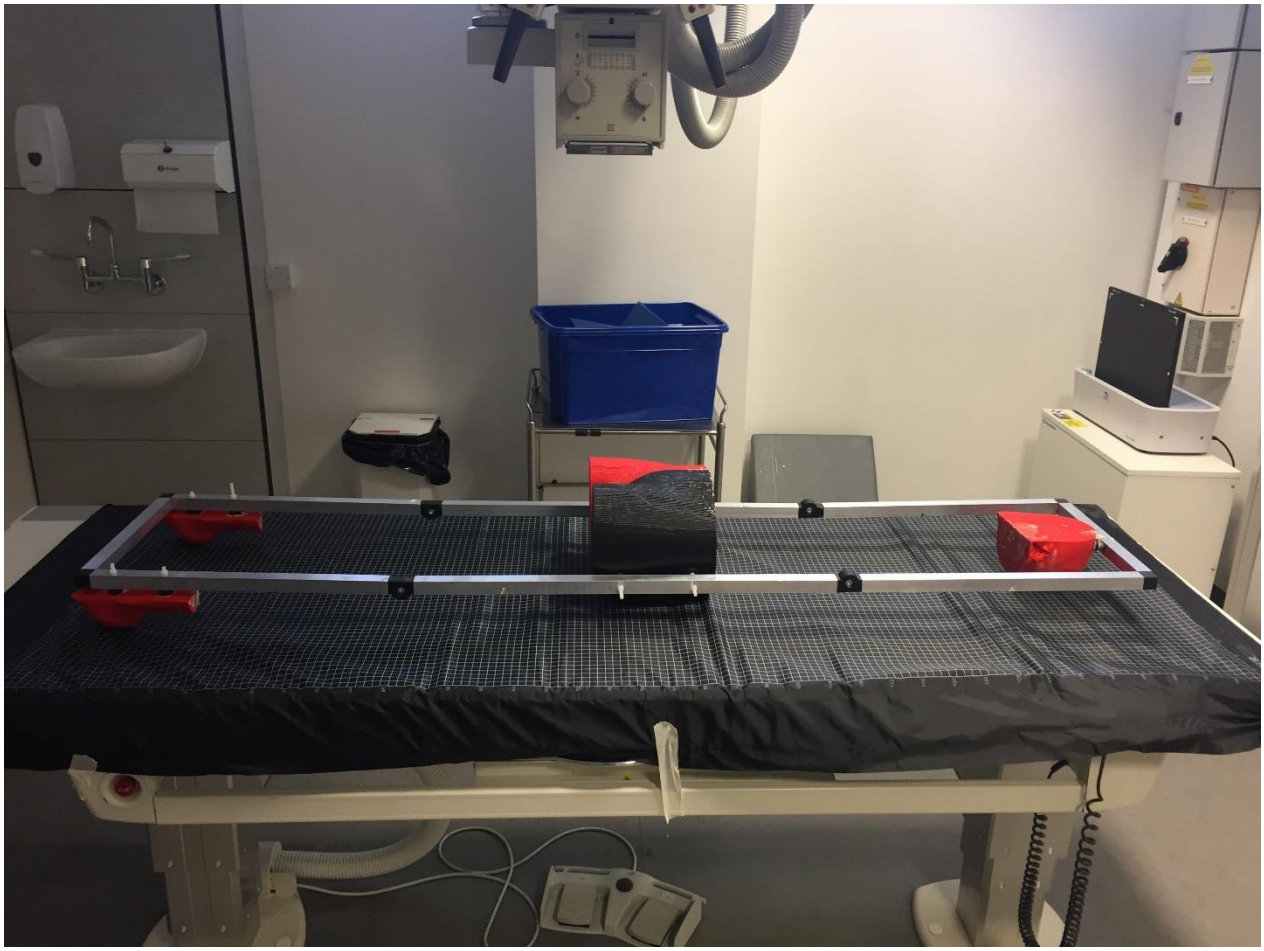

Figure 4.11: The XSensor P x 100 system fixed to the X-ray table with the 3D phantom placed on top of it.

4.4.1.3. Procedure for pressure mapping

Four large hospitals in the North West of England, one X-ray table mattress manufacturer and The University of Salford's medical imaging laboratory were asked to make their X-ray table mattresses available for this thesis. Hospitals only provided one mattress of each type, because they were in high demand for clinical usage.

Data were collected for 18 X-ray mattresses from four different hospitals, as well as two used mattresses from The University of Salford laboratory. The hospital mattress surface data were collected over approximately two months with the dates and times being decided

upon by the hospitals' administration and the researcher. Owing to the high demand for the imaging facilities, data were only collected at weekends.

4.4.2. The experimental design for collecting pressure measurements

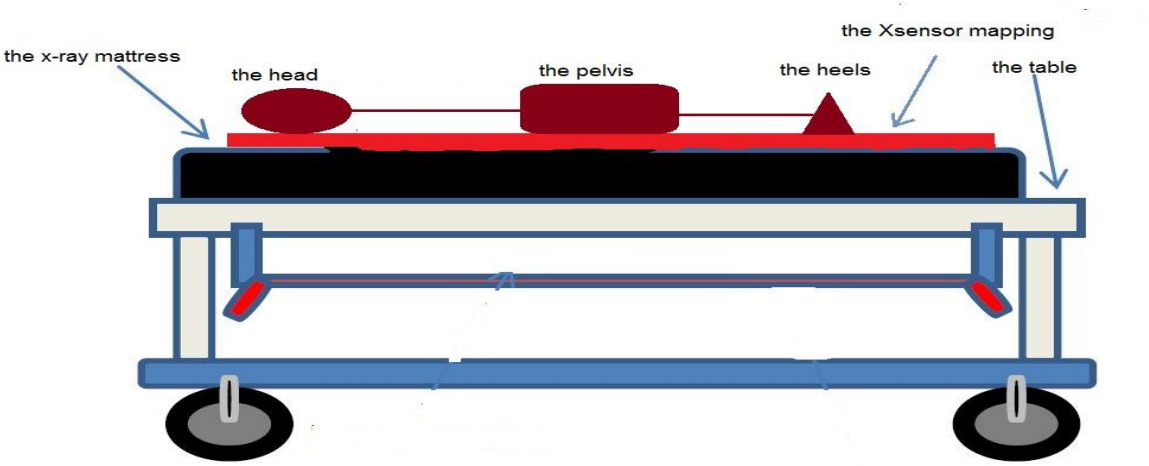

Figure 4.12: Setup for the 3D phantom on the X-ray mattress.

In total, 24 X-ray table mattresses were examined, ranging in thickness from 2.5 cm to 13 cm. The mattresses varied in age and were made by different manufacturers. The PPIs were measured at the head, pelvis, and heels using XSensor pressure imaging equipment (Figure 4.11) with and without a mattress. The XSensor was placed between the 3D phantom and mattress, and a control was created in which the XSensor was placed between the phantom and the X-ray table without a mattress. Five different weights of sand were used to simulate the adult head, pelvis, and heels for five body compositions.

During the pressure measurements, the 3D phantom was placed on the mattress for three minutes while the mattress stabilised. Data collection occurred over a 15-minute period for each of the five weights.

To reduce random error, the procedure was repeated three times for each weight category, and pressure measurements were taken. From these, averages, means and confidence intervals (CIs) were calculated. A stabilisation period of three minutes was established as optimal for a non-human object, as a single human subject would have to lie in the supine position on each mattress for 30 minutes in a clinical setting. Three minutes was deemed to be the point at which sensor creep due to mattress instability would be nullified.

4.4.3. Data and statistical analysis

For the statistical analysis, SPSS version 22 (Ghasemi and Zahediasl, 2012) was used to correlate the numerical data obtained by the XSensor, as were inferential statistics. The paired t-test for parametric data determined the significance of the differences between the experimental groups, and a *p*-value of $< .05$ was considered statistically significant. In addition, the mean IPR was determined using the XSensor, and the 3D phantom's segment calculations for the PPIs were also obtained.

4.5. Radiation Dose Measurements

4.6.1. QC tests

The functioning of an X-ray system is assured by planned testing and maintenance programmes, and these are fundamentals of their operating procedures (IPEM, 2005). Therefore, prior to the experimental work for this thesis, QC tests were performed on the X-ray machines to check for any errors. The results showed that all the technical performances fell within the expected limits. The QC tests are outlined in the IPEM recommendations (2005).

The QC test used included radiation dose output assessments and the variation in kVp, mAs and time. Appendix 3 presents the QC data.

4.6.2. Method for Radiation Dose Measurements

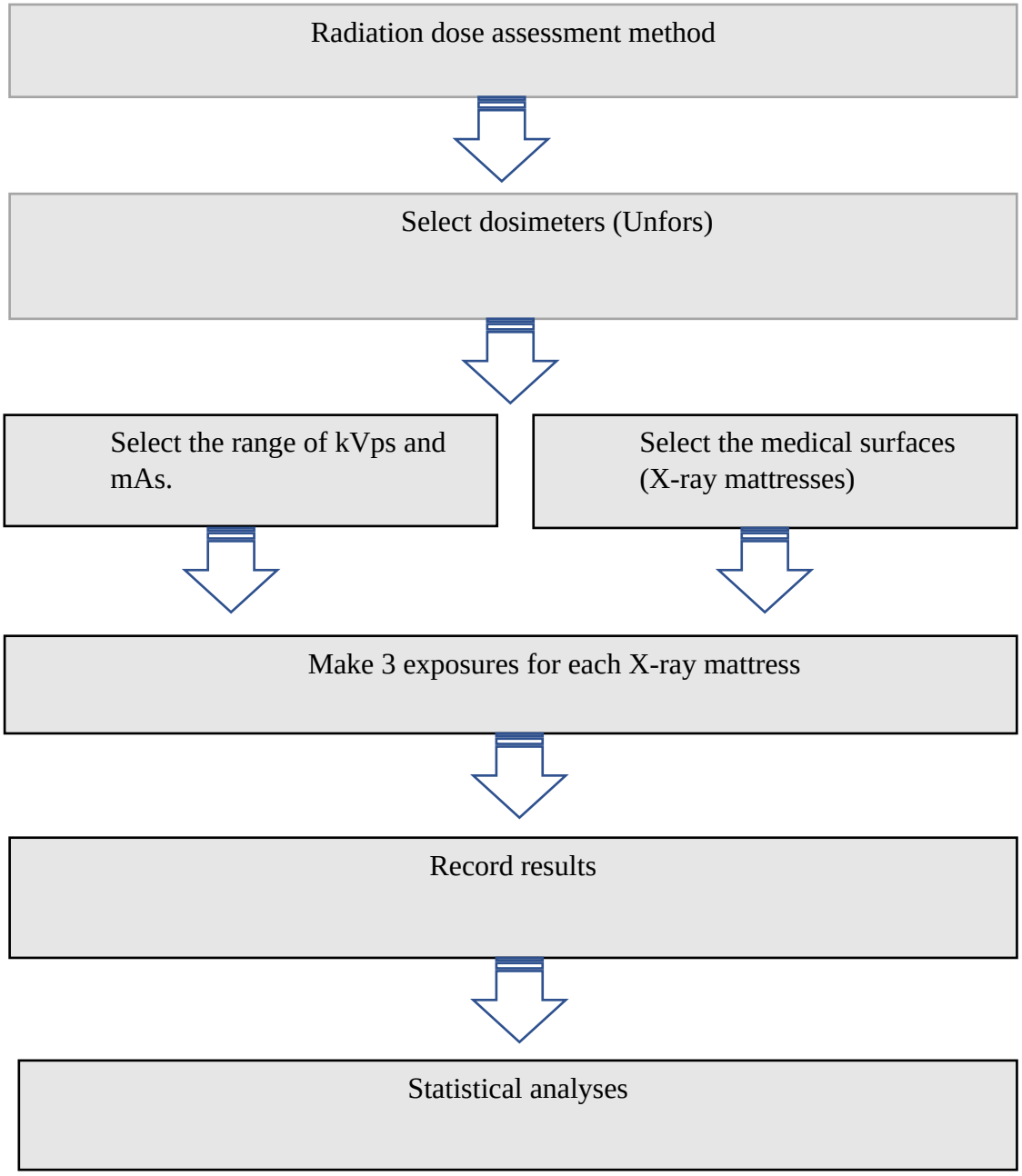

Figure 4.13: Flowchart of the radiation dose assessment method.

The radiation dose was measured using a solid-state dosimeter (RaySafe X2, Unfors Ray Safe AB, Billdal, Sweden) and represented as incident air kerma (IAK). The IAK was measured with and without a mattress (Figure 4.15). Three repeated exposures were measured for each protocol and the mean was calculated to reduce random error. For radiation acquisitions, manual exposure control was used with different kVp and mAs values (Table 4.2) to justify the use of the different kVp and mAs values.

For abdominal X-ray examinations, a common protocol for clinical practice was used. The parameters for the radiation dose were automatic exposure control (AEC), kVp of 80, with a grid, SID of 120 cm, and a broad focal spot without additional filtration. However, to achieve suitable dose measurements, a wide range of exposure parameters with different kVp and mAs were required. This allowed for the generation of images with a wide range of IQs, as expected in a clinical setting, and for sufficient data for conducting the statistical analysis.

In this thesis, kVp values ranging from 65 to 110 in five increments were used for image acquisition and their corresponding mAs values generated by the AEC were recorded. To conduct the experiment in the lab, the values of the kVp and their corresponding mAs values were set using manual exposure control instead of AEC. This is because AEC would make it impossible to investigate the influence of mattresses on the radiation dose.

Table 4.2: Exposure Parameters used for Image Acquisition and Radiation Dose Measurements

SID = 120 cm, filtration = zero										
kVp	65	70	75	80	85	90	95	100	105	110
mAs	40	25	20	14	10	8	6.3	5.6	4.5	4

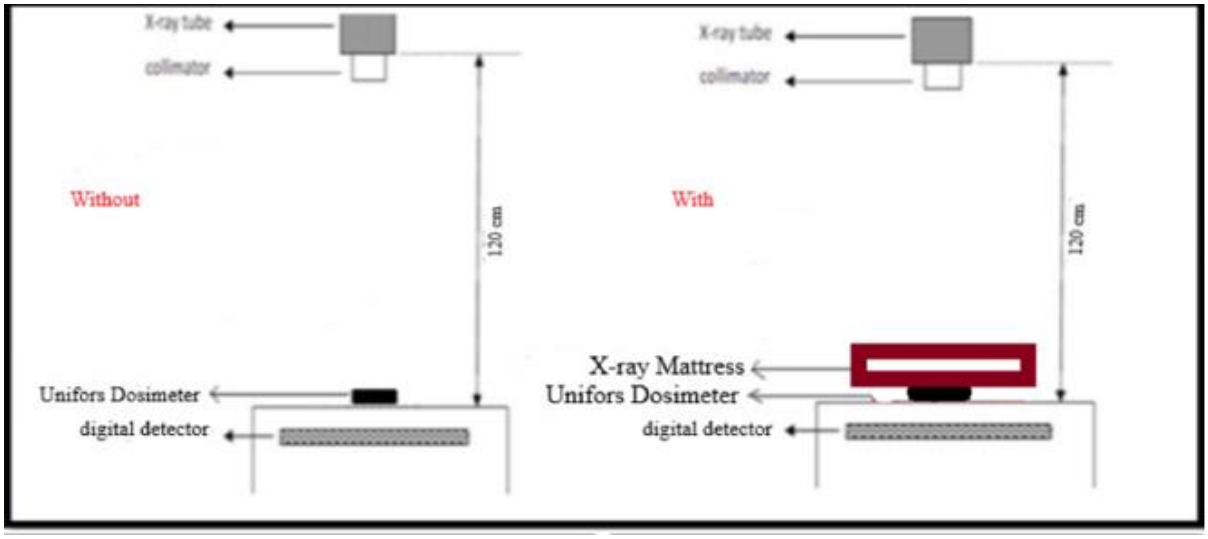

Figure 4.14: The experimental setup for radiation dose measurements with mattress and without a mattress.

4.6.2.1.The dose detector used in this thesis

4.6.2.1.1 RaySafe X2 dosimeter (Unfors)

A commercially available solid-state dosimeter (RaySafe X2, Unfors RaySafe AB, Billdal, Sweden) (Figure 4.14) was used to measure the IAK (μGy) at the surface of the X-ray table (with/without) mattress. This was the point of entry for the central focus of the X-ray beam. The RaySafe X2 dosimeter was used to ensure a precise measurement of the radiation dose. The RaySafe X2 has a working range of 40-150 kVp and can detect a wide range of radiation doses (1nGy to 9999 Gy). The manufacturer suggests that this dosimeter has an accuracy of within ± 5% of the calibrated values.

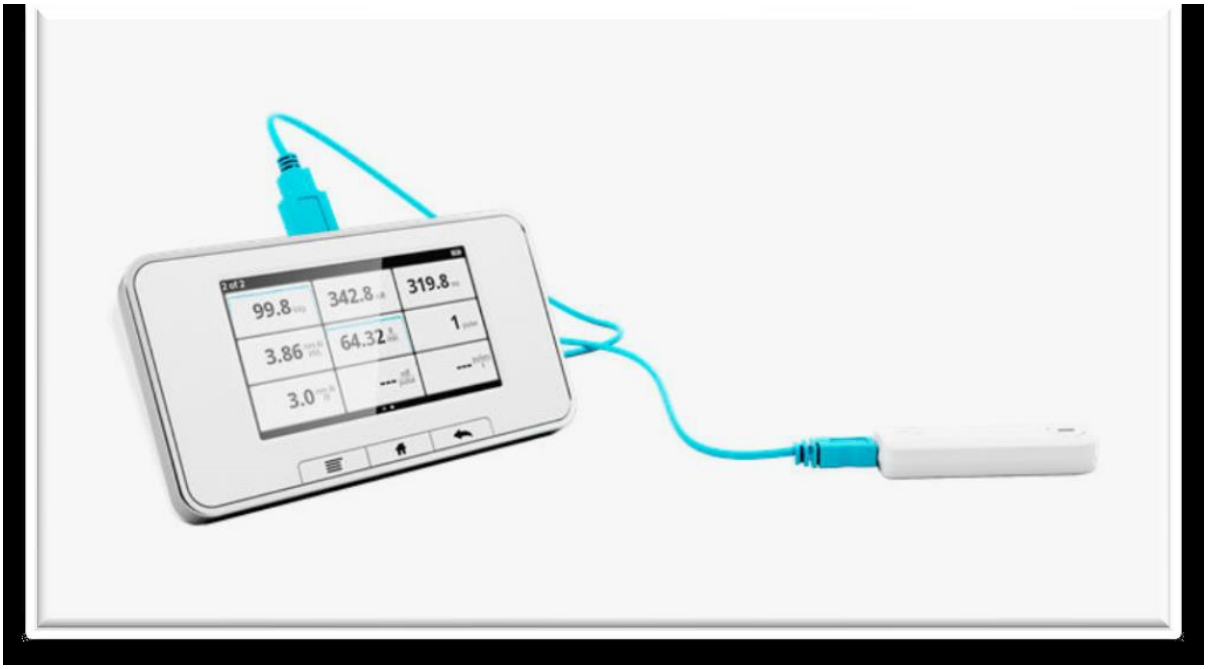

Figure 4.15: The RaySafe X2 dosimeter (RaySafe X2, 2016).

4.6.1.2 Dosimetry experiment

The collimation size of the X-ray beam was 10 x 10 cm and was kept constant for each mattress. Keeping the X-ray beam at a constant size enhances durability and reduces the effect of a collimation radiation dose. Figure 4.15 shows the X-ray room used for image recording.

For the dosimetry test, the RaySafe X2 (Unfors RaySafe AB, Billdal, Sweden) dosimeter was placed directly on an X-ray table without a mattress, as shown in Figure 4.16. The radiation field was defined tightly around the dosimeter's edges, and three exposures were made to reduce random error. These exposures were averaged to produce the mean values and SDs. A 120-cm SID was used throughout. Table 4.2 lists the kVp and mAs values used. A broad spot size was used without additional filtration. The IAK values were recorded with and without a mattress using the RaySafe X2 so that the imposition of the mattress on the IAK could be assessed. Repeat radiation dose measurements were undertaken with the only difference between the two conditions being the presence or absence of the mattress. The

respective tables report the mean level of recorded doses for the ‘mattress removed’ and ‘mattress present’ percentage differences at both low and high kV. Figure 4.16 shows the method used to record the mean dose levels with and without a mattress.

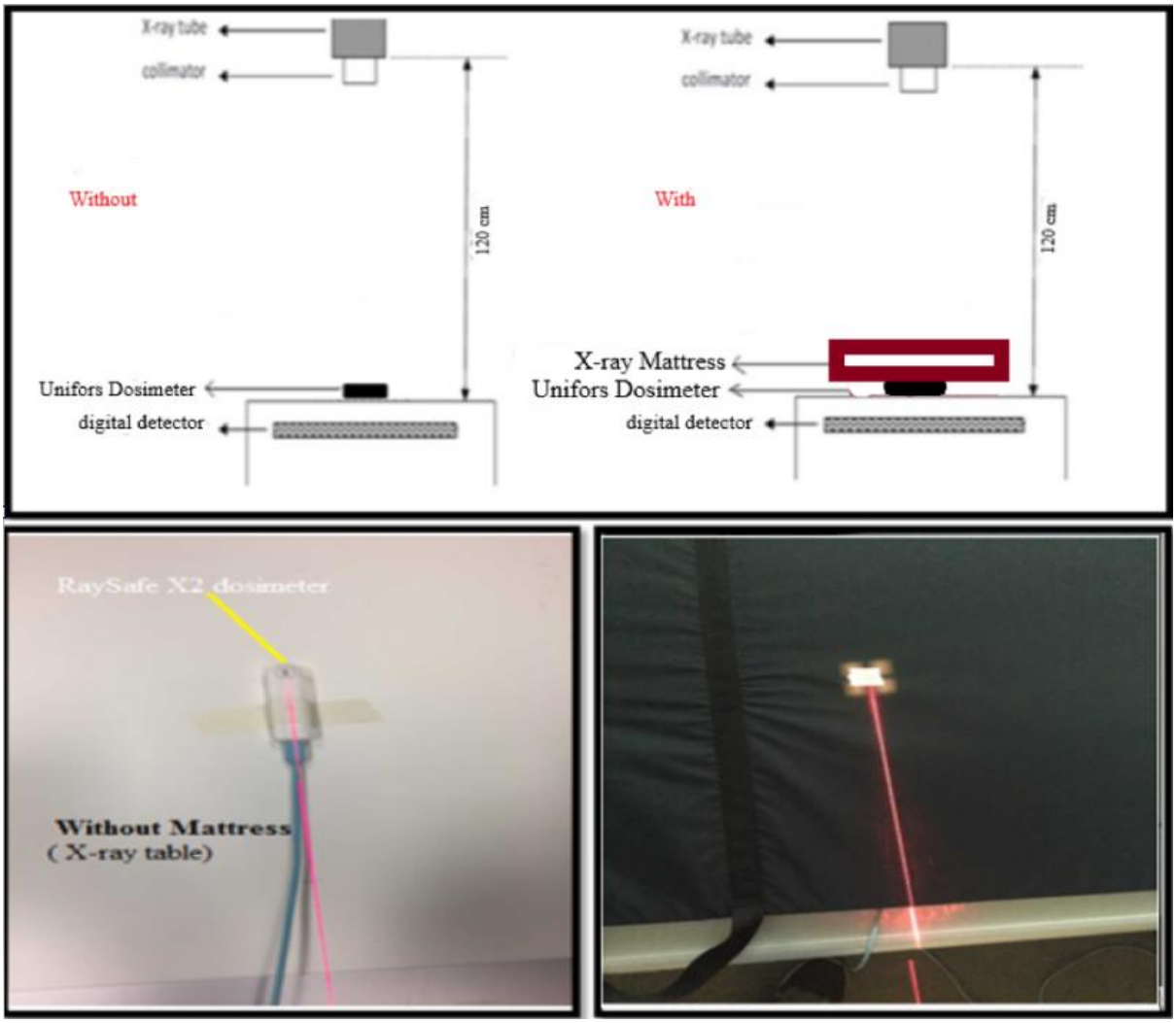

Figure 4.16: The setup for the RaySafe X2 dosimeter with and without the mattress.

4.7. IQ Measurements

4.7.1. Phantoms used for IQ evaluation

4.7.1.1. Rationale for using the CDRAD 2.0 phantom

The choice of using physical phantoms, such as the CDRAD 2.0 phantom, was supported by previous studies that used low-contrast detectability (LCD) and a CDRAD 2.0 phantom to compare IQ and radiation doses between hospitals (Geleijns et al., 1993; Almén et al., 1996; Van Soldt et al., 2003; Veldkamp et al., 2006). There are several advantages to this method. Firstly, it makes it easy to simulate the three types of X-ray table/mattress combinations by increasing or decreasing the PMMA slab thickness. This was an influential factor in the study's using LCD and the CDRAD 2.0 phantom as its aim was to compare a range of X-ray table mattresses and an X-ray table surface. It would have been impossible to achieve this aim using any of the currently available anthropomorphic phantoms on the mattress, as they were not suitable because of no commercially available phantoms could cover all the X-ray mattresses and table surfaces. The second advantage of using LCD with a CDRAD 2.0 phantom is its enabling the use of automatic analyser computer software for physically evaluating the IQ. This provided a mechanism for making extremely reliable IQ comparisons between mattresses. Finally, using a physical phantom was deemed to be the simplest method available. This is necessary for survey studies such as this, wherein large amounts of data are expected to be collected.

Moreover, the additional advantages of the physical evaluation method for CDRAD 2.0 phantom images using the CDRAD analyser software are as follows. This approach has high reliability and consistency on the evaluation criteria utilised to assess the threshold CD detection and it does not suffer from the subjectivity of the human visual and cognition systems (Pascoal et al., 2005). Many studies were investigated that found that there is good correlation

between the visual and physical IQ evaluation methods of CDRAD 2.0 phantom images (De Crop et al., 2012; Norrman et al., 2005). Finally, using the CDRAD software analyser in this thesis is extremely useful due to the large amount of data (CDRAD 2.0 phantom images) that was collected, since using visual assessment for CDRAD 2.0 image evaluation would have been extremely time consuming.

Selecting the PMMA thicknesses

A 17.5 cm thick slab of PMMA was combined with the CDRAD 2.0 phantom to simulate the abdominal area for a standard sized adult. This thickness was chosen because the radiation attenuation achieved was equal to that experienced when imaging the abdominal area of a standard sized adult (the anthropomorphic phantom represented the standard size).

The 17.5 cm measurement was decided upon because the AP dimensions of the adult anthropomorphic abdominal phantom used in the imaging lab (PH-5 CT Abdomen Phantom, Kyoto Kagaku Company, Japan) (Figure 4.17) were equal to 16 cm and represented an underweight adult. An additional 4 cm of fat thickness was added to the phantom to simulate a standard sized patient with an AP thickness equal to 20 cm. This represents a patient who weighs 59 kg, is 1.78 m tall, and has a BMI of 18.6. The additional 4 cm of fat thickness added to the phantom was estimated using the following equation:

$$\text{AP dimension (cm)} = 111.4 + 1.376W + 0.003573W^2,$$

where W is the weight of the patient

To estimate the thicknesses of the PMMA that needed to be added to the CDRAD phantom to represent the abdomen of a standard-sized adult, the adult anthropomorphic abdominal phantom (PH-5 CT Abdomen Phantom, Kyoto Kagaku Company, Japan) with an additional 4 cm of fat was imaged using a standard clinical protocol. That meant an SID of 120, a broad focal spot, a grid, a kVp of 85 and a mAs of 450 using an AEC.

A value of 7.6 mAs was recorded when imaging the phantom with additional fat. The same experiment was repeated using the CDRAD phantom with the PMMA, instead of the anthropomorphic abdominal phantom with 4 cm of additional fat. Different thicknesses of PMMA were used with the CDRAD phantom and achieved the same mAs value of 7.6, indicating that the attenuation was the same. The thicknesses of the PMMA that accompanied the CDRAD phantom with a mAs of 7.6 had similar attenuation to that of the anthropomorphic phantom, wherein the fat was equal to 17.5 cm of PMMA.

Taking this into account, 17.5 cm of PMMA was used with the CDRAD 2.0 phantom to represent the abdominal area of a standard sized adult patient.

Figure 4.17: The adult anthropomorphic abdominal phantom (PH-5 CT Abdomen Phantom, Kyoto Kagaku Company, Japan).

4.7.2. Procedure for image acquisition

4.7.2.1. IQ parameters

The CDRAD 2.0 phantom (Artinis Medical System, Netherlands) combined with 17.5 cm of PMMA slabs was used for IQ evaluation. The CDRAD phantom has been widely used in studies evaluating IQ (Al-Murshedi et al., 2018; Geijer et al., 2001), and a good correlation has been typically found between visual IQ and lesion visibility (Al-Murshedi et al., 2018; De Crop, 2012).

The CDRAD+PMMA phantom was imaged using a commercial X-ray machine (Wolverson X-ray Ltd, Willenhall, West Midlands, UK), both with and without an X-ray table mattress (Figure 4.18) to determine its impact on IQ. For image acquisitions, manual exposure controls were used with different kVp and mAs values (Table 1) with a SID of 120 cm, a broad focal spot size and an anti-scatter grid as constants. For each set of acquisition conditions, three images were taken of the CDRAD phantom, as recommended by the manufacturer (Burght et al., 2014).

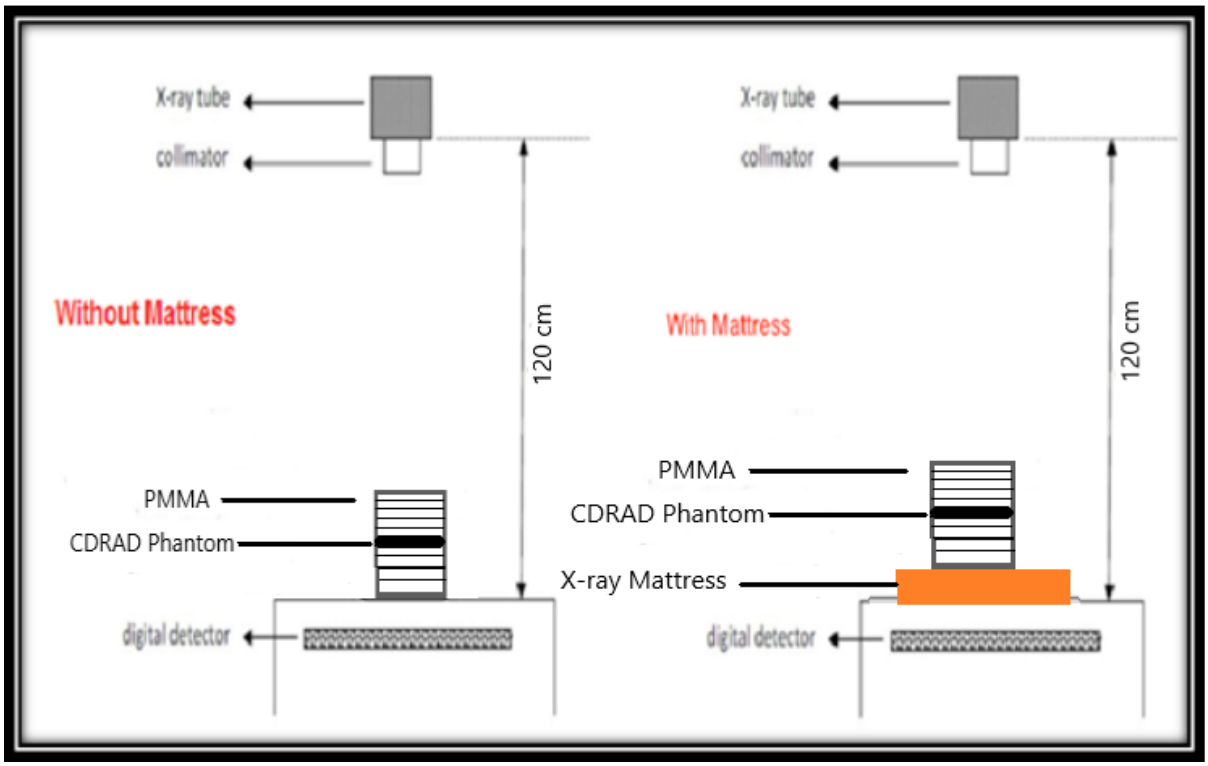

Figure 4.18: Experimental setup for the CDRAD phantom imaging with and without a mattress.

4.7.3. Method for IQ Measurements

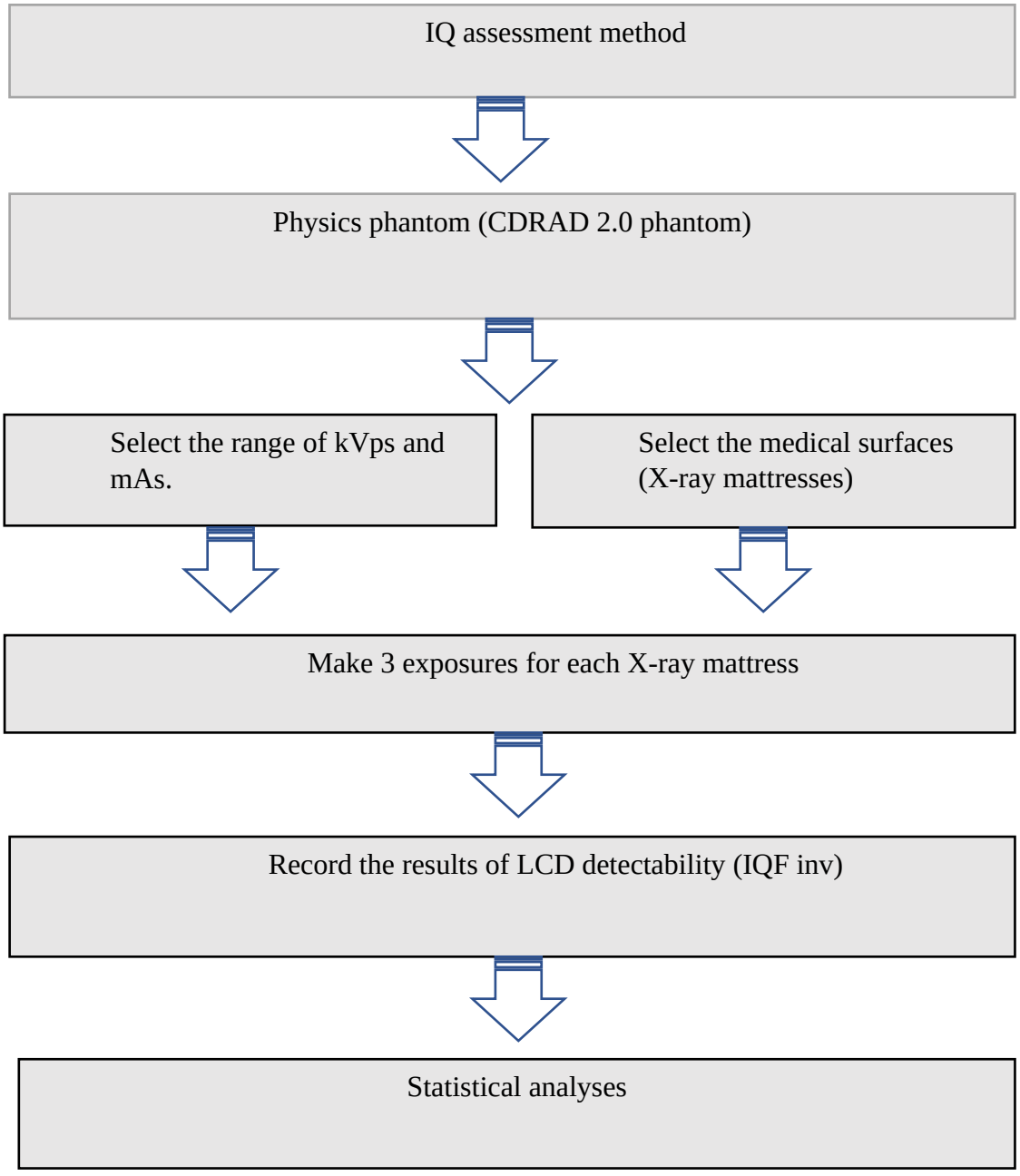

Figure 4.19: Flowchart of the IQ method.

As noted by Bourne (2010), IQ relates to how able diagnostic images are to present visual information regarding a patient's physiology and anatomy. This includes the

physiological and anatomical differences that can occur due to trauma or disease. The IQ can be affected by five distinct characteristics: noise, contrast, spatial resolution (Tapiovaara, 2008), sharpness (blurring) and artefacts (Hendee and Ritenour, 2003).

4.7.3.1. Physical IQ evaluation

4.7.3.1.1 IQFinv Calculations

The physical evaluation of LCD was performed using CDRAD analyser software with its output displayed as IQFinv values (the average of three consecutive values). The CDRAD software has three input parameters: Alpha, APD and SID.

The default value for Alpha is 1e-8, as proposed by Burght et al. (2014). The reason for choosing this value is that, according to Pascoal et al. (2005), this value best matches the perceptual IQ APD, is considered in the calculation of the automated scoring method and is set relative to image bit depth. To use different bit depths, the APD value must be 0 to allow for valid comparison between images (Brosi et al., 2011; Burght et al., 2014). For the CDRAD 2.0 phantom, the APD is set to 0 in different X-ray machines which have various bit numbers stored per pixel.

The main benefits of using the physical evaluation method for the CDRAD 2.0 phantom images alongside the CDRAD analyser software include its high reliability and consistency in the evaluation criteria used to assess the threshold contrast–detail (CD) detection and because subjectivity from human visual and cognitive systems does not occur (Pascoal et al., 2005).

In addition, many studies have found good agreements and correlations between the visual and physical IQ evaluation methods of the CDRAD 2.0 phantom images (Norrman et al., 2005; De Crop et al., 2012). The CDRAD software analyser was useful in this thesis

because analysing the large amount of data collected from the visual assessment of the CDRAD 2.0 image evaluation would have been extremely time-consuming.

4.7.3.2.The CD phantom (CDRAD 2.0)

The low-contrast detail perceptibility strategy typically utilises CD phantoms. The CDRAD phantom is well-established in the examination of IQ for imaging systems, imaging conventions/procedures and the acquisition of parameters. Accordingly, as observed by radiologists, this phantom has the capability to determine the visibility levels of various contrasts, which may then be utilised in different diagnostic imaging modalities (e.g. fluoroscopy and digital subtraction angiography) (Van der Burght, 2003).

4.7.3.3. Description of the CD phantom (CDRAD 2.0)

The CDRAD 2.0 phantom is a plexiglass tablet (26.5 x 26.5 x 1 cm^3) (Figure 4.20), which was constructed with 225 cylindrical holes drilled into it at various diameters and depths (logarithmically sized 0.3-8.0 mm). A total of 225 squares were placed onto the X-ray image on a grid (15 x 15 cm). The contrast (depth of the holes) was increased left to right across the grid's rows. Moreover, across the grid's columns, the hole diameters decreased from top to bottom. Therefore, while there was only a single hole within each square in the first three rows, from the fourth row onwards, there were two holes in each square, which were placed in the middle and in any random corner of the squares.

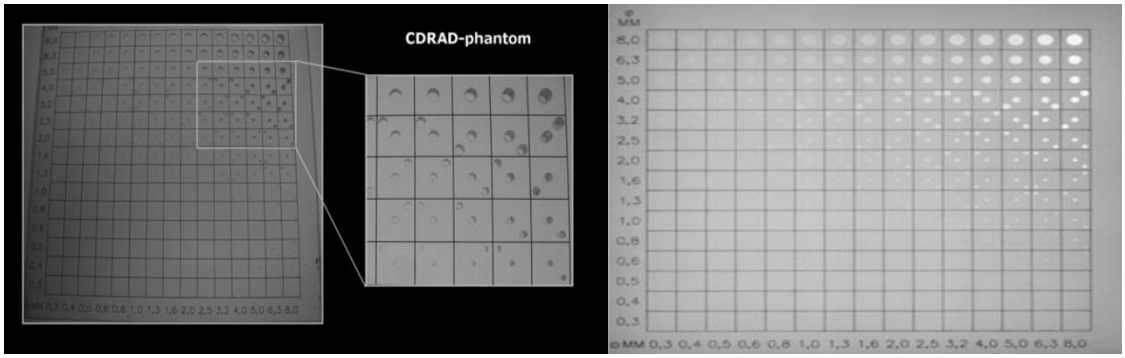

Figure 4.20: Diagrammatic illustration of the CDRAD 2.0 phantom.

4.7.3.4. Features of CDRAD

The CDRAD 2.0 phantom is commonly used to test the physical properties of an X-ray system, which define the IQ together with the perceptions of the observers. Observers' perceptions are vital for achieving the correct diagnosis. Accordingly, the CDRAD phantom quantifies the contrast and details of the system's CD properties of the images along with the perceptions of the observers. Specifically, the Artinis CDRAD 2.0 phantom can be applied to the complete diagnostic imaging system.

The CDRAD phantom was placed on the imaging table and the AEC was used to control the exposure with and without a mattress. When the image receptor was placed within its holder it needed to align with the median sagittal location.

4.7.3.5. CDRAD analyser, data, and statistical analyses

Two methods were used to present the results: first, the utilisation of the formulas, and second, the utilisation of the CD curve (Van der Burght, 2003).

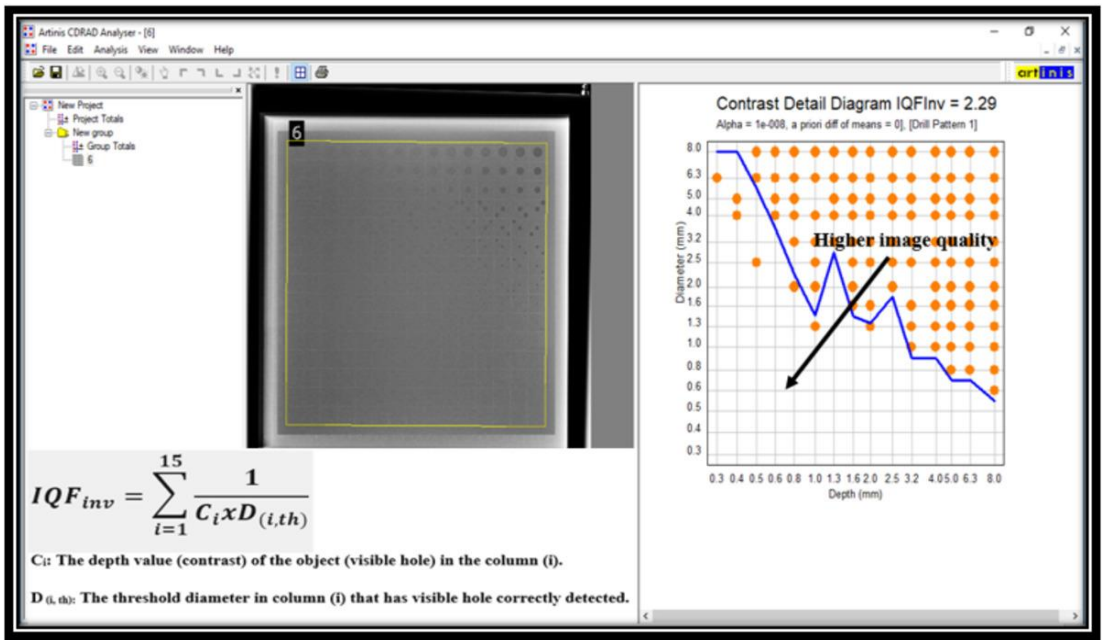

Figure 4.21: Physical evaluation of the CDRAD phantom images using CDRAD 2.0 phantom analyser software.

The analysis of the CDRAD data involved evaluating the IQ and providing a statistical method that helped determine whether many holes were observed in the various sections of the image. SDs were utilised with the value of the average pixel signal of the images being evaluated, as well as their pixel background/variables.

This analysis was imperative for identifying the 225 different images of the holes for the image phantom and was deemed to be of help in determining the two variables (with mattress and without mattress) correctly (Van der Burght, 2003). Initially, the locations of the holes for the image phantom were identified through the software program, which was completed by applying the statistical method which indicates the images of the holes (Figure 4.21).

4.7.4 The method for using the CDRAD phantom

4.7.4.1 The rationale for the change in collimation when imaging thin and thick mattresses

Due to the two different size of thickness of mattress (thin and thick) in this thesis, the collimation size of the X-ray beam remained constant for each mattress based on the size of the mattress used (i.e. different constant collimation sizes were used according to the sizes of the mattresses used during all image acquisitions. This was necessary for increasing reliability and ensuring that collimation did not influence the IQ.

The CDRAD phantom was utilised as a measurement function to show the lowest level of contrast detectable in each image. An evaluation of all the CDRAD DICOM images was then provided, which included finding the threshold CD curves through the CDRAD analyser software version 1 (Bourne, 2010). To enable scatter and provide attenuation levels that were like those of an adult patient, the CDRAD phantom combined with 17.5 cm of PMMA slabs was used for IQ evaluation (Figure 4.22).

Figures 4.22 and 4.23 show the setup for the CDRAD phantom both with and without the mattress. The X-ray tables were exposed three times and manual exposure controls were used with the kVp and mAs values listed in Table 4.2. The 20 x 25 cm^2 CDRAD was collimated to reduce the radiation beam field. First, three exposures were taken from the range of 50–110 kVp on the CDRAD+PMMA phantom, which was placed on the X-ray table (Figure 4.22).

The CDRAD+PMMA phantom was placed on the X-ray table and each mattress was exposed using the same range of kVp and mAs values. The CDRAD+PMMA phantom was then removed and another set of three exposures was taken using a similar range of kV exposure factors. In total, three exposures were taken for each mattress with the CDRAD+PMMA phantom for every kVp value listed in Table 4.2 (see Figure 4.23).

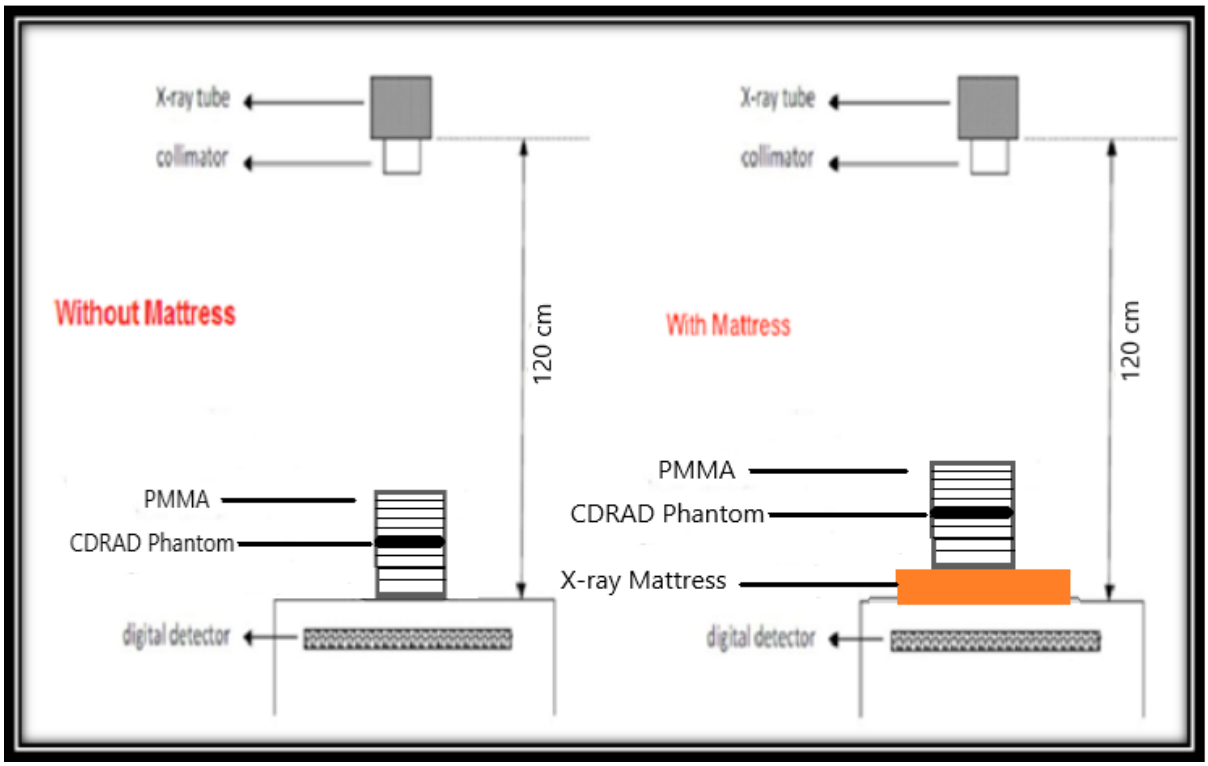

Figure 4.22: Setup for the CDRAD phantom both with and without the mattress.

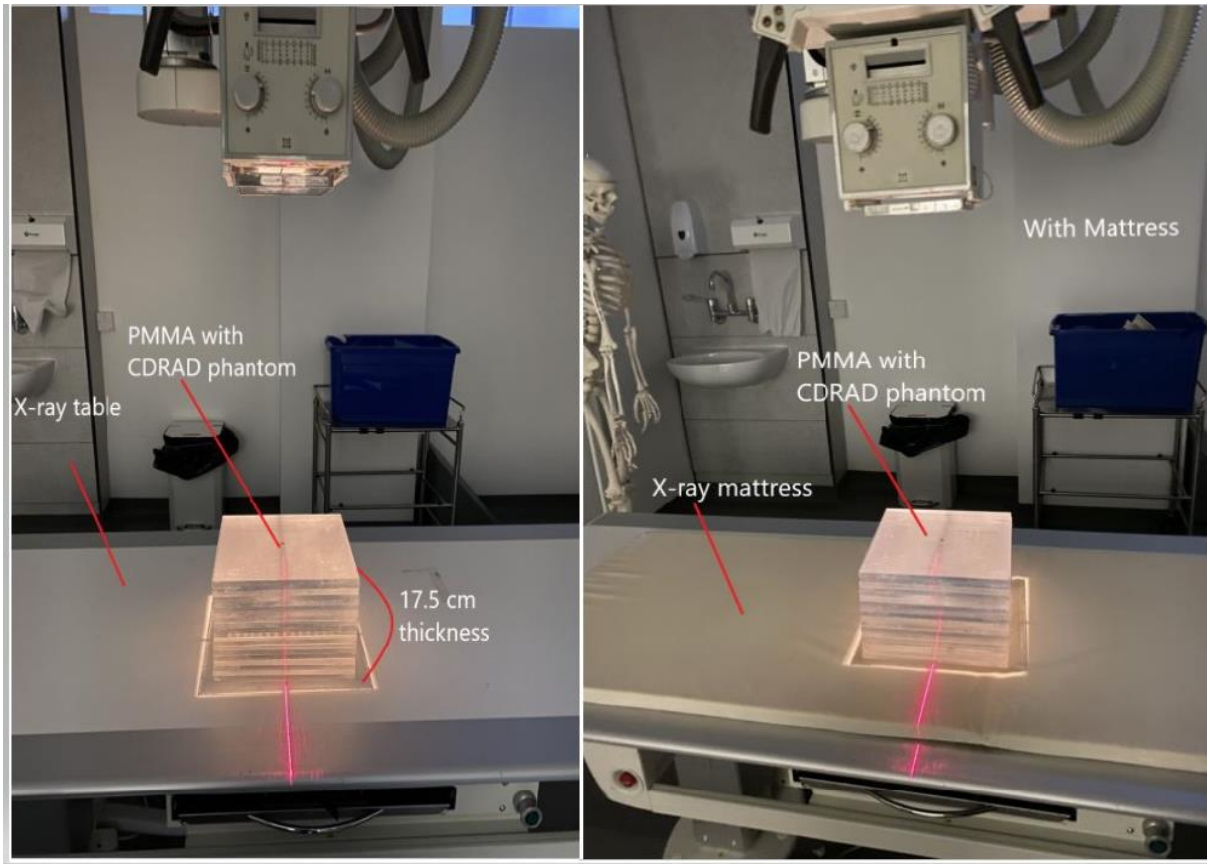

Figure 4.23: Photos showing the setup for the CDRAD phantom both with and without the mattress

4.8. Data Analysis

4.8.1. Normality tests

Frequency distributions in the form of histograms can be used to visually inspect the normal distribution of data points in various forms, such as stem-and-leaf plots, box plots, probability-probability (P-P) plots and quantile-quantile (Q-Q) plots. These types of plots are preferred over Shapiro-Wilk tests because they are more sensitive when detecting normality differences (Field, 2013). However, Shapiro-Wilk tests can be significant even with a slight deviation in data values from a normal distribution.

4.8.2. Statistical tests

Paired sample t-tests were performed to compare the mattress surface and the hard surface of the X-ray table. The differences between PPIs for the head, the PPIs for the sacrum and the PPIs for the heels were analysed for all mattresses. This test was also used to measure radiation doses and IQ across all the X-ray mattresses. These tests were performed because the Shapiro-Wilk test results showed that the data were normally distributed.

The results of the paired t-test for parametric data showed that there was a statistically significant difference in the peak pressure index PPI for the jeopardy areas on all X-ray mattresses (Shapiro–Wilk test: $p < .05$). All mattresses showed lower PPI than non-mattress measurements. The age of the mattress had an impact on PPI, with older mattresses performing worse.

A statistically significant decrease ($p < .05$) in IQ was observed between the 'no mattress' and 'with mattress' conditions. It was found that these differences have a clinically insignificant impact on the primary beam and the image quality measured through IQFinv. While mattress age does correlate with the amount of attenuation, it does not with image quality and also this also applies to new mattresses.

In assessing the radiation attenuation properties of the X-ray mattresses, a statistically significant increase ($p < .05$) was observed in the IAK between the 'no mattress' and 'with mattress' conditions. It was found that clinically these differences are insignificant as the change in mAs to compensate for the attenuation would be between 0.01 and 0.13 mAs. Practically, it is unlikely any X-ray equipment would have this level of precision when setting mAs values for bucky work.

The next section describes the pilot study that was conducted for method development and validation before it was applied to a range of X-ray mattresses.

4.9. Pilot Study

A pilot study was applied to validate the method for assessing a range of X-ray mattresses used in clinical practice. Three Rothband mattresses supplied by WSR Medical Solutions Ltd. were used for the pilot study. These included the complete range of X-ray table mattress used in general X-ray rooms; two were the same thickness (2.5 cm) and one was a thicker trolley mattress (13 cm).

4.9.1. Introduction

The pilot study was undertaken to determine the feasibility and validity of the method used to assess three types of X-ray mattresses before applying it to a wider range of commercially available mattresses for the main study.

4.9.2. Method for Pilot study

4.9.2.1.The X-ray mattresses selected for the pilot study

Mattresses supplied by WSR Medical Solutions Ltd., which trades as Rothband (UK), Incorporating WS Rothband & Co. Ltd., were used for the pilot study. These mattresses were used because Rothband is a popular supplier of mattresses to clinical departments and thus they are currently used in imaging. As the trolley mattresses are used in UK hospitals, the pilot study has ecological validity (Thompson, 2012; Stone, 2012; Briody and Walker, 2013). These mattresses were chosen due to their physical characteristics, as shown in Table 4.3.

Table 4.3: Summary of the X-Ray Mattresses Selected for the Pilot Study

Name of the Mattress	**Foam Grade**	**Dimension (L x W x T in cm) ***	**Weight (kg)**	**Features**
Sewn Mattress New	rx39-200	198 x 61 x 2.5 cm	5 kg	-Functionally radiolucent and general artefact free -High-density foam (39 kg/m³) -Excellent durability -Excellent longevity -Premium replacement for fibre-filled cushions -Adheres to strict British fire regulations
Anti-static Mattress New	rx39-200	198 x 61 x 2.5 cm	5 kg	-Completely welded seams for infection control purposes -High-density foam (39 kg/m³) -Excellent durability -Excellent longevity -Premium replacement for fibre-filled cushions -Adheres to strict British fire regulations -Certified anti-static
Trolley Mattress 10 years	foam	195 x 56 x 13 cm	unknown	-Pressure re-distributing mattress

4.9.3. Results for Pilot study

4.9.3.1. For pressure measurements (PPI)

PPI of Head

Table 4.4: Mean PPI and Standard Deviation (SD) of the Five Weights for the Head on the Three Medical Imaging Mattresses.

	PPI of Head (mmHg) ± SD				
Mattress name (thickness 2.5 cm)	**Max±SD**	**3Q±SD**	**Mean ±SD**	**1Q±SD**	**Min±SD**
Hard Surface/X-ray table	95.4±1.8	74.8±1.2	71.5±1.5	65.9±1.5	60.5±1.8
Sewn Mattress RC new	54.8±2.1	50.9±2.3	47.8±1.5	46.8±1.5	42.2±1
Anti-Static Mattress RC new	49.6±1.1	44.4±1.1	43.4±0.7	40.8±0.9	38.8±1.4
Trolley Mattress-L (13 cm) ¥	56.5±2.3	57.2±2.5	50.4±1.3	48.3±1.6	49.2±1.8

Note. RC: Rothband Company, ¥: 10 years.

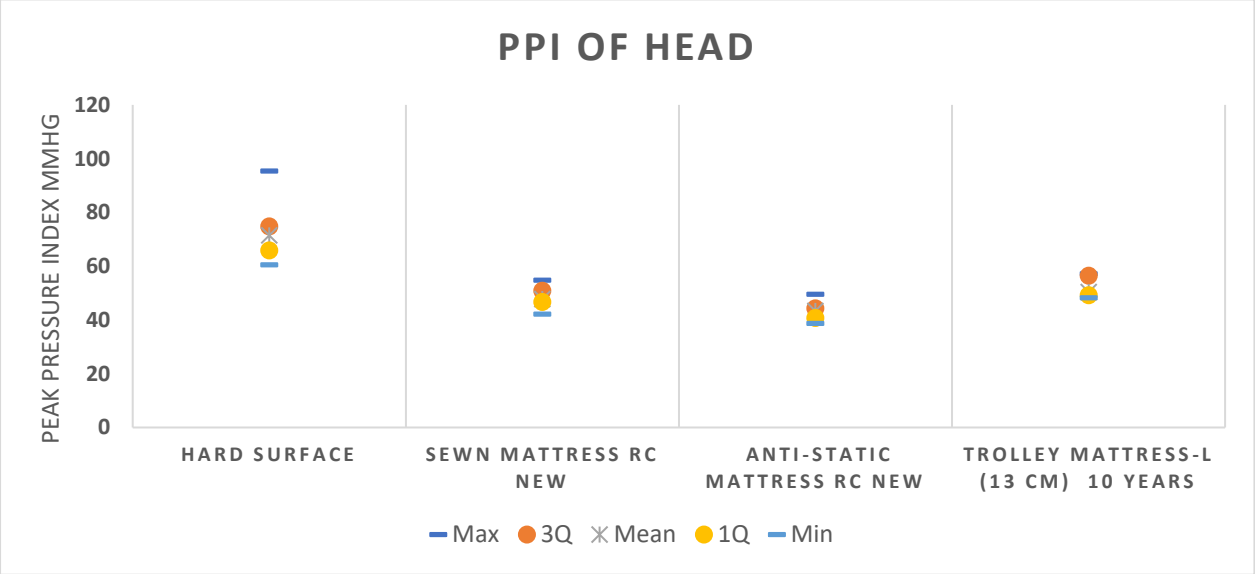

Figure 4.24: Comparison of the mean PPIs with the SD of the five weights for the head on the three medical imaging mattresses.

PPI of Sacrum

Table 4.5: 4.5 Mean PPI and SD of the Five Weights for the Sacrum on the Three Medical Imaging Mattresses

	PPI of Sacrum (mmHg) ±SD				
Mattress name (thickness 2.5 cm)	**Max±SD**	**3Q±SD**	**Mean ±SD**	**1Q±SD**	**Min±SD**
Hard Surface/X-ray table	95.4±1.8	74.8±1.2	71.5±1.5	65.9±1.5	60.5±1.8
Sewn Mattress RC new	81.1±2.1	75.8±1.3	54.2±1.3	51.6±1.9	42.6±2.4
Anti-Static Mattress RC new	55.4±1.8	50.6±1.4	44.1±1.5	40.1±1.5	36.1±1.0
Trolley Mattress-L (13 cm) ¥	54.8±2.3	50.8±2.0	46.9±0.5	46.1±2.2	38±1.0

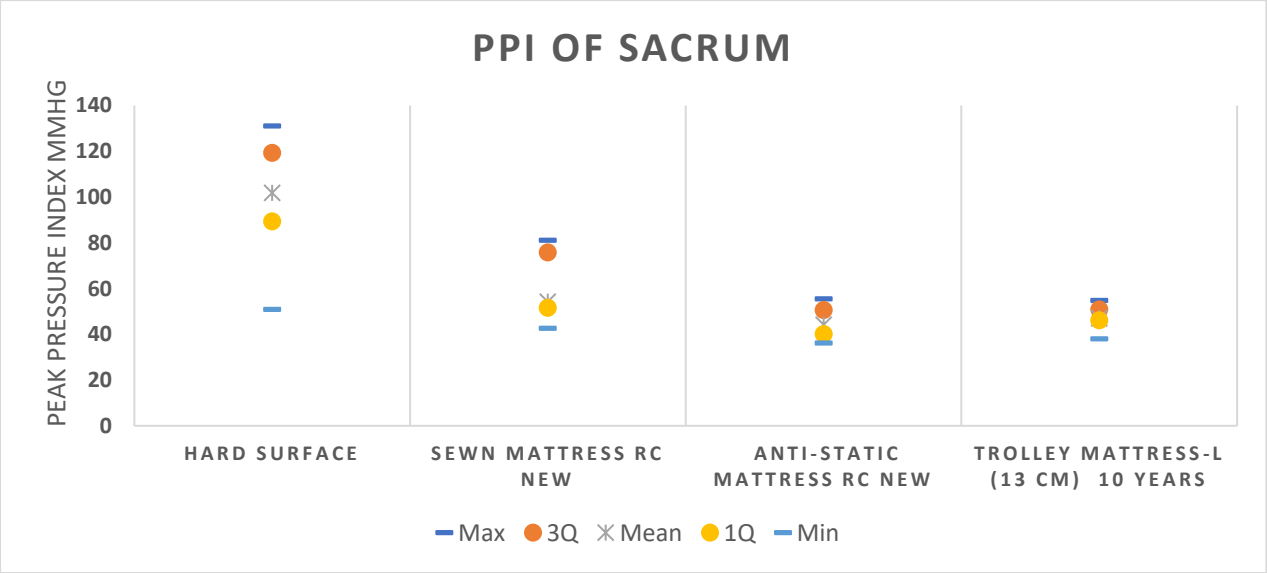

Figure 4.25: Comparison of the mean PPI with the SD of the five weights for the sacrum on the three medical imaging mattresses.

PPI of Heels

Table 4.6: Mean PPI and SD of the Five Weights for the Heels on the Three Medical Imaging Mattresses.

	PPI of Heels (mmHg) ± SD				
Mattress name (thickness 2.5 cm)	**Max±SD**	**3Q±SD**	**Mean ±SD**	**1Q±SD**	**Min±SD**
Hard Surface/X-ray table	95.4±1.8	74.8±1.2	71.5±1.5	65.9±1.5	60.5±1.8
Sewn Mattress RC new	91.9±2.6	82±0.9	60.3±1.7	54.3±2.6	25.9±2.3
Anti-Static Mattress RC new	84±1.2	73.9±1.3	54.4±1.8	30.4±1.1	29.7±1.0
Trolley Mattress-L (13 cm) ¥	90.2±1.8	79.9±3.9	44.1±1.6	43.3±1.8	28.5±0.9

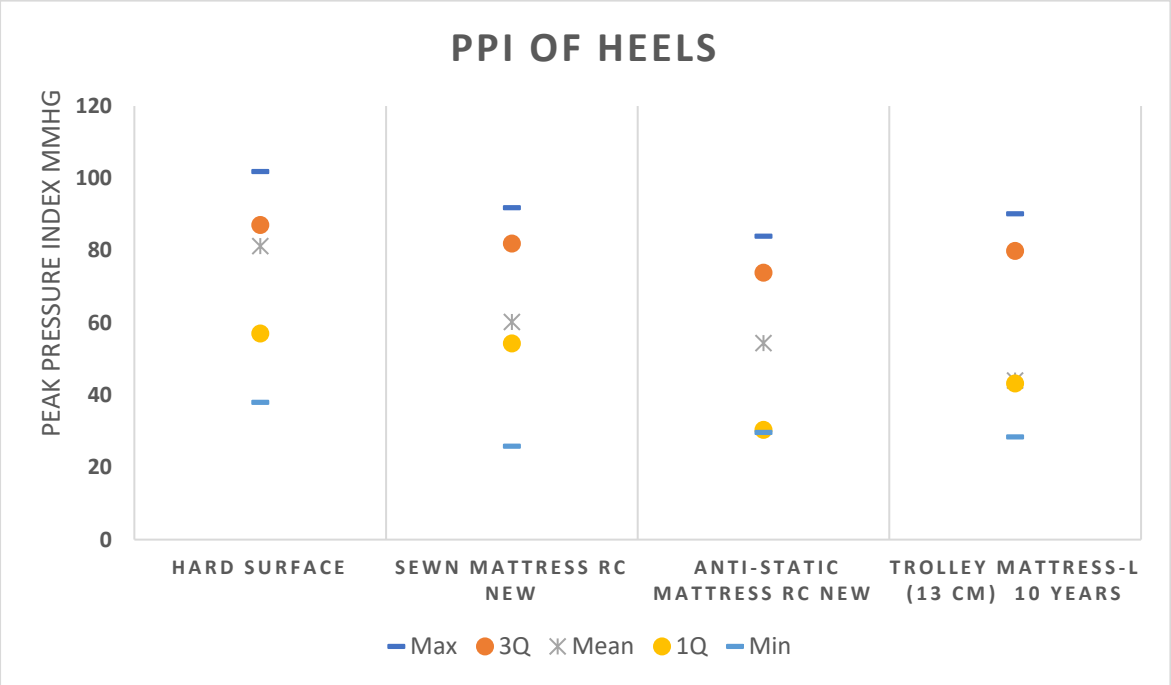

Figure 4.26: Comparison of the mean PPI with the SD of the five weights for the heels on the three medical imaging mattresses.

IPR Results

Table 4.7: IPR Values for the Five Weights for the Head on the Three Medical Imaging Mattresses.

	IPR of Head				
Mattress name (thickness 2.5 cm)	**Max Weight**	**3Q Weight**	**Mean Weight**	**1Q Weight**	**Min Weight**
Sewn Mattress RC new	0.57	0.68	0.67	0.71	0.70
Anti-Static Mattress RC new	0.52	0.59	0.61	0.62	0.64
Trolley Mattress-L (13 cm) ¥	0.59	0.76	0.70	0.73	0.81

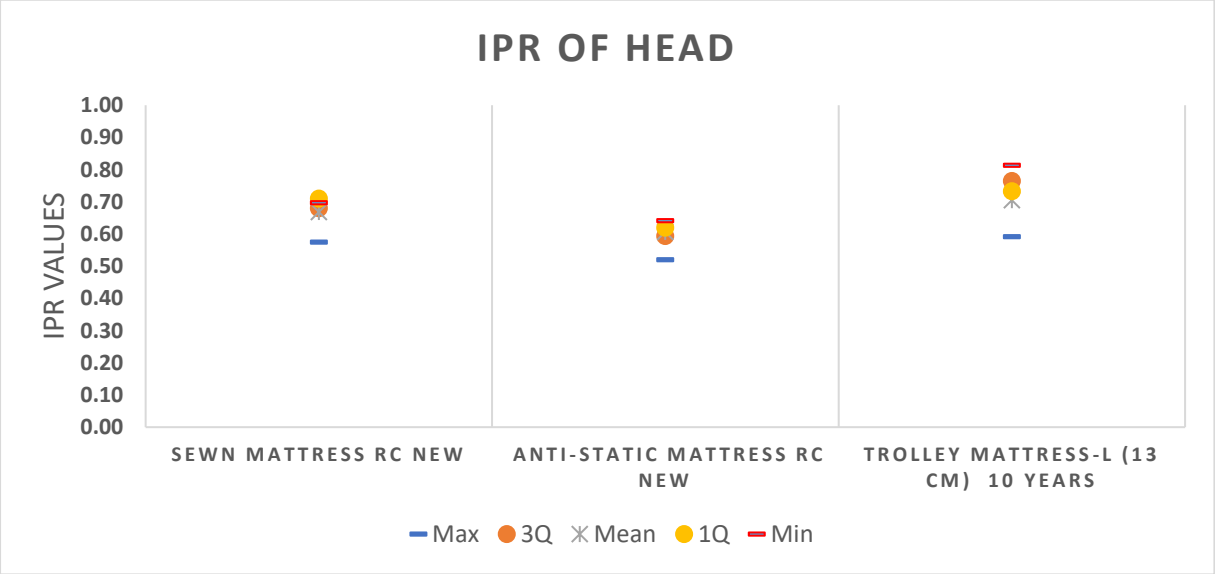

Figure 4.27: IPR values for the head on the three medical imaging mattresses.

Table 4.8: IPR Values for the Five Weights for the Sacrum on the Three Medical Imaging Mattresses.

	IPR of Sacrum				
Mattress name (thickness 2.5 cm)	**Max Weight**	**3Q Weight**	**Mean Weight**	**1Q Weight**	**Min Weight**
Sewn Mattress RC new	0.60	0.64	0.70	0.58	0.84
Anti-Static Mattress RC new	0.42	0.42	0.43	0.45	0.71
Trolley Mattress-L (13 cm) ¥	0.42	0.43	0.46	0.52	0.75

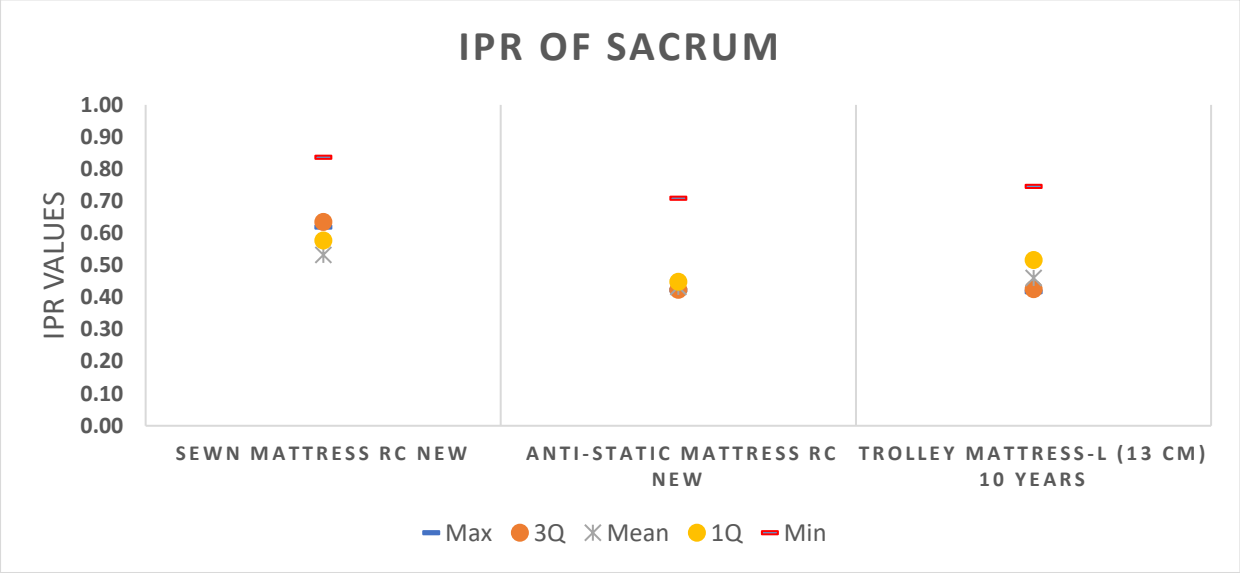

Figure 4.28: IPR values for the sacrum on the three medical imaging mattresses.

Table 4.9: IPR Values for the Heels on the Three Medical Imaging Mattresses.

	IPR of Heels				
Mattress name (thickness 2.5 cm)	**Max Weight**	**3Q Weight**	**Mean Weight**	**1Q Weight**	**Min Weight**
Sewn Mattress RC new	0.90	0.94	0.74	0.95	0.68
Anti-Static Mattress RC new	0.82	0.85	0.67	0.53	0.78
Trolley Mattress-L (13 cm) ¥	0.89	0.92	0.54	0.76	0.75

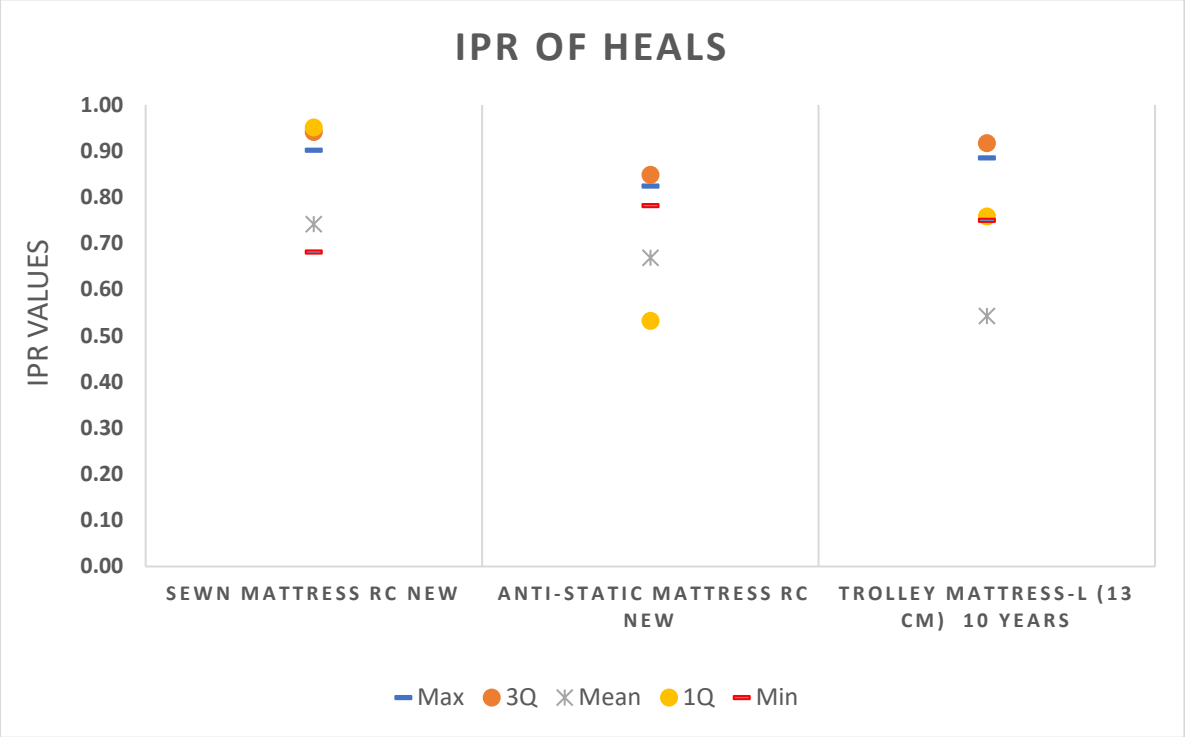

Figure 4.29: IPR values for the heels on the three medical imaging mattresses.

4.9.3.2. For radiation measurements

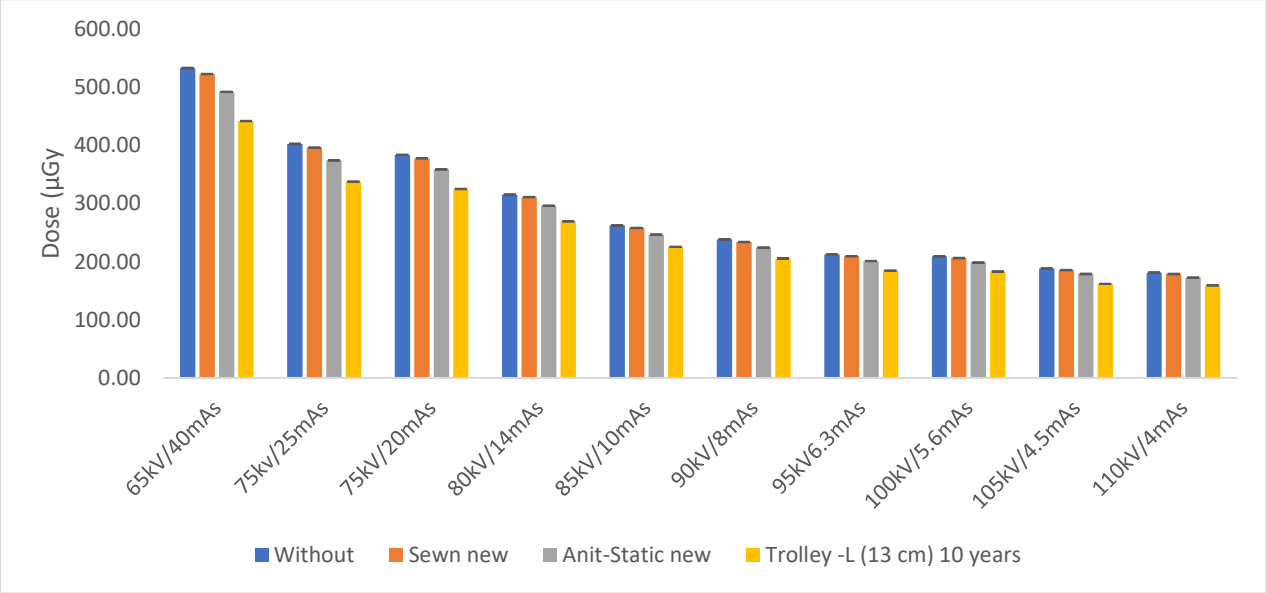

Figure 4.30: Variations in radiation attenuation for the three mattresses with SD.

4.9.3.3. For IQ measurements

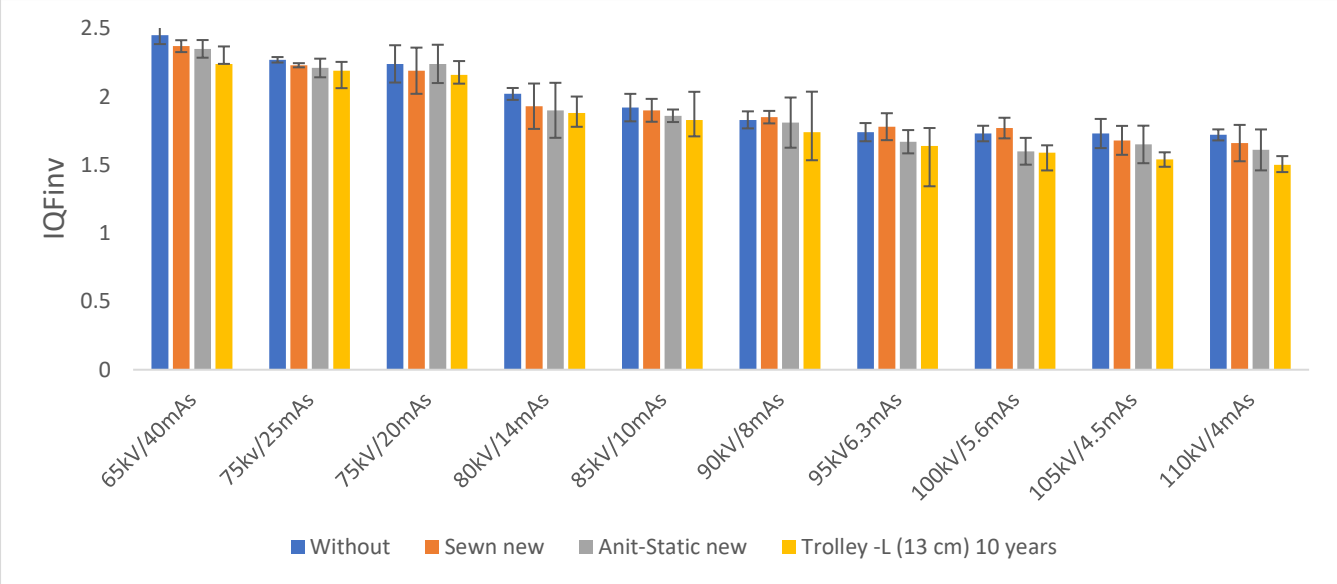

Figure 4.31: Variations in physical IQ for the three mattresses and the new mattresses with SD.

Statistically significant differences ($p < .05$) were found between the PPIs with and without the X-ray table mattress for all body parts and mattress types. The type and age of the mattress were also found to affect the reduction in PPIs.

IQ and radiation dose data were analysed using SPSS version 22.0 (IBM Inc., Armonk, NY, USA). To select the most valid statistical test, the Shapiro–Wilk test was used to investigate the normality of the data. As both IQ and radiation dose data were found to be normally distributed ($p > .05$), a paired t-test was used to compare the IQ and radiation doses with and without a mattress.

4.9.4. Benefits of conducting the pilot study

The pilot study had three benefits. First, by using a phantom instead of humans, the X-ray table mattresses could be compared in a reliable, valid, and reproducible fashion, which

may not have been possible with human volunteers. Data arising from this study could have value in the testing of X-ray mattresses that are in routine use. It could help assess different designs for mattress development and provide baseline/performance data for manufacturers to present at point of sale. Such data could be provided by mattress manufacturers to enable buyers to match mattress characteristics to imaging demands and underlying patient populations.

Second, PPIs were significantly reduced when an X-ray table mattress was used, meaning that using a mattress reduces the probability of PU formation. The two X-ray table mattresses displayed a range of interface pressure distributions, with the older mattress (the trolley mattress) being less able to redistribute pressure. These findings could be either because mattress design has changed in recent years, with new materials being used that have better pressure redistribution properties or that the older mattress could be worn down, negatively affecting its ability to redistribute pressure. To minimise PU formation, this method could be used to identify clinical mattresses that need replacing.

Finally, the results of the pilot study showed that the thin (2.5 cm) mattresses had little impact on dose attenuation and thus had no negative impact on diagnostic quality. By contrast, the thicker mattresses showed the most absorption. Regarding IQ, a statistically significant reduction was found for the thin mattresses. Each mattress type had a different impact on IQ, which reduced as kVp increased. Additionally, the thicker mattress (Trolley-L, 13 cm) demonstrated the lowest IQ for all acquisition values.

After validation, the method was applied to the main study using 24 X-ray mattresses from four hospitals and one company. These X-ray table mattresses were used in general X-ray rooms and all had the same thickness (2.5 cm), except for three of the mattresses: one X-ray trolley mattress (13 cm) and two mattresses used on X-ray screening tables (8 cm and 5 cm). In medical imaging, the thickness of a mattress is a physical parameter. Standard polyfoam

mattresses are regulated to ensure uniform thickness, tensile strength, and their ability to withstand fire. The standard polyfoam used in mattresses and wheelchair seats has a low density and can bear the weight of the patient spread evenly over a large surface area. A search of the literature indicated that almost no studies exist regarding pressure redistribution, X-ray attenuation or image degradation in the design and development of X-ray table mattresses. As such, it is not possible to describe the characteristics of the mattresses used in this validation study regarding these characteristics.

4.10. Chapter Summary

This chapter presented the proposed method for evaluating X-ray mattresses by measuring the pressure redistribution in the three areas most at risk of PUs: the head, the sacrum, and the heels. The rationale for using a 3D anthropomorphic phantom created by 3D printing and based on CT datasets was also explained. In addition, this chapter evaluated the steps required to convert DICOM image data into STL format ready for 3D printing. Subsequently, further work within this chapter has been shown to be necessary in developing the correct use of this method which also includes radiation dose measurements and the forms of dose detectors; the experiment for the dosimetry test; and the description of solid-state dosimeter (RaySafe X2, Unfors RaySafe AB, Billdal, Sweden). Also included was a description of the evaluation method development for image quality measurements of patient physiology and anatomy, a contrast-detail phantom (CDRAD 2.0) description, and CDRAD Analyser and Data and Statistical Analyses, which involved normality tests and Shapiro-Wilk tests. The following chapter presents the results of this research.

Chapter Five: Results

5.1. Overview

This chapter presents the results of the validation and the main study in a descriptive form using means, SDs, tables, graphs and scatter plot graphs. The deductive statistics results are also displayed, while significance levels show any statistical differences between the variables. The results of the interface pressure distribution, radiation dose and IQ experiments are provided for all mattresses.

The results are presented under five subheadings: pressure distribution, IPR values, radiation dose, IQ versus radiation dose and access parameters used. The results of the pressure distribution from the 3D phantom validation experiments, which were subsequently used in the main study, are given first with an explanation of each method. To obtain the required weights, the ratio of each anatomic part of a human was calculated and applied to the phantom using dried sand. The shape of the patients was also compared with that of the phantom parts. This method was useful for verifying the validity of the use of phantoms instead of humans. The weights were applied to different mattresses used in diagnostic imaging practices to ascertain the validity of this new method. The results of the validation study show that the new method is satisfactory and can thus be used to measure the pressure of the specific IP jeopardy areas of a human. The results of the radiation dose experiment and the IQ data are presented as a series of bar charts.

5.2. Pressure Distribution Results

This section contains pressure data from the initial pilot study used to validate the 3D phantom and the associated method. It also presents the interface pressure data results from the main study, which assessed 24 mattresses.

5.2.1. Validation data for the 3D phantom and associated method

5.2.1.1.Data sources

To establish the weight of the sand needed to simulate a range of human weights in the phantom, data were accessed from an existing study that used human volunteers (Webb, 2018). The volunteers' characteristics reflecting the characteristics of 24 females and 3 males were as follows: average height of 164.63 cm (SD = 7.64), average BMI of 28.18 (SD = 6.75), average weight of 77.04 kg (SD = 22.18) and a weight range of 50-148 kg. For the 3D phantom, these 27 volunteers were grouped into five weight categories: maximum (148 kg), third quartile (84 kg), mean (76 kg), first quartile (64 kg) and minimum (50 kg). To represent these five categories, the average weights for each were calculated from XSensor data using a memory foam mattress to determine the amount of sand to be added to the phantom's heels, pelvis and head (see the last column of Table 5.1).

Table 5.1: PPI for the Phantom and Humans.

Weight category	PPI for human volunteer data (average and SD) (mmHg)			PPI for the 3D phantom data (average and SD) (mmHg)			Weight added to 3D phantom (kg)		
	Head	**Pelvis**	**Heels**	**Head**	**Pelvis**	**Heels**	**Head**	**Pelvis**	**Heels**
Maximum	47.3 ± 1.18	54.6 ± 1.24	56 ± 3.49	46.6 ± 2.76	57.4 ± 2.41	55.4 ± 1.38	**6**	**37**	**3**
Third quartile	38.7 ± 2.02	44.1 ± 2.67	34.7 ± 2.00	39.1 ± 2.33	47.1 ± 1.75	37.6 ± 1.93	**3**	**30**	**1.3**
Mean	33.6 ± 1.66	39.6 ± 1.00	29.8 ± 1.25	35.3 ± 2.08	41.5 ± 2.52	31 ± 2.60	**2.5**	**24**	**1**
First quartile	30 ± 1.77	34.3 ± 2.40	22.5 ± 2.21	30.3 ± 2.31	35.9 ± 1.81	24.9 ± 1.66	**2**	**21**	**0.8**
Minimum	22.1 ± 1.32	25.4 ± 2.61	18.8 ± 0.50	22.5 ± 1.34	24.9 ± 1.10	22.5 ± 1.67	**1.5**	**10**	**0.3**

5.2.2. Validation of the 3D phantom

For the pelvis, heels and head, PPI and interface pressure profiles were compared between the 3D phantom and the human volunteers. In both cases, a memory foam mattress was used to collect data on interface pressure.

Prior to conducting the phantom pressure experiments, QC was undertaken to determine whether the weights placed on one ‘body part’ had an impact on the XSensor interface pressure reading of another ‘body part’. That is, whether the weight placed on the pelvis impacted the readings taken at the heels and head, as all sections of the phantom were linked. It was essential to ensure that this did not occur, as the weights added had been

calculated to mimic those that would be expected for each respective weight group. This experiment involved placing the maximum sand weights on the head, then the pelvis, then the heels one at a time to determine whether a change in interface pressure occurred at the other locations (see Figures 4.8A, 4.8B, Section 4.3.5, Page 92). The percentage difference in the weights was calculated using the equation shown in Section 4.3.5, Page 92. The results show that the percentage differences varied from 1.3% to 5.8%, indicating that the weight transference is quite small and only minor errors are imposed.

5.2.2.1. Comparison between human volunteers and the 3D phantom – pressure profile shape analysis using ImageJ software

5.2.2.1.1. Pressure Profiles

Multiple pressure profile graphs were created using phantom and human volunteer XSensor interface pressure data to compare the five weight categories for the pelvis, head, and heels of the phantom and human volunteers. Figure 5.1 shows an example of a pressure profile comparison between the human (top) and phantom (bottom). As can be seen, the whole-body outline of the human is visible compared to only the jeopardy areas (head, pelvis and heels) of the phantom.

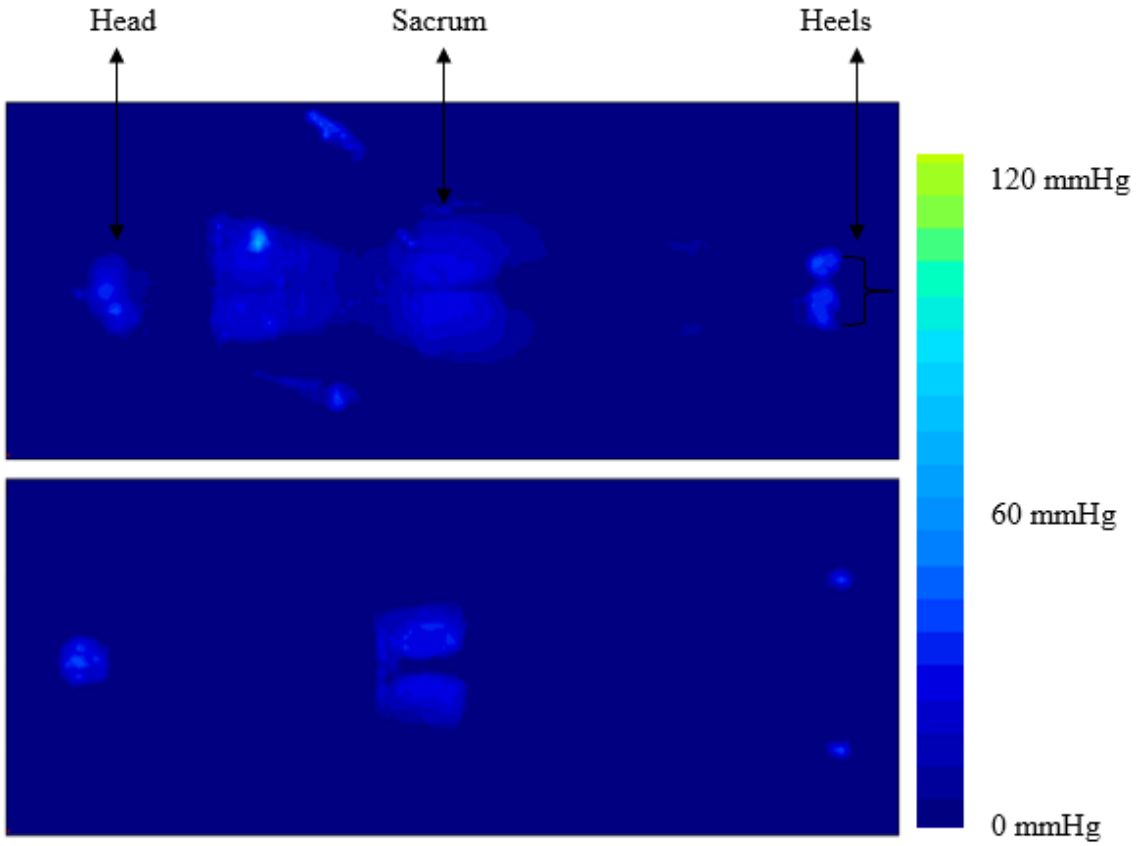

Figure 5.1: The interface pressure map of a human (top) and the phantom (bottom). The interface pressure values are mapped as a colour gradient. The scale to the right of the maps displays the interface pressure for the corresponding colours of the scale, ranging from 0 mmHg to 120 mmHg.

Figures 5.2A, 5.2B and 5.2C show example interface pressure line profiles for the head, pelvis, and heels, respectively, for one human volunteer's data in the minimum weight group. A visual comparison of the human/phantom profiles shows similarity for the three jeopardy (remarkably dissimilar, especially the pelvis) areas in the five weight categories between the phantom and the human. An applied assessment of the data for all 27 human volunteers showed similarity between them.

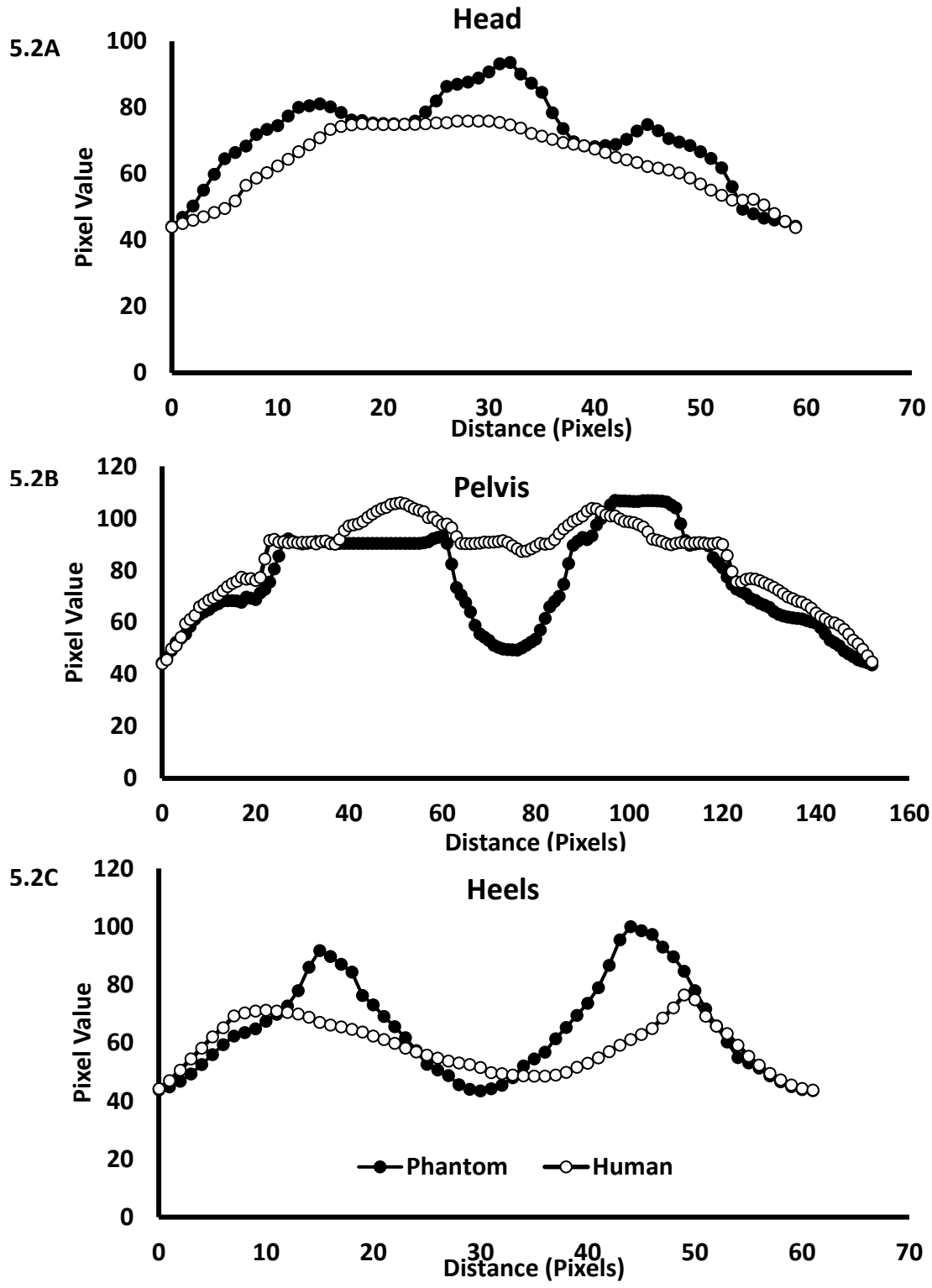

Figure 5.2: (A), (B) and (C) show example line profiles of interface pressure for the head, pelvis and heels, respectively, for the minimum weight group. Phantom data are indicated by the black dots, and human data are indicated by the white dots.

5.2.2.1.2. Pressure results of the X-ray mattresses

The main study tested a complete range of X-ray table mattresses from four hospitals and one company. 21 mattresses had the same thickness of 2.5 cm, one X-ray trolley mattress had 13 cm, and two mattresses used on X-ray screening tables had 8 cm and 5 cm. Pressure data using the phantom was also obtained from a hard surface – a typical X-ray table in the radiography suite at the University of Salford. The pressure data for all mattress types and the hard surface is presented below.

5.2.3 Pressure data – thin mattresses

5.2.3.1 3D phantom – head

Table 5.2 shows the PPIs for the head. Compared with the newer mattresses, older mattresses, such as the H3 Clinic R Mattress and H3 R1 Mattress which were both 20 years of age, had higher mean PPIs for the head: 88.9 ± 1.4 and 86.9 ± 1.9 mmHg, respectively. Conversely, new mattresses, such as the Sewn Mattress and Anti-Static Mattress RC, recorded the lowest mean PPIs for the head: 54.8 ± 2.1 and 49.6 ± 1.1, respectively.

Table 5.2: The PPIs for the head for thin mattresses.

	PPI for the head (mmHg) ± SD				
Mattress name (thickness of 2.5 cm)	**Max ± SD**	**3Q ± SD**	**Mean ± SD**	**1Q ± SD**	**Min ± SD**
Hard surface/X-ray table	95.4 ± 1.8	74.8 ± 1.2	71.5 ± 1.5	65.9 ± 1.5	60.5 ± 1.8
H3 Clinic R Mattress &	88.9 ± 1.4	71.3 ± 1.5	68.6 ± 2.4	60.1 ± 1.8	58.8 ± 2.6
H3 R1 Mattress &	86.9 ± 1.9	70.9 ± 1.1	63.3 ± 2.9	59.1 ± 2.4	49.2 ± 2.0
H1 R1R1 Mattress @	92.3 ± 3.6	68 ± 1	61.2 ± 1.8	52.6 ± 2.5	49.3 ± 1.7

H1 R1R5 Mattress @	88.5 ± 2.5	68.9 ± 2	60.6 ± 3.5	55.4 ± 4	50.1 ± 3
H3 Phase R1 Mattress ¥	93.6 ± 2.4	73.9 ± 3	66.4 ± 2.1	59 ± 1.9	56.5 ± 2.6
H3 R2 Mattress ¥	90.2 ± 2.1	63.5 ± 1.9	54 ± 2.1	48.4 ± 1.7	41.3 ± 2.7
H3 R4 Mattress ¥	83 ± 0.7	61.7 ± 1.2	57.7 ± 2.2	55.6 ± 1.5	43.3 ± 2.1
H3 R3 Mattress ¥	79.7 ± 3.5	57.1 ± 2	52.6 ± 1.5	45.9 ± 1	42 ± 2.2
H1 R2R2 Mattress ¥	76.2 ± 1.5	61.7 ± 1.7	59.1 ± 1.9	57.3 ± 2.2	52 ± 1.6
H1 R2R4 Mattress ¥	66.1 ± 2.6	56.3 ± 3.2	52.1 ± 1.5	49.2 ± 2.5	46.9 ± 2
Salford Lab Mattress L ¥	65.2 ± 1.2	54.6 ± 1.9	50.1 ± 1.3	46.7 ± 1.9	44.6 ± 1.4
H1 R2R3 Mattress ©	71 ± 1.4	62.8 ± 1.2	56.7 ± 2.1	53.1 ± 1.1	48.5 ± 1.6
H1 R1 R2 Mattress #	81.6 ± 1.5	68.3 ± 1.3	61.1 ± 1	55.6 ± 2.3	51.2 ± 2.3
H2 R4 Mattress #	65.9 ± 1.4	59.1 ± 1.8	55.3 ± 1.1	54.7 ± 1.1	52.8 ± 2.4
H3 Phase R2 Mattress £	79.8 ± 1.7	55.6 ± 2.2	50.7 ± 1.6	48.8 ± 2.1	39.9 ± 1.2
H2 R3 Mattress §	71.9 ± 2.7	69.5 ± 1.6	62.9 ± 1.4	60.9 ± 1.5	55 ± 2
H4 R6 Mattress Ø	77.3 ± 2.4	50.3 ± 1.7	45.9 ± 2.1	45.1 ± 1.8	42.3 ± 1.6
H1 R1R3 Mattress ~~A~~	63.9 ± 1.4	53 ± 1.6	48 ± 2.1	40.8 ± 1.8	34.4 ± 1.7
Sewn Mattress RC ~~A~~	54.8 ± 2.1	50.9 ± 2.3	47.8 ± 1.5	46.8 ± 1.5	42.2 ± 1
Anti-Static Mattress RC ~~A~~	49.6 ± 1.1	44.4 ± 1.1	43.4 ± 0.7	40.8 ± 0.9	38.8 ± 1.4
Black-Grey (Welded) Mattress RC ~~A~~	81.3 ± 1.6	61.2 ± 2.6	55.2 ± 1.4	50.2 ± 1.1	47.5 ± 1

Note. The symbols indicate the mattresses' age: **&**: 20 years, **@**: 15 years, **¥**: 10 years, ©: 8 years, **#**: 7 years, **£**: 6 years, **§**: 4 years, **Ø**: 1 year, **~~A~~**: new. **H1**: hospital A, **H2**: hospital B, **H3**: hospital C, **H4**: hospital D, **L**: University of Salford lab, **RC**: Rothband Company, **R**: room number. Weight categories: Max = maximum, 3Q = 3rd quartile, 1Q = 1st quartile, min = minimum.

Figure 5.3 shows a graphic representation of the PPIs for the 3D phantom head for all 2.5 cm mattresses across the five weight categories. Excluding the hard surface, data are presented from left to right, from the oldest to the newest mattress.

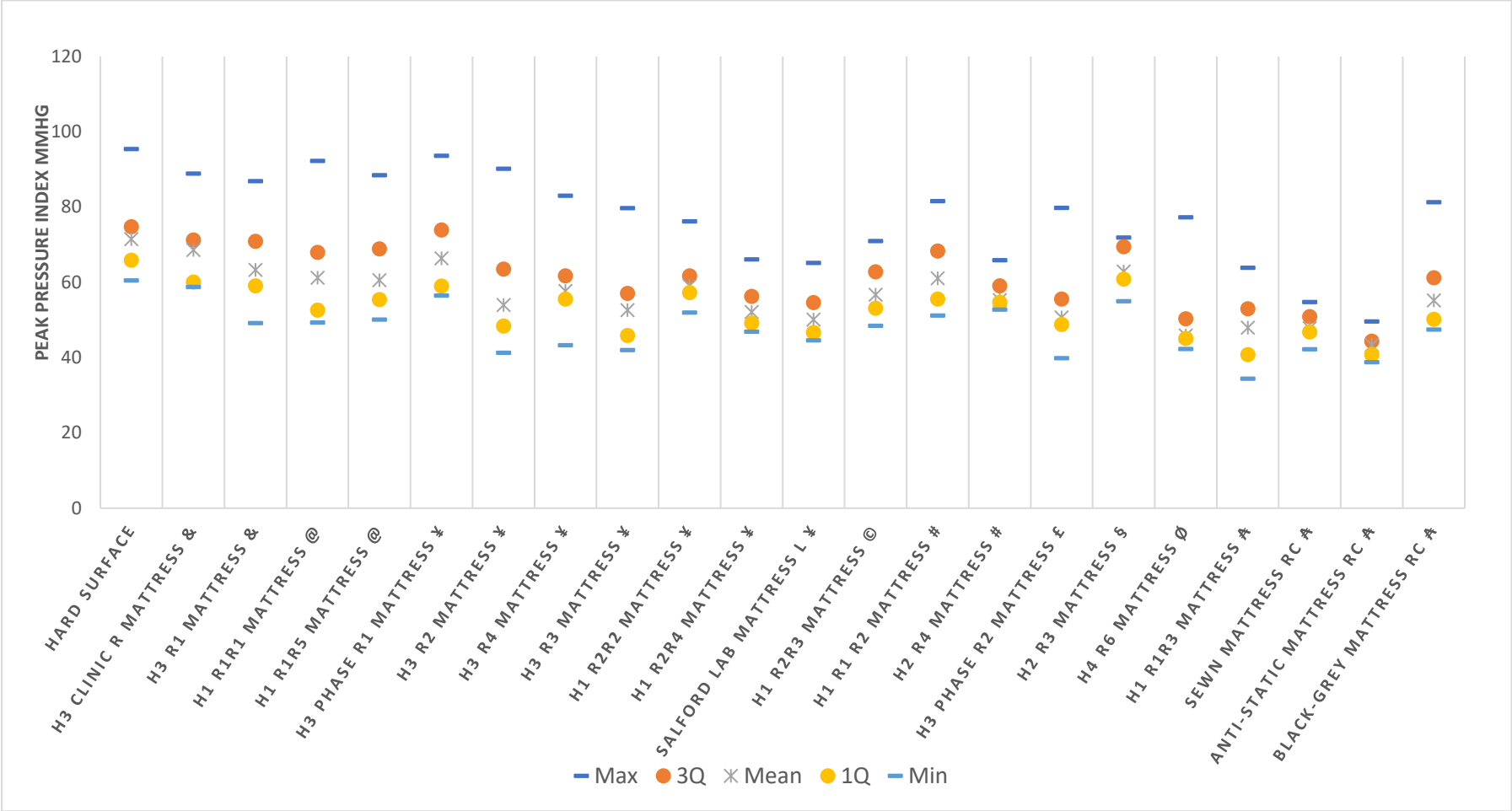

Figure 5.3: PPIs for the 3D phantom heads for all 2.5-cm mattresses in the five weight categories. Excluding the hard surface, data are presented from left to right, from the oldest to the newest mattress.

5.2.3.2. 3D phantom – sacrum

Table 5.3 shows the PPIs for the 3D phantom sacrum for all 2.5 cm mattresses in the five weight categories. The highest PPI for the 3D phantom sacrum was recorded on the hard surface/X-ray table (131 ± 2.4 mmHg), the mean PPI for the sacrum was on the Anti-Static Mattress RC (55.4 ± 1.8 mmHg), and the lowest PPI was seen for the H4R6 Mattress (43 ± 1.3 mmHg).

Table 5.3: The PPIs for the 3D phantom sacrum for thin mattresses.

	PPI for the sacrum (mmHg) ± SD				
Mattress name (thickness of 2.5cm)	**Max ± SD**	**3Q ± SD**	**Mean ± SD**	**1Q ± SD**	**Min ± SD**
Hard surface/X-ray table	131.0 ± 2.4	119.3 ± 1.8	101.8 ± 1.4	89.3 ± 1.6	50.9 ± 0.8
H3 Clinic R Mattress &	120.9 ± 3.6	111.6 ± 3.5	99.1 ± 1.5	75.3 ± 1.9	44.2 ± 1.7
H3 R1 Mattress &	122.7 ± 4.9	109.8 ± 3.6	93.7 ± 2.6	73.8 ± 2.6	47.9 ± 1.2
H1 R1R1 Mattress @	122.5 ± 3.0	113.8 ± 0.9	98.3 ± 1.2	65.8 ± 1.4	45.7 ± 2.9
H1 R1R5 Mattress @	110.7 ± 3.6	93.4 ± 1.4	79.2 ± 2.6	62.5 ± 2.4	47.5 ± 3.1
H3 Phase R1 Mattress ¥	128.9 ± 4.8	108.7 ± 1.9	70.4 ± 1.9	66.4 ± 2.8	51.8 ± 2.2
H3 R2 Mattress ¥	107.7 ± 1.8	81.5 ± 1.7	56.8 ± 1.8	54.1 ± 4.2	39.8 ± 2.7
H3 R4 Mattress ¥	80.5 ± 1.5	72.5 ± 0.9	68.4 ± 1.7	63.7 ± 1.7	41.6 ± 1.6
H3 R3 Mattress ¥	130.5 ± 3.9	100.6 ± 2.7	78.9 ± 2.6	61.4 ± 1.8	41.2 ± 2.1
H1 R2R2 Mattress ¥	106.5 ± 2.9	98.8 ± 2.8	86.1 ± 2.1	82.7 ± 0.7	48.6 ± 0.9
H1 R2R4 Mattress ¥	91.6 ± 2.9	87.9 ± 2.5	82.6 ± 1.3	73.9 ± 2.1	45.5 ± 2.3
Salford Lab Mattress L ¥	73.2 ± 1.9	68.0 ± 1.2	56.3 ± 1.2	45.3 ± 2.4	39.0 ± 1.2
H1 R2R3 Mattress ©	128.0 ± 2.4	107.0 ± 1.3	86.9 ± 2.6	79.5 ± 1.3	47.1 ± 1.4
H1 R1 R2 Mattress #	96.2 ± 1.5	87.6 ± 1.8	78.4 ± 1.6	71.9 ± 1.4	42.7 ± 1.2
H2 R4 Mattress #	95.0 ± 1.8	60.7 ± 1.3	47.3 ± 1.3	41.6 ± 2.2	35.1 ± 1.0
H3 Phase R2 Mattress £	93.9 ± 3.0	74.9 ± 2.4	57.4 ± 1.4	51.7 ± 0.8	47.4 ± 3.2
H2 R3 Mattress §	91.0 ± 1.5	76.6 ± 0.8	54.5 ± 1.1	43.1 ± 1.1	32.5 ± 2.0
H4 R6 Mattress Ø	77.6 ± 2.9	49.3 ± 1.3	43.0 ± 1.3	39.8 ± 1.2	35.2 ± 1.3
H1 R1R3 Mattress Ѧ	75.0 ± 1.4	65.2 ± 1.7	53.8 ± 1.7	47.5 ± 1.8	39.8 ± 1.2
Sewn Mattress RC Ѧ	81.1 ± 2.1	75.8 ± 1.3	54.2 ± 1.3	51.6 ± 1.9	42.6 ± 2.4
Anti-Static Mattress RC Ѧ	55.4 ± 1.8	50.6 ± 1.4	44.1 ± 1.5	40.1 ± 1.5	36.1 ± 1.0

Black-Grey (Welded) Mattress RC Ⱥ	85.7 ± 1.9	79.9 ± 1.5	60.4 ± 1.7	58.6 ± 1.8	40.3 ± 1.7

Note: The symbols indicate the age of the mattresses: **&**: 20 years, **@**: 15 years, **¥**: 10 years, **©**: 8 years, **#**: 7 years, **£**: 6 years, **§**: 4 years, **Ø**: 1 year, **Ⱥ**: new. **H1**: hospital A, **H2**: hospital B, **H3**: hospital C, **H4**: hospital D, **L**: University of Salford lab, **RC**: Rothband Company, **R**: room number. Weight categories: Max = maximum, 3Q = 3rd quartile, 1Q = 1st quartile, min = minimum.

Figure 5.4 shows the PPIs for the 3D phantom sacrum for all 2.5 cm mattresses in the five weight categories. Excluding the hard surface, data are presented from the oldest mattress on the left to the newest mattress on the right.

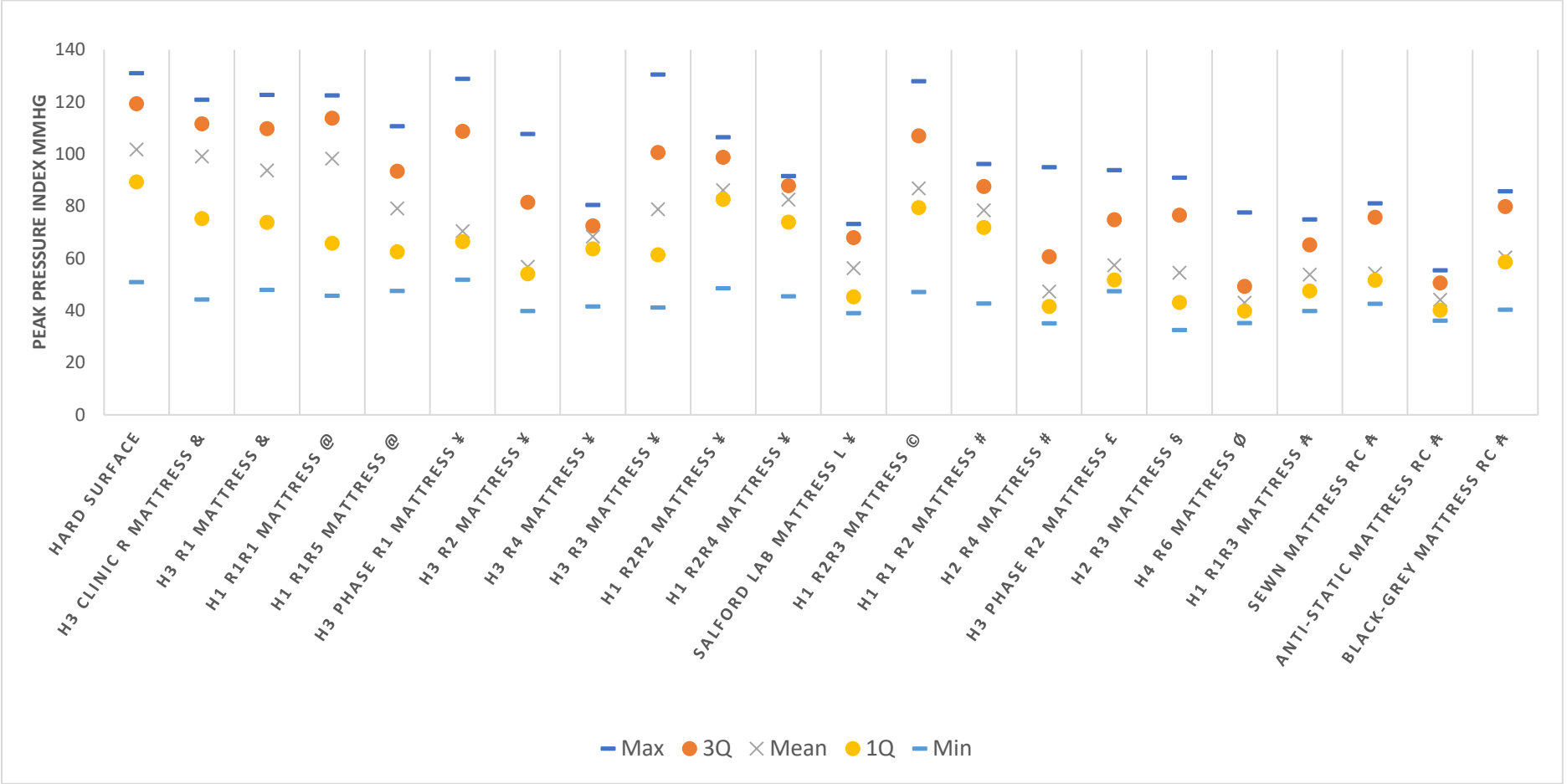

Figure 5.4: The PPI of the 3D phantom sacrum for all 2.5-cm mattresses in the five weight categories. Excluding the hard surface, data are presented with the oldest mattress on the left to the newest mattress on the right.

5.2.3.3. 3D phantom – heels

Table 5.4 shows the PPIs for the 3D phantom heels for all 2.5 cm mattresses in the five weight categories. The highest PPI for 3D phantom heels was recorded on the hard surface/X-ray table (101.9 ± 1.9 mmHg). The lowest PPIs were obtained for the H2 R3 Mattress (4 years) and the H4 R6 Mattress (1 year) with 58.7 ± 1.2 and 44.4 ± 2.0 mmHg, respectively.

Table 5.4: The PPIs for the 3D phantom heels for thin mattresses.

	PPI for the heels (mmHg) ± SD				
Mattress name (thickness of 2.5cm)	**Max ± SD**	**3Q ± SD**	**Mean ± SD**	**1Q ± SD**	**Min ± SD**
Hard surface	101.9 ± 1.9	87.1 ± 0.9	81.3 ± 2.5	57.1 ± 1.1	38 ± 1.2
H3 Clinic R Mattress &	88.9 ± 1.0	75.4 ± 1.6	72 ± 2.0	51.7 ± 1.9	34.5 ± 2.3
H3 R1 Mattress &	97.7 ± 2.4	78.2 ± 1.9	73.3 ± 1.8	49.8 ± 1.5	33.9 ± 1.3
H1 R1R1 Mattress @	97 ± 2.4	81.9 ± 0.5	60.5 ± 1.7	46.3 ± 1.9	34.2 ± 1.1
H1 R1R5 Mattress @	97.3 ± 3.5	78.1 ± 2.3	70.2 ± 2.4	53.9 ± 3.5	35.1 ± 2.4
H3 Phase R1 Mattress ¥	70.6 ± 2.2	67.3 ± 2.4	65.4 ± 2.0	41.2 ± 2.5	35.3 ± 1.8
H3 R2 Mattress ¥	53 ± 1.7	42.3 ± 2.1	41.9 ± 1.3	31.5 ± 3.1	29.3 ± 1.8
H3 R4 Mattress ¥	73.1 ± 2.0	65.8 ± 2.8	63.2 ± 2.7	37.8 ± 2.3	36.4 ± 1.2
H3 R3 Mattress ¥	89.9 ± 4.1	77.3 ± 2.6	56.7 ± 1.7	40.6 ± 2.5	39 ± 2.1
H1 R2R2 Mattress ¥	87.3 ± 0.8	78.3 ± 1.8	77.3 ± 1.4	46.7 ± 1.2	34 ± 1.9
H1 R2R4 Mattress ¥	96.5 ± 0.9	80.4 ± 2.0	78.4 ± 1.3	50.2 ± 1.3	36.6 ± 2.1
Salford Lab Mattress L ¥	68.6 ± 1.7	51.5 ± 1.9	45.9 ± 1.2	37.4 ± 1.8	31.5 ± 1.7
H1 R2R3 Mattress ©	88.7 ± 1.9	72.2 ± 1.5	70.3 ± 1.3	45.4 ± 2.9	37.4 ± 1.6
H1 R1 R2 Mattress #	79.2 ± 1.8	65 ± 1.7	65.2 ± 1.7	51.1 ± 1.5	28.2 ± 1.5

H2 R4 Mattress #	54.8 ± 1.4	49.6 ± 1.6	44.4 ± 2.1	43.1 ± 1.2	32.9 ± 2.3
H3 Phase R2 Mattress £	60.7 ± 0.9	58.1 ± 1.9	53 ± 1.6	39.6 ± 2.2	29.9 ± 1.9
H2 R3 Mattress §	58.7 ± 1.2	43.7 ± 1.5	35.8 ± 2.1	32 ± 1.5	29.3 ± 1.3
H4 R6 Mattress Ø	44.4 ± 2.0	38.5 ± 0.6	36.7 ± 1.2	36.1 ± 1.7	35.2 ± 1.6
H1 R1R3 Mattress Ⱥ	70.3 ± 0.6	65.1 ± 1.3	61.4 ± 1.5	36 ± 1.4	32.1 ± 1.5
Sewn Mattress RC Ⱥ	91.9 ± 2.6	82 ± 0.9	60.3 ± 1.7	54.3 ± 2.6	25.9 ± 2.3
Anti-Static Mattress RC Ⱥ	84 ± 1.2	73.9 ± 1.3	54.4 ± 1.8	30.4 ± 1.1	29.7 ± 1.0
Black-Grey (Welded) Mattress RC Ⱥ	76.2 ± 1.2	46 ± 2.6	41.4 ± 1.4	39.8 ± 1.0	33.4 ± 1.3

Note. The symbols indicate the mattresses' age: **&**: 20 years, **@**: 15 years, **¥**: 10 years, **©**: 8 years, **#**: 7 years, **£**: 6 years, **§**: 4 years, **Ø**: 1 year, **Ⱥ**: new. **H1**: hospital A, **H2**: hospital B, **H3**: hospital C, **H4**: hospital D, **L**: University of Salford lab, **RC**: Rothband Company, **R**: room number. Weight categories: Max = maximum, 3Q = 3rd quartile, 1Q = 1st quartile, min = minimum.

Figure 5.5 shows the PPI of the 3D phantom heels for all 2.5 cm mattresses in the five weight categories. Excluding the hard surface, data are presented from left to right starting with the oldest mattress.

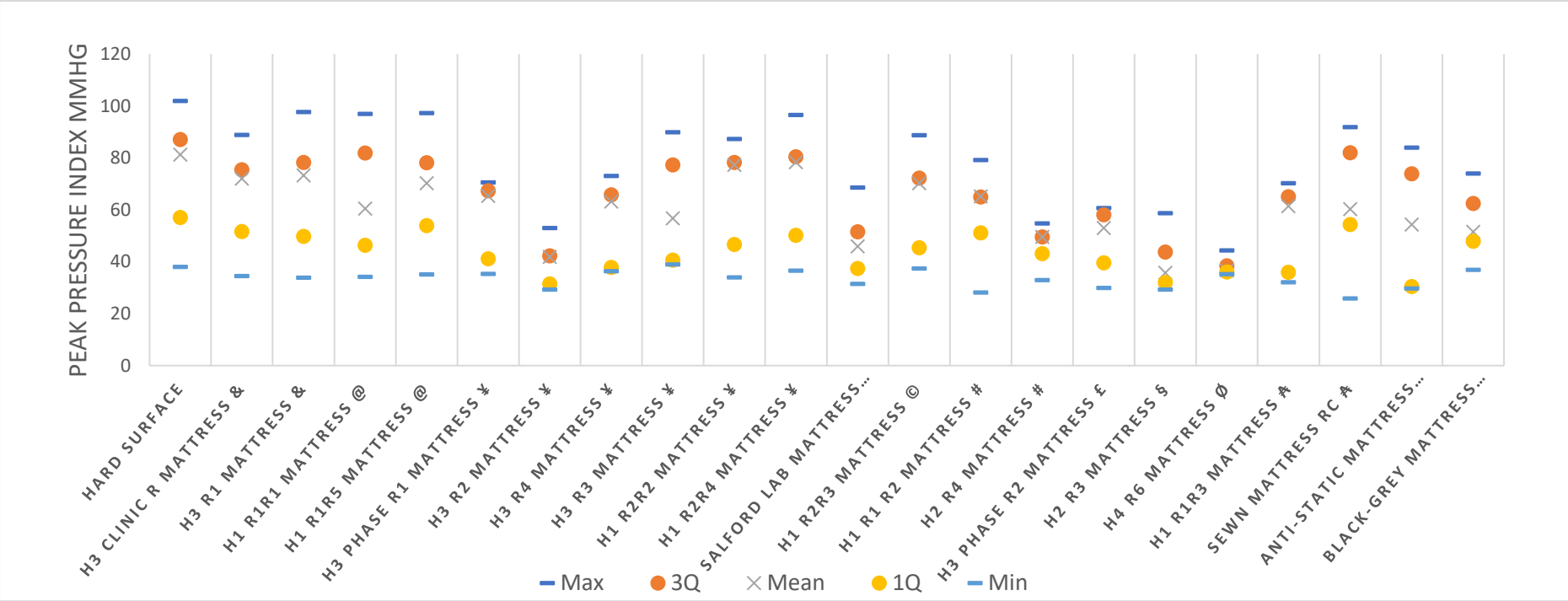

Figure 5.5: The PPI for the 3D phantom heels for all 2.5-cm mattresses in the five weight categories. Excluding the hard surface, data are presented from left to right starting with the oldest mattress.

Statistically significant differences ($p > .05$) were found between the PPI values, with and without using the X-ray table mattresses, for all 2.5 cm mattress types. The type and age of the mattresses were observed to have an impact on the PPI values, with the older mattresses showing a worse performance.

5.2.4. Pressure data – thicker mattresses

5.2.4.1. 3D phantom – head

Table 5.5 shows the PPI for the 3D phantom head for all thicker mattresses in the five weight categories. The highest PPI for the 3D phantom heels was recorded on a hard surface/s-ray table (71.5 ± 1.5 mmHg), while the lowest PPI was recorded for the H4 screening R mattress (8 cm) with 1 year of age (34.4 ± 1.0 mmHg). The 10-year-old Trolley Mattress L (13 cm) had a higher PPI (50.4 ± 1.3 mmHg) than the new mattress (40.5 ± 0.6 mmHg).

Table 5.5: The PPI for the 3D phantom head for thicker mattresses

	PPI for the head (mmHg) ± SD				
Mattress name (varying thicknesses)	**Max ± SD**	**3Q ± SD**	**Mean ± SD**	**1Q ± SD**	**Min ± SD**
Hard surface/X-ray table	95.4 ± 1.8	74.8 ± 1.2	71.5 ± 1.5	65.9 ± 1.5	60.5 ± 1.8
Trolley Mattress L (13 cm) ¥	56.5 ± 2.3	57.2 ± 2.5	50.4 ± 1.3	48.3 ± 1.6	49.2 ± 1.8
H4 Screening R Mattress (8 cm) Ø	41.1 ± 2.2	36.3 ± 1.8	34.4 ± 1.0	33.8 ± 2.2	34.9 ± 1.9
Black-Grey Mattress (Welded) RC (5 cm) Ⱥ	52.4 ± 1.0	40.5 ± 0.6	38.4 ± 1.7	37.1 ± 0.9	34.8 ± 1.8

Note. The symbols indicate the mattresses' age: **¥**: 10 years, **Ø**: 1 year, **Ⱥ**: new. **H1**: hospital A, **H2**: hospital B, **H3**: hospital C, **H4**: hospital D, **L**: University of Salford lab, **RC**: Rothband Company, **R**: room number. Weight categories: Max = maximum, 3Q = 3rd quartile, 1Q = 1st quartile, min = minimum.

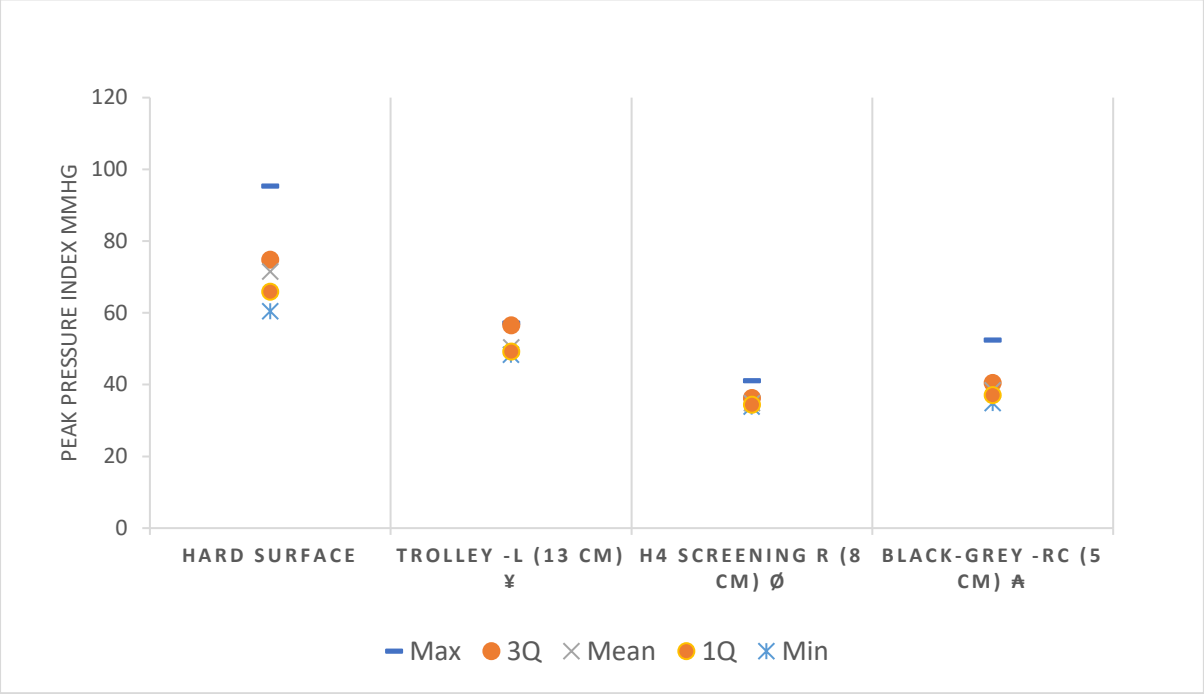

Figure 5.6: PPIs for the three thicker mattresses using the range of (sand) weights and the 3D phantom.

5.2.4.2. 3D phantom – sacrum

Table 5.6 shows the PPI of the 3D phantom head for all thicker mattresses in the five weight categories. The highest PPI for the 3D phantom heels was recorded on a hard surface/X-ray table (101.8 ± 1.4 mmHg), while the lowest PPI was obtained for the one-year-old H4 screening R mattress (8 cm) (34.2 ± 2.2 mmHg).

Table 5.6: The PPI of the 3D phantom head for thicker mattresses

	PPI for the sacrum (mmHg) ± SD				
Mattress name (varying thicknesses)	**Max ± SD**	**3Q ± SD**	**Mean ± SD**	**1Q ± SD**	**Min ± SD**
Hard surface/X-ray table	131 ± 2.4	119.3 ± 1.8	101.8 ± 1.4	89.3 ± 1.6	50.9 ± 0.8
Trolley Mattress L (13 cm) ¥	54.8 ± 2.3	50.8 ± 2.0	46.9 ± 0.5	46.1 ± 2.2	38 ± 1.0

H4 Screening R Mattress (8 cm) Ø	45.2 ± 2.7	41 ± 1.1	34.2 ± 2.2	30.2 ± 0.9	26.5 ± 1.8
Black–Grey Mattress (Welded) RC (5 cm) ₳	62.7 ± 1.3	49.5 ± 1.2	47.3 ± 1.2	43 ± 1.1	30.5 ± 1.5

Note. The symbols indicate the mattresses' age: **¥**: 10 years, **Ø**: 1 year, **₳**: new. **H1**: hospital A, **H2**: hospital B, **H3**: hospital C, **H4**: hospital D, **L**: University of Salford lab, **RC**: Rothband Company, **R**: room number. Weight categories: Max = maximum, 3Q = 3rd quartile, 1Q = 1st quartile, min = minimum.

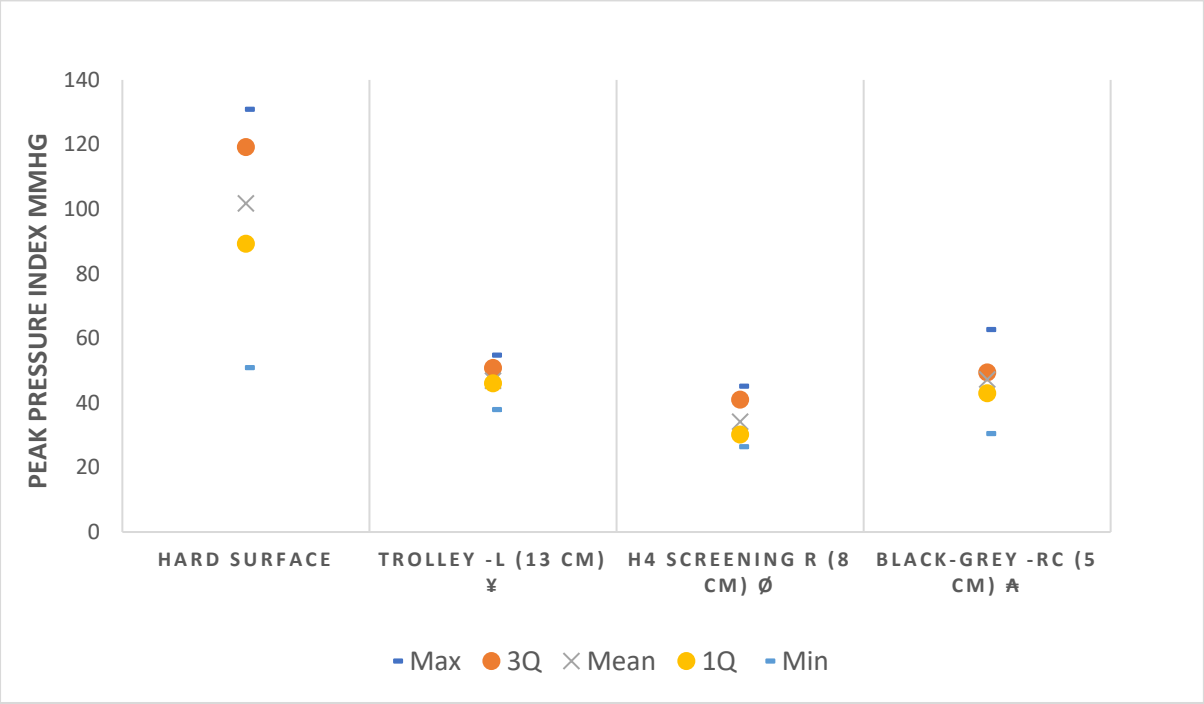

Figure 5.7: PPIs for the three thicker mattresses using the range of (sand) weights and the 3D phantom.

5.2.4.3.3D phantom – heels

Table 5.7 shows the PPI of the 3D phantom heels for all thicker mattresses across the five weight categories. The highest PPI for 3D phantom heels was recorded on a hard surface/s-ray table (81.3 ± 2.5 mmHg), and the lowest PPI was obtained for the one-year-old H4 screening R mattress (8 cm) (28.6 ± 2.5 mmHg).

Table 5.7: The PPI of the 3D phantom heels for thicker mattresses					
	PPI for the heels (mmHg) ± SD				
Mattress name (varying thicknesses)	**Max ± SD**	**3Q ± SD**	**Mean ± SD**	**1Q ± SD**	**Min ± SD**
Hard surface	101.9 ± 1.9	87.1 ± 0.9	81.3 ± 2.5	57.1 ± 1.1	38 ± 1.2
Trolley Mattress L (13 cm) ¥	90.2 ± 1.8	79.9 ± 3.9	44.1 ± 1.6	43.3 ± 1.8	28.5 ± 0.9
H4 Screening R Mattress (8 cm) Ø	37 ± 0.6	30.5 ± 1.0	28.6 ± 2.5	27.5 ± 1.9	25.8 ± 1.4
Black–Grey Mattress RC (5 cm) Ⱥ	76.2 ± 1.2	46 ± 2.6	41.4 ± 1.4	39.8 ± 1.0	33.4 ± 1.3

Note. The symbols indicate the mattresses' age: **¥**: 10 years, **Ø**: 1 year, **Ⱥ**: new. **H1**: hospital A, **H2**: hospital B, **H3**: hospital C, **H4**: hospital D, **L**: University of Salford lab, **RC**: Rothband Company, **R**: room number. Weight categories: Max = maximum, 3Q = 3rd quartile, 1Q = 1st quartile, min = minimum.

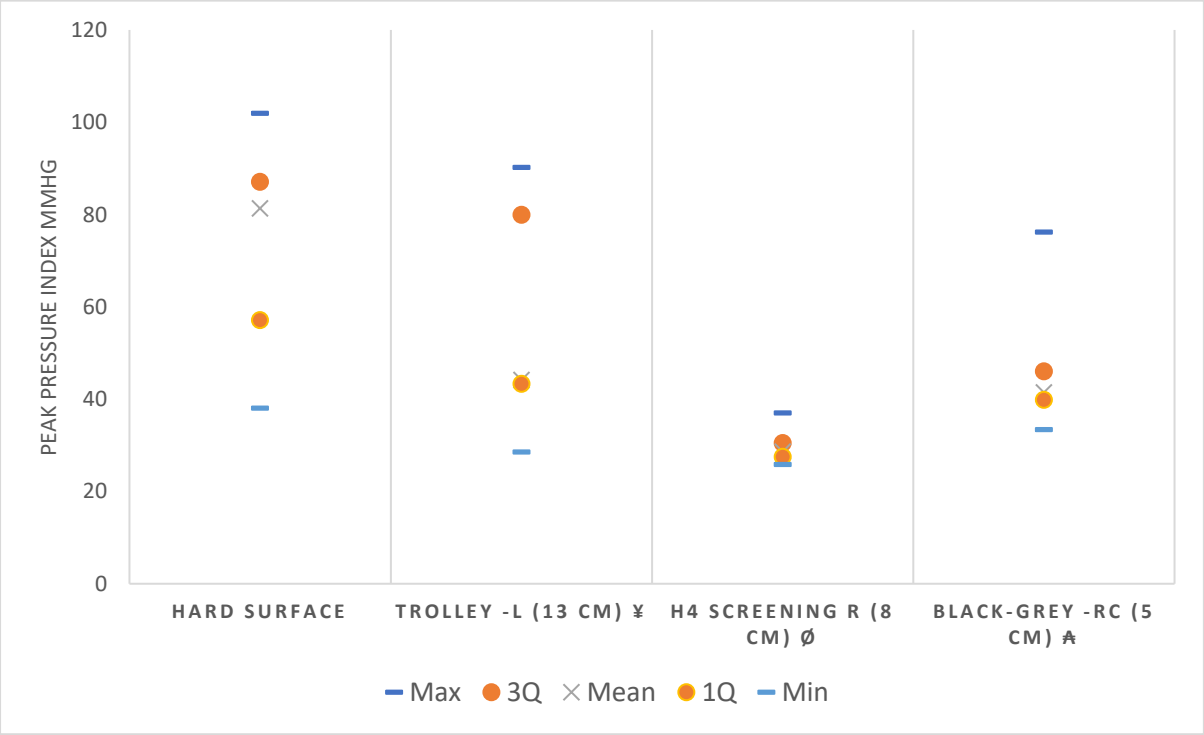

Figure 5.8: PPIs for the three thicker mattresses using the range of (sand) weights and the 3D phantom

Statistically significant differences ($p < .05$) were found between the PPI values with and without the X-ray table mattress for all body parts and mattress types. The type and age of the mattresses were observed to have an impact on the PPI, with older mattresses performing worse.

5.3. IPR Values

Using the phantom data, a novel IPR was developed to indicate a mattress's IPR efficiency. The IPR serves as a simple indicator that can be used to make comparisons among different mattresses and for the same mattress over time. It uses phantom PPIs from the head, pelvis and heels for comparing a 'mattress' (experimental condition) against 'no mattress' (control condition). This calculation was repeated for all five weights. Thus, for one mattress there were five IPR values for the head, five for the pelvis and five for the heels (where only one average value for both heels is presented). The formula for the IPR is indicated in Section 4.3.4.3.

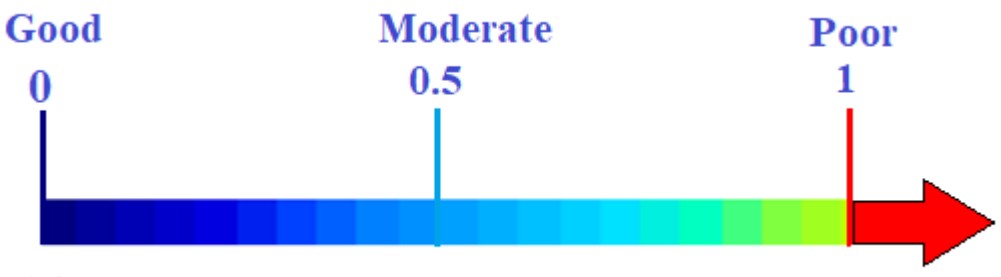

Figure 5.5.9: The IPR values from the best to the worst performance.

5.3.1. IPR Values for the 2.5-cm Mattresses

5.3.1.1. Head

Table 5.8 shows the IPR values. The highest mean value, along with the 1Q and 3Q, was for the H3 Clinic R Mattress.

Table 5.8: The IPR values of the head for the 2.5 -cm Mattresses

	IPR for the head				
Mattress name (thickness of 2.5 cm)	**Max Weight**	**3Q Weight**	**Mean Weight**	**1Q Weight**	**Min Weight**
H3 Clinic R Mattress &	0.93	0.95	0.96	0.91	0.97
H3 R1 Mattress &	0.91	0.95	0.89	0.90	0.81
H1 R1R1 Mattress @	0.97	0.91	0.86	0.80	0.81
H1 R1R5 Mattress @	0.93	0.92	0.85	0.84	0.83
H3 Phase R1 Mattress ¥	0.98	0.99	0.93	0.90	0.93
H3 R2 Mattress ¥	0.95	0.85	0.76	0.73	0.68
H3 R4 Mattress ¥	0.87	0.82	0.81	0.84	0.72
H3 R3 Mattress ¥	0.84	0.76	0.74	0.70	0.69
H1 R2R2 Mattress ¥	0.80	0.82	0.83	0.87	0.86
H1 R2R4 Mattress ¥	0.69	0.75	0.73	0.75	0.78
Salford Lab Mattress L ¥	0.68	0.73	0.70	0.71	0.74
H1 R2R3 Mattress ©	0.74	0.84	0.79	0.81	0.80
H1 R1 R2 Mattress #	0.86	0.91	0.85	0.84	0.85
H2 R4 Mattress #	0.69	0.79	0.77	0.83	0.87
H3 Phase R2 Mattress £	0.84	0.74	0.71	0.74	0.66
H2 R3 Mattress §	0.75	0.93	0.88	0.92	0.91
H4 R6 Mattress Ø	0.81	0.67	0.64	0.68	0.70
H1 R1R3 Mattress ~~A~~	0.67	0.71	0.67	0.62	0.57
Sewn Mattress RC ~~A~~	0.57	0.68	0.67	0.71	0.70
Anti-Static Mattress RC ~~A~~	0.52	0.59	0.61	0.62	0.64
Black–Grey Mattress RC ~~A~~	0.85	0.82	0.77	0.72	0.83

&: 20 years, **@**: 15 years, **¥**: 10 years, **©**: 8 years, **#**: 7 years, **£**: 6 years, **§**: 4 years, **Ø**: 1 year, **~~A~~**: new, **H1**: hospital A, **H2**: hospital B, **H3**: hospital C, **H4**: hospital D, **L**: Salford University lab, **RC**: Rothband Company, **R**: room number. Weight categories: Max = maximum, 3Q = 3rd quartile, 1Q = 1st quartile, min = minimum.

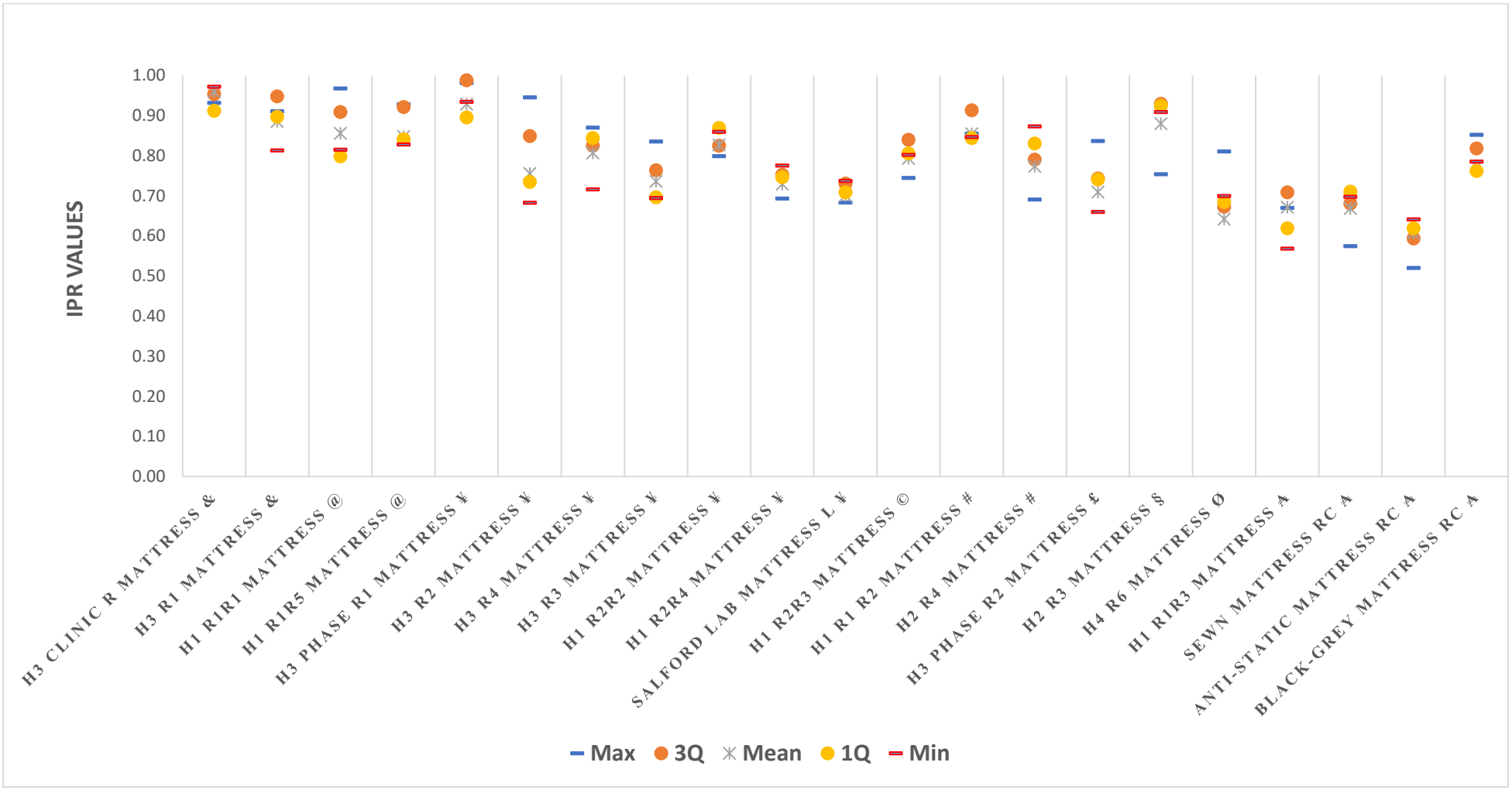

Figure 5.10: IPRs for the head when using the 2.5-cm mattresses; from left to right, the mattresses are presented starting with the oldest.

5.3.1.2. Sacrum

Table 5.9 shows the IPR values for the sacrum measurements using the 2.5cm mattresses. The mattress with the lowest mean and 1Q and 3Q values was the Anti-Static Mattress RC.

Table 5.9:The IPR values of the sacrum for the 2.5 -cm Mattresses

	IPR for the sacrum				
Mattress name (thickness of 2.5cm)	**Max Weight**	**3Q Weight**	**Mean Weight**	**1Q Weight**	**Min Weight**
H3 Clinic R Mattress &	0.92	0.94	0.97	0.84	0.87
H3 R1 Mattress &	0.94	0.92	0.92	0.83	0.94
H1 R1R1 Mattress @	0.94	0.95	0.97	0.74	0.90
H1 R1R5 Mattress @	0.85	0.78	0.78	0.70	0.93
H3 Phase R1 Mattress ¥	0.98	0.91	0.69	0.74	0.99
H3 R2 Mattress ¥	0.82	0.68	0.56	0.61	0.78
H3 R4 Mattress ¥	0.61	0.61	0.67	0.71	0.82
H3 R3 Mattress ¥	1.00	0.84	0.78	0.69	0.81
H1 R2R2 Mattress ¥	0.81	0.83	0.85	0.93	0.95
H1 R2R4 Mattress ¥	0.70	0.74	0.81	0.83	0.89
Salford Lab Mattress L ¥	0.56	0.57	0.55	0.51	0.77
H1 R2R3 Mattress ©	0.98	0.90	0.85	0.89	0.93
H1 R1 R2 Mattress #	0.73	0.73	0.77	0.81	0.84
H2 R4 Mattress #	0.73	0.51	0.46	0.47	0.69
H3 Phase R2 Mattress £	0.72	0.63	0.56	0.58	0.93
H2 R3 Mattress §	0.69	0.64	0.54	0.48	0.64
H4 R6 Mattress Ø	0.59	0.41	0.42	0.45	0.69
H1 R1R3 Mattress ~~A~~	0.57	0.55	0.53	0.53	0.78
Sewn Mattress RC ~~A~~	0.60	0.64	0.70	0.58	0.84
Anti-Static Mattress RC ~~A~~	0.42	0.42	0.43	0.45	0.71
Black–Grey Mattress RC ~~A~~	0.65	0.67	0.59	0.66	0.79

&: 20 years, **@**: 15 years, **¥**: 10 years, ©: 8 years, **#**: 7 years, **£**: 6 years, **§**: 4 years, **Ø**: 1 year, **~~A~~**: new. **H1**: hospital A, **H2**: hospital B, **H3**: hospital C, **H4**: hospital D, **L**: Salford University lab, **RC**: Rothband Company, **R**: room number. Weight categories: Max = maximum, 3Q = 3rd quartile, 1Q = 1st quartile, min = minimum.

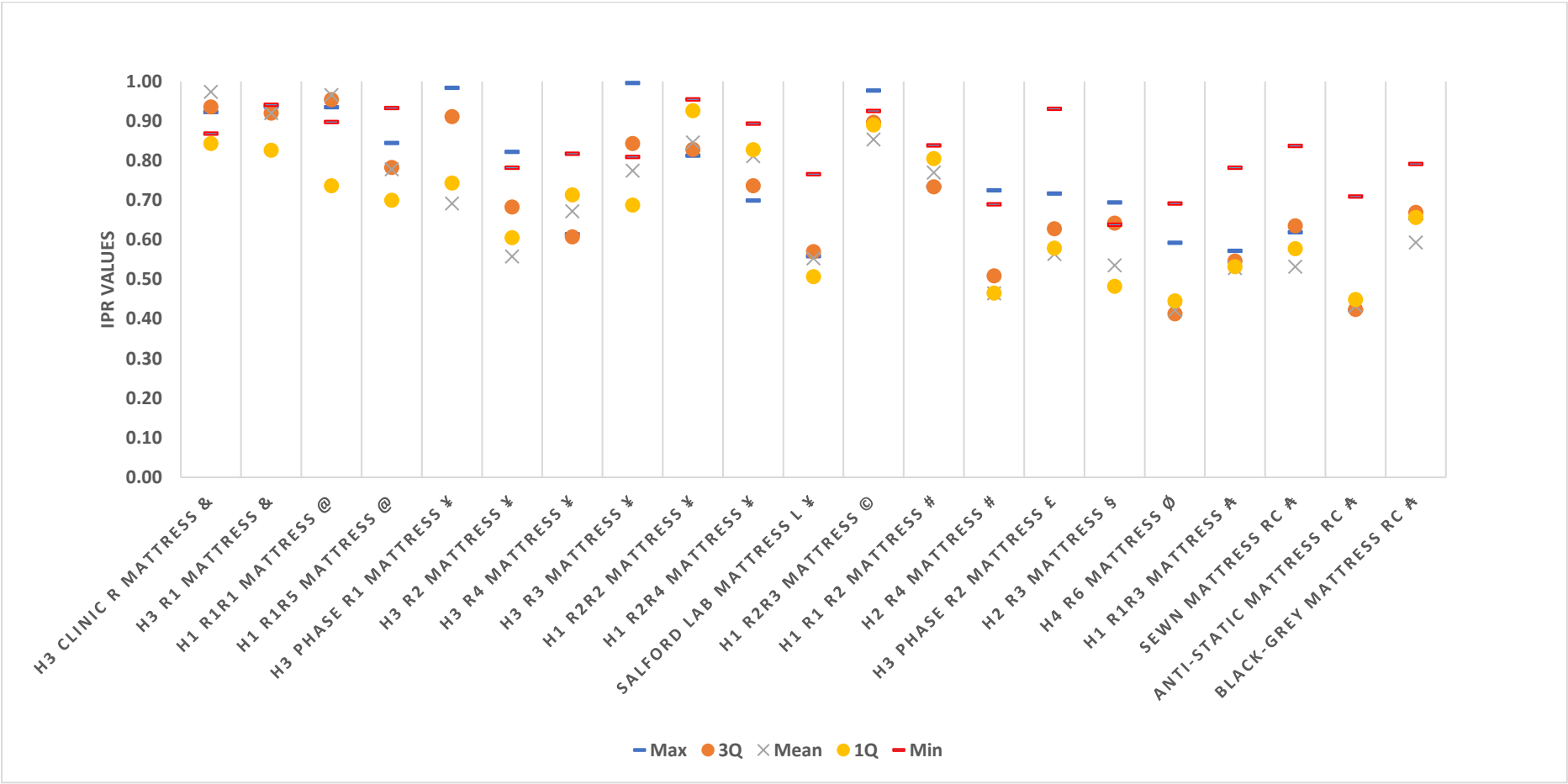

Figure 5.11: IPRs for the sacrum on the 2.5-cm mattresses; from left to right, the mattresses are presented starting with the oldest.

5.3.1.3. Heels

Table 5.10 shows the IPR for the heels. The highest mean weight and 1Q and 3Q values were found for the H1 R2R4 Mattress, and the lowest mean weight and 1Q and 3Q values were for the H3 R2 Mattress.

Table 5.10: Table 5.9:The IPR values of the heels for the 2.5 -cm Mattresses

	IPR for the heels				
Mattress name (thickness of 2.5cm)	**Max Weight**	**3Q Weight**	**Mean Weight**	**1Q Weight**	**Min Weight**
H3 Clinic R Mattress &	0.87	0.87	0.89	0.91	0.91
H3 R1 Mattress &	0.96	0.90	0.90	0.87	0.89
H1 R1R1 Mattress @	0.95	0.94	0.74	0.81	0.90
H1 R1R5 Mattress @	0.95	0.90	0.86	0.94	0.92
H3 Phase R1 Mattress ¥	0.69	0.77	0.80	0.72	0.93
H3 R2 Mattress ¥	0.52	0.49	0.52	0.55	0.77
H3 R4 Mattress ¥	0.72	0.76	0.78	0.66	0.96
H3 R3 Mattress ¥	0.88	0.89	0.70	0.71	1.03
H1 R2R2 Mattress ¥	0.86	0.90	0.95	0.82	0.89
H1 R2R4 Mattress ¥	0.95	0.92	0.96	0.88	0.96
Salford Lab Mattress L ¥	0.67	0.59	0.56	0.65	0.83
H1 R2R3 Mattress ©	0.87	0.83	0.86	0.80	0.98
H1 R1 R2 Mattress #	0.78	0.75	0.80	0.89	0.74
H2 R4 Mattress #	0.54	0.57	0.55	0.75	0.87
H3 Phase R2 Mattress £	0.60	0.67	0.65	0.69	0.79
H2 R3 Mattress §	0.58	0.50	0.44	0.56	0.77
H4 R6 Mattress Ø	0.44	0.44	0.45	0.63	0.93
H1 R1R3 Mattress ~~A~~	0.69	0.75	0.76	0.63	0.84
Sewn Mattress RC ~~A~~	0.90	0.94	0.74	0.95	0.68
Anti-Static Mattress RC ~~A~~	0.82	0.85	0.67	0.53	0.78
Black–Grey Mattress RC ~~A~~	0.73	0.72	0.63	0.84	0.97

&: 20 years, **@**: 15 years, **¥**: 10 years, **©**: 8 years, **#**: 7 years, **£**: 6 years, **§**: 4 years, **Ø**: 1 year, **~~A~~**: new. **H1**: hospital A, **H2**: hospital B, **H3**: hospital C, **H4**: hospital D, **L**: Salford University lab, **RC**: Rothband Company, **R**: room number. Weight categories: Max = maximum, 3Q = 3rd quartile, 1Q = 1st quartile, min = minimum.

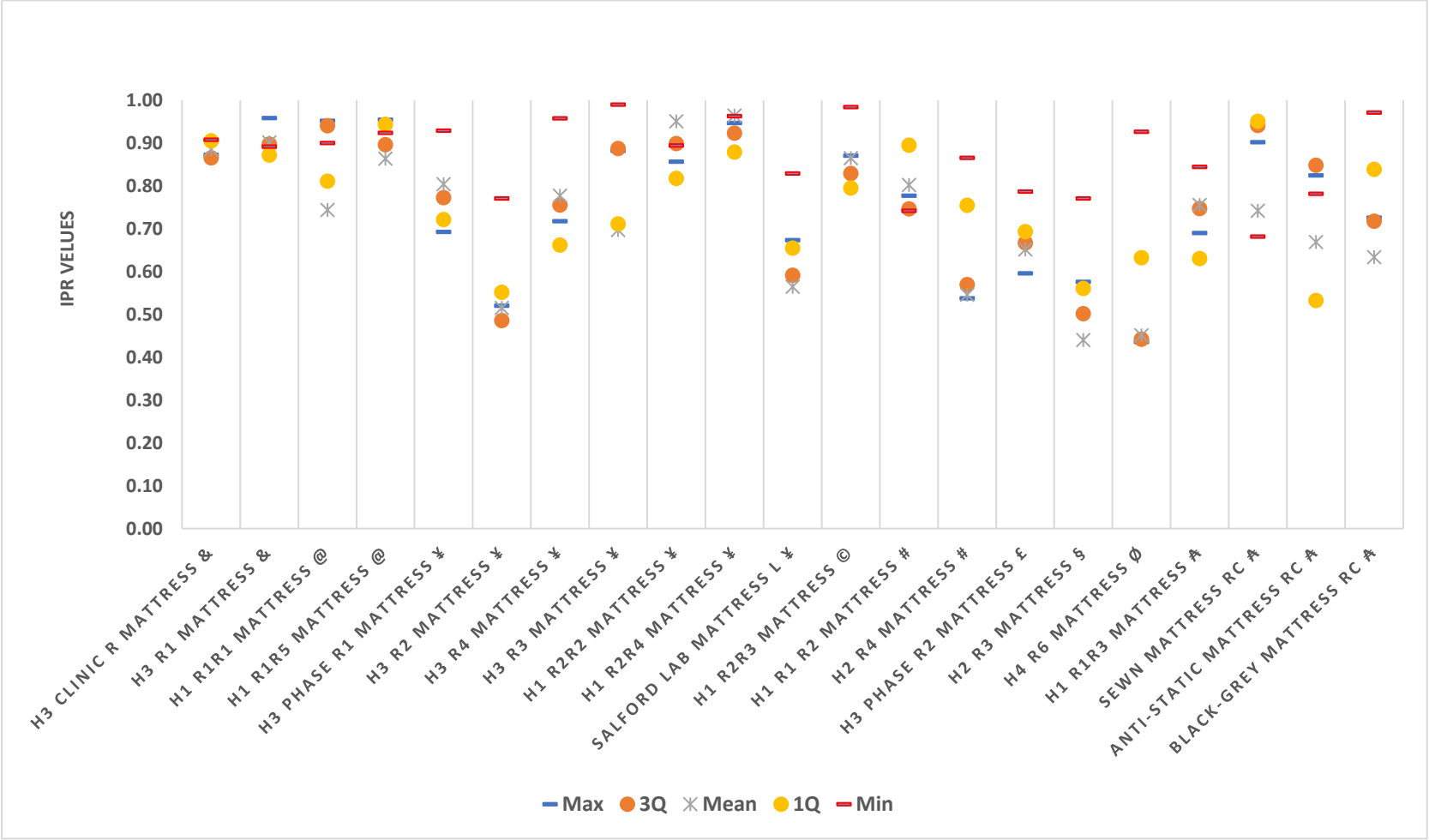

Figure 5.12: The IPR for the heels for the 2.5-cm mattresses; from left to right, the mattresses are presented starting with oldest.

5.3.2. IPR Values for the Thicker Mattresses

5.3.2.1. Head

Table 5.11 shows the IPRs for the head. The highest maximum, 3Q, mean, 1Q and minimum values were for the Trolley Mattress L (13 cm).

Table 5.11: The IPR values of the head for the Thicker Mattresses.

	IPR for the head				
Mattress name (varying thicknesses)	**Max Weight**	**3Q Weight**	**Mean Weight**	**1Q Weight**	**Min Weight**
Trolley Mattress L (13 cm) ¥	0.59	0.76	0.70	0.73	0.81
H4 Screening R Mattress (8 cm) Ø	0.43	0.49	0.48	0.51	0.58
Black–Grey Mattress RC (5 cm) Ⱥ	0.55	0.54	0.54	0.56	0.58

¥: 10 years, **Ø**: 1 year, **Ⱥ**: new. **H1**: hospital A, **H2**: hospital B, **H3**: hospital C, **H4**: hospital D, **L**: University of Salford lab, **RC**: Rothband Company, **R**: room number. Weight categories: Max = maximum, 3Q = 3rd quartile, 1Q = 1st quartile, min = minimum.

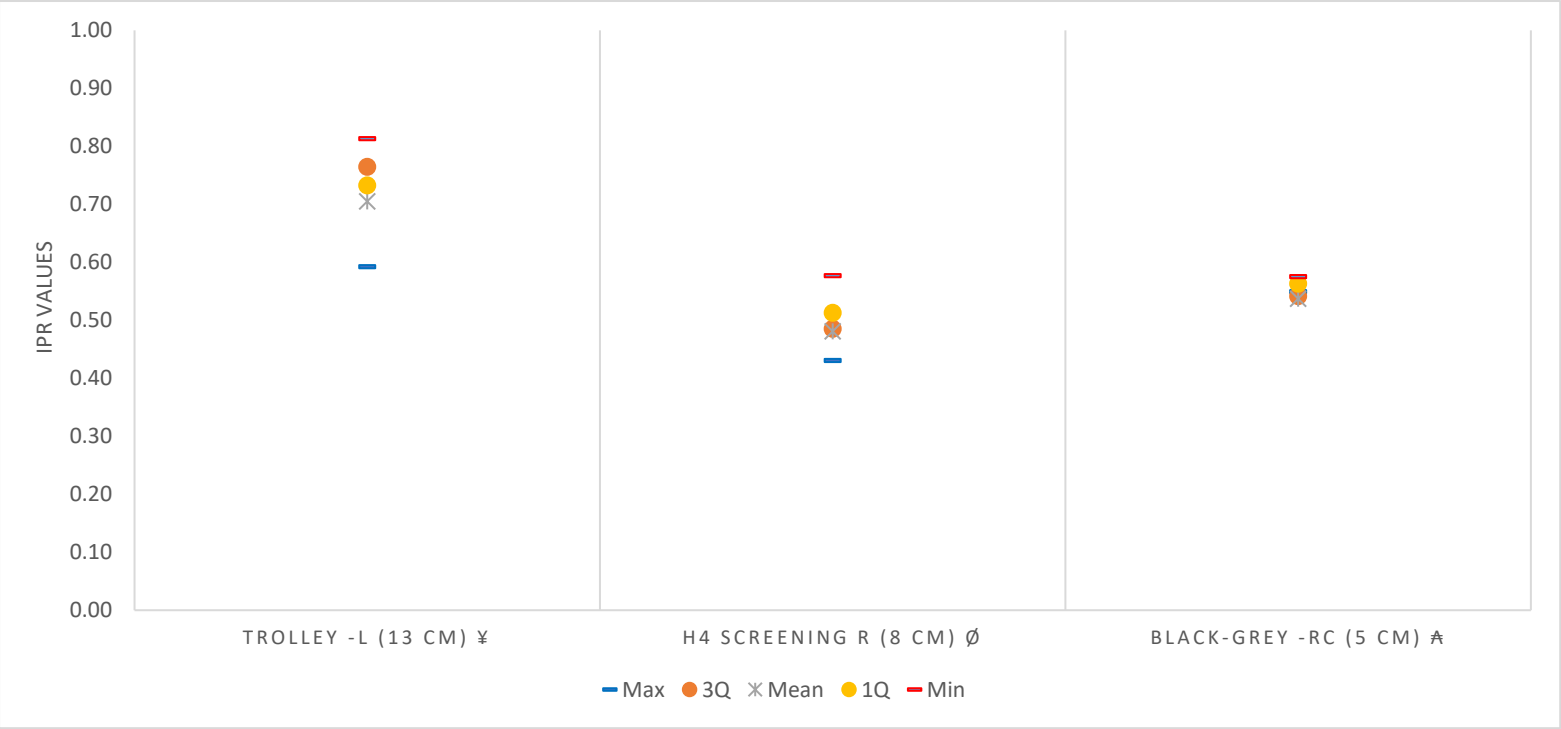

Figure 5.13: IPR values for the head for the three thicker mattresses.

5.3.2.2. Sacrum

Table 5.12 shows the IPR for the sacrum. The highest maximum, 3Q, mean, 1Q and minimum values values were for the Trolley Mattress L (13 cm).

Table 5.12: : The IPR values of the sacrum for the Thicker Mattresses.

	IPR for the sacrum				
Mattress name (varying thicknesses)	**Max Weight**	**3Q Weight**	**Mean Weight**	**1Q Weight**	**Min Weight**
Trolley Mattress L (13 cm) ¥	0.42	0.43	0.46	0.52	0.75
H4 Screening R Mattress (8 cm) Ø	0.35	0.34	0.33	0.34	0.52
Black–Grey Mattress RC (5 cm) ₳	0.48	0.41	0.46	0.48	0.60

¥: 10 years, **Ø**: 1 year, **₳**: new. **H1**: hospital A, **H2**: hospital B, **H3**: hospital C, **H4**: hospital D, **L**: University of Salford lab, **RC**: Rothband Company, **R**: room number. Weight categories: Max = maximum, 3Q = 3rd quartile, 1Q = 1st quartile, min = minimum.

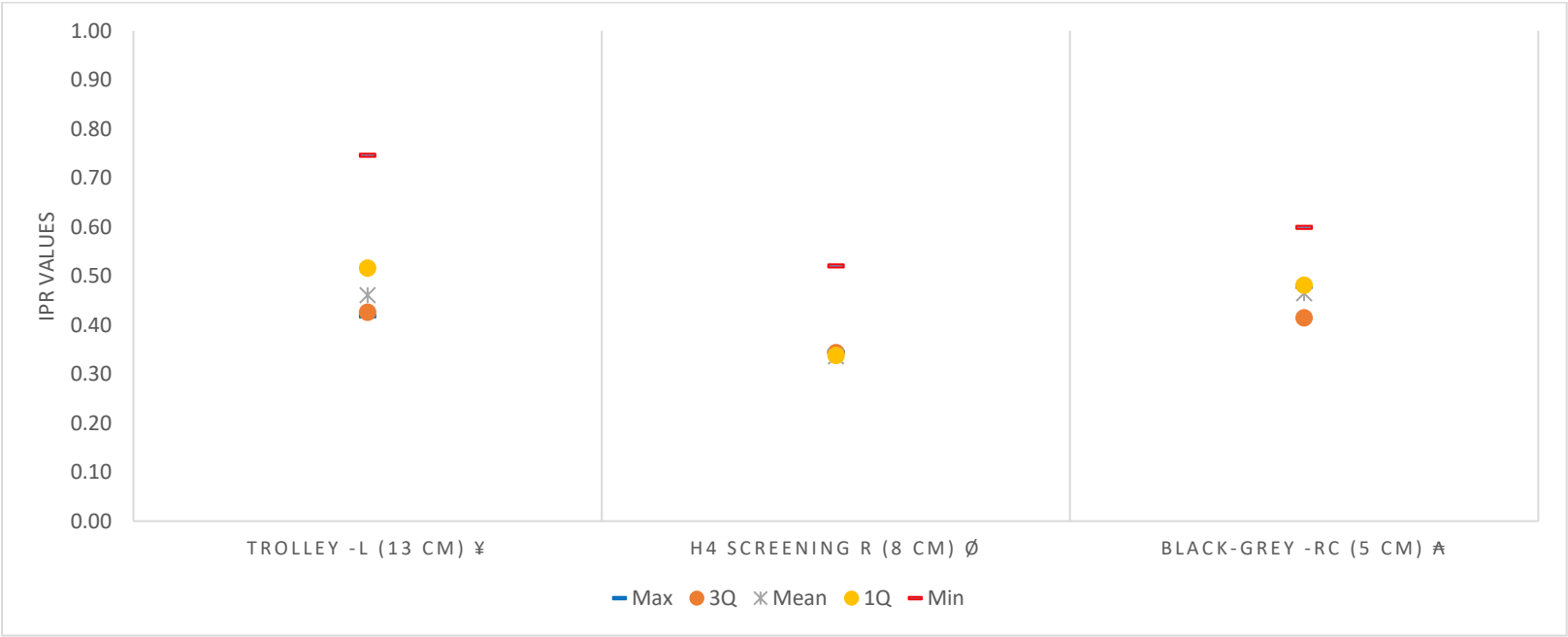

Figure 5.14: The IPR values for the sacrum for the three thicker mattresses

5.3.2.3. Heels

Table 5.13 shows the IPR for the heels. The highest maximum, mean, 1Q and minimum values were for the Trolley Mattress L (13 cm).

Table 5.13: The IPR values of the head for the Thicker Mattresses.

	IPR for the heels				
Mattress name (varying thicknesses)	**Max Weight**	**3Q Weight**	**Mean Weight**	**1Q Weight**	**Min Weight**
Trolley Mattress L (13 cm) ¥	0.89	0.92	0.54	0.76	0.75
H4 Screening R Mattress (8 cm) Ø	0.36	0.35	0.34	0.48	0.68
Black–Grey Mattress RC (5 cm) ₳	0.75	0.53	0.51	0.70	0.88

¥: 10 years, **Ø**: 1 year, **₳**: new. **H1**: hospital A, **H2**: hospital B, **H3**: hospital C, **H4**: hospital D, **L**: University of Salford lab, **RC**: Rothband Company, **R**: room number. Weight categories: Max = maximum, 3Q = 3rd quartile, 1Q = 1st quartile, min = minimum.

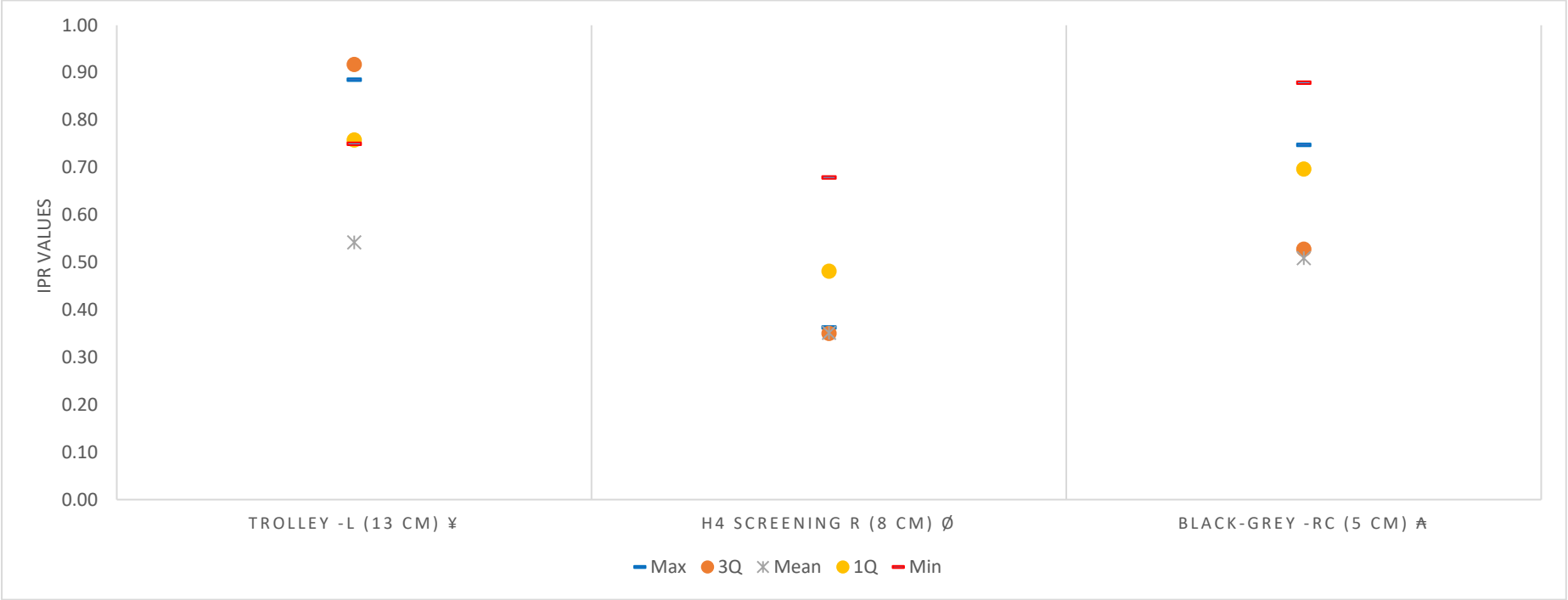

Figure 5.15: The IPR values for the heels for the three thicker mattresses.

5.4. Radiation Dose Results

The following figures illustrate the variation in radiation dose (IAK) for all mattresses. These were obtained using the X2 R/F dosimeter and the University of Salford's X-ray machine (Wolverson X-ray Ltd, Willenhall, West Midlands, UK). Figure 5.16 shows the 2.5 cm mattresses with 20, 15 and 10 years of age; Figure 5.17 shows the new 2.5 cm mattress with 8, 7, 6, 4 and 1 years of age; and Figure 5.18 shows the thicker mattresses.

Figure 5.16 shows that all older mattresses performed similarly, having the lowest absorption of the primary X-ray beam.

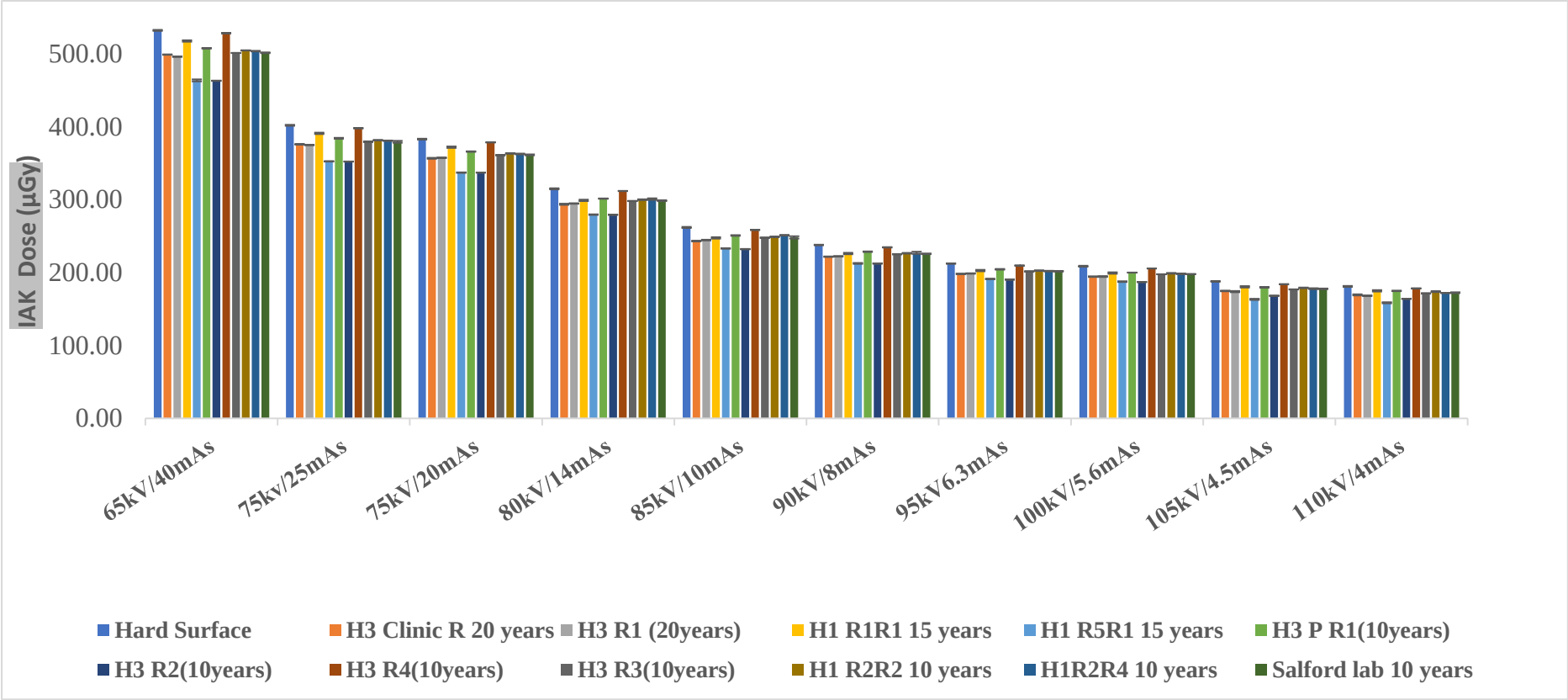

Figure 5.16*:* IAK values for the 2.5-cm mattresses aged 20, 15 and 10 years.

As shown in Figure 5.17, all mattresses aged 10 years or less performed similarly, with the new mattress having the lowest absorption of the primary X-ray beam.

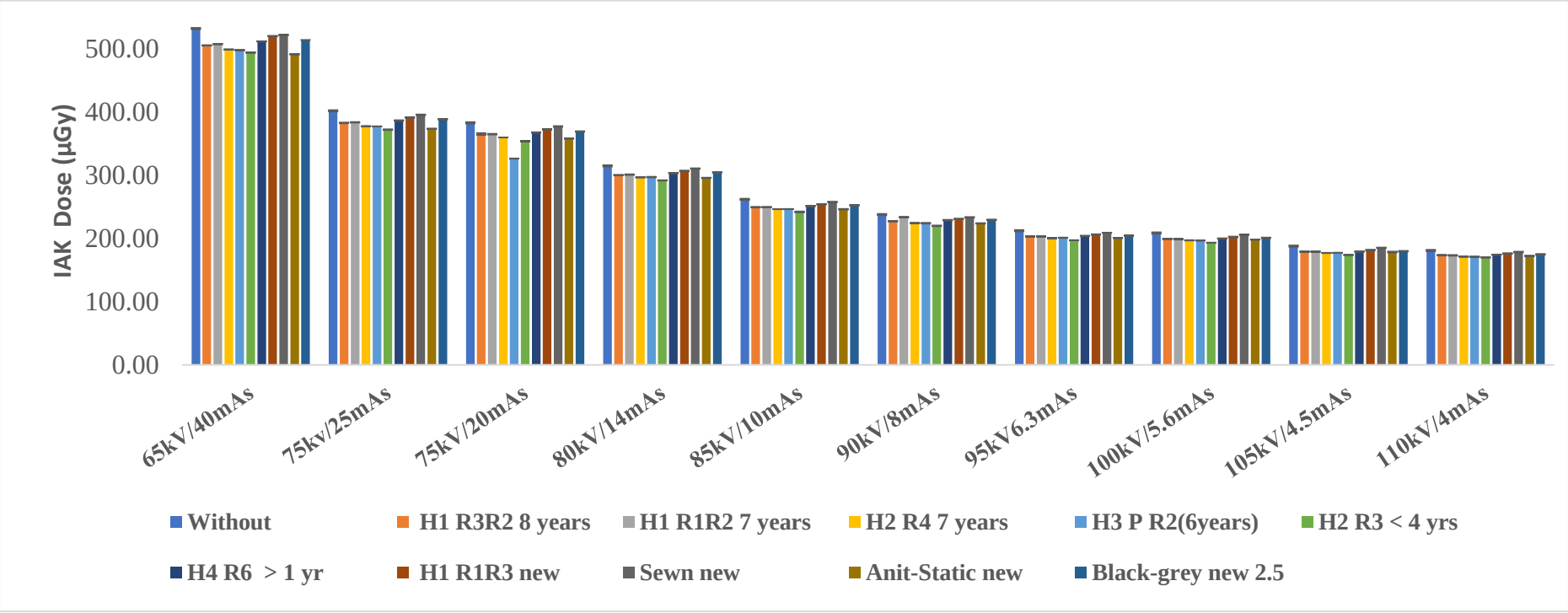

Figure 5.17: The IAK values of the new 2.5-cm mattress and those aged 8, 7, 6, 4 and 1 years

Figure 5.18 shows that the Black-Grey (5 cm) mattress had the lowest absorption of the primary X-ray beam among the thicker mattresses.

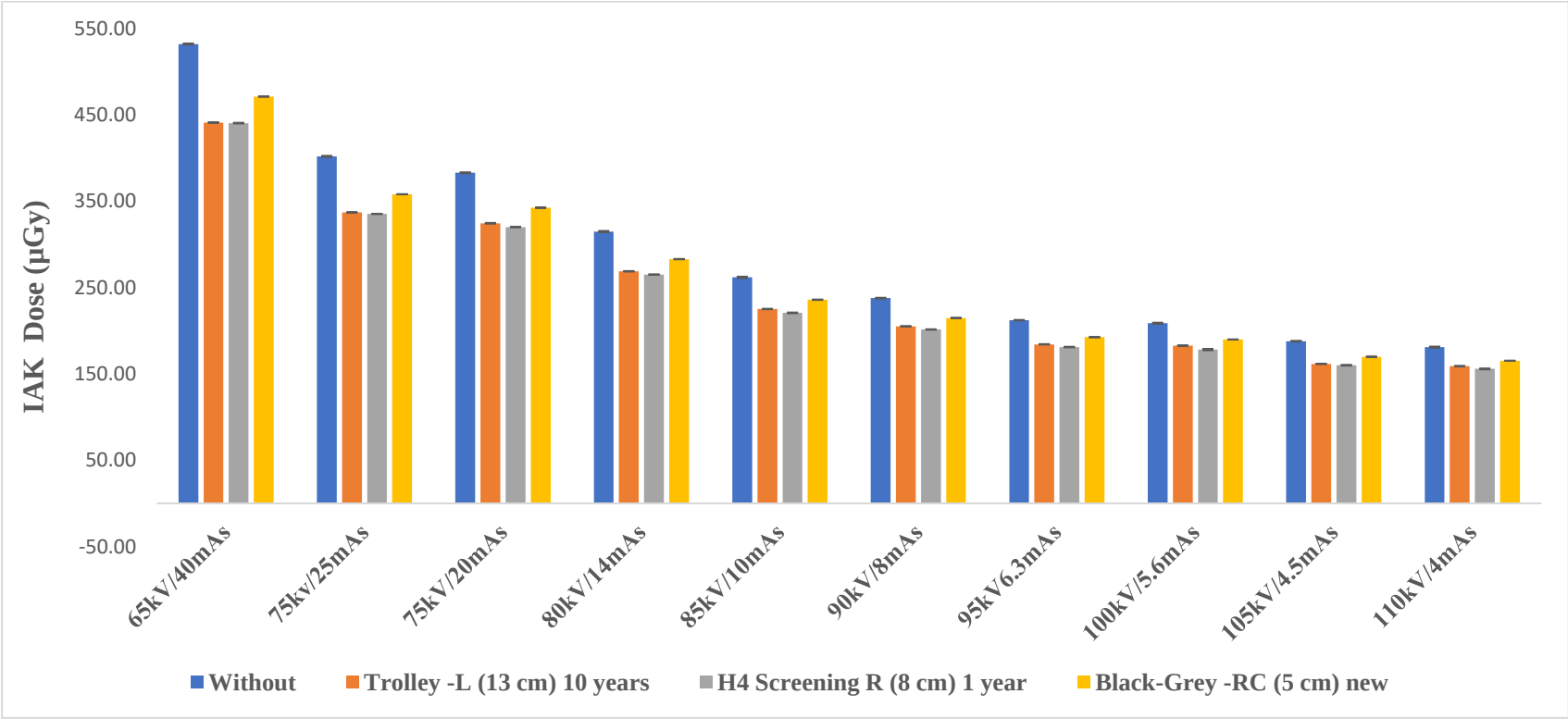

Figure 5.18: IAK values for the thicker mattresses.

Table 5.14: Percentage of Dose Attenuates for all Thinner (2.5 cm) Mattresses

Mattress Name	**Percentage decrease in IAK (%) for used mattresses**																	
	H3 Clinic	**H3 R1**	**H1 R1R1**	**H1R1R 5**	**H3 Phase**	**H3 R2**	**H3 R4**	**H3 R3**	**H1 R2R2**	**H1 R2R4**	**Salford Lab**	**H1 R2R3**	**H1 R1R2**	**H2 R4**	**H3Pha se R2**	**H2 R3**	**H4 R6**	**H1 R1R3**
Age (years)	**20**	**20**	**15**	**15**	**10**	**10**	**10**	**10**	**10**	**10**	**10**	**8**	**7**	**7**	**6**	**4**	**1**	**0**
65kV 40mAs	6.79	6.25	2.74	12.89	5.16	5.35	4.62	5.82	0.73	6.10	12.99	5.02	4.64	6.23	6.44	7.17	3.82	2.26
70kV 25mAs	6.73	6.48	2.74	12.29	5.07	5.26	4.42	5.61	0.99	5.90	12.36	4.75	4.52	6.07	6.13	7.41	3.81	2.66
75kV 20mAs	6.67	6.85	2.87	11.98	5.12	5.30	4.44	5.74	1.14	5.91	11.98	4.61	4.68	6.04	5.37	7.59	3.99	2.71
80kV 14mAs	6.39	6.72	5.03	11.24	4.73	4.47	4.27	5.29	0.94	5.84	11.32	4.64	4.40	5.77	5.63	7.30	3.64	2.55
85kV 10mAs	6.60	7.11	5.45	11.01	4.91	4.06	4.19	5.37	1.28	5.83	11.35	4.71	4.68	5.91	5.86	7.58	4.03	2.98
90kV 8mAs	6.50	6.74	4.89	10.60	4.74	4.48	3.85	5.31	1.34	5.64	10.70	4.42	1.70	5.64	5.73	7.49	3.72	2.87
95kV 6.3mAs	6.38	6.64	4.48	9.91	4.49	4.85	3.67	5.03	1.26	5.40	10.32	4.32	4.30	5.56	5.26	7.10	3.85	2.81
100kV 5.6mAs	6.76	6.83	4.47	10.12	4.66	5.01	4.19	5.29	1.48	5.62	10.40	4.54	4.63	5.57	5.69	7.42	4.18	3.07
105kV 4.5mAs	7.46	6.98	3.97	13.12	4.74	5.31	4.32	5.84	2.07	6.22	10.53	4.71	4.70	5.77	5.65	7.46	4.64	3.40
110kV 4mAs	7.05	6.36	3.31	12.37	3.88	4.95	3.34	5.22	1.48	5.51	9.40	4.05	4.24	5.37	5.50	6.05	3.64	2.63

Table 5.15: Percentage Change Applied to mAs

Mattress Name	**Effective mAs**																	
	H3 Clinic	**H3 R1**	**H1 R1R1**	**H1R1R5**	**H3 Phase**	**H3 R2**	**H3 R4**	**H3 R3**	**H1 R2R2**	**H1 R2R4**	**Salford Lab**	**H1 R2R3**	**H1 R1R2**	**H2 R4**	**H3 Phase**	**H2 R3**	**H4 R6**	**H1 R1R3**
Age (years)	**20**	**20**	**15**	**15**	**10**	**10**	**10**	**10**	**10**	**10**	**10**	**8**	**7**	**7**	**6**	**4**	**1**	**0**
65kV 40mAs	39.9	39.9	40.0	39.9	39.9	39.9	40.0	39.9	40.0	39.9	39.9	39.9	40.0	39.9	39.9	39.9	40.0	40.0
70kV 25mAs	24.9	24.9	25.0	24.9	24.9	24.9	25.0	24.9	25.0	24.9	24.9	25.0	25.0	24.9	24.9	24.9	25.0	25.0
75kV 20mAs	19.9	19.9	20.0	19.9	19.9	19.9	20.0	19.9	20.0	19.9	19.9	20.0	20.0	19.9	19.9	19.9	20.0	20.0
80kV 14mAs	13.9	13.9	13.9	13.9	14.0	14.0	14.0	13.9	14.0	13.9	13.9	14.0	14.0	13.9	13.9	13.9	14.0	14.0
85kV 10mAs	9.9	9.9	9.9	9.9	10.0	10.0	10.0	9.9	10.0	9.9	9.9	10.0	10.0	9.9	9.9	9.9	10.0	10.0
90kV 8mAs	7.9	7.9	8.0	7.9	8.0	8.0	8.0	7.9	8.0	7.9	7.9	8.0	8.0	7.9	7.9	7.9	8.0	8.0
95kV 6.3mAs	6.2	6.2	6.3	6.2	6.3	6.3	6.3	6.2	6.3	6.2	6.2	6.3	6.3	6.2	6.2	6.2	6.3	6.3
100kV 5.6mAs	5.5	5.5	5.6	5.5	5.6	5.5	5.6	5.5	5.6	5.5	5.5	5.6	5.6	5.5	5.5	5.5	5.6	5.6
105kV 4.5mAs	4.4	4.4	4.5	4.4	4.5	4.4	4.5	4.4	4.5	4.4	4.4	4.5	4.5	4.4	4.4	4.4	4.5	4.5
110kV 4mAs	3.9	3.9	4.0	3.9	4.0	4.0	4.0	3.9	4.0	3.9	3.9	4.0	4.0	3.9	3.9	3.9	4.0	4.0

Table 5.16: The Percentage of Dose Attenuates for all Thicker Mattresses.

Exposure factors	Percentage Decrease in IAK		
	Trolley 13 cm	Screening 8 cm	Black-Grey (Welded) 5 cm
65kV 40mAs	17.10	17.22	11.44
70kV 25mAs	16.13	16.58	10.90
75kV 20mAs	15.27	16.41	10.56
80kV 14mAs	14.60	15.80	10.13
85kV 10mAs	13.99	15.72	9.90
90kV 8mAs	13.73	15.27	9.67
95kV 6.3mAs	13.20	14.67	9.28
100kV 5.6mAs	12.45	14.62	9.03
105kV 4.5mAs	14.01	14.84	9.62
110kV 4mAs	12.13	13.90	8.67

The paired t-test for parametric data (Shapiro–Wilk test: $p < .05$) was utilised to assess the radiation attenuation properties of the X-ray mattresses. For all mattresses, a statistically significant increase ($p < .05$) was observed in the IAK between the 'no mattress' and 'with mattress' conditions.

It was found that clinically these differences are insignificant as the change in mAs to compensate for the attenuation would be between 0.01 and 0.13 mAs. Practically, it is unlikely any X-ray equipment would have this level of precision when setting mAs values for bucky work.

5.5. IQ Results

The bar graphs that follow display the variation in the physical IQ parameters (IQFinv) for the range of mattresses obtained using the CDRAD method. These measurements were obtained from CDRAD phantom images, as detailed in Chapter Three. These graphs show considerable variation in the physical IQ. Figure 5.19 shows the 2.5 cm mattresses aged 20, 15 and 10 years; and Figure 5.20 shows the new 2.5 cm mattress aged 8, 7 6, 4 and 1 years; and figure 5.21 shows the thicker mattresses.

Each mattress impacted the IQ differently, with IQ reducing as the kVp increased for all mattresses. As can be seen, the oldest mattress demonstrated the lowest IQ for all acquisition values, except for the Clinic's mattresses (20 years) with a value of 65 kV/40mAs, as indicated in Figure 5.19.

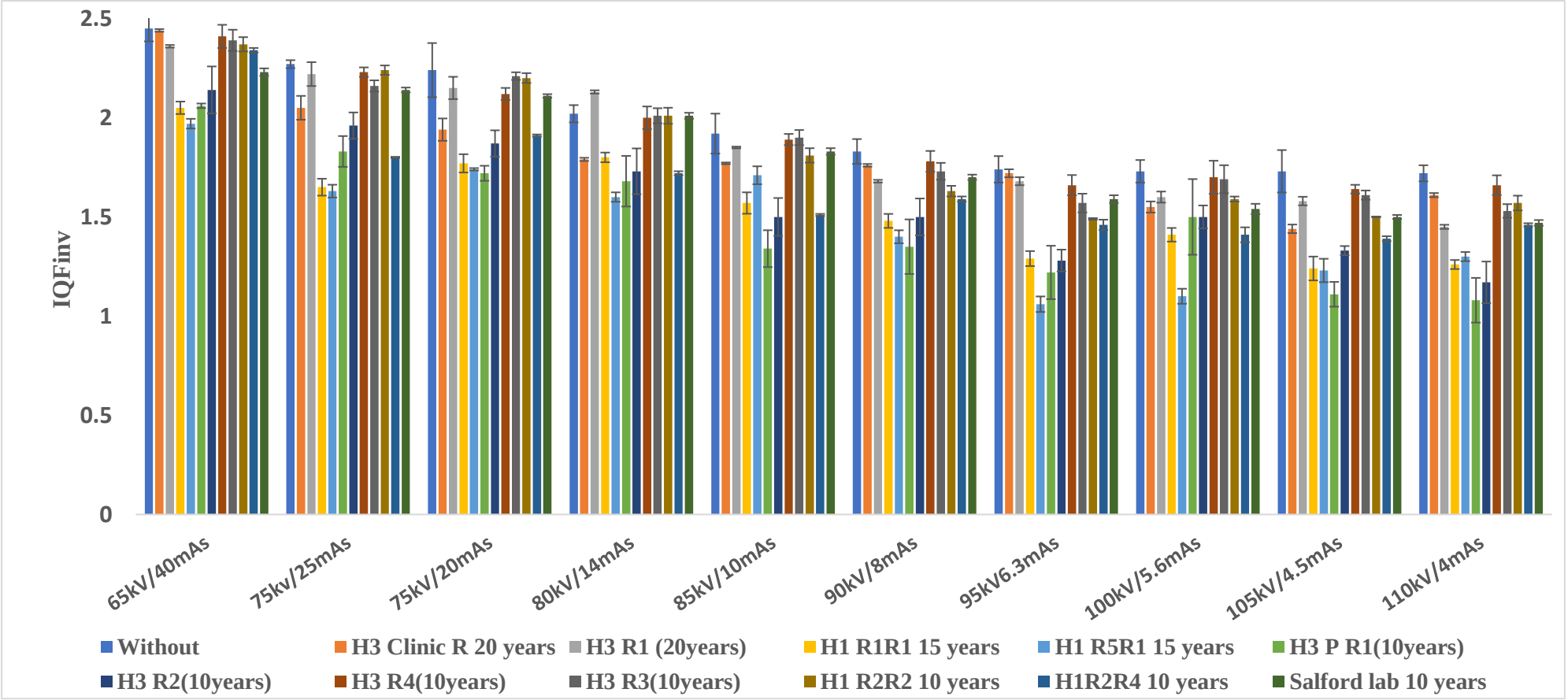

Figure 5.19: The IQFinv for mattresses aged 20, 15 and 10 years

Figure 5.20 shows that each mattress impacted the IQ differently, with the IQ decreasing as the kVp increased for all mattresses. Furthermore, the newest mattresses (Sewn Anti-Static and Black–Grey mattresses) demonstrated the best IQ for all acquisition values. The H1R1R2 and H1R1R3 mattresses produced the lowest IQ.

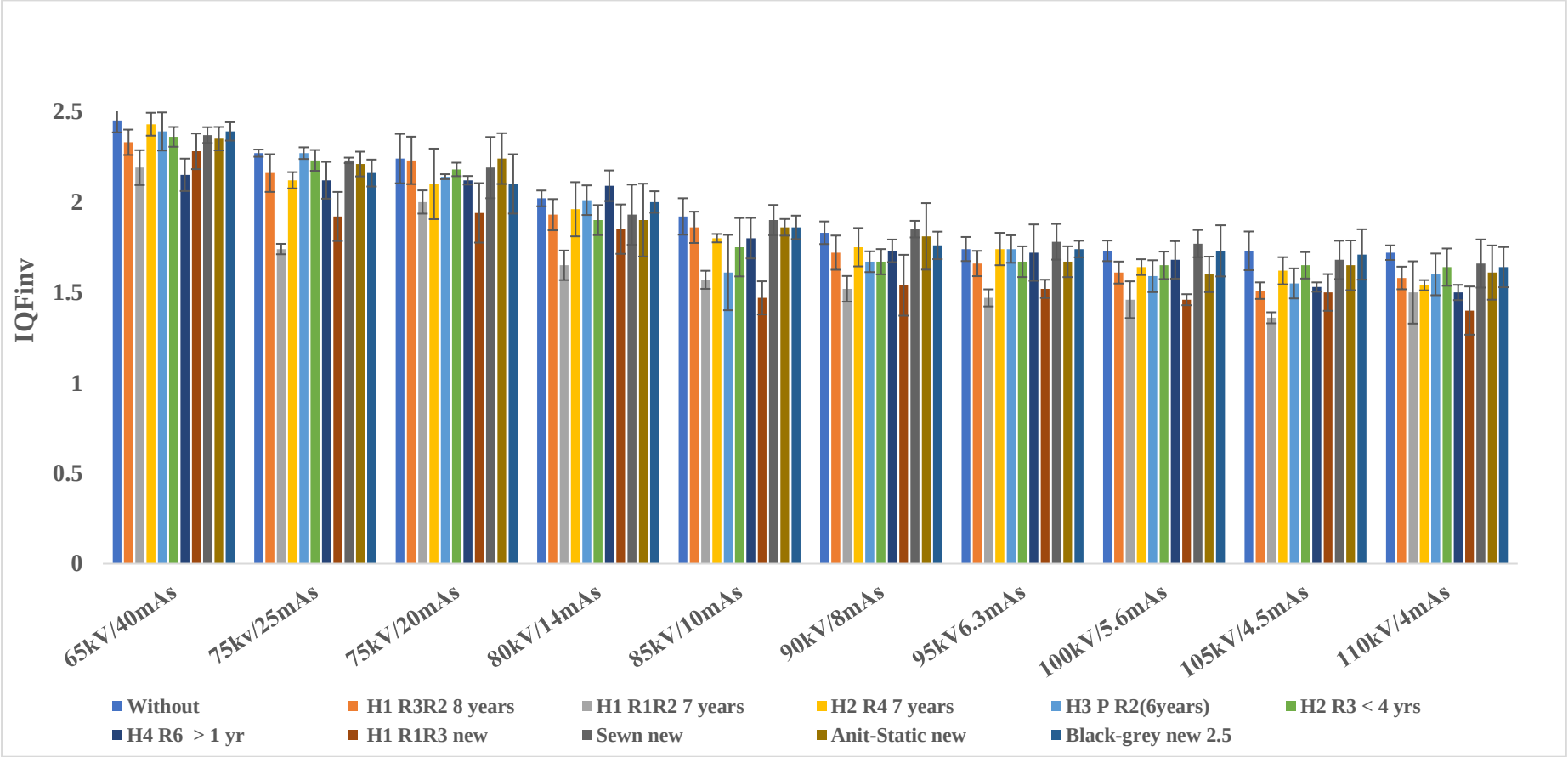

Figure 5.20: The IQFinv for the new 2.5-cm mattress and those aged 8, 7, 6, 4 and 1 years

Figure 5.21 shows that each mattress impacted the IQ differently, with the IQ decreasing as the kVp increased for all mattresses. The thickest mattress (Trolley L, 13 cm) demonstrated the best IQ for all acquisition values, except for the 105 keV value. The 8 cm mattress, H4 Screening R, produced the lowest IQ.

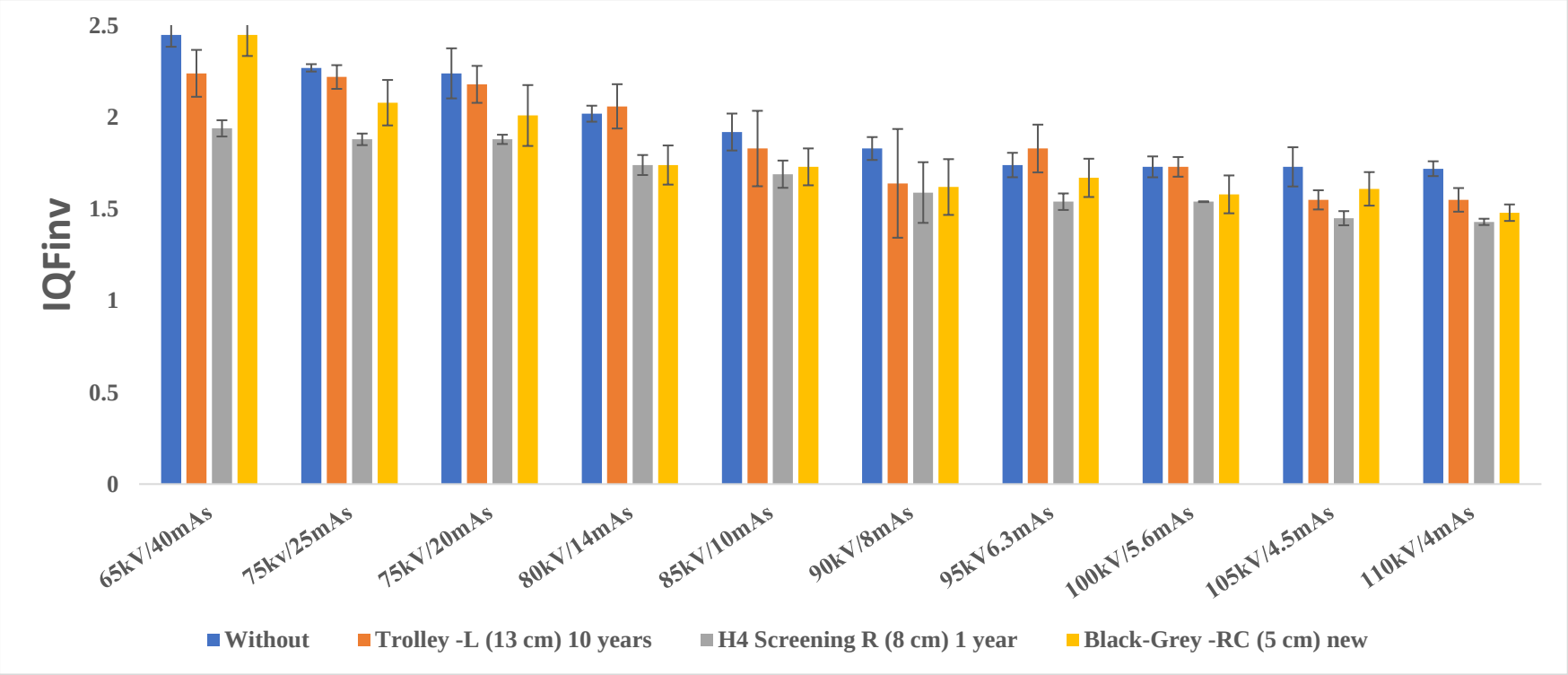

Figure 5.21: The IQFinv for the thicker mattresses

.

The paired t-test for parametric data (Shapiro–Wilk test: $p > .05$) was conducted to assess the IQ using IQF_{inv}. A statistically significant decrease ($p < .05$) in IQ was observed between the 'no mattress' and 'with mattress' conditions. It was found that clinically these differences that mattresses have a clinically insignificant impact on the primary beam and the image quality measured through IQFinv.

5.6. Chapter Summary

This chapter reported the results of the 3D phantom validation, phantom-based pressure method, image quality and radiation dose results. The positive correlations between the human volunteer and 3D phantom PPI values indicated that the 3D phantom and the phantom-based pressure method are valid and reasonable approximations of the human body PU jeopardy areas. This was established by assessing the shape of the pressure line profiles between human volunteers and a 3D phantom (Figure 5.2 A, B, and C). This was validated by the good positive correlations (R values: 0.993, 0.997 and 0.996, respectively) between the PPI of patients and PPI of the 3D phantom. Also, the shape analysis conducted by ImageJ between patient and 3D phantoms proved that there was a similarity between their jeopardy areas. In addition, all X-ray table mattresses displayed a range of pressure distributions, with older mattresses having a lesser ability to redistribute pressure.

This chapter also presented the results of the radiation dose for the X-ray mattresses. A large difference was observed when the 'no mattress' condition compared to the 'with mattress' condition ($p < .05$). In addition, there was a considerable variation between in the percentage of photon absorption of each mattress in the jeopardy areas for all mattresses that were used. This chapter also illustrated the IQ results using a physical method (CDRAD 2.0). Overall, the introduction of a mattress demonstrated a significant decrease ($p < .05$) in IQFinv values.

Chapter Six: Discussion

6.1. Overview

This thesis developed a novel method to compare the pressure distribution of a 3D anthropomorphic phantom on X-ray table mattresses and to evaluate the impact of X-ray table mattresses on IQ and radiation attenuation. The method used to analyse pressure redistribution needed to be objective and repeatable to compare not only different mattresses but also the same mattress over time. Therefore, in contrast to methods presented in existing literature which used human participants, a repeatable and objective method for pressure analysis was required to avoid variations caused by potential weight and body shape changes in humans. The movement of human participants can also cause complications that impact data collection and produce anomalies. Developing a repeatable and objective method for pressure analysis thus enabled the PPI risks from lying on X-ray mattresses currently in use in radiology departments in hospitals to be assessed.

With IQ, radiation attenuation and patient comfort and wellbeing in mind, the aim of any radiographic examination is to generate an image of sufficient quality using the lowest dose of radiation. However, several factors relating to X-ray table mattresses can lead to variations in pressure distribution, radiation dose and IQ. Differences in IQ could impact the diagnosis and lead to inappropriate treatment, increase in radiation dose and therefore the risk for the patient, and heighten the chance of patient discomfort and PU development.

Currently, no established standard method is available that considers pressure distribution properties, IQ, and radiation attenuation among X-ray mattresses. This thesis thus presents a novel method to compare pressure distribution, IQ and radiation doses among X-ray

mattresses which can be used as part of the mattress development process and in the ongoing testing of a mattresses in clinical use.

The following discussion is conducted in four parts: (1) 3D Phantom development and validation for use with the XSensor pressure imaging system to analyse the pressure redistribution of X-ray table mattresses; (2) an analysis of mattress performance for pressure distribution; (3) an evaluation of X-ray table mattresses for radiation attenuation; and (4) an evaluation of X-ray table mattresses for IQ. The chapter concludes with a summary and recommendations for future research.

6.2. Part 1: 3D Phantom Development and Validation for Use with the XSensor Pressure Imaging System to Analyse the Pressure Redistribution of X-ray Table Mattresses

As part of the evidence-based design and development process, the 3D anthropomorphic phantom was assessed to ensure its similarity with human pressure data. A strong positive correlation was observed between the human PPI data and the 3D phantom PPI data across the five phantom weights for the three PU jeopardy areas. R^2 values for the head, pelvis and heels were 0.993, 0.997 and 0.996, respectively. The correlations between the interface pressure distribution properties of the X-ray mattresses indicated that the 3D phantom was a reasonable representation of the three jeopardy areas.

After validating the 3D phantom using human weight data, ImageJ software was used to conduct a shape analysis to compare the phantom pressure profile characteristics against the same set of human data. Using ImageJ software, multiple pressure profile graphs were created using 3D phantom and human XSensor interface pressure data from the pelvis, head, and heels. For the 3D phantom, this profile analysis included data in the five weight categories for

comparison. Figure 5.1 (Page 135, Section 5.2.2) and Figure 5.2 (Page 136, Section 5.2.2) showed an example of the interface pressure map of a human and 3D phantom. Figure 5.2 A, B, and C demonstrated the similarity in terms of the profile curve shape trend between the human and 3D phantom for the three jeopardy areas. Figure 5.2 A, B and C showed further examples of interface pressure line profiles for the head, pelvis, and heels for one set of human pressure data in the minimum weight group. This also showed similarity. Pressure profile assessments for all 27 human volunteers showed similarity with the 3D phantom datasets.

The interface pressure map is a visualisation of the pressure distribution, allowing for a visual comparison of the phantom and human data. As shown in Figure 5.1, an outline of the whole human body could be seen compared to only the jeopardy areas (head, pelvis, and heels) of the phantom. Visual comparisons of the human and phantom pressure maps showed similarity for the three jeopardy areas in the five weight categories.

The human and 3D phantom profile curves for each jeopardy area were not the same. There are two possible explanations for this. First, humans are not homogenous; thus, any two humans are unlikely to have the same pressure profiles. Second, the 3D phantom only represents one physical size and does not have deformable material on its exterior inferior surfaces, unlike humans. Consequently, it is unlikely for a 3D phantom and a human to have the same profile.

The data of the 3D phantom PPIs, pressure profiles and visual pressure maps showed similarity with the human data. Therefore, one could argue that the 3D phantom represents a variant of a human profile that is suitable for use as an alternative for pressure mapping studies.

The 3D-printed phantom used herein has advantages over the one produced by Bain et al. (2003). First, the simple design of the 3D-printed phantom, combined with the availability of 3D printing, allows it to be produced quickly, cheaply and easily. Second, the 3D-printed

phantom allowed a range of human weights/sizes to be simulated, thus enabling mattresses to be tested under a range of realistic weight conditions and sizes. Limitations of 3D- printed phantom included its lack of deformability and its singular size. In humans, deformability would be expected because soft tissues, such as skin, muscle, and fat, would change shape, resulting in different pressure distribution characteristics. The variability induced would enable evaluations of pressure redistribution across a range of human characteristics, which the 3D-printed phantom does not allow.

Despite using a singular phantom size, size variations could be introduced using a range of human CT images which could then be 3D printed to create a range of phantom size options. For deformability, a suitable deformable material or materials needed to be identified and added to the external inferior surfaces of the 3D phantom to mimic human tissue deformability. Aside from having suitable human soft tissue deformability characteristics, the material would need to maintain the same deformable characteristics over a sustained period so that pressure distribution studies could be conducted over weeks, months or years as needed. This setup was intended be suitable for the longitudinal testing of mattresses and wherein the baseline measures could be compared against those at future instances. Further work is needed to identify suitable deformable materials.

If studies examining the interface pressure properties of mattresses begin regularly using 3D anthropomorphic phantoms, human involvement in mattress testing would require some consideration. Until now, pressure analysis studies have only involved humans, except for Bain et al.'s (2003) proposition which was not supported by actual studies. Mixed method approaches could therefore be adopted to include 3D-printed phantoms and humans. In future studies, it could be that only subjective measures will require human volunteers (e.g. comfort/quality of sleep/pain scales) and interface pressure mapping using humans will only

be needed in quite specific circumstances. For instance, 3D phantoms could be used for a common range of human shapes, sizes, and weights, whereas studies that address human outliers (e.g. grossly overweight) would still require humans. Further methodological work is needed to determine when a 3D phantom should and should not replace humans for pressure mapping. Validation work is also needed to refine the methodological details for when phantoms and humans are used together in pressure mapping studies.

It is reasonable to conclude that the 3D-printed phantom is a fair representation of a human for the pressure mapping purposes of this thesis. Additionally, as its physical characteristics will not change over time, unlike humans, it can be used to obtain objective, repeatable and comparable measurements between different mattresses and for the same mattress at varying points in time. Additionally, access and ethical issues that arise for human volunteers did not apply.

6.3. Part 2: Analysis of Mattress Performance for Pressure Distribution

This section of the discussion focuses on the 3D phantom pressure data arising from the mattresses in clinical use and the new ones. The key metrics used for comparison were the PPI and IPR, as outlined in the method.

6.3.1. PPI

The PPI is a widely reported metric for assessing interface pressure risk areas in seating and mattresses. However, the added benefit of this approach within this thesis relates to the standardisation imposed by the 3D-printed phantom. This standardisation allowed for objective repeatable PPI comparisons of the same mattress over time and between different mattresses at the same point in time. The controllable phantom characteristics also allowed further

analyses to be made using interface pressure data. Mattresses 2.5 cm thick are considered first, followed by the thicker mattresses. Subsequently, the PPI and IPR will be discussed. The IPR is a new objective ratio developed within this thesis (see Section 5.3, Page 150) which allows for an easy numeric objective comparison between mattresses.

6.3.1.1. PPI for mattresses 2.5 cm thick

Statistically significant differences ($p < .05$) were found between the PPIs with and without X-ray table mattresses for the 3D phantom head, sacrum, and heels for all 2.5-cm mattresses.

Table 5.2 and Figure 5.3 (Section 5.2.3.1, Page 137) show the PPIs for the 3D phantom head. As expected, the PPI for head on the hard surface/X-ray table had the highest PPI (95.4 ± 1.8 mmHg). This contrasted with the various X-ray table mattresses, such as the H1 R2R4 Mattress (66.1 ± 2.6 mmHg) and Salford Lab Mattress L (65.2 ± 1.2 mmHg), whose maximum PPI for the head were found to be lower. The PPI values for the 3D phantom head were the highest on a hard surface/X-ray table without a mattress. This result was similar to that obtained in the pilot study (Page 120, Section 4.9) , which recorded PPI values of 107.1 ± 19.29 mmHg for the head on a hard surface/X-ray table without a mattress and 53.93 ± 14.42 mmHg when using an X-ray mattress. This result indicates a pattern whereby the mean PPI for the head was higher while on hard surface/X-ray table than on x-ray mattresses which contain cushioning material.

Justham et al. (1996) shared similar findings, obtaining a PPI of 59.2 ± 25.1 mmHg for the head on a hard surface/X-ray table compared to 48.0 ± 25.25 mmHg when using a 2.5 cm thick mattress. However, the mean PPI for the head on hard surface recorded in this thesis had a maximum value of 95.4 ± 1.8 mmHg, which is much higher than that recorded by Justham et

al. (1996). Given that the two studies were conducted on similar hard surfaces, one would expect the findings to be similar. Such a big discrepancy could be because Justham et al.'s (1996) study experimented on healthy adult individuals, while the study for this thesis used a 3D-printed phantom. Additionally, the technology used was different in the two studies. This thesis used state-of-the-art and quality controlled XSensor pressure mapping equipment (SUMED International UK, 2014).

As shown in Table 5.2 and Figure 5.3 (Section 5.2.3.1, Page 137), the PPI for the hard surface/X-ray table gave the highest PPI values. It was expected that the X-ray table mattresses with the same thickness would have the same mean PPI values. However, differences ($p < .05$) were found between the PPI values of the different types of X-ray table mattresses, even with the same thickness. It is possible that the PPI differences between the 2.5 cm thick mattresses could be explained by their construction specifications (e.g. foam inserts/exterior coverings), denoting differences between manufacturers' development techniques. However, the mattresses in clinical use had no information associated with them, even of the manufacturer, rendering follow-up for further information impossible. Nevertheless, the PPI data demonstrated that a mattress's age can significantly influence the properties of pressure redistribution. As indicated in Table 5.2 (Section 5.2.3.1, Page 137), older mattresses, such as H3 Clinic R Mattress and H3 R1 Mattress, whose ages were given as 20 years, had higher mean PPI values for the head (88.9 ± 1.4 and 86.9 ± 1.9 mmHg, respectively) compared with newer mattresses, such as the Sewn Mattress and Anti-Static Mattress RC, which recorded the lowest mean PPI values for the head (54.8 ± 2.1 and 49.6 ± 1.1, respectively).

PPI values varied between mattresses, with newer mattresses demonstrating better pressure redistribution properties than older ones. One explanation for this finding is that the longer the X-ray table mattresses are in use, the less dense they become and therefore their

ability to support patients' weight declines. This would then result in a higher mean PPI among older X-ray table mattresses, especially those aged 10 years and above. Another hypothesis for this finding relates to the materials used in their construction and construction methods. However, no information could be obtained about these factors, and, because the clinical mattresses were still in use, permission was not granted for their destructive testing.

However, while the general trend is that older mattresses have higher mean PPI values for the head compared to those of newer mattresses, this does not apply uniformly to all types of mattresses. For example, the mean PPI for the 3D phantom head for all mattresses used for 10 years ranged from 93.6 ± 2.4 to 65.2 ± 1.2 mmHg. Some mattresses that had been in use for several years had a higher mean PPI than other mattresses used for 10 years. This can be exemplified by the H1R1 R2 Mattress, which had a mean PPI of 81.6±1.5 mmHg. These inconsistencies may be attributable to differences in the quality and type of raw materials used by different manufacturers or even the amount of use to which they have been exposed.

Table 5.3 and Figure 5.4 (Section 5.2.3.2, Page 140) show that the mean PPI findings for the 3D phantom head are similar to those recorded for sacrum for all 2.5 cm mattresses using the five weight categories. The data show the PPI values across the range of weights for 3D phantom sacrum for all 2.5 cm thick X-ray table mattresses. The highest mean value can be seen for the hard surface/X-ray table. A comparison of the mean PPI values for the sacrum on different surfaces (hard surface/X-ray mattress) showed significant differences ($p < .05$). Like the 3D phantom head, the highest mean PPI for the 3D phantom sacrum was recorded on the hard surface (131 ± 2.4 mmHg), and the lowest mean PPI was recorded for an X-ray table with a mattress, i.e. the Anti-Static Mattress RC (55.4 ± 1.8 mmHg). The age of mattresses was also found to have a direct impact on the mean PPI for the different weight categories of the 3D phantom sacrum. X-ray mattresses that had been in use for 20 years had a higher mean PPI

than those used for 10 years and less. For example, the H3 Clinic R and H1 R1R1 Mattresses had mean PPIs for the sacrum of 120.9±3.6 and 122.5±3.0 mmHg, respectively. Mattresses that had been used for one year, such as the H4 R6 Mattress, had a maximum mean PPI of 77.62.9 mmHg, while the new mattresses, such as the H1 R1R3, Black-Grey Mattress RC and the Anti-sewn Mattress RC, had mean PPIs of 75±1.4, 85.7±1.9 and 55.4±1.8 mmHg, respectively. As seen, the PPIs vary between mattresses, with newer mattresses demonstrating better pressure redistribution properties than older ones. Although there are still some deviations, the older mattresses recorded a higher mean PPI for the 3D phantom sacrum than did newer ones, as was found with the head.

A similar trend was reported for the PPIs with different weights for the 3D phantom heels. These data are presented in Table 5.4 and Figure 5.5 (Section 5.2.3.3, Page 143), which show the PPI data across the range of weights for 3D phantom heels for all 2.5 cm thick X-ray table mattresses. As expected, the highest mean PPI value was recorded for the hard surface/X-ray table and the lowest PPI values were recorded for X-ray tables with mattresses. The 3D phantom heels achieved a mean PPI of 101.9±1.9 on the hard surface, while the mean PPI on X-ray tables with mattresses varied depending on the age of the mattress and the type of mattress material used in its construction. In this regard, the mean PPI was higher for X-ray mattresses that had been used for a longer period and lower for newer mattresses. The lowest value was seen for the H2 R3 Mattress (4 years) and the H4 R6 Mattress (1 year) with the mean PPI for the two types of mattresses being 58.7 ± 1.2 mmHg and 44.4 ± 2.0 mmHg, respectively. This variation is likely due to mattress age and frequency of use, and possibly also construction method.

Based on the above, the following conclusions can be drawn for the 2.5 cm thick mattresses. First, their use incurs a statistically significant reduction in PPI for all three

jeopardy areas, compared with not using a mattress. Second, PPI variations between mattresses occur. The trend suggests that older mattresses have poorer pressure redistribution properties than newer ones, indicating that 2.5 cm thick X-ray table mattresses might have limited lifetimes in clinical use. An alternative or additional explanation could relate to their construction techniques and/or their physical components.

6.3.1.2. PPI for thicker mattresses

According to Table 5.5 (Section 5.2.4.1, Page 146), the thicknesses of the mattresses were categorised as hard surface/X-ray table, Trolley Mattress L (13 cm), H4 Screening R Mattress (8 cm) and Black-Grey Mattress RC (5 cm).

The PPI results in Table 5.5 show that the mean and PPI values for the above four types of mattresses are 71.5 ± 1.5, 50.4 ± 1.3, 34.4 ± 1.0 and 38.4 ± 1.7, respectively. Maximum PPIs were obtained for the hard surface/X-ray table (95.4 ± 1.8 mmHG), the trolley mattress L (13 cm) used for 10 years (56.5 ± 2.3 mmHG), the H4 screening R mattress (8 cm) used for 1 year (41.1 ± 2.2 mmHG), and for the Black-Grey mattress RC (5 cm) which was newly purchased (52.4 ± 1.0 mmHG). The differences in PPI values are associated with the different mattress manufacturers and the number of years the mattresses had been used. For example, the mean PPI for Mattress L (13 cm) of 10 years is 50.4 ± 1.3 mmHG, compared to that of the Black-Grey mattress RC (5 cm), which is 38.4 ± 1.7 mmHG. The highest PPI in Table 5.5 is the hard surface/X-ray table with a mean of 71.5 ± 1.5 mmHG, and the mattress with the lowest PPI is the H4 screening R mattress (8 cm) with one year of use (34.4 ± 1.0 mmHG). The fact that the Trolley Mattress L (13 cm) has a higher PPI than a new mattress shows that manufacturing and design aspects, as well as age are likely to have played an important role in the PPI scores. The thickness of the mattresses also played an important role in the PPI scores, as shown in Table

5.5. Where the Black-Grey (Welded) mattress RC is new, its thickness (5 cm) resulted in a lower PPI compared to the Trolley Mattress L (13 cm) of 10 years. Additionally, the PPI of the new Black-Grey mattress RC had a mean difference of 4.0 with the H4 screening R mattress (8 cm) of 1 year. The length of time the mattresses had been used also affected the PPI scores, as recorded in Table 5.5. Potentially, repetitive use of the mattresses over time incurs a statistically significant reduction in their PPIs. Additionally, PPI variations indicate a trend that older mattresses have poorer pressure redistribution properties than newer ones, suggesting that thicker X-ray table mattresses have varied lifetimes when in clinical use. An alternative or perhaps additional explanation could also be provided, relating to their physical components and manufacturing methods.

Table 5.6 (Section 5.2.4.2, Page 147) shows the PPI values across the range of weights for the 3D phantom sacrum for all thicker X-ray table mattresses. The highest mean value was obtained for the hard surface (101.8 ± 1.4), and the lowest value was obtained for the H4 Screening R Mattress (8 cm) (34.2 ± 2.2), which had been used for one year. The PPI of the sacrum might be explained by the duration of the use of the mattresses, whereby they could become squashed through regular use and therefore thinner than newly bought ones. This deterioration is likely to lead to ‘bottoming out’ of the foam. A comparison of three mattresses of different thickness shows that the Trolley Mattress L (13 cm) used for 10 years had a mean PPI at the sacrum of 46.9 ± 0.5 mmHg, the H4 Screening R Mattress (8cm) had a mean of 34.2 ± 2.2 after one year of use, and the new Black-Grey mattress RC (5 cm) had a mean of 47.3 ± 1.2. Despite being considerably older, the Trolley Mattress L (13 cm) had a mean value that was only 0.4 lower than the new Black-Grey mattress RC (5 cm), suggesting that the thickness and material contributed to its longevity. Thus, the point of comparability is the material used

in the manufacturing of the Trolley Mattress L (13 cm), as its durability was evident in the thickness measured in the PPI for the sacrum (mmHg).

Table 5.7 (Section 5.2.4.3, Page 149) shows the PPI weights for the 3D phantom heels for all thicker X-ray table mattresses. The results of the mean and SDs indicate that the hard surface mattress category scored 81.3 ± 2.5 (highest), while the H4 Screening R Mattress (8 cm) used for one year had a mean and SD of 28.6 ± 2.5. The PPI of the 3D phantom heels for the thicker X-ray table mattress means also varied for the Trolley Mattress L (13 cm) which had been used for 10 years, which had a mean and SD of 44.1 ± 1.6; the H4 Screening R Mattress (8 cm) of one year, which had a mean and SD of 28.6 ± 2.5; and the Black-Grey Mattress RC (5 cm), which had a mean and SD of 41.4 ± 1.4. The variations in the means relating to the phantom heels for the thicker mattresses and the X-ray table could be because of their material and surface. The hard X-ray table surface had the highest mean PPI for the heels, indicating that the material used for the surfaces of the thicker mattresses contributed to the weight of the 3D phantom heels. Trolley Mattress L (13 cm) had the second highest mean of 44.1 ± 1.6 mmHG, despite being used for 10 years.

Figure 5.6 shows the PPI for the 3 thicker mattresses using the range of [sand] weights and the 3D phantom. The box plots indicate the PPI for 3D phantom thicker mattresses. As already indicated by the means and SDs, the H4 Screening R mattress (8 cm) that had been in use for one year had a mean SD, and quartiles and maximum and minimum that were close together. The closeness of the data points indicates that the data is tightly grouped together in the case of the H4 screening R (8cm) mattress on the X-ray table. The smaller standard deviation of the H4 screening mattress R (8 cm) is shown by the closeness of the ranges to the mean, indicating

the mean weight and the relationship to the X-ray (thicker) mattress' age and the material used in its manufacturing.

In Figure 5.7, the box plots show the PPI for the 3 thicker mattresses using the range of [sand] weights and the 3D phantom. According to the results shown in Table 5.7, the Trolley Mattress L (13 cm) and the Black-Grey RC (Waded) (5 cm) are the two mattresses that show closeness, symmetry, and dispersion of the data points in terms of the means and SDs of the heels. Figure 5.8's box plots show that the H4 screening L (8 cm) thicker mattresses have a smaller mean, maximum and minimum, and standard deviation dispersion.

The benefits of thicker X-ray table mattresses are like those of the trolley mattresses, which offer more comfort and safety to patients as they are designed to reduce pressure on PU regions (ArjoHuntleighs, 2010). As one would expect, appropriate thickness and age of an X-ray table mattress is significant in terms of reducing the risk of PUs. In the same way, the maximum weight limit of the X-ray table mattress is associated with the safety and ability of a mattress to reach its optimal performance. Therefore, the lower the weight limit, the lower the optimal performance for patient comfort (Kneip et al., 2010; Masschaele et al., 2007). To ensure the best efficacy of the equipment, consideration should be given to the distribution of pressure. In some comorbidities, patients have very heavy weight, as in the case of lymphoedema, wherein patients have heavy legs while the rest of the body is of average weight.

PUs remains a major problem and are among the costliest and most physically unbearable complications of 20th century healthcare (Agrawal and Chauhan, 2012). The main cause of PUs is prolonged contact of body parts with surfaces, especially when patients remain in the same position. The EPUAP and NPUAP (2009) guidelines state that patients in a supine position should be repositioned every two hours to relieve their body of sustained pressure. Presently, in imaging and emergency departments, some patients can remain on trolley

mattresses or X-ray tables for prolonged periods. However, Dharmarajan and Ugalino (2006) demonstrated that 20 minutes is long enough to produce tissue breakdown caused by prolonged interface pressure.

While many X-ray imaging examinations are short (<20 minutes) and potentially induce no detrimental effects with respect to PU formation, some radiological procedures are lengthy and require patients to lie in one position for two hours or more (Moore and Cowman, 2014). Such lengthy radiological studies occur within operating theatres, interventional imaging rooms and on emergency department trolleys. Intermediate length imaging studies also exist, for example MR and hybrid imaging, wherein a patient may have to lie perfectly still for 30 minutes or more. These radiological procedures have the potential to induce PUs due to the length of time a potential at-risk patient must remain very still or even motionless (Liao et al., 2013; Stojadinovic et al., 2013). Furthermore, mattresses used in imaging contexts need consideration in terms of their usage frequency and variation in the sizes of patients who are to use them. Consequently, deterioration over time should be considered as a mattress in one locality could remain serviceable for years whereas the same mattress in a different locality might not (Bain, 2001).

6.3.2. The Ratio of Pressure Distribution

Using the 3D phantom, the IPR can be presented as an array of data for the sacrum, head and heels in the five weight categories - see Figures 5.11, 5.12, 5.13, 5.14 and 5.15 (Section 5.3.1 and 5.3.2, Page 150 to 162). The IPR is a simple metric that permits quick and objective comparisons to be made between different mattresses at a given point in time and for the same mattress over time. Manufacturers could consider providing this sort of data to help consumers make more informed procurement decisions. If such data were provided at point of

sale, each mattress would have baseline anthropomorphic phantom IPR and PPI data and, if needed, repeat testing could be conducted to see whether the mattress continues to perform adequately over time. Such data could also help inform procurement decisions for matching mattress characteristics to imaging demands/frequency and underlying patient populations.

An IPR value closer to 1 approaches the equivalent performance of a hard surface while a value closer to 0 reflects a better performing mattress in terms of its redistribution properties (see Figure 5.9).

6.3.2.1. IPR for 2.5-cm thick mattresses

Table 5.8 and Figure 5.10 shows the IPR values for 21 2.5 cm thick mattresses (head), with different weights indicated as mean, 1st and 3rd quartiles, and minimum and maximum. The 20-year-old H3 Clinic R and the 10 year old H3 Phase R1 X-ray mattresses had maximum IPR values of 0.93, a mean value of 0.99 and a minimum value of 0.93, suggesting that these older mattresses performed extremely poorly in pressure redistribution. Additionally, the IPR for the head shows that the new Anti-Static RC mattress (new) and Sewn Mattress RC (new) had a maximum IPR value of 0.52, a mean value of 0.61, and a minimum value of 0.64; these mattresses performed moderately well in pressure redistribution compared with older ones. Table 5.9 (sacrum) showed that the mattress with the least significant values was the new Anti-Static Mattress RC with a mean of 0.43, a 1Q value of 0.45, a 3Q value of 0.42 and a maximum of 0.71. The H4 R6 mattress (1 year old) had good IPR values, with a mean of 0.42, a 1Q value of 0.45, a 3Q value of 0.41 and a maximum of 0.59. Figure 5.9 showed that the three newer mattresses and the mattress with only one year of use had good to moderate performance. Figure 5.11 indicated that the Salford Lab Mattress close values for the 1st and 3rd quartiles, mean, and maximum and minimum values, indicating little dispersion in the values compared

to the other 20 X-ray mattresses. Table 5.10 highlights the 1st and 3rd quartiles, mean, and maximum and minimum IPRs of the mattresses for the heels. The results showed that the H3 R2 Mattress (10 years old) had a minimum value of 0.77, a 3rd quartile of 0.49, a mean of 0.52, a 1st quartile of 0.55, and a maximum value of 0.52. The box plot in Figure 5.12 showed that the dispersion of data points for the H3 R2 Mattress were clustered, except for the outlying minimum value of the IPR weight of the mattress.

6.3.2.2. IPR for thicker mattresses

Tables 5.11, 5.12 and 5.13 focused on the thicker mattresses. Table 5.11 shows the IPR values for the thicker (head) Trolley Mattress R (13 cm) used for 10 years, the H4 Screening R Mattress (8 cm) used for one year, and the new Black-Grey (Welded) Mattress RC (5 cm).

The thicker Trolley Mattress R (13 cm) used for 10 years had the highest IPR value of 0.70, followed by 0.54 for the Black-Grey (Welded) Mattress, and 0.48 for the H4 screening R mattress (8 cm) for the head. The best performance for pressure redistribution was the Screening mattress 8 cm (one year), likely due to its thickness and age in contrast with the trolley mattress 13 cm (10 years) which potentially lost its ability to distribute pressure because of its age and long period of use in clinical practice. Figure 5.13 shows the dispersion of IPR values and the normality and variation of the data for the three sampled mattresses. Figure 5.13 shows that the Black-Grey RC (5 cm) mattress IPR data values are clustered, indicating a normal distribution of data. The mean, 3Q, and minimum and maximum ranges are close together, indicating minimal variability in the IPR values for the head for the three thicker mattresses tested.

Table 5.12 outlines the sacrum IPR values for the three thicker mattresses. The highest mean weight value for the sacrum was for found the Trolley Mattress L (13 cm) and Black-

Grey Mattress RC (5 cm), which both had a mean of 0.46. The H4 Screening R (8 cm) had the lowest IPR sacrum mean of 0.33. The Screening mattress 8 cm (one year) performed better in distributing the pressure compared with the other mattresses. Figure 5.14 showed that the data points for the IPR values of the three thicker mattresses are not clustered.

For the H4 Screening (8 cm), the minimum IPR value for the H4 screening mattress was an outlier (0.52), but the maximum (0.35), 3Q values (0.34), and 1Q (0.34) IPR values are clustered, indicating that the H4 screening R (8 cm) mattress data is the least variable and close to normal distribution.

Table 5.13 showed the IPR values of the thicker mattresses for the heels. Focusing on the three mattresses, the IPR mean value for the H4 Screening R (8 cm) was the lowest at 0.34, the Black-Grey mattress RC (5 cm) had a mean of 0.51, and the mean of the Trolley Mattress (13 cm) was 0.54. Figure 5.15 shows the dispersion of the IPR values for the heels for all three thicker mattresses. The dispersion showed significant variability because the data points for the 1Q, 3Q, maximum, minimum, and mean values were not clustered. Overall, a wide range of IPR and PPI values existed across the new, in use 2.5-cm thickness mattresses and the thicker X-ray table mattresses, with newer mattresses tending to have better pressure redistribution properties than the older ones. Statistically significant differences (p >.05) were found for the heels, head, and sacrum between the PPI values with and without using an X-ray table mattress.

The impact of medical imaging and radiotherapy surfaces on patients who undergo radiography/therapy procedures needs to be analysed and improved (Ahmed et al., 2012). The results of this PhD thesis have significance for radiology departments. For the four hospitals and the mattress manufacturer included in the analysis, there is a wide variation in PPI and IPR values between mattresses, with some performing extremely poorly. Extrapolating the findings, one can speculate that they could be similar for other radiology departments and that

many mattresses do not offer maximum protection to patients, thus putting them at risk of developing PUs. The trend that older mattresses perform worse than newer mattresses raises the question about how long a mattress should be kept in service and whether quality testing of the mattress should be conducted at intervals to ensure its pressure redistribution properties are preserved at a level that is considered adequate for clinical use. An important problem that was identified when requesting the mattresses from hospitals was the lack of information among radiology staff about their build quality. As no manufacturer product information was retained about any of the mattresses, their constructions methods, materials, and age were unknown. Aside from conducting initial radiolucency testing prior to clinical use, X-ray table mattresses are not considered adequately in quality assurance testing. This assertion is partly confirmed when considering that some mattresses are still in continual use after 20 years' service, despite the association between increasing age and decreasing pressure redistribution properties. If a quality assurance programme is to be introduced to assess mattress pressure redistribution properties, then manufacturers will have to provide baseline data for a range of pressure-related metrics. Detailed information about mattress construction would also be needed, along with a maximum patient weight, up to which the mattress is effective.

6.3.3. Potential clinical implications of BMI and X-ray table mattresses

6.3.3.1. Pressure versus weight of patients

It has been shown that a higher BMI, defined as the measure of the body size, calculated by dividing a person's weight by the square of his height, is related to a higher PPI (Hyun et al., 2014). Some studies have indicated that there is an increased risk of PU among patients with a high BMI, while others argue that, in some circumstances, a low BMI can cause an

increased risk of PU development (Baumgarten et al., 2006; Casimiro et al., 2002; Compher et al., 2007; Uzun and Tan, 2007; VanGilder et al., 2009b).

Average IP and BMI are positively correlated for the patient's whole body during the processes of radiography imaging. Health professionals involved in radiotherapy ought to be aware that patients with different BMIs are subject to varying levels of IP risk when lying on treatment or imaging tables. In this regard, a plan to prevent the development of PUs needs to be targeted to the specific needs of individual patients rather than being generalised to all patients. For instance, having a thin mattress fitted onto an imaging table could be deemed suitable for minimising the IP of a slim and bony patient but may not be appropriate for reducing for a patient with a higher BMI. This is because a slim and bony patient is at the highest risk of PU development due to less padding at the jeopardy areas, and therefore any damage to their imaging surface would further increase their risk. Thus, the patient with a higher BMI may need to be provided with a mattress that has a higher specification pressure distribution to protect their skin from developing tissue ischemia, the skin of their slimmer peers (Pieper, 2012).

The redistribution of the pressure on the X-ray table is important in the development of PUs in populations that are at risk. The head, sacrum and heels' pressure distribution on the X-ray table mattress performance is an important aspect, particularly for considering the relatively smaller size (2.5 cm thickness) of the mattresses on the X-ray table.

The pressure distribution of X-ray mattresses differs, and inappropriate distribution predisposes at-risk populations to PUs. Although previous study findings have shown that mattresses used on X-ray tables that show a poor distribution of pressure increase the occurrence of ulceration among at-risk populations, there are still X-ray clinics that use thin mattresses without considering their pressure properties. Patients above the weight limit of the

mattresses used on the X-ray tables, as denoted by the product manufacturer, have a damaging effect on both the mattresses and the tables. This increases the risk of pressure ulceration among the at-risk population.

6.3.4. Types of patients and procedures that do not require a mattress

Despite the increased risk of PUs during lengthy radiography procedures, it is worth discussing whether all procedures require the use of an X-ray table mattress. For lengthier studies exceeding 20 minutes, the use of a mattress is indicated, especially for those at risk of developing a PU. For studies of duration less than 20 minutes on patients who are not at risk of developing a PU, the need for using a table mattress should be questioned.

Another point of consideration is that in some radiology units, the use of mattresses is not required, and some manufacturers have been marketing their products without indicating the need to use mattresses on their X-ray tables (Everton et al. (2014a)). Nonetheless, some studies (Beadle et al., 2014, Rieber et al., 2016, Franks et al., 2015) have indicated that the discomfort of patients on the X-ray tables is a result of a prolonged duration of the X-ray procedure. Consequently, not using a mattress in some situations may increase a patient's discomfort and movement on the X-ray table and thus reduce the quality of the image obtained.

Notwithstanding the above, regarding the non-use of a mattress Pope (1999a) noted that the external pressure applied to the skin can be up to 3-5 times higher than at the skin surface when the concentration of pressure is at the muscle/bone interface. Meanwhile, Simpson et al. (1996) indicated that high interface pressures are generated by most standard hospital mattresses. Pressure is a significant causative factor in PU development, which is shown as the vertical weight-force exerted upon a specific part of the skin (Agrawal and Chauhan, 2012; Messer, 2012). Accordingly, this pressure is a primary causative factor, as it significantly

impacts an individual's blood flow which can cause partial or even complete blood vessel occlusion (Demarre et al., 2012). Skin shears commonly occur when forces bear down upon a body in parallel with friction caused by body and surface resistance (Messer, 2012; Pieper, 2012). This leads to the stretching and tearing of the skin and reduced blood flow and stasis in the subcutaneous tissues, resulting in blood and lymph vessel damage (Byrant, 2012).

Moreover, Defloor (1999) argued that the progress of PUs is intermediarily affected by tissue tolerance rather than the actual contributors. The main causative factors to tissue damage are the time duration and intensity of pressure, which varies from patient to patient depending upon the capability of the patient's skin tissues to withstand pressure. Brienza (2007) stated that the interface pressure measurement is a vital tool to assess the risk of developing PUs. Gomez-batiste et al. (2014) and Pieper (2012) stated that within the healthcare setting, patients' health is commonly threatened by PUs, particularly in relation to the elderly or partially/fully immobile individuals or those suffering from chronic diseases.

The aetiology, treatment and prevention of PUs have been analysed through different research studies (Yap et al., 2013; Garcia-Fernandez et al., 2014a). Nevertheless, published material regarding the risks of PUs on patients who need to undergo radiography and the consequential procedures is minimal. Only six studies (Messer, 2012; Justham and Rolfe 2002; Brown, 2002; Justham and Rolfe, 2001; Howatson-Jones, 2001; Justham et al., 1996) directly or indirectly evaluate these risks, together with rates of prevalence, and assessment tools regarding the procedures of radiotherapy (Messer, 2012; Brown, 2002).

The results obtained in this thesis confirm that the PPI for jeopardy areas is higher on hard surfaces. All the recorded PPI values for the X-ray table mattresses in this thesis showed an improvement compared to the hard surfaces. By using radiolucent mattresses, the PPIs for jeopardy areas can be minimised below the PU risk level, though bony parts may require thicker

and more highly specialised mattresses. However, the recorded values from both surfaces were still higher than the standard values (60 mmHg) for hospital mattresses. Mattress surfaces are designed to provide an even distribution of pressure across jeopardy areas, supporting the conclusion that higher specification surfaces can reduce the incidence of PUs. The difference in average interface pressure is the medical surface, however more investigation is needed to justify the using of pressure-reducing surfaces in radiographic mattresses. The main objective of this thesis was to investigate this justification. Mattresses reduce the peak interface and average pressure on the whole body and on three jeopardy areas and can thus minimise the probability of developing PUs.

The pressure-related results in this thesis show that new X-ray table mattresses assist much more in redistributing the interface pressure and thus help to minimise patient risk of sustaining PUs that can be generally described as MDR. For some European, Middle East and African countries that use X-ray tables without mattresses, this novel method is likely to have far-reaching implications for radiography practices. The application of the novel method developed in this thesis in radiography settings in these developing countries would result in improved radiography practices. This is because the findings show that X-ray tables should be fitted with mattresses that enhance patient comfort and reduce pain caused by hard surfaces, and these may have the added benefit of reducing PU formation. Consequently, patient management should be improved while advancing patient care, since the fitting of mattresses on X-ray beds is associated with a reduction in PPI, thus minimising the patients' risk of sustaining MDR PUs in the course of radiotherapy planning and medical imaging.

Similarly, the elevated risk of interface pressure linked to X-ray tables not fitted with mattresses is likely to cause tissue ischemia, which may in turn contribute to the development of PUs among patients being subjected to lengthy imaging sessions, such as interventional

radiography processes. The high risk of these imaging processes is associated with the long periods they take to complete, some taking two or more hours. In radiotherapy facilities in countries whose imaging tables have no mattresses, patients who must undergo lengthy imaging procedures, such as cervical vertebroplasty, have to lie on hard imaging tables with no mattresses for prolonged periods. Cervical vertebroplasty is briefly described as percutaneous modestly invasive interventional radiography performed as a treatment modality for painful vertebral compression fractures (VCFs) (Yang et al., 2016; Zhao et al., 2016a).

Considering the attributes of patients who usually undergo cervical vertebroplasty, it is evident that lengthy radiography therapy may cause severe MDR PUs. Patients receiving cervical vertebroplasty therapy are normally elderly, on extended steroid therapy, or diagnosed with cervical vertebral compression because of a malignant tumour or a chronic metabolic disorder (Zhao et al., 2016b). Additionally, as many patients are elderly, they suffer from conditions such as osteoporosis and thus have weak bone structures coupled with the presence of multi-comorbidities (Akintade, 2015; Svensson et al., 2016). Moreover, the older cohort represents the largest proportion of patients that undergo lengthened radiotherapy treatment processes, including cranial stereotactic radiotherapy (SRT). Existing statistics demonstrate that older patients constitute approximately 50% of all reported cancer cases (CR-UK, 2015). Inadvertently, older patients are highly vulnerable to developing PUs mainly because of the poor condition of their skin. Advanced age is associated with a notable reduction in the amount of collagen and elastin found in the skin (Reddy, 2018). The notable deterioration in the content of these valuable skin protective fibres negatively affects the skin's flexibility and ability to recoil, which safeguard the superficial skin and the subcutaneous tissue from the effects of high levels of pressure (Kelly, 2014). In addition, older groups of patients constitute the largest proportion of patients diagnosed with neurological disorders such as Parkinson's disease,

chronic spinal cord injuries and multiple sclerosis (MS), which affect the functioning of the immune system and sensation. Thus, they cannot feel discomfort associated with increased ICP and therefore fail to shift position to relieve the pressure, making them more vulnerable to developing PUs. The presence of these neurological disorders and sensation deficits negatively impacts the patients' nutritional status and general wellbeing, which in turn escalates their risk of developing PUs. Therefore, the results of the main study of this thesis, which have highlighted the augmented risks of interface pressure for hazardous regions on X-ray table mattresses in use for 15 years old or more, have implications for older patients who receive therapeutic or imaging sessions for lengthy periods. The result of this lengthened exposure to elevated interface pressure is damage to skin tissue that may result in the development of PUs.

The risk of MDR PUs is profound on the jeopardy areas of X-ray table mattresses that have been subjected to clinical use for a long time. This risk tends to be higher for the head because of the high interface pressure it exerts on the X-ray table surface. As such, these findings present the possibility of a negative impact for patients receiving lengthy therapeutic radiography procedures in countries whose radiography facilities use X-ray tables without mattresses, such as countries in the Middle East, Africa and Europe. The presence of high interface pressure on various parts of the body, such as the head, sacrum or heels, while the patient lies motionless on an X-ray table without a mattress, has a high chance of causing skin damage among patients receiving a radiotherapy intervention. Recently introduced advancements in radiography therapies, such as cranial SRT, have extended the time taken from 10 minutes to about an hour, which means that patients undergoing cranial SRT have to lie still in a supine position without moving their whole or part of their body throughout the course of treatment. In most cases, an immobilisation device is used to ensure that the patient remains still throughout the radiotherapy procedure. The immobilisation device can escalate

the already elevated interface pressure exerted by the head's contact with the hard X-ray tabletop, raising the patients' risk of sustaining PUs.

In summary, many patients receiving radiotherapy planning or radiotherapy procedures are likely to be elderly patients with deteriorated health and are thus considered to be at high risk of developing PUs. As demonstrated by past research (Reddy, 2008, Pittman, 2007), advanced age is usually associated with declining amounts of elastin and collagen in the skin, which implies that the skin of elderly patients undergoing comprehensive treatment radiotherapy, radiotherapy planning and interventional procedures is potentially devoid of the critical protective capacity needed to protect it from possible injury. As a result, the risk of developing MDR PUs among these elderly patients increases. Further research should thus be conducted to identify possible approaches to reduce the interface pressure risks likely to cause injury to patients' heads when lying on X-ray tables without a mattress.

6.3.4.1. Pressure analysis summary

Previous studies have highlighted the concerns of patients remaining on the X-ray table for a prolonged period during a procedure, depending on the condition or nature of their injury. Because of the risk of pressure injury, it is important to consider whether the mattresses used on the X-ray table attain the objectives of reducing patient movement due to discomfort while maintaining a high-quality X-ray image. The pursuit of these objectives leads to the proposal mattresses which redistribute the patients' pressure on the X-ray table be used. While most mattress manufacturers provide varying size measurements in terms of the thickness of the mattresses, unique patient X-ray needs make it necessary to consider the optimum mattress that ensures pressure redistribution of patients with different weights.

6.4. Part 3: Evaluation of X-Ray Table Mattresses for Radiation Attenuation

This thesis evaluated the radiation attenuation of X-ray table mattresses and their subsequent IQ performance. This section analyses and determines the influence of the thickness and age of the mattress and the mAs and kVp have on radiation attenuation and IQ. Interpretations are also made based on the findings of existing literature.

The thickness and composition of an X-ray mattress could have a negative impact on IQ and radiation attenuation. Given that radiation deposits energy while travelling through matter, the quantity of X-ray dose received by an individual depends on the way radiation attenuation is achieved (Korsfeldt and Tais, 2014). As radiation passes through material, its intensity decreases as it interacts with it. Given that ionising radiation damages the human body, the linear non-threshold model dictates that the smallest amount of radiation should be used to achieve the medical aim at hand, whether for diagnostic or therapeutic purposes, or for routine assessment.

The imposition of a mattress between the X-ray source and image detector could mean additional radiation is needed to penetrate the mattress. This means that the patient could receive an additional radiation dose because of the mattress. It was initially proposed that the thickness and construction of the X-ray table mattress can influence the radiation dose administered to the patient and potentially reduce the clarity of captured images.

6.4.1. Thinner mattresses (2.5 cm)

For the 21 2.5 cm mattresses assessed in this study, there was a mean reduction of 16.47 mGy IAK. Clinically, this radiation dose difference is insignificant as the change in mAs required to compensate for the attenuation is 0.05 mAs.

The results show the attenuation properties of all thinner mattresses that were tested by comparing the IAK in the presence and absence of a mattress and with a RaySafe X2 (Unfors RaySafe AB, Billdal, Sweden). Its R/F sensor was positioned in the central beam with a source to image distance (SID) of 120 cm (source to object) and a dosimeter distance [SOD] of 100 cm.

Figure 5.16 (Section 5.4, Page 164) shows the results for the 2.5 cm mattresses aged 20, 15 and 10 years; Figure 5.17 (Section 5.4, Page 165) shows the results for the new mattresses and for the 2.5 cm mattresses aged 8, 7, 6, 4 and 1 years; and Figure 5.18 (Section 5.4, Page 166) shows the results for the thicker mattresses. In general, the radiation attenuation of all mattresses increased with mattress age and thickness.

A moderate negative correlation was found between the age of a mattress and measured IAK, with correlation coefficients ranging from -0.41 to -0.28 (Table 6.1). The reasons for this finding could be the material used, with older material being denser or having greater deterioration through repeated use. Table 5.14 (Page 167) showed that the percentage of dose attenuation for mattresses of 20 years at all mAs values was 6.25%-7.46%. For mattresses of 15 years, the range was 2.74%-13.12%, while for mattresses of 10 years it ranged from 0.73% to 12.99%.

Therefore, the Salford mattress aged 10 years showed higher percentages of dose attenuation, ranging from 9.40% to 12.99%. This could be because of its construction method and/or construction materials. However, it is still in the range that would not have a clinical impact on the choice of exposure factors. For the mattress of eight years, the range of dose attenuation was 4.05%-5.02%; for the mattress of seven years, the range was 1.7%-6.23%; for the mattress of six years, the range was 5.26%-6.44%; for the mattress of four years, the range

was 6.05%-7.59%; for the mattress of one year, the range was 3.64%-4.64%; and for the newer mattress, the range was 2.26%-3.40%.

In summary, the mattresses aged 10 years (H3 R4, H1 R2R2, H1R1R4, Salford lab, H3R3) had a similar radiation attenuation rate to the mattresses aged eight years (H1 R3R2), seven years (H1 R1R2, H2 R4), six years (H3 P R2) and less than four years (H2 R3), except for the Salford Mattress. However, the new mattresses generally exhibited lower attenuations compared to the older mattresses with a 2.5 cm thickness. Based on the statistical analysis of the radiation dose, the presence of an X-ray mattress significantly increased the radiation dose compared to the no mattress condition ($p < .05$). There was a statistically significant difference between the dose for mattress and no mattress, the mattress dose being higher. However, this was not a significant increase, it is in the range of 2.26% - 3.40% for newer mattresses. This is hardly significant.

The clinical impact of the mattress shown in the percentage decrease in IAK applied to the mAs in Table 5.15 (Page 168). This shows that a clinically insignificant decrease in mAs would be delivered to the image receptor with a decrease no greater than 0.1 mAs. A change of 25%-35% is required to make a visible change in image noise; therefore, reductions below this level are not considerable (Fauber, 2013). The change in signal detected by the image receptor in this thesis ranged from 0.73% to 12.99%.

The variability in radiation attenuation is due to the variability of the attenuation characteristics of the component materials of the mattresses, which result in the absorption of some photons. However, these data were not available. Thus, a prospective longer-term study is needed for conclusions to be made.

Nevertheless, the difference in the radiation attenuation of all thin (2.5 cm) X-ray mattresses came more at lower voltages (i.e. 65kV, 0.73%-12.99%) than at higher voltages (i.e.

110kV, 1.26%-9.91%). This dose variability is important in compensating for the decrease in primary photons in the presence of certain X-ray mattresses. Thus, to reduce the risk of increasing the photon flux when a mattress is present, optimising the voltage to produce the effective dose is preferred (Tugwell et al., 2017).

The newer mattresses attenuated the least amount of the primary beam, which could be because the newer materials have a lower density sponge and/or coating material. The radiation dose method and resulting data could be of use to manufacturers in the development of new mattresses and new materials. Significant decreases in IAK and effective mAs could indicate that the material used is either too dense or too thick.

An analysis of correlations in Table 6.1 showed a moderate negative correlation between the IAK and the age of the mattress being tested.

Table 6.1: Correlations Between IAK and Age of the Mattresses 2.5 cm Thick

Exposure factors	Correlation
65kV 40mAs	-0.28
70kV 25mAs	-0.29
75kV 20mAs	-0.31
80kV 14mAs	-0.37
85kV 10mAs	-0.36
90kV 8mAs	-0.37
95kV 6.3mAs	-0.36
100kV 5.6mAs	-0.36
105kV 4.5mAs	-0.37
110kV 4mAs	-0.41

6.4.2. Thicker Mattresses

The absorption of the primary X-ray beam by the mattresses decreases the radiation dose, consequently affecting the number of photons reaching the image detector. Mattress thickness correlates with radiation attenuation, wherein the thicker the mattress, the more

radiation it attenuates. Conversely, the thinner the mattress, the less radiation it attenuates. This finding is typified by the generally higher IAK dose in thinner mattresses (2.5 cm > 5 cm) than in thicker mattresses (8 cm and 13 cm). However, as shown in Table 5.14 (Page 167), the addition of a thicker mattress resulted in the absorption of the primary beam and a mean reduction of IAK of 39.77 mGy. As with the thinner mattresses, these differences are clinically insignificant as the change in mAs to compensate for the attenuation would be 0.05 mAs.

The outcomes presented (Section 5.4, Page 163) demonstrate the differences in radiation dose (IAK) for the X-ray table mattresses. Figure 5.18 indicated that thicker mattresses had lower sensor doses because they absorbed more X-ray photons compared to thinner mattresses.

A negative correlation was found between the thickness of a mattress and the measured IAK, with correlation coefficients ranging from -0.77 to -0.49 (Table 6.2). However, as shown in Table 5.16 (Page 169), the percentage of dose attenuation for the 13 cm mattress with 10 years of age at all mAs values was 12.13%-17.10%. For the 8 cm mattress with one year of age, the range was from 13.90%-17.22%, while the new 5 cm mattress ranged from 8.67% to 11.44%. For mattresses with different thicknesses, the new 5 cm thickness, named the Black-Grey (Welded) mattress, had the highest radiation dose indicating low radiation attenuation compared to other thicker mattresses.

While little research into mattress attenuation exists, research has been performed on other pieces of apparatus that can sit in the primary beam. Mutch and Wentworth (2007) arrived at the same results in their study investigating incubator trays in the special care baby unit. They determined that the incubator with the broadest mattress (10 cm thick) showed the lowest reduction factor of 40% and produced the same quality of images compared to the other mattresses and incubator models. This finding highlights the significance of considering

several factors linked to an object or piece of equipment in the path of the primary beam. The density and thickness of the absorbent medium between the X-ray tube are essential factors that should be considered when procuring imaging equipment (ArjoHuntleighs, 2010).

The difference observed between the absorbing characteristics of these mattresses (thinner and thicker) could be due to the thickness or scatter produced. Once again, as the data of these mattresses were not available, conclusions cannot be made without a prospective longer-term study being undertaken.

Table 6.2: Correlations of IAK and Breadth of Thicker Mattresses

Exposure factors	Correlation
65kV 40mAs	-0.77
70kV 25mAs	-0.74
75kV 20mAs	-0.66
80kV 14mAs	-0.65
85kV 10mAs	-0.57
90kV 8mAs	-0.59
95kV 6.3mAs	-0.59
100kV 5.6mAs	-0.49
105kV 4.5mAs	-0.69
110kV 4mAs	-0.54

In principle, the 'denser' the material composition of the matter, the higher the probability of interaction between the photons and the materials of the mattress. Thus, when considering a mattress made of the same material and density, a thicker mattress provides more opportunity for the primary photons to ionize the atomic structures of the mattress, thereby absorbing these and making them unable to reach the patient due to a decreased exit dose (Becker et al., 2007).

In this situation, the image detector requires the X-ray tube to increase the radiation output to compensate for the attenuated beams and allow the transmission of enough photons to create an acceptable X-ray image. However, doing so increases the patient dose, which may have a negative effect on the patient by increasing the exposure time and the quantity of scattered radiation (Carucci, 2013; Uppot et al., 2007; Yanch et al., 2009).

However, the purpose of the AEC is to regulate the amount of radiation reaching the detector to ensure the signal and noise reaches a level set by the manufacturer, which is deemed to be adequate for IQ. The AEC can help limit the over-radiation of a patient; however, in the mattress scenarios the AEC would have compensated for lost photons and increase the exposure time to achieve the required noise and signal levels. Thus, the AEC increases the

radiation dose administered to the patient when an attenuator, such as a table mattress, is introduced.

6.5. Part 4: Evaluation of X-ray table mattresses for IQ

6.5.1. Thinner (2.5 cm) and thicker mattresses

X-ray table mattresses should not reduce the quality of an image since it may lead to an inaccurate diagnosis. A near radiolucent material like a mattress between the patient and the detector is likely to absorb photons, hence causing further scatter which reduces the quality of an image (Hess and Neitzel, 2012; Whitley et al., 2015).

According to Uffman and Schaefer-Prokop (2009), noise in an image is inversely associated with the detector radiation dose, which demonstrates a sign of the quality of an image. By utilising the CDRAD IQ inverse (IQF_{inv}), a measurement of the object quality was undertaken. This process was conducted for all the mattresses. Overall, there were statistically significant differences of $p < .05$ in the quality of physical objects between the 'no mattress' and 'with mattress' conditions. This finding confirmed that, in all cases, the inclusion of mattresses reduces IQ.

In this thesis, each mattress affected the IQ differently, with IQ reducing as the kVp increased for all mattresses. As can be seen in Figures 5.19 and 5.20 (Section 5.5, Page 172), the oldest mattress demonstrated the lowest IQ for all acquisition values. This is excluding the H3 clinic R mattress (20 years) 2.5 cm, which had a value of 65 kV/40 mAs as indicated in Figure 5.18. Furthermore, the Black-Grey (Welded) mattress (5cm) had the lowest IQ compared to the acquisition values found in the other mattresses.

These results show that, compared with a 'no mattress' condition, the addition of a mattress resulted in a deterioration in IQ of 0.21 for those measured through the IQFinv across

all the mattresses used in this thesis. However, it is highly likely that a decrease in IQ of 0.21 would be undetectable to anyone viewing the image (Al-Murshedi, 2018). Clinically, these differences are therefore insignificant because the change in mAs needed to compensate for the attenuation would be as low as 0.1 mAs.

Clinically, the differences between the mattress and no mattress conditions would be imperceptible to an observer, suggesting no deterioration in the clinical quality of the image. Notably, there is no correlation between IQFinv and the age of the mattress (correlation coefficients range from -0.25 to 0.25; see Table 6.3).

Table 6.3: Correlation of IQFinv and Age of Mattress

Exposure factors	**Correlation**
65kV 40mAs	0.07
70kV 25mAs	-0.08
75kV 20mAs	-0.17
80kV 14mAs	-0.05
85kV 10mAs	0.25
90kV 8mAs	0.04
95kV 6.3mAs	-0.11
100kV 5.6mAs	-0.25
105kV 4.5mAs	-0.16
110kV 4mAs	-0.02

The oldest 2.5 cm thick mattresses demonstrated the lowest IQ for all acquisition values. This is excluding the H3 clinic R mattress (20 years), which had a value of 65 kV/40 mAs as indicated in Figure 5.19. The newest mattresses (Sewn Anti-Static and Black-Grey (Welded) mattresses) demonstrated the best IQ for all acquisition values. The H1R1R2 (7 years old) and H1R1R3 (0 years old) mattresses produced the lowest IQ. However, among the thicker mattresses, the thickest mattress (13 cm) demonstrated the best IQ for all acquisition values. The 8-cm mattress, H4 Screening R, produced the lowest IQ.

6.5.2. The influence of mattress thickness on IQ

In principle, radiation attenuation correlates with IQ since the effective dose connects the two concepts. Therefore, the lower the attenuation caused by the mattress, the more exit dose/photons will reach the image detector to generate the image, resulting in a higher quality image. However, the quality, type, design, and thickness of a mattress may compromise the IQ due to the interactions of the primary beam, which decreases the exit dose (Aichinger et al., 2004).

As seen in the results (Figures 5.19 to 5.21), the 2.5 cm X-ray mattresses showed better IQ than the thicker mattresses. This difference is likely due to the type of material, density, foam, and thickness of the mattresses. Thus, it can be concluded that thickness is proportional to the IQ since the specifications of the mattresses were not consistent. However, thinner mattresses produce the best IQ, which can be further optimised.

These data suggest that regular ongoing quality assurance of mattress performance may not be required to maintain attenuation properties or IQ. Manufacturers in the development of new mattresses and mattress materials should use tests. These data should also be made available to X-ray departments for further mattress testing, as needed.

6.5.3. Summary of radiation attenuation and IQ

Based on the results of this study, the new mattress with a 2.5 cm thickness is the best at ‘transmitting’ radiation, thus imposing a minimal dose to the patient. It also had the best IQ. However, the type of material, composition, structure, morphology, design, and foam used should be verified since there is variability in the values generated. These results can be applied

to the improvement of X-ray imaging and diagnosis as well as to the innovation of methods and intervention to compensate for the poor quality and performance of other X-ray mattresses.

It has been demonstrated that mattresses have a clinically insignificant impact on the primary beam and the IQ measured through IQFinv. While a correlation exists between age and attenuation, a correlation was not found between age and IQ. Additionally, clinically, the age of the mattress has no impact on the exposure factors an operator would select, the mAs delivered by an automatic exposure control system or the perceptible quality of an image. The method developed in this thesis could be used by manufacturers to objectively evaluate the performance of new materials and provide potential users with specifications of new products.

The next chapter discusses the limitations of this thesis, including the 3D phantom, and highlights possible avenues for future work.

Chapter Seven: Conclusions, Limitations and Future Work

This thesis validated a novel 3D phantom to evaluate the pressure distribution of X-ray mattresses and developed a new method to evaluate IQ impact and radiation attenuation. This chapter summarises the key findings of the thesis and presents the overall conclusion.

Following a review of the literature to enhance the understanding of the topic, this thesis developed a method of measurement to assess X-ray mattress requirements. This opened the possibility of examining the quality of mattresses before using them to ensure they limit the harm caused to patients who are required to lie on them for long periods.

A novel method to test X-ray mattresses for interface pressure was developed and validated as an index of mattress performance. This method could be used for assessing bed mattresses during the design and development by manufacturers. Manufacturers could then provide phantom interface pressure data to inform procurement decisions when matching mattress characteristics to medical imaging examinations. Additionally, the data collected for this thesis provide valuable new information about the attenuation properties of clinically used mattresses, the impact on IQ and the pressure redistribution for X-ray table mattresses. These findings could be used as a catalyst for future work to examine medical mattresses, such as X-ray, CT and MR scanners mattresses, as these data are currently not available. In addition, PPI reduces significantly when an X-ray table mattress is used and thus consideration needs to be given to determining circumstances when a mattress is not to be used. Given that X-ray mattresses in clinical use display a wide range of pressure distribution properties, it is important that clinical

standards be established, perhaps using PPI and IPR, for mattress performance and testing to occur.

The findings of the pilot study presented in Sections 5.1 and 5.2 suggest that the 3D phantom models used in this study are valid representations of the human body and jeopardy areas. Positive correlations were observed between the PPI values obtained for the patients and the 3D phantoms. The shape analysis, comparing the images of patients and 3D phantoms, proved that similarities exist between the jeopardy areas of the human body and the 3D phantoms.

The results presented the radiation attenuation properties of each type of X-ray mattress (e.g. thickness). A statistically significant difference in radiation doses was observed between the X-ray mattresses compared with hard surfaces (X-ray tables) but It was found that clinically these differences are insignificant as the change in mAs to compensate for the attenuation would be between 0.01 and 0.13 mAs. Practically, it is unlikely any X-ray equipment would have this level of precision when setting mAs values for bucky work. Among all mattresses tested, considerable variation was found in the percentage of absorption by each mattress. Increased mattress thickness could increase the radiation dose due to the need to increase mAs to compensate for the attenuated primary beam.

The results demonstrate that mattresses have a clinically insignificant impact on the image quality measured through IQFinv. While age does correlate with attenuation, it does not correlate with image quality. However, clinically, the age of a mattress has no impact on the exposure factors an operator would select or the mAs delivered by an automatic exposure control system, or on the perceptible quality of an image.

Overall, the outcome of the thesis presents a novel method that could measure and assess X-ray mattress requirements for pressure redistribution, X-ray transmission and low contrast detail detection. Furthermore, the method described could be used by manufacturers to evaluate objectively the performance of new materials and could also provide specifications on new products.

Implications for practice for this study: The 3D phantom can be used to help investigate pressure redistribution properties of new and existing X-ray table mattresses. On the same basis the CDRAD and associated analyser software can be used to investigate whether image quality is affected by the imposition of a mattress. Similarly, the IAK method can investigate mattress radiation attenuation properties. It is unlikely that radiation attenuation or image quality would alter as the mattress ages, and these tests have value in the design, construction, and initial testing of mattresses prior to use in clinics. Whereas the pressure analysis method would have value in the design, construction, initial testing, and ongoing use at regular intervals. For the latter, it is hypothesised that mattress pressure redistribution properties would change through use as time progresses. The data could therefore be used to inform decisions about mattress replacement.

7.1. Limitations

The 3D phantom is limited in that it is not deformable, and, unlike for humans, there is no soft tissue component, meaning it is not truly anthropomorphic. Therefore, using 3D phantoms to examine the X-ray mattresses in this thesis raised some issues. This is because phantoms are limited by their lack of movement and anatomical variation, especially for testing

the risk of PUs, despite these 3D phantoms simulating the shape of a human body. Owing to the limitations that the 3D phantom demonstrated, the findings of the thesis should be applied with caution. Notably, the 3D phantom was a satisfactory representation of the human body in the jeopardy areas, but it was not an exact representation of a patient.

7.2. Recommendations

The pressure-related work in this thesis showed the limited evidence and study gaps in addressing X-ray table mattress use. This can be seen in the scarcity of literature found to support the reviews and the conflicting findings about the use of mattresses on X-ray tables. Future studies should expand the evidence on patient discomfort issues associated with the decision to use or not to use a mattress and the effect of different thickness sizes.

Other types of imaging tables use thinner mattresses or do not have a mattress at all. As such, this thesis could be extended to include and/or focus on other types of mattresses, such as those found on MR and CT tables. Unlike X-ray tables, tables used for CT and MR procedures are curved and the mattresses superimposed onto the tables are very thin (thinner than 2.5 cm).

Data collected within this thesis provides valuable and up-to-date information on a novel method for comparing the performance of X-ray table mattresses. The method described in this thesis could be used by manufacturers in the development of new mattresses and mattress materials. The findings can be used as a baseline for future local and national reference for manufacturers and to inform mattress procurement. These data should be made available to X-ray departments for further mattress testing and ongoing quality testing when in clinical use. Baseline and clinical standards' data can thus be used to inform decisions about when to replace mattresses in clinical use.

7.3. Statement of Novelty

The following list presents the novel contributions of this thesis:

1. A novel method for comparing the performance of X-ray table mattresses in several hospitals with an analysis of new, commercially available X-ray table mattresses that determined whether x-ray mattresses might have maximum (patient) weights beyond which bottoming out would occur. This method could help in the design of new X-ray table mattresses.
2. The provision of new information on the relationship between initial radiolucency testing and X-ray table mattresses which should be considered in quality assurance testing and in the imaging department. This assertion is partly confirmed when it is considered that some mattresses are still in continual use after 20 years' service.
3. The provision of information about mattress construction with maximum patient weights to show for how long the mattress will be effective. Manufacturers should provide baseline data for a range of pressure-related metrics to assess mattress pressure redistribution properties.
4. A novel method that allows users to objectively evaluate the performance of their mattresses and make informed decisions about when they require replacement.
5. The manufacturers of mattresses for radiology departments can use these methods to test their products at the development stage and obtain a set of values to quote in their specification to illustrate the performance of their products. This would provide purchasers with an objective measurement by which to inform their procurement decisions.

6. A novel method for comparing the impact of X-ray mattresses on radiation dose and IQ. This new method is also likely to be beneficial for the assessment of X-ray mattresses within radiography departments in hospitals. Establishing this novel method was necessary since it was observed that there is no standardised method which considers both IQ and dose levels within radiography departments in hospitals.

7.4. Future work

- Future studies could replicate this study with a larger number of hospitals and X-ray table mattresses.
- Further investigations should be conducted to test different X-ray machines used in various radiology departments to identify variations in IQ and radiation dose.
- To investigate the interface pressure risks, the study should be duplicated for all medical imaging and radiotherapy surfaces for elderly cancer patients who use these medical surfaces.
- Additional attention should be given to the examining of mattresses of different qualities and specifications and those used in other areas of the hospital, such as CT and MR scanning, procedure rooms and medical trolleys.

References

Agrawal, K. and Chauhan, N. (2012). ‘Pressure ulcers: Back to the basics’, *Indian Journal of Plastic Surgery: Official Publication of the Association of Plastic Surgeons of India*, 45(2), p. 244-254.

Ahmed, N.A., Nayl, A.I. and Suliman, I.I., 2012. ‘Equipment performance and radiation protection status in X-ray fluoroscopy units in Sudan’, *Radiation protection dosimetry*, 148(2), pp. 174-180.

Aichinger, H., Joachim, D. and Sigrid Joite-Barfuβ, M.S. (2004). *Radiation exposure and image quality in X-ray diagnostic radiology.* Berlin: Springer-Verlag. Available at: https://doi.org/10.1017/CBO9781107415324.004 (Accessed: 30/11/2017).

Al-Murshedi, S., Hogg, P. and England, A. (2018). 'An investigation into the validity of utilising the CDRAD 2.0 phantom for optimisation studies in digital radiography', *Br J Radiol*, [Online]. Available at: https://europepmc.org/articles/PMC6223154 (Accessed 25/2/2019).

Al-Murshedi, S., Hogg, P., Lanca, L. and England, A. (2018). 'A novel method for comparing radiation dose and image quality between and within different X-ray units in a series of hospitals', *Journal of Radiological Protection,*. [Online]. Available at: https://doi.org/10.1088/1361-6498/aae3fa (Accessed: 25/2/2019).

Alfaro-Almagro, F., Jenkinson, M., Bangerter, N.K., Andersson, J.L., Griffanti, L., Douaud, G., Sotiropoulos, S.N., Jbabdi, S., Hernandez-Fernandez, M., Vallee, E. and Vidaurre, D. (2018). ‘Image processing and quality control for the first 10,000 brain imaging datasets from UK Biobank’, *Neuroimage*, 166, pp. 400-424.

Alresheedi, N., Walton, A.L., Tootell, A.K., Webb, J. and Hogg, P. (2020). 'A phantom-based method to assess X-ray table mattress interface pressures', *Journal of Medical Imaging*

and Radiation Sciences, pp. 30/7/2020. [Online]. Available at: http://www.jmirs.org/article/S1939865420300473/fulltext (Accessed 22 June 2020).

Alvarez, O.M., Brindle, C.T., Langemo, D., Kennedy-Evans, K.L., Krasner, D.L., Brennan, M.R. and Levine, J.M. (2016). 'The VCU pressure ulcer summit', *Journal of Wound, Ostomy and Continence Nursing*, 43(5), pp. 455-463.

Anatoli Vladimirov, K. K. (n.d.). *A definition of image quality: The image quality figure*.

Angmorterh, S.K. (2016). *An investigation into interface pressure (IP) risk of healthy volunteers on modern medical imaging and radiotherapy tables.* PhD. University of Salford.

Angmorterh, S.K., England, A., Webb, J., Szczepura, K., Stephens, M., Anaman-Torgbor, J., Ofori, E.K. and Hogg, P. (2019). 'An investigation of pressure ulcer risk, comfort, and pain in medical imaging', *Journal of Medical Imaging and Radiation Sciences*, pp. 1-10. [Online]. Available at: https://doi.org/10.1016/j.jmir.2018.07.003 (Accessed: 17/01/2020)

Arora, N. (2007). 'Mosfet modeling for VLSI simulation: Theory and practice', *Chemistry &amp*.

Aydin, C., Donaldson, N., Stotts, N.A., Fridman, M. and Brown, D.S., 2015. 'Modeling hospital-acquired pressure ulcer prevalence on medical-surgical units: Nurse workload, expertise, and clinical processes of care', *Health Services Research*, 50(2), pp. 351-373.

Aziz, Z. and Bell-Syer, S.E.M. (2015). 'Electromagnetic therapy for treating pressure ulcers', *Cochrane Database of Systematic Reviews*,. [Online]. Available at: https://doi.org/10.1002/14651858.CD002930.pub6 (Accessed: 12/6/2018).

Badano, A., Revie, C., Casertano, A., Cheng, W.C., Green, P., Kimpe, T., Krupinski, E., Sisson, C., Skrøvseth, S., Treanor, D. and Boynton, P. (2015). 'Consistency and

standardization of color in medical imaging: A consensus report', *Journal of Digital Imaging*, 28(1), pp. 41-52.

Bader, D.L. and White, S.H. (1998). 'The viability of soft tissues in elderly subjects undergoing hip surgery', *Age Ageing*, 27, pp. 217-21.

Bain, D.S., Ferguson-Pell, M.W. and Davies, P. (2001). 'An instrument for in-service testing of mattresses', *Journal of Tissue Viability*, 11(4), pp. 161-165.

Bain, D., Ferguson-Pell, M. and McLeod, A. (2003). 'Evaluation of mattresses using interface pressure mapping', *Journal of Wound Care*, 12(6), pp. 231-235.

Balonov, M.I. and Shrimpton, P.C. (2012). 'Effective dose and risks from medical x-ray procedures.' *Annals of the ICRP*, 41(3-4), pp. 129-141.

Bangova, A. (2013). Prevention of pressure ulcers in nursing home residents. *Nursing Standard*, 27(24), pp. .

Banks, M.D., Graves, N., Bauer, J.D. and Ash, S. (2013). 'Cost effectiveness of nutrition support in the prevention of pressure ulcer in hospitals', *European Journal of Clinical Nutrition* [Online]. Available at: https://doi.org/10.1038/ejcn.2012.140 (Accessed: 20/5/2019).

Barateau, M. and Salles, N. (2015). 'The contribution of telemedicine in the management of pressure ulcers in palliative care', *Soins; la revue de reference infirmiere*, (792), pp. 46-48.

Båth, M. (2010). 'Evaluating imaging systems: Practical applications', *Radiation Protection Dosimetry*, 139(1-3), pp. 26-36.

Bauer, C. (2012). 'Pressure ulcer update for primary care', *Journal for Nurse Practitioners*,. [Online]. Available at: https://doi.org/10.1016/j.nurpra.2012.09.015 (Accessed: 12/6/2018).

Bauer, K., Rock, K., Nazzal, M., Jones, O. and Qu, W. (2016). 'Pressure ulcers in the United States' inpatient population from 2008 to 2012: Results of a retrospective nationwide study. *Ostomy/Wound Management*, 62(11), pp. 30-38.

Beaman, J.J., Barlow, J.W., Bourell, D.L., Crawford, R.H., Marcus, H.L. and McAlea, K.P. (1997). 'Solid freeform fabrication: A new direction in manufacturing', *Kluwer Academic Publishers, Norwell, MA*, 2061, pp. 25-49.

Beeckman, D., Defloor, T., Demarré, L., Van Hecke, A. and Vanderwee, K. (2010). 'Pressure ulcers: Development and psychometric evaluation of the attitude towards pressure ulcer prevention instrument (APuP)', *International Journal of Nursing Studies*.

Benbow, M. (2009). 'Principles of pressure ulcer prevention', *Practice Nursing*, 20(10), pp. 504-509.

Benner, T., Campagna, S., Feiweier, T., Kuehn, B., Loeffler, T., Speckner, T., Speier, P., Splitthoff, D.N., Stoecker, S., Sukkau, J. and Wullenweber, M. (2019). Medical imaging apparatus having multiple subsystems, and operating method therefor. US Patent Application: 10/241, pp. 175.

Bennett, G., Dealey, C. and Posnett, J. (2004). The cost of pressure ulcers in the UK. *Age and Ageing*, 33(3), pp. 230-235.

Bennett, M.K., Shao, M. and Gorodeski, E.Z. (2017). 'Home monitoring of heart failure patients at risk for hospital readmission using a novel under-the-mattress piezoelectric sensor: A preliminary single center experience', *Journal of Telemedicine and Telecare*, 23(1), pp. 60-67.

Bhattacharya, S., and Mishra, R. K. (2015). 'Pressure ulcers: Current understanding and newer modalities of treatment', *Indian Journal of Plastic Surgery: Official Publication of the Association of Plastic Surgeons of India*, 48(1), p. 4.

Birkfellner, W. (2016). *Applied medical image processing: A basic course.*: CRC Press.

Bishop, C.H. and Droste, L.R. (2014). 'Pressure ulcer prevention in the patient with spinal cord injury on hemodialysis', *Nephrology Nursing Journal: Journal of the American Nephrology Nurses' Association*, 41(1), p. 14.

Black, J., Alves, P., Brindle, C.T., Dealey, C., Santamaria, N., Call, E. and Clark, M. (2015). 'Use of wound dressings to enhance prevention of pressure ulcers caused by medical devices', *International Wound Journal*, 12(3), pp. 322-327.

Black, J., Baharestani, M., Cuddigan, J., Dorner, B., Edsberg, L., Langemo, D., Posthauer, M.E., Ratliff, C. and Taler, G. (2007). 'National Pressure Ulcer Advisory Panel's updated pressure ulcer staging system', *Advances in Skin & Wound Care*, 20(5), pp. 269-274.

Black, J., Baharestani, M., Cuddigan, J., Dorner, B., Edsberg, L., Langemo, D., Posthauer, M.E., Ratliff, C. and Taler, G. (2007). 'National Pressure Ulcer Advisory Panel's updated pressure ulcer staging system', *Dermatology Nursing / Dermatology Nurses' Association*.

Bly, D., Schallom, M., Sona, C. and Klinkenberg, D. (2016). 'A model of pressure, oxygenation, and perfusion risk factors for pressure ulcers in the intensive care unit', *American Journal of Critical Care*, 25(2), pp. 156-164.

Bontrager, K.P.L. (2005). *Handbook of radiographic positioning and techniques*.

Bordier, C., Klausz, R. and Desponds, L. (2014). 'Patient dose map indications on interventional X-ray systems and validation with gafchromic XR-RV3 film', *Radiation Protection Dosimetry*, [Online]. Available at: https://doi.org/10.1093/rpd/ncu181 (Accessed: 10/12/2019).

Bourne, R. (2010), *Fundamentals of digital imaging in medicine.* New York: Dordrecht.

Bouten, C.V.C. and Oomens, E.B.C. (1999). ‘The aetiology of pressure sores: A tissue and cell mechanics approach’, *Biomedical Aspects of Manual Wheelchair Propulsion: The State of the Art II*, 5, pp. 52.

Bouten, C.V., Oomens, C.W., Baaijens, F.P. and Bader, D.L. (2003). ‘The etiology of pressure ulcers: Skin deep or muscle bound? *Archives of Physical Medicine and Rehabilitation*, 84(4), pp. 616-619.

Bowling, A. (2014). *Research methods in health: Investigating health and health services*. UK: McGraw-Hill Education.

Boyko, T.V., Longaker, M.T. and Yang, G.P. (2018). 'Review of the current management of pressure ulcers', *Advances in Wound Care*, 7(2), pp. 57-67. [Online]. Available at: https://doi.org/10.1089/wound.2016.0697 (Accessed: 30/3/2019).

Brennan, M.R., Laconti, D. and Gilchrist, R. (2014). ‘Using conformational positioning to reduce hospital-acquired pressure ulcers’, *Journal of Nursing Care Quality*, 29(2), pp. 182-187.

Brenner, D.J. (2008). Effective dose: A flawed concept that could and should be replaced. *The British Journal of Radiology*, 81(967), pp. 521-523.

Brenner, D.J. (2014). ‘What we know and what we don’t know about cancer risks associated with radiation doses from radiological imaging’, *The British Journal of Radiology*, 87(1035), pp. 20130629.

Brienza, D. (2007). Pressure ulcers, more questions than answers, *Proceedings of the 23rd International Seating Symposium*, Orlando, Fl..

Brienza, D. (2007). Rollin’, rollin’, rollin’ … Get this wheelchair rollin: Selecting access methods for power mobility. *23rd International Seating Symposium, Moving into the Age of Accountability*, 8th – 10th March 2007. [Online] Available at:

http://www.iss.pitt.edu/ISS_Pre_Bro/ISS_2007.pdf (Accessed: 12/2/2018).

Brienza, D.M., Karg, P.E., Geyer, M.J., Kelsey, S. and Trefler, E. (2001). 'The relationship between pressure ulcer incidence and buttock-seat cushion interface pressure in at-risk elderly wheelchair users', *Archives of Physical and Medical Rehabilitation*, 4, pp. 529-33.

Brix, G., Lechel, U., Veit, R., Truckenbrodt, R., Stamm, G., Coppenrath, E.M., Griebel, J. and Nagel, H.D. (2004). 'Assessment of a theoretical formalism for dose estimation in CT: An anthropomorphic phantom study', *European Radiology*, 14(7), pp. 1275-1284.

Brosi, P., Stuessi, A., Verdun, F.R., Vock, P. and Wolf, R. (2011). 'Copper filtration in pediatric digital X-ray imaging: Its impact on image quality and dose', *Radiological Physics and Technology*, 4(2), pp. 148-155. [Online]. Available at: https://doi.org/10.1007/s12194-011-0115-4 (Accessed: 15/8/2019_).

Bryant, R. and Nix, D. (2015). 'Acute and chronic wounds: Current management concepts', *Elsevier Health Sciences*.

Burger, W. and Burge, M.J. (2016). 'Digital image processing: An algorithmic introduction using Java'.

Bush, T.R., Leitkam, S., Aurino, M., Cooper, A. and Basson, M.D. (2015). 'A comparison of pressure mapping between two pressure-reducing methods for the sacral region', *Journal of Wound, Ostomy and Continence Nursing*, 42(4), pp. 338-345.

Bushberg, J.T., Seibert, J.A., Leidholdt, E.M. and Boone, J.M. (2002). *The essential physics of medical imaging.* 2nd edn. Philadelphia: Lippincott Williams & Wilkins, 16, p. 933.

Bushong, S.C. (2013). 'Radiologic science for technologists-E-book: Physics, biology, and protection', *Elsevier Health Sciences*,.

Campbell, B. (2013). 'Inditherm OTM1 heated mattress: Measurement of aluminium

equivalent and assessment of radiographic appearance', 44(0),.

Casey, J. and Gittins, L. (2013). ‘Use of tilt-in-space in seating systems for adults with physical disabilities’, *Physical Therapy Reviews*, 18(4), pp. 285-299.

Chai, C.Y. and Bader, D.L. (2013). 'The physiological response of skin tissues to alternating support pressures in able-bodied subjects', *Journal of the Mechanical Behavior of Biomedical Materials*, _____, _____. [Online]. Available at: https://doi.org/10.1016/j.jmbbm.2013.05.014 (Accessed: 10/4/2020.

Chai, C.Y., Sadou, O., Worsley, P.R. and Bader, D.L. (2017). 'Pressure signatures can influence tissue response for individuals supported on an alternating pressure mattress', *Journal of Tissue Viability*. [Online]. Available at: https://doi.org/10.1016/j.jtv.2017.05.001 (Accessed: 03/5/2018).

Chen, H., Zhang, Y., Kalra, M.K., Lin, F., Chen, Y., Liao, P., Zhou, J. and Wang, G. (2017). ‘Low-dose CT with a residual encoder-decoder convolutional neural network’, *IEEE Transactions on Medical Imaging*, 36(12), pp. 2524-2535.

Chen, H., Zhang, Y., Zhang, W., Liao, P., Li, K., Zhou, J. and Wang, G. (2017). ‘Low-dose CT via convolutional neural network’, *Biomedical Optics Express*, 8(2), pp. 679-694.

Chopra, P., Tinkle, B., Hamonet, C., Brock, I., Gompel, A., Bulbena, A. and Francomano, C. (2017). 'Pain management in the Ehlers–Danlos syndromes', *American Journal of Medical Genetics, Part C: Seminars in Medical Genetics*,. [Online]. Available at: https://doi.org/10.1002/ajmg.c.31554 (Accessed: 10/4/2020).

Clements, L., Moore, M., Tribble, T. and Blake, J. (2014). ‘Reducing skin breakdown in patients receiving extracorporeal membranous oxygenation’, *Nursing Clinics*, 49(1), pp. 61-68.

Cohnen, M., Wittsack, H.J., Assadi, S., Muskalla, K., Ringelstein, A., Poll, L.W., Saleh, A. and Mödder, U. (2006). ‘Radiation exposure of patients in comprehensive computed tomography of the head in acute stroke’, *American Journal of Neuroradiology*, 27(8), pp. 1741-1745.

Conine, T.A., Hershler, C., Daechsel, D., Peel, C. and Pearson, A. (1994). 'Pressure ulcer prophylaxis in elderly patients using polyurethane foam or Jay® wheelchair cushions', *International Journal of Rehabilitation Research*, 17, pp. 123-137.

Costa, P., Galdran, A., Meyer, M.I., Niemeijer, M., Abràmoff, M., Mendonça, A.M. and Campilho, A. (2018). ‘End-to-end adversarial retinal image synthesis’, *IEEE Transactions on Medical Imaging*, 37(3), pp. 781-791.

Crawford, S.A., Stinson, M.D., Walsh, D.M. and Porter-Armstrong, A.P. (2005). ‘Impact of sitting time on seat-interface pressure and on pressure mapping with multiple sclerosis patients’, *Archives of Physical Medicine and Rehabilitation*, 86(6), pp. 1221-1225.

Davis, S. and Affatato, A. (2006). 'Blunt chest trauma: Utility of radiological evaluation and effect on treatment patterns', *American Journal of Emergency Medicine*. [Online]. Available at: https://doi.org/10.1016/j.ajem.2006.03.022 (Accessed: 18/12/2017).

Dealey, C., Posnett, J. and Walker, A. (2012). ‘The cost of pressure ulcers in the United Kingdom’, *Journal of Wound Care*, 21(6), pp. 261-266.

Defloor, T. (1999). ‘The risk of pressure sores: A conceptual scheme’, *Journal of Clinical Nursing*, 8(2), pp. 206-216.

Demarré, L., Beeckman, D., Vanderwee, K., Defloor, T., Grypdonck, M. and Verhaeghe, S. (2012). 'Multi-stage versus single-stage inflation and deflation cycle for alternating low pressure air mattresses to prevent pressure ulcers in hospitalised patients: A randomised-controlled clinical trial', *International Journal of Nursing Studies*,. [Online]. Available

at: https://doi.org/10.1016/j.ijnurstu.2011.10.007 (Accessed: 30/5/2018).

Demarré, L., Van Lancker, A., Van Hecke, A., Verhaeghe, S., Grypdonck, M., Lemey, J., Annemans, L. and Beeckman, D. (2015). 'The cost of prevention and treatment of pressure ulcers: A systematic review', *International Journal of Nursing Studies*, 52(11), pp. 1754-1774.

Demarre, L., Vanderwee, K., Defloor, T., Verhaeghe, S., Schoonhoven, L. and Beeckman, D. (2012). 'Pressure ulcers: Knowledge and attitude of nurses and nursing assistants in Belgian nursing homes', *Journal of Clinical Nursing*, 21, pp. 1425-1434.

Denk, F., Bennett, D.L. and McMahon, S.B. (2017). 'Nerve growth factor and pain mechanisms', *Annual Review of Neuroscience*,. [Online]. Available at: https://doi.org/10.1146/annurev-neuro-072116-031121 (Accessed: 18/4/2018).

Department of Health and Essence of Care (2010). *Benchmarks for the fundamental aspects of nursing care*, In: HEALTH, D. O. (ed.). London, UK.

Desai, N., Singh, A. and Valentino, D.J. (2010). 'Practical evaluation of image quality in computed radiographic (CR) imaging systems', In *Medical Imaging 2010: Physics of Medical Imaging*, 7622, p. 76224Q. *International Society for Optics and Photonics*.

Dharmarajan, T.S. and Ugalino, J.T. (2002). 'Pressure ulcers: Clinical features and management', *Hospital Physician*, March 2002, pp. 64-71.

Dillavou, M.W., Shum, P.C., Guthrie, B.L., Shenai, M.B., Deaton, D.S. and May, M.B., Help Lightning Inc. and University of Alabama at Birmingham Research Foundation (2019). System and method for image registration of multiple video streams. US Patent Application: 10/181,361.

Dobbins, J.T., Rice, J.J., Beam, C.A. and Ravin, C.E. (1992). 'Threshold perception performance with computed and screen-film radiography: Implications for chest

radiography', *Radiology*, 183(1), pp. 179-187. [Online]. Available at: https://doi.org/10.1148/radiology.183.1.1549669 (Accessed: 11/2/2018).

Dobrzyński, L., Fornalski, K.W. and Feinendegen, L.E. (2015). 'Cancer mortality among people living in areas with various levels of natural background radiation', *Dose-Response*, 13(3), p. 1559325815592391.

Dowsett, D.J., Kenny, P.A. and Johnston, R.E. (2006). *The physics of diagnostic imaging*. 2nd edn..

Doxastakis, M., Suh, H.S., Chen, X., Rincon Delgadillo, P.A., Wan, L., Williamson, L., Jiang, Z., Strzalka, J., Wang, J., Chen, W., Ferrier, N., Ramirez-Hernandez, A., de Pablo, J.J., Gronheid, R. and Nealey, P. (2015). 'Grazing-incidence small angle X-ray scattering studies of nanoscale polymer gratings', *Metrology, Inspection, and Process Control for Microlithography XXIX*,. [Online]. Available at: https://doi.org/10.1117/12.2085824 (Accessed: 19/7/2019).

Dumville, J.C., Land, L., Evans, D. and Peinemann, F. (2015). 'Negative pressure wound therapy for treating leg ulcers', *Cochrane Database of Systematic Reviews*,. [Online]. Available at: https://doi.org/10.1002/14651858.CD011354.pub2 (Accessed: 12/1/2018).

Dumville, J.C., Webster, J., Evans, D. and Land, L. (2015). 'Negative pressure wound therapy for treating pressure ulcers', *Cochrane Database of Systematic Reviews*, (5), pp. [Online]. Available at: https://doi.org/10.1002/14651858.CD011334.pub2 (Accessed: 12/1/2018).

Drummond, D.S., Narechania, R.G., Rosenthal, A.N., Breed, A.L., Lange, T.A. and Drummond, D.K. (1985). 'A study of pressure distributions measured during balanced and unbalanced sitting', *The Journal of Bone and Joint Surgery*, 64-A(7), pp. 1034-1039.

Edsberg, L.E., Black, J.M., Goldberg, M., McNichol, L., Moore, L. and Sieggreen, M.

(2016). 'Revised National Pressure Ulcer Advisory Panel pressure injury staging system', *Journal of Wound, Ostomy and Continence Nursing*, [Online]. Available at: https://doi.org/10.1097/WON.0000000000000281 (Accessed: 22/6/2019).

Edwars, S.L. (2006). 'Tissue viability: Understanding the mechanisms of injury and repair', *Nursing Standard*, 21**,** pp. 48-56.

Ehman, M.O., Bao, Z., Stiving, S.O., Kasam, M., Lanners, D., Peterson, T., Jonsgaard, R., Carter, R. and McGee, K.P. (2017). 'Automated low-contrast pattern recognition algorithm for magnetic resonance image quality assessment', *Medical Physics*, 44(8), pp. 4009-4024.

Eltorai, I.M. (2003). *History of spinal cord medicine*. New York: Demos Medical Publishing.

Engels, D., Austin, M., McNichol, L., Fencl, J., Gupta, S. and Kazi, H. (2016). 'Pressure ulcers: Factors contributing to their development in the OR', *AORN Journal*, 103(3), pp. 271-281. [Online]. Available at: https://doi.org/10.1016/j.aorn.2016.01.008 (Accessed: 15/5/2018).

Eskicioglu, A.M. and Fisher, P.S. (1995). 'Image quality measures and their performance', *IEEE Transactions on Communications*, [Online]. Available at: https://doi.org/10.1109/26.477498 (Accessed: 10/11/2019).

European Pressure Ulcer Advisory Panel (1999). 'Guidelines to treatment of pressure ulcers', *EPURAP Review*, 1(2), pp. 31-33.

European Pressure Ulcer Advisory Panel and National Pressure Ulcer Advisory Panel (2009). *Treatment of pressure ulcers: quick reference guide.* EPUAP and NPUAP.

European Pressure Ulcer Advisory Panel and National Pressure Ulcer Advisory Panel (2009). 'Tratamiento de las úlceras por presión: Guía de referencia rápida', *Gneaupp*.

European Pressure Ulcer Advisory Panel, National Pressure Ulcer Advisory Panel and Pan

Pacific Pressure Injury Alliance (2014). 'Prevention and treatment of pressure ulcers : Quick reference guide', *Clinical Practice Guideline*.

Everton, C., Bird, S., Brito, W., Collé, P., Franco, A.P. and Lutjeber, S. (2014). 'Experimental article: An experimental study to compare the interface pressure and experience of healthy participants when lying still for 20 minutes in a supine position on two different imaging surfaces', , pp. 75-80.

Everton, C., Bird, S., Brito, W., Collé, P., Franco, A.P., Lutjeber, S., Nodeland, K., Rième, S., Siddika, M., Webb, J. and Angmorterh,, S. (2014a). 'Review article – The effects of clinical support surfaces on pressure as a risk factor in the development of pressure ulcers, from a radiographical perspective: A narrative literature review', In P. Hogg, L. Lança (Eds.), Radiation dose and image quality optimisation in medical imaging, Erasmus Intensive Programme OPTIMAX#2014: Lisbon, Portugal.

Everton, C., Bird, S., Brito, W., Collé, P., Franco, AP., Lutjeber, S., Nodeland, K., Rième, S., Siddika, M., Webb, J., and Angmorterh, S. (2014b). 'Experimental article – An experimental study to compare the interface pressure and experience of healthy participants when lying still for 20 minutes in a supine position on two different imaging surfaces', In P. Hogg, L. Lança (Eds.), Radiation dose and image quality optimisation in medical imaging, Erasmus Intensive Programme OPTIMAX#2014: Lisbon, Portugal.

Everton, C., Bird, S., Brito, W., Collé, P., Franco, A.P., Lutjeber, S. and Angmorterh, S. (2015). 'An experimental study to compare the interface pressure and experience of healthy participants when lying still for 20 minutes in a supine position on two different imaging surfaces'.

Fader, M., Bain, D. and Cottenden, A. (2004). 'Effects of absorbent incontinence pads on pressure management mattresses', *Journal of Advanced Nursing*, 48(6), pp. 569-574.

Fauber, T.L. (2013). 'Radiographic imaging & exposure', p. 341. [Online]. Available at: www.elsevier.com/permissions (Accessed 17 June 2020).

Film Badges (2017). Retrieved January 30, 2018 from NDT Resource Center.

Filius, A., Damen, T.H.C., Schuijer-Maaskant, K.P., Polinder, S., Hovius, S.E.R. and Walbeehm, E.T. (2013). 'Cost analysis of surgically treated pressure sores stage III and IV', *Journal of Plastic, Reconstructive and Aesthetic Surgery*, 66(11), pp. 1580-1586. [Online]. Available at: http://dx.doi.org/10.1016/j.bjps.2013.05.014 (Accessed: 19/10/2019).

Fletcher, J. (2015). 'Case series evaluating the use of the dolphin fluid immersion simulation mattress', *Wounds UK*.

Foamrite (2020). *Buy foam and rubber sheets and products online*, Foamrite. [Online]. Available at: https://www.foamrite.co.uk/ (Accessed 26 June 2020). Lin, E.C. (2010). 'Radiation risk from medical imaging', *Mayo Clinic Proceedings*, 85(12), pp. 1142-1146. Fogel, G.R., Toohey, J.S., Neidre, A. and Brantigan, J.W. (2008). 'Fusion assessment of posterior lumbar interbody fusion using radiolucent cages: X-ray films and helical computed tomography scans compared with surgical exploration of fusion', *Spine Journal*. [Online]. Available at: https://doi.org/10.1016/j.spinee.2007.03.013 (Accessed: 05/11/2017).

Forde-Johnston, C. (2014). 'Intentional rounding: A review of the literature', *Nursing Standard*, 28(32), pp. 37.

Funama, Y., Awai, K., Nakayama, Y., Kakei, K., Nagasue, N., Shimamura, M., Sato, N., Sultana, S., Morishita, S. and Yamashita, Y. (2005). 'Radiation dose reduction without degradation of low-contrast detectability at abdominal multisection CT with a low-tube voltage technique: Phantom study', *Radiology*, 237(3), pp. 905-910. [Online]. Available

at: https://doi.org/10.1148/radiol.2373041643 (Accessed: 05/11/2017).

García-Fernández, F.P., Pancorbo-Hidalgo, P.L. and Agreda, J.J.S. (2014). 'Predictive capacity of risk assessment scales and clinical judgment for pressure ulcers: A meta-analysis. *Journal of Wound Ostomy & Continence Nursing*, 41(1), pp. 24-34.

Gardiner, J.C., Reed, P.L., Bonner, J.D., Haggerty, D.K. and Hale, D.G. (2016). 'Incidence of hospital-acquired pressure ulcers–a population-based cohort study', *International Wound Journal*, 13(5), pp. 809-820.

Gelis, A., Dupeyron, A., Legros, P., Benaim, C., Pelissier, J. and Fattal, C. (2009). 'Pressure ulcer risk factors in persons with spinal cord injury part 2: The chronic stage', *Spinal Cord*, 47(9), pp. 651.

Gissibl, T., Thiele, S., Herkommer, A. and Giessen, H. (2016). 'Two-photon direct laser writing of ultracompact multi-lens objectives', *Nature Photonics*, 10(8), p. 554.

Gómez-Batiste, X., Martínez-Muñoz, M., Blay, C., Amblàs, J., Vila, L., Costa, X. and Mitchell, G.K. (2014). 'Prevalence and characteristics of patients with advanced chronic conditions in need of palliative care in the general population: A cross-sectional study', *Palliative Medicine*, 28(4), pp. 302-311.

Goode, P.S. and Allman, R.M. (1998). 'Pressure ulcers', In Duthie. *Practice of Geriatric* pp. 228-35.

Gorecki, C., Lamping, D.L., Brown, J.M., Madill, A., Firth, J. and Nixon, J. (2010). 'Development of a conceptual framework of health-related quality of life in pressure ulcers: A patient-focused approach', *International Journal of Nursing Studies*, 47(12), pp. 1525-1534.

Gould, T.W. and Enomoto, H. (2009). 'Neurotrophic modulation of motor neuron development', *The Neuroscientist*, 15(1), pp. 105-116.

Gravenstein, N., Van Oostrom, J.H. and Caruso, L.J. (2013). ‘Patient repositioning and pressure ulcer risk-monitoring interface pressures of at-risk patients’, *Journal of Rehabilitation Research and Development*, 50(4), pp. 477.

Gulshan, V., Peng, L., Coram, M., Stumpe, M.C., Wu, D., Narayanaswamy, A., Venugopalan, S., Widner, K., Madams, T., Cuadros, J. and Kim, R. (2016). ‘Development and validation of a deep learning algorithm for detection of diabetic retinopathy in retinal fundus photographs’, *Jama*, 316(22), pp. 2402-2410.

Gutjahr, R., Halaweish, A.F., Yu, Z., Leng, S., Yu, L., Li, Z., Jorgensen, S.M., Ritman, E.L., Kappler, S. and McCollough, C.H. (2016). ‘Human imaging with photon-counting-based CT at clinical dose levels: Contrast-to-noise ratio and cadaver studies’, *Investigative Radiology*, 51(7), pp. 421.

Hashemi-Malayeri, B. and Williams, J. (2003). ‘A practical approach for the assessment of patient doses from CT examinations’, Radiography, 64, pp. 35.

Health and Social Care Information Centre (2015). ‘Statistics on obesity, physical activity and diet: England 2015’, *Health and Social Care Information Centre*,).

Hendee, W.R. and Ritenour, E.R. (2003). *Medical imaging physics*. Wiley: Hoboken.

Hendrichova, I., Castelli, M., Mastroianni, C., Piredda, M., Mirabella, F., Surdo, L., Marinis, M.G.D., Heath, T. and Casale, G. (2010). 'Pressure ulcers in cancer palliative care patients', *Palliative Medicine*. [Online]. Available at: https://doi.org/10.1177/0269216310376119 (Accessed: 23/01/2018).

Heywood, N., Brown, L., Arrowsmith, M. and Poppleston, A. (2015). ‘A quality improvement programme to reduce pressure ulcers’, *Nursing Standard (Royal College of Nursing, Great Britain*, 1987), 29**,** pp. 62-70.

Hiles, P., Mackenzie, A., Scally, A. and Wall, B. (2005). 'Recommended standards for the routine performance testing of diagnostic X-ray imaging systems: Institute of Physics and Engineering in Medicine (IPEM); Report No. 91. York: IPEM.

Hine, G.J. and Brownell, G.L. (2013). 'Radiation dosimetry', *Elsevier*.

Hobbie, R.K. and Roth, B.J. (2007). *Intermediate physics for medicine and biology*. Springer Science & Business Media.

Hollingsworth, C.L., Yoshizumi, T.T., Frush, D.P., Chan, F.P., Toncheva, G., Nguyen, G. and Hurwitz, L.M. (2007). 'Pediatric cardiac-gated CT angiography: Assessment of radiation dose', *American Journal of Roentgenology*, 189(1), pp. 12-18.

Hommel, A., Gunningberg, L., Idvall, E. and Bååth, C. (2017). 'Successful factors to prevent pressure ulcers: An interview study', *Journal of Clinical Nursing*, 26(1-2), pp. 182-189.

Hourdakis, J. and Nowotny, R. (2014). 'Instrumentation for dosimetry', in *Diagnostic radiology physics: A handbook for teachers and students*. Endorsed by: American Association of Physicists in Medicine, Asia-Oceania Federation of Organizations for Medical Physics, European Federation of Organisations for Medical Physics.

Hristova, M.G. (2013). 'Metabolic syndrome: From the neurotrophic hypothesis to a theory', *Medical Hypotheses*, 81(4), pp. 627-634.

HSCIC (2014). NHS Safety Thermometer: Patient Harms and Harm Free Care. England December 2012-December 2013, official statistics, in HEALTH, D.O. (Ed.). London.

Huang, J.Y., Kerns, J.R., Nute, J.L., Liu, X., Balter, P.A., Stingo, F.C., Followill, D.S., Mirkovic, D., Howell, R.M. and Kry, S.F. (2015). 'An evaluation of three commercially available metal artifact reduction methods for CT imaging', *Physics in Medicine & Biology*, 60(3), pp. 1047.

Huang, Y.N., Peng, X.C., Ma, S., Yu, H., Jin, Y.B., Zheng, J. and Fu, G.H. (2018). 'Development of whole slide imaging on smartphones and evaluation with Thin Prep cytology test samples: Follow-up study', *JMIR mHealth and uHealth*, 6(4), pp. e82.

ICRP Publication 102 (2007). 'International Commission on Radiological Protection. Managing patient dose in multi-detector computed tomography (MDCT)', *Annals of the ICRP Publication 102 (0702030473).*

Jardini, A.L., Larosa, M.A., Macedo, M.F., Bernardes, L.F., Lambert, C.S., Zavaglia, C.A.C., Maciel Filho, R., Calderoni, D.R., Ghizoni, E. and Kharmandayan, P. (2016). 'Improvement in cranioplasty: Advanced prosthesis biomanufacturing', *Procedia CIRP*, 49, pp. 203-208.

Jessen, K.A. (2004). 'Balancing image quality and dose in diagnostic radiology', *European Radiology Supplements,* 14(1), pp. 9-18.

Jin, K.H., McCann, M.T., Froustey, E. and Unser, M. (2017). 'Deep convolutional neural network for inverse problems in imaging', *IEEE Transactions on Image Processing*, 26(9), pp. 4509-4522.

Johnston, J. and Fauber, T.L. (2015). *Essentials of radiographic physics and imaging.* 2nd edn. Missouri: Elsevier.

Jones, A., Pazik, F., Hintenlang, D. and Bolch, W. (2005). 'MOSFET dosimeter depth-dose measurements in heterogeneous tissue-equivalent phantoms at diagnostic x-ray energies', *Medical Physics,* 32(10), pp. 3209-3213.

Jung, J.Y., Kim, Y.S., LEE, C.L. and Yi, J.H., Samsung Electronics Co. Ltd. (2019). Radiographic imaging apparatus, method of controlling radiographic imaging apparatus and computed tomography apparatus. US Patent Application: 10/219, pp. 771.

Kang, E., Min, J. and Ye, J.C. (2017). ‘A deep convolutional neural network using directional wavelets for low-dose X-ray CT reconstruction’, *Medical Physics*, 44(10), pp. 360-375.

Karssemeijer, N. and Thijssen, M.A.O. (1996). 'Determination of contrast-detail curves of mammography systems by automated image analysis', *Digital Mammography*, pp. 155-160.

Kermany, D.S., Goldbaum, M., Cai, W., Valentim, C.C., Liang, H., Baxter, S.L., McKeown, A., Yang, G., Wu, X., Yan, F. and Dong, J. (2018). ‘Identifying medical diagnoses and treatable diseases by image-based deep learning’, *Cell*, 172(5), pp. 1122-1131.

Kernozek, T.W., Wilder, P.A., Amundson, A. and Hummer, J. (2002). ‘The effects of body mass index on peak seat-interface pressure of institutionalized elderly’, *Arch Phys Med Rehabil*, 83, pp. 868-871.

Knežević, Ž., Stolarczyk, L., Bessieres, I., Bordy, J.M., Miljanić, S. and Olko, P. (2013). 'Photon dosimetry methods outside the target volume in radiation therapy: Optically stimulated luminescence (OSL), thermoluminescence (TL) and radiophotoluminescence (RPL) dosimetry', *Radiation Measurements*. [Online]. Available at: https://doi.org/10.1016/j.radmeas.2013.03.004 (Accessed: 12/6/2018).

Kriete, A. (1998). 'Image quality', *Journal of Computer-Assisted Microscopy,*. [Online]. Available at: https://doi.org/10.1023/A:1023486104392 (Accessed: 05/11/2017).

Kudo, K., Osanai, M., Tsushima, M., Hirota, J., Otani, Y., Naraki, S., Suzaki, K., Aoki, M. and Hosokawa, Y. (2019). *Quantitative and visual image quality evaluation between CsI and Gd2O2S: Tb scintillator types of irradiation side sampling flat-panel detector systems for reduction of radiation exposure*.

Kwong, L., Jasty, M., Mulroy, R., Maloney, W., Bragdon, C. and Harris, W. (2018). 'The histology of the radiolucent line', *The Journal of Bone and Joint Surgery*. British

Volume, 74-B(1), pp. 67-73. [Online]. Available at: https://doi.org/10.1302/0301-620x.74b1.1732269 (Accessed: 12/6/2019).

Lahmann, N.A., Tannen, A., Dassen, T. and Kottner, J. (2011). 'Friction and shear highly associated with pressure ulcers of residents in long-term care: Classification tree analysis (CHAID) of Braden items', *Journal of Evaluation in Clinical Practice*, 17(1), pp. 168-173.

Larsen, J.R., Horton, P.H., Puterbaugh, D.E. and Anderson, T.R., Sound Sleep Products, Inc. (2016). *Foam mattress with resilient reinforcing members and air channels*. US Patent: 9,259,099.

Le Jeune, L., Robert, S., Villaverde, E.L. and Prada, C. (2016). 'Plane wave imaging for ultrasonic non-destructive testing: Generalization to multimodal imaging', *Ultrasonics*, 64, pp. 128-138.

Lechel, U., Becker, C., Langenfeld-Jäger, G. and Brix, G. (2009). 'Dose reduction by automatic exposure control in multidetector computed tomography: Comparison between measurement and calculation', *European Radiology*, 19(4), pp. 1027-1034.

Levine, J.M. (1992). 'Historical notes on pressure ulcers: The cure of Ambrose Paré', *Decubitus*, 5**,** pp. 23-24.

Levine, J.M. (2005). 'Historical perspective on pressure ulcers: The Decubitus ominosus of Jean-Martin Charcot', *Journal of the American Geriatrics Society*, 53(7), pp. 1248-1251.

Levy, A., Kopplin, K. and Gefen, A. (2013). Simulations of skin and subcutaneous tissue loading in the buttocks while regaining weight-bearing after a push-up in wheelchair users', *Journal of the Mechanical Behavior of Biomedical Materials*, 28**,** pp.436-447.

Liao, F., Burns, S. and Jan, Y.K. (2013). ‘Skin blood flow dynamics and its role in pressure ulcers’, *Journal of Tissue Viability*, 22(2), pp. 25-36. [Online] Available at: http://dx.doi.org/10.1016/j.jtv.2013.03.001 (Accessed: 22/3/2018).

Lindenmayer, D. (2013). 'From biodiversity to bioperversity: From good science to poor environmental policy', *Pacific Conservation Biology*, 19(3-4), pp. 250-255.

Linder-Ganz, E. and Gefen, A. (2007). ‘The effects of pressure and shear on capillary closure in the microstructure of skeletal muscles’, *Annals of Biomedical Engineering*, 35(12), pp. 2095-2107.

Little, M.P., Wakeford, R., Tawn, E.J., Bouffler, S.D. and Berrington de Gonzalez, A. (2009). ‘Risks associated with low doses and low dose rates of ionizing radiation: Why linearity may be (almost) the best we can do’, *Radiology*, 251(1), pp. 6-12.

Liu, Y., Liu, S. and Wang, Z. (2015). ‘A general framework for image fusion based on multi-scale transform and sparse representation’, *Information Fusion*, 24, pp. 147-164.

Lundstrom, M. (1997). 'Elementary scattering theory of the Si MOSFET', *IEEE Electron Device Letters*. [Online]. Available at: https://doi.org/10.1109/55.596937 (Accessed: 12/6/2018).

Maklebust, J. (1997). ‘Pressure ulcer assessment’, *Clinics in Geriatric Medicine*, 13, pp. 455-481.

Månsson, L. (2000). ‘Methods for the evaluation of image quality: A review’, *Radiation Protection Dosimetry*, 90(1-2): pp. 89-99.

Marchesini, S., Boutet, S., Sakdinawat, A.E., Bogan, M.J., Bajt, S., Barty, A., Chapman, H. N., Frank, M., Hau-Riege, S.P., Szöke, A., Cui, C., Shapiro, D.A., Howells, M.R., Spence, J.C.H., Shaevitz, J.W., Lee, J.Y., Hajdu, J. and Seibert, M.M. (2008). 'Massively parallel X-ray holography', *Nature Photonic*. [Online]. Available at:

https://doi.org/10.1038/nphoton.2008.154 (Accessed: 30/7/2019).

Martin, C.J. (2007). ‘The importance of radiation quality for optimisation in radiology.’ *Biomedical Imaging and Intervention Journal COMMENTARY,* 3(2), pp. 1-38.

Mathiesen, A.S., Norgaard, K., Andersen, M.F., Moller, K.M. and Ehlers, L.H. (2013). 'Are labour-intensive efforts to prevent pressure ulcers cost-effective?', *J Med Econ*, 16, pp. 1238-45.

Matsumoto, J.S., Morris, J.M., Foley, T.A., Williamson, E.E., Leng, S., McGee, K.P., Kuhlmann, J.L., Nesberg, L.E. and Vrtiska, T.J. (2015). ‘Three-dimensional physical modeling: Applications and experience at Mayo Clinic’, *Radiographics, 35*(7), pp.1989-2006.

Mcginnis, E. and Stubbs, N. (2014). 'Pressure-relieving devices for treating heel pressure ulcers', *Cochrane Database of Systematic Reviews,*. [Online]. Available at: https://doi.org/10.1002/14651858.CD005485.pub3 (Accessed: 12/6/2018).

Mcginnis, E., Briggs, M., Collinson, M., Wilson, L., Dealey, C., Brown, J., Coleman, S., Stubbs, N., Stevenson, R., Nelson, E.A. and Nixon, J. (2014). ‘Pressure-ulcer-related pain in community populations: A prevalence survey’, *BMC Nurs*, 13**,** pp. 16.

Mcinnes, E., Jammali-Blasi, A., Bell-Syer, S.E.M., Dumville, J.C., Middleton, V. and Cullum, N. (2015). 'Support surfaces for pressure ulcer prevention', *Cochrane Database of Systematic Reviews,*. [Online]. Available at: https://doi.org/10.1002/14651858.CD001735.pub5 (Accessed: 12/6/2018).

Mert, A., Ozaras, R., Tabak, F., Pekmezci, S., Demirkesen, C. and Ozturk, R. (2004). 'Erythema nodosum: An experience of 10 years', *Scandinavian Journal of Infectious Diseases,*. [Online]. Available at: https://doi.org/10.1080/00365540410027184 (Accessed: 07/9/2019).

Messer, M.S. (2012). ‘Development of a tool for pressure ulcer risk assessment and preventive interventions in ancillary service patients’, University of South Florida.

Minnich, L., Bennett, J. and Mercer, J. (2014). ‘Partnering for perioperative skin assessment: A time to change a practice culture’, *Journal of Peri Anesthesia Nursing*, 29(5), pp. 361-366.

Mitchell, F., Lindsay, H., Joan, S., Evelyn, M., Tim, B., Susan, R., Mohammad, A. and Tara, T. (2005). ‘Pressure measurement applications for humans. Unpublished (supplied by Xsensor Inc.).

Moore, Z. (2004). ‘Pressure ulcer prevention: Nurses’ knowledge, attitudes and behaviour’, *Journal of Wound Care*, 13(8), pp. 330-334.

Moore, Z.E.H. and Cowman, S. (2013). 'Wound cleansing for pressure ulcers', *Cochrane Database of Systematic Reviews*,. [Online]. Available at: https://doi.org/10.1002/14651858.CD004983.pub3 (Accessed: 12/4/2019_).

Moore, Z.E.H. and Cowman, S. (2014). 'Risk assessment tools for the prevention of pressure ulcers', *Cochrane Database of Systematic Reviews*,. [Online]. Available at: https://doi.org/10.1002/14651858.CD006471.pub3 (Accessed: 25/6/2018

Moore, Z.E. and Cowman, S. (2015). ‘Repositioning for treating pressure ulcers’, *Cochrane Database of Systematic Reviews*, ___(1), pp. [Online]. Available at: https://doi.org/10.1002/14651858.CD006898.pub4 (Accessed: 10/8/2019).

Moscovitch, M. and Horowitz, Y.S. (2006). ‘Thermoluminescent materials for medical applications: LiF: Mg, Ti and LiF: Mg, Cu, P’, *Radiation Measurements*, 41, pp. S71-S77.

Narwaria, M., Mantiuk, R., Da Silva, M.P. and Le Callet, P. (2015). HDR-VDP-2.2: A calibrated method for objective quality prediction of high-dynamic range and standard images. *Journal of Electronic Imaging*, 24(1), pp. 010501.

National Institute for Health and Care Excellence (2011). *Inditherm patient warming mattress for the prevention of inadvertent hypothermia*. London: NICE.

National Pressure Ulcer Advisory Panel (2014). Pressure ulcer category/staging illustrations. In: Health, D.O. (ed.). London.

National Pressure Ulcer Advisory Panel (2016). *National Pressure Ulcer Advisory Panel (NPUAP) announces a change in terminology from pressure ulcer to pressure injury and updates the stages of pressure injury*. (Accessed: 12/6/2018).

NICE, 2014. *Behaviour change: Individual approaches | Glossary | Guidance and guidelines | NICE*.

Norman, G., Dumville, J.C., Moore, Z.E., Tanner, J., Christie, J. and Goto, S. (2016). 'Antibiotics and antiseptics for pressure ulcers', *Cochrane Database of Systematic Reviews*, 4. [Online]. Available at: https://doi.org/10.1002/14651858.CD011586.pub2 (Accessed: 10/4/2018).

Norrman, E., Gårdestig, M., Persliden, J. and Geijer, H. (2005). 'A clinical evaluation of the image quality computer program, CoCIQ', *Journal of Digital Imaging*, 18(2), pp. 138-144. [Online] Available at: https://doi.org/10.1007/s10278-004-1036-0 (Accessed: 05/11/2017).

Orlinsky, M. and Bright, A.A. (2006). 'The utility of routine X-rays in all glass-caused wounds', *American Journal of Emergency Medicine*. [Online]. Available at: https://doi.org/10.1016/j.ajem.2005.06.008 (Accessed: 19/7/2018).

Pacific, P.A.N. and European Pressure Ulcer Advisory Panel and National Pressure Ulcer

Advisory Panel, P.P.P.I.A. (2014). 'npuap 2014', *Clinical Practice Guideline,*. [Online]. Available at: https://doi.org/10.1103/PhysRevLett.97.258103 (Accessed: 19/7/2018).

Papp, J. (2018). *LIC-quality management in the imaging sciences*. *Elsevier Health Sciences*,

Pascoal, A., Lawinski, C.P., Honey, I. and Blake, P. (2005). 'Evaluation of a software package for automated quality assessment of contrast detail images: Comparison with subjective visual assessment', *Physics in Medicine and Biology*, 50(23), pp. 5743-5757. [Online]. Available at: https://doi.org/10.1088/0031-9155/50/23/023 (Accessed: 12/6/2018).

Pereira, S., Pinto, A., Alves, V. and Silva, C.A. (2016). 'Brain tumor segmentation using convolutional neural networks in MRI images', *IEEE Transactions on Medical Imaging*, *35*(5), pp. 1240-125.

Pessanha, E.M.R., Matlakhova, L.A., Paes, H.R., Rodriguez, R.J.S., Candido, V.S. and Monteiro, S.N. (2014). 'Thermal treatment related structure and property changes in a TiNi alloy presenting shape memory effect', *Materials Science Forum*. [Online]. Available at: https://doi.org/10.4028/www.scientific.net/MSF.775-776.733 (Accessed: 12/6/2018).

(1990). 'Power MOSFETs: Theory and applications', *Choice Reviews Online*. [Online]. Available at: https://doi.org/10.5860/choice.27-2740 (Accessed: 12/6/2018).

Peterson, M.J., (2013). 'Patient repositioning and pressure ulcer risk: Monitoring interface pressures of at-risk patients', *Journal of Rehabilitation Research & Development (JRRD)*, 50(4), pp. 477-488.

Phantoms, Sectional (2014). The Phantom laboratory. Sectional lower Torso SK250. [Online]. Available at: http://www.phantomlab.com/library/pdf/sectional_ SK250DS.pd (Accessed 1 June 2015).

Pieper, 2012. ‘Pressure ulcers: Impact, etiology, and classification’, *Acute and Chronic Wounds: Current Management Concepts.* 4th edn. St Louis, MO: Mosby, pp.123-135.

Plaskitt, A., Heywood, N. and Arrowsmith, M. (2015). ‘Recording pressure ulcer risk assessment and incidence’, *Nursing Standard (2014+)*, 29(46), pp. 54.

Pocket dosimeter (2017). NTD Resource Center. [Online]. Available at: _ (Accessed 30 January 2018).

Qaseem, A., Humphrey, L.L., Forciea, M.A., Starkey, M. and Denberg, T.D. (2015). ‘Treatment of pressure ulcers: A clinical practice guideline from the American College of Physicians’, *Annals of Internal Medicine*, 162(5), pp. 370-379.

Quartz fiber dosimeter (2017). Revolvy. [Online]. Available at: _ (Accessed 30 January 2018).

Rajan, J.I. (2017). ‘Review of radiation oncology physics: A handbook for teachers and students’, Retrieved January 30, 2018.

Raju, D., Su, X., Patrician, P.A., Loan, L.A. and Mccarthy, M.S. (2015). ‘Exploring factors associated with pressure ulcers: A data mining approach’, *International Journal of Nursing Studies*, 52(1), pp. 102-111.

Reenalda, J. (2009). ‘Analysis of healthy sitting behaviour: Interface pressure distribution and subcutaneous tissue oxygenation’, *Journal of Rehabilitation Research & Development.* 46, pp. 577-586.

Regan, M.A., Teasell, R.W., Wolf, D.L., Keast, D., Mortenson, W.B. and Aubut, J.A.L. (2009). ‘A systematic review of therapeutic interventions for pressure ulcers after spinal cord injury’, *Archives of Physical Medicine and Rehabilitation*, 90, pp. 213-231.

Riordan, J. and Voegeli, D. (2009). ‘Prevention and treatment of pressure ulcers’, *British Journal of Nursing*, 18(7), pp. 20-27.

Ristic, G.S. (2017). ‘Radiation dosimeters for medical use’, _ (Accessed: 30 January 2018).

Rose, A. (1974). 'Vision: Human and electronic. *Applied Solid State Physics, Springer*, pp. 79-160. [Online] Available at: https://doi.org/10.1016/B978-1-4832-3089-4.50032-7 (Accessed: 12/2/2018).

Roth, H.R., Lu, L., Liu, J., Yao, J., Seff, A., Cherry, K., Kim, L. and Summers, R.M. (2016). ‘Improving computer-aided detection using convolutional neural networks and random view aggregation’, *IEEE Transactions on Medical Imaging*, 35(5), pp. 1170-1181.

Russ, J.C. (2016). *The image processing handbook*.: CRC Press.

Samuriwo, R. (2012). ‘Pressure ulcer prevention: The role of the multidisciplinary team’, *British Journal of Nursing*, 21(5), pp. 4-13.

Sankaran, B.M., Chakraborty, S., Patil, V.M., Raghavan, S.N., Thomas, S. and Sen, S. (2015). ‘Burden and outcomes of pressure ulcers in cancer patients receiving the kerala model of home based palliative care in India: Results from a prospective observational study’, *Indian J Palliat Care*, 21, pp. 152-7.

Santamaria, N., Gerdtz, M., Sage, S., McCann, J., Freeman, A., Vassiliou, T., De Vincentis, S., Ng, A.W., Manias, E., Liu, W. and Knott, J. (2015). ‘A randomised controlled trial of the effectiveness of soft silicone multi-layered foam dressings in the prevention of sacral and heel pressure ulcers in trauma and critically ill patients: The border trial’, *International Wound Journal*, 12(3), pp. 302-308.

Sato, H., Kittaka, D., Ohsawa, M. and Kato, K. (2019). ‘A study on fluoroscopic images in exposure reduction techniques ― Focusing on the image quality of fluoroscopic images and exposure images’, *Journal of Applied Clinical Medical Physics*,

Sayar, S., Turgut, S., Dogan, H., Ekici, A., Yurtsever, S., Denirkan, F., Doruk, N. and Tasdelen, B. (2009). ‘Incidence of pressure ulcers in intensive care unit patients at risk

according to the Waterlow scale and factors influencing the development of pressure ulcers', *J Clin Nurs,* 18**,** pp. 765-74.

Scalchi, J.E. (2009). 'Mosfet dosimetry in radiotherapy', *Cygler*.[Online]. (Accessed 30 January 2018).

Scott, E.M., Baker, E.A., Kelly, P.J., Stoddard, E.J. and Leaper, D.J. (1999). 'Measurement of interface pressures in the evaluation of operating theatre mattresses', *Journal of Wound Care*, 8(9), pp. 437-441.

Seeram, E. (2015). 'Computed tomography: Physical principles, clinical applications, and quality control', *Elsevier Health Sciences*.

Sezdi, M. (2011). 'Dose optimization for the quality control tests of X-ray equipment', In A.B. Eldin (Ed.), *Modern approaches to quality control: InTech*,

Sheikh, H.R. and Bovik, A.C. (2006). 'Image information and visual quality', *IEEE Transactions on Image Processing,*. [Online]. Available at: https://doi.org/10.1109/TIP.2005.859378 Accessed: 30/8/2018).

Siddharth, P.D. and Deshpande, S. (2016). Embedded system design for real-time interaction with smart wheelchair, *2016 Symposium on Colossal Data Analysis and Networking (CDAN 2016),*Available at: https://doi.org/10.1109/CDAN.2016.7570917 (Accessed: 28/8/2018_).

Sidhil Ltd. (2013). *Pressure reducing static mattresses*. Sidhil Ltd.

Siebel, O.F., Pereira, J.G., Souza, R.S., Ramirez-Fernandez, F.J., Schneider, M.C. and Galup Montoro, C. (2015). 'A very-low-cost dosimeter based on the off-the-shelf CD4007 MOSFET array for in vivo radiotherapy applications', *Radiation Measurements,* 75(C), pp. 53-63.

Singh, A.K., Kumar, B., Dave, M. and Mohan, A. (2015). 'Multiple watermarking on

medical images using selective discrete wavelet transform coefficients', *Journal of Medical Imaging and Health Informatics*, 5(3), pp. 607-614.

Spadavecchia, C., Villa, R., Pasquali, C., Paruccini, N. and Crespi, A. (2016). 'Comparison among three different approaches for low contrast detectability evaluation in digital radiography', *February*,

Spilsbury, K., Nelson, A., Cullum, N., Iglesias, C., Nixon, J. and Mason, S. (2007). 'Pressure ulcers and their treatment and effects on quality of life: Hospital inpatient perspectives', *Journal of Advanced Nursing*, 57(5), pp. 494-504.

Statkiewicz-Sherer, M.A., Visconti, P.J. and Ritenour, E.R. (2010). *Radiation protection in medical radiography*. 6th edn. London: Mosby.

Stekelenburg, A., Strijkers, G.J., Parusel, H., Bader, D.L., Nicolay, K. and Oomens, C.W. (2007). 'Role of ischemia and deformation in the onset of compression-induced deep tissue injury: MRI-based studies in a rat model', *Journal of Applied Physiology*, 102(5), pp. 2002-2011.

Stock, S.R. (2008). 'Recent advances in X-ray microtomography applied to materials', *International Materials Reviews*. [Online]. Available at: https://doi.org/10.1179/174328008X277803 (Accessed: 22/6/2018).

Stojadinovic, O., Minkiewicz, J., Sawaya, A., Bourne, J.W., Torzilli, P., De Rivero Vaccari, J.P., Dietrich, W.D., Keane, R.W. and Tomic-Canic, M. (2013). 'Deep tissue injury in development of pressure ulcers: A decrease of inflammasome activation and changes in human skin morphology in response to aging and mechanical load', *PLoS ONE*, 8(8), 1-9.

Stotts, N.A., Brown, D.S., Donaldson, N.E., Aydin, C. and Fridman, M. (2013). 'Eliminating hospital-acquired pressure ulcers: Within our reach', *Advances in Skin & Wound Care*, 26(1), pp. 13-18.

Suetens, P. (2017). *Fundamentals of medical imaging*. : Cambridge University Press.

Sumed International, UK (2014). *Products and specifications.* [Online]. Available at: http://www.xsensor.com/files/galleries/XSensor_Automotive_Catalogue_Augu st-2014-0002.pdf (Accessed 19 August 2018).

Suzuki, K. and Yamashita, S. (2012). 'Low-dose radiation exposure and carcinogenesis', *Japanese Journal of Clinical Oncology*, 42(7), pp. 563-568.

Tajbakhsh, N., Shin, J.Y., Gurudu, S.R., Hurst, R.T., Kendall, C.B., Gotway, M.B. and Liang, J. (2016). 'Convolutional neural networks for medical image analysis: Full training or fine tuning?', *IEEE Transactions on Medical Imaging*, 35(5), pp. 1299-1312.

Tapiovaara, M. (2008). 'Radiation protection dosimetry', *Review of Relationships between Physical Measurements and User Evaluation of Image Quality*, 129(1-3), pp. 244-248.

Teslim Onigbinde, A., Ogunsanya, G.I. and Oniyangi, S.O. (2012). 'Pressure ulcer incidence among high-risk inpatients in Nigeria', *British Journal of Nursing*, 21(12), pp. 4-10.

The Ionising Radiations Regulations. Queen's Printer of Acts of Parliament; 2017. [Online]. Available at: http://www.legislation.gov.uk/uksi/2017/1075/contents/made (Accessed: 12/6/2018).

The Joint Commission (2017). 'Joint Commission enhances pain assessment and management requirements for accredited hospitals', *The Official Newsletter of The Joint Commission*, _____, _____.

Thermo Scientific (2007). *Method development guide for hypercarb columns*. Runcorn, UK: Thermo Scientific.

Thijssen, M.A., Thijssen, H.O., Merx, J.L. and van Woensel, M.P. (1988). 'Quality analysis of DSA equipment', *Neuroradiology*, 30(6), pp. 561-568.

Thijssen, M.A.O., Bijkerk, H.R. and Van der, B.R. (1988). *Manual CDRAD-phantom type 2.0: Project quality assurance in radiology.* St. Radboud, The Netherlands: Department of Radiology, University Hospital Nijmegen.

Thomas, D.R. (1997). 'Pressure ulcers', In: Cassel, *Geriatric Medicine*, 3, pp. 767-785.

Thomas, D.R. (2001). 'Improving outcome of pressure ulcers with nutritional interventions: Review of the evidence', *Nutrition*, 17, pp. 121-125.

Thompson, T.M. and Marks-Maran, D. (2015). 'A programme to reduce acquired pressure ulcers in care homes', *British Journal of Nursing*, 24(12), pp. 4-12.

Toennies, K.D. (2017). *Guide to medical image analysis*. London: Springer.

(2017). *Thermoluminescent dosimeter*.

Tootell, A., Szczepura, K. and Hogg, P. (2014). 'An overview of measuring and modelling dose and risk from ionising radiation for medical exposures', *Radiography*, 20(4), pp. 323-332.

Tootell, A.K., Szczepura, K.R. and Hogg, P. (2013). 'Optimising the number of thermoluminescent dosimeters required for the measurement of effective dose for computed tomography attenuation correction data in SPECT/CT myocardial perfusion imaging', *Radiography*, 19(1), pp. 42-47.

Toshiba, M.S.C. (2004). Operation manual for whole-body X-ray CT scanner, Toshiba Medical Systems Corporation. Toshiba Aquilion 16. (2B201-313E*B).

Trewartha, M. and Stiller, K. (2011). 'Comparison of the pressure redistribution qualities of two air-filled wheelchair cushions for people with spinal cord injuries', *Australian Occupational Therapy Journal*, 58(4), pp. 287-292.

Trzeciak, S. and Rivers, E.P. (2003). 'Emergency department overcrowding in the United States', *Emerg Med J*., [Online]. Available at: https://doi.org/10.1136/emj.20.5.402 (Accessed: 12/6/2018).

Tubaishat, A., Papanikolaou, P., Anthony, D. and Habiballah, L. (2018). 'Pressure ulcers prevalence in the acute care setting: A systematic review, 2000-2015', *Clinical Nursing Research*,. [Online]. Available at: https://doi.org/10.1177/1054773817705541 (Accessed: 12/5/2018).

Tugwell, J.R., England, A. and Hogg, P. (2017). 'Antero-posterior (AP) pelvis x-ray imaging on a trolley: Impact of trolley design, mattress design and radiographer practice on image quality and radiation dose', *Radiography*,. [Online]. Available at: https://doi.org/10.1016/j.radi.2017.04.002 (Accessed: 12/6/2018).

Van der, B.V.R. and B-TNAMS (2006). Manual CDRAD analyser.

Van der Burght, R.J.M. (2003). *Manual CDRAD analyser*. The Netherlands: Artinis Medical Systems BV.

Van Gaal, B.G., Schoonhoven, L., Mintjes-de Groot, J.A., Defloor, T., Habets, H., Voss, A. and Koopmans, R.T. (2014). 'Concurrent incidence of adverse events in hospitals and nursing homes', *Journal of Nursing Scholarship*, 46(3), pp. 187-198.Van Gilder, C., MacFarlane, G.D. and Meyer, S. (2008). 'Results of nine international pressure ulcer prevalence surveys: 1989 to 2005', *Ostomy Wound Management*, 54(2), pp. 40.

Vanderwee, K., Clark, M., Dealey, C., Gunningberg, L. and Defloor, T. (2007). 'Pressure ulcer prevalence in Europe: A pilot study', *Journal of Evaluation in Clinical Practice*, 13(2), pp. 227-235.

Vangilder, C., Amlung, S., Harrison, P. and Meyer, S. (2009). 'Results of the 2008-2009 international pressure ulcer prevalence™ survey and a 3-year, acute care, unit-specific

analysis', *Ostomy Wound Management*,.

Vangilder, C., MacFarlane, G.D. and Meyer, S. (2008). 'Feature: Results of nine international pressure ulcer prevalence surveys: 1989 to 2005', *Ostomy Wound Management*.

Veldkamp, W.J.H., Kroft, L.J.M. and Geleijns. J. (2007). 'Dose and perceived image quality in chestradiography', *European Journal of Radiology*, 72(2), pp. 209-217.

Venkataraman, K., Jabbi, A.S., Mullis, R.H. and Pelican, C. (2016). 'Systems and methods for measuring depth using images captured by a camera array including cameras surrounding a central camera' 9, pp. 485-496.

Verschakelen, J., Bellon, E. and Deprez, T. (2003). 'Digital chest radiography: Quality assurance', *Journal of Thoracic Imaging*, 18(3), pp. 169-177.

Viergever, M.A., Maintz, J.A., Klein, S., Murphy, K., Staring, M. and Pluim, J.P. (2016). 'A survey of medical image registration: Under review'.

Vokhmintsev, A.S., Weinstein, I.A. and Kortov, V.S. (2013). 'Dosimetric application of green luminescence in irradiated TLD-500 detectors', *Radiation Measurements*, [Online]. Available at: https://doi.org/10.1016/j.radmeas.2013.01.050 (Accessed: 22/6/2019).

Walker, S., Allen, D., Burnside, C. and Small, L. (2011). 'Determining the between exposure factors, dose and exposure index value in digital radiographic imaging. *Imaging & Therapy Practice*, 14.

Wall, B.F., Haylock, R., Jansen, J.T., Hillier, M.C., Hart, D. and Shrimpton, P.C. (2011). 'Medical x-rays: Radiation risks by age and sex of patient', *Public Health England*,.

Wang, G. (2016). 'A perspective on deep imaging', *IEEE Access*, 4, pp. 8914-8924.

Wang, Z., Bovik, A.C. and Lu, L. (2002). 'Why is image quality assessment so difficult?', *IEEE*, 4(___), pp. 3313-3316.

Wang, Z., Bovik, A.C., Sheikh, H.R. and Simoncelli, E.P. (2004). 'Image quality assessment: From error visibility to structural similarity', *IEEE Transactions on Image Processing*, [Online]. Available at: https://doi.org/10.1109/TIP.2003.819861 (Accessed: 12/5/2020).

Webb, J. (2018). Levitex foam: An innovation in pressure redistribution and comfort. *Poster presentation at Wounds UK Conference*, Harrogate, North Yorkshire, England. 2018. [Online] Available at: epostersonline.com/wounds2018/node/382 Accessed: 12/4/2020).

Welsh, L. (2014). 'Ethical issues and accountability in pressure ulcer prevention', *Nursing Standard (Royal College of Nursing (Great Britain):1987)*, 29(8), pp. 56-63.

West, J.B., Maurer Jr, C.R., Fu, D., Dooley, J.R. and Accuray, I. (2016). 'Non-invasive method for using 2D angiographic images for radiosurgical target definition', *U.S. Patent*, 9(___), pp. 427-201.

Westby, M.J., Dumville, J.C., Soares, M.O., Stubbs, N. and Norman, G. (2017). 'Dressings and topical agents for treating pressure ulcers', *Cochrane Database of Systematic Reviews*,

Whitfield, M.D., Kaltenthaler, E.C., Akehurst, A.L., Walters, S.J. and Paisley, S. (2000). 'How effective are prevention strategies in reducing the prevalence of pressure ulcers?', *Journal of Wound Care*, 9(6), pp. 261-266.

Williams, M.B., (2007). 'Digital radiography image quality: Image acquisition', *Journal of the American College of Radiology,* 4(6): pp. 371-388.

Xavier Ortega, M.G. (2000). 'Advantages and limitations of electronic devices', *Institut d Tècniques Energètiques – Universitat Politècnica de Catalunya,* (Accessed 30 January 2018).

Yamaguchi, Y. and Miura, M. (2015). 'Programmed cell death in neurodevelopment', *Dev Cell*, 32, pp. 478-90.

Yap, T.L., Kennerly, S.M., Simmons, M.R., Buncher, C.R., Miller, E., Kim, J. and Yap, W.Y. (2013). 'Multidimensional team-based intervention using musical cues to reduce the odds of facility-acquired pressure ulcers in long-term care: A paired randomized intervention study', Journal of the American Geriatrics Society, 61(9), pp. 1552-1559.

Yoshizumi, T.T., Goodman, P.C., Frush, D.P., Nguyen, G., Toncheva, G., Sarder, M. and Barnes, L. (2007). 'Validation of metal oxide semiconductor field effect transistor technology for organ dose assessment during CT: Comparison with thermoluminescent dosimetry', *American Journal of Roentgenology*, 188(5), pp. 1332-1336.

Yu, E.Y., Bishop, M., Zheng, B., Ferguson, R.M., Khandhar, A.P., Kemp, S.J., Krishnan, K.M., Goodwill, P.W. and Conolly, S.M. (2017). 'Magnetic particle imaging: A novel in vivo imaging platform for cancer detection', *Nano Letters*, 17(3), pp. 1648-1654.

Yusuf, S., Okuwa, M., Shigeta, Y., Dai, M., Iuchi, T., Rahman, S., Usman, A., Kasim, S., Sugama, J., Nakatani, T. and Sanada, H. (2015). 'Microclimate and development of pressure ulcers and superficial skin changes', *International Wound Journal*, 12(1), pp. 40-46. [Online]. Available at: https://doi.org/10.1111/iwj.12048 (Accessed: 12/9/2019).

Zaman, M., Fatima, N., Naqvi, M., Parveen, R. and Sajjad, Z. (2011). 'Short communication radiation dosimetry: From thermoluminescence dosimeter (TLD) to Optically Stimulated Luminescence Dosimeter (OSLD)', *Pakistan Journal of Radiology*,

Zamani, A., Abbosh, A.M. and Mobashsher, A.T. (2016). 'Fast frequency-based multistatic microwave imaging algorithm with application to brain injury detection', *IEEE Transactions on Microwave Theory and Techniques*, 64(2), pp. 653-662.

Zhou, Z., Shin, J., Zhang, L., Gurudu, S., Gotway, M. and Liang, J. (2017). Fine-tuning convolutional neural networks for biomedical image analysis: Actively and

incrementally, *Proceedings of the IEEE Conference on Computer Vision and Pattern Recognition*, pp. 7340-7351.

Zhu, T.C. (2009). 'Diode dosimetry for diode dosimetry for mega voltage electron and photon beams', [Online]. (Accessed 30 January 2018).

Appendix 1: The Xsensor Px100 system

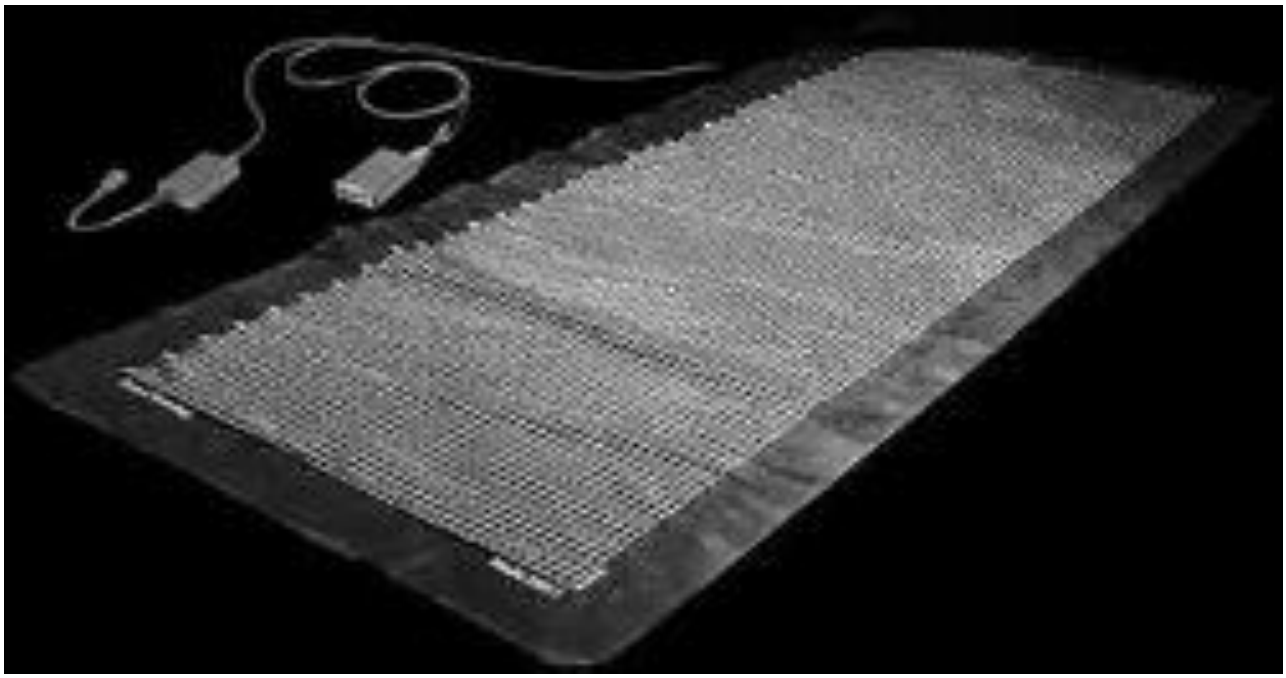

A full body image showing the pressure distribution of a healthy volunteer using the Xsensor:

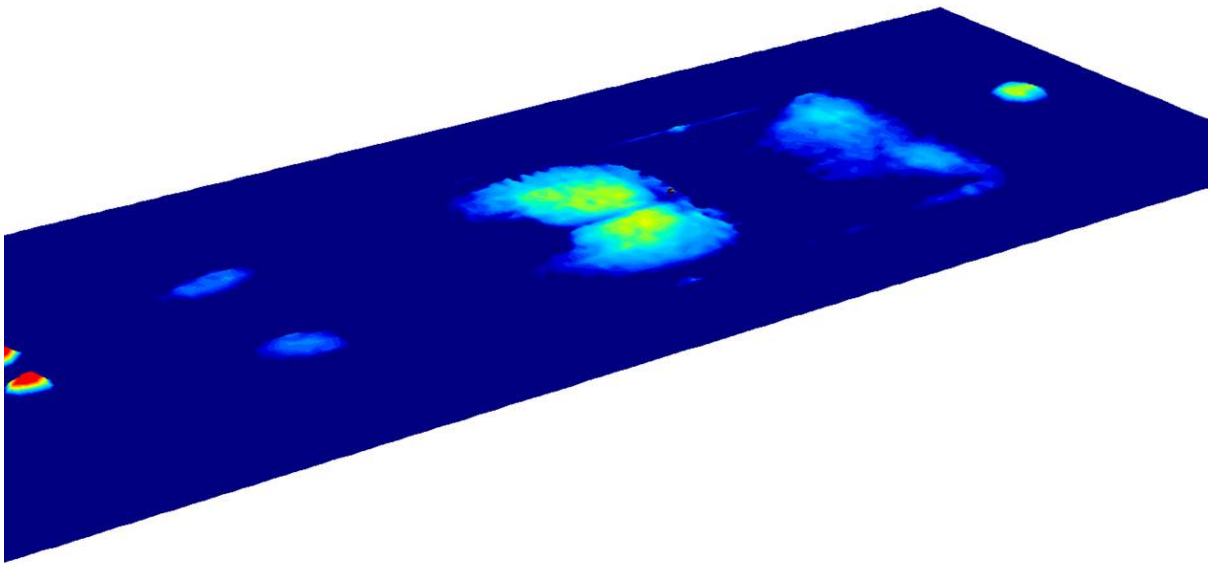

Appendix 2: Creating a 3D Skin Model STL File Ready for 3D Printing

Step 1: Load DICOM Image data into the Slicer

The Launch Slicer - From the file pack, drag and drop the DICOM folder onto the Slicer window to load; for example, the head CT scan data set (see Figure 1).

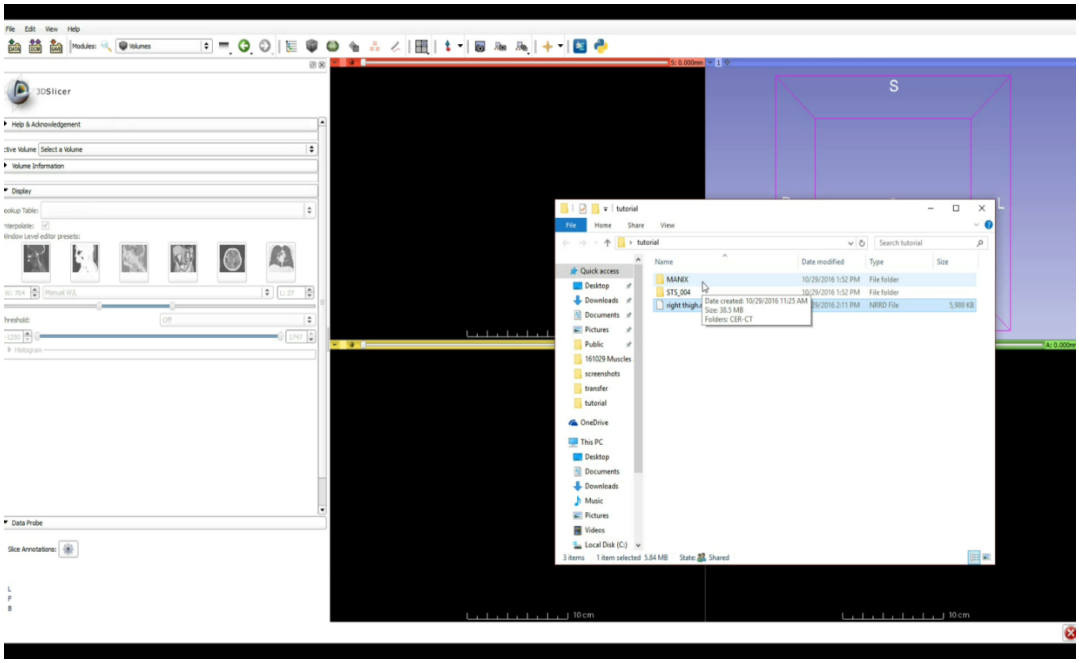

Figure 1: Loading the Head CT Scan into Slicer**.**

It may take a minute or two to load. From the DICOM browser, click on the CT series as shown in Figure 2.

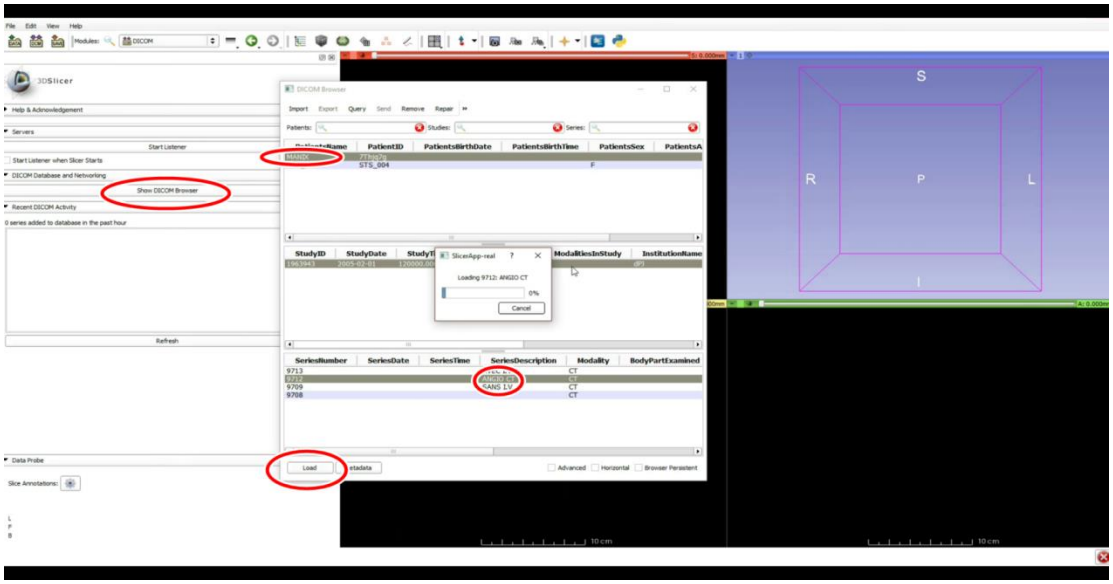

Figure 2: Loading the CT series from the data set**.**

Step 2: Save the CT scan in NRRD Format.

Save the volume in the NRRD format. Click on the save button and make sure that the checkbox for the NRRD file is selected and all other checkboxes are deselected. Specify the correct directory that you want the file to be saved in, and then click “Save”.

Step 3: Upload your NRRD file of the head to the embodi3D website.

Upload the head NRRD file to the embodi3D.com website. Enter in the required fields. In this case, however, under Operation, choose the CT NRRD to Skin STL operation.

Step 4: Download your New Skin STL File

Following approximately 5 minutes, you should receive an email that says your file processing has been completed. Follow the link in the email or look for your file in the list of files you own in your profile. You should see that your skin STL file has been completed, with several rendered images (see Figure 3). Go ahead and download your file. You can then check the quality of your file in Meshmixer, as shown in Figure 8. In this instance everything looks great and the file is error free and ready for 3D printing.

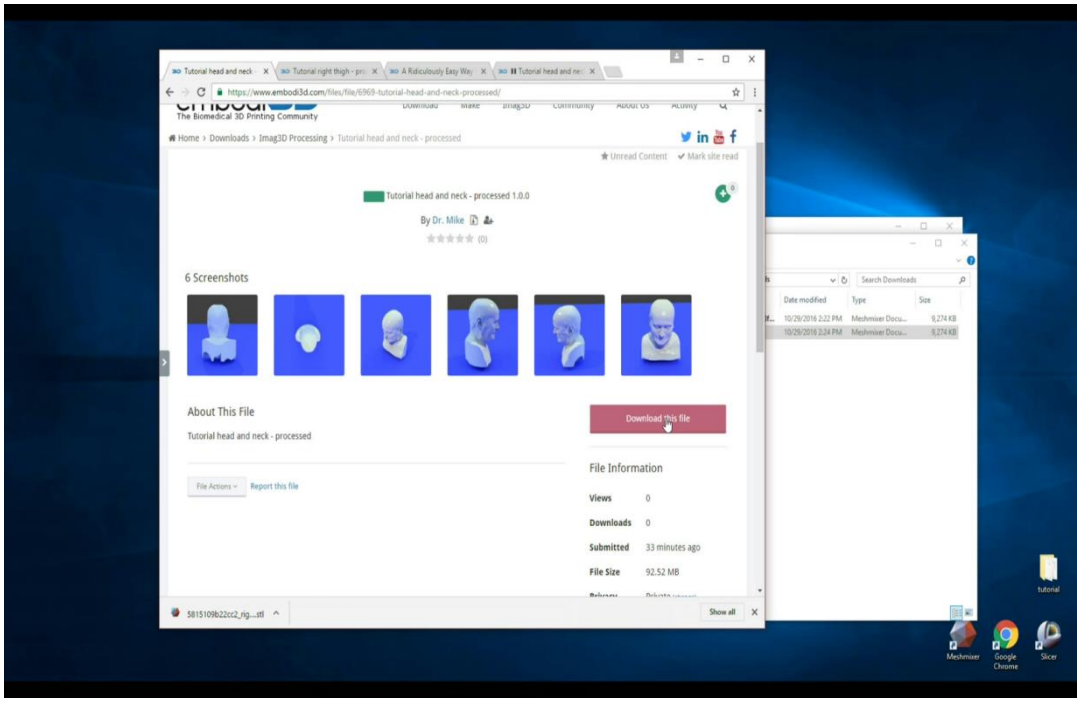

Figure 3: The download page for your newly created 3D printable skin STL file.

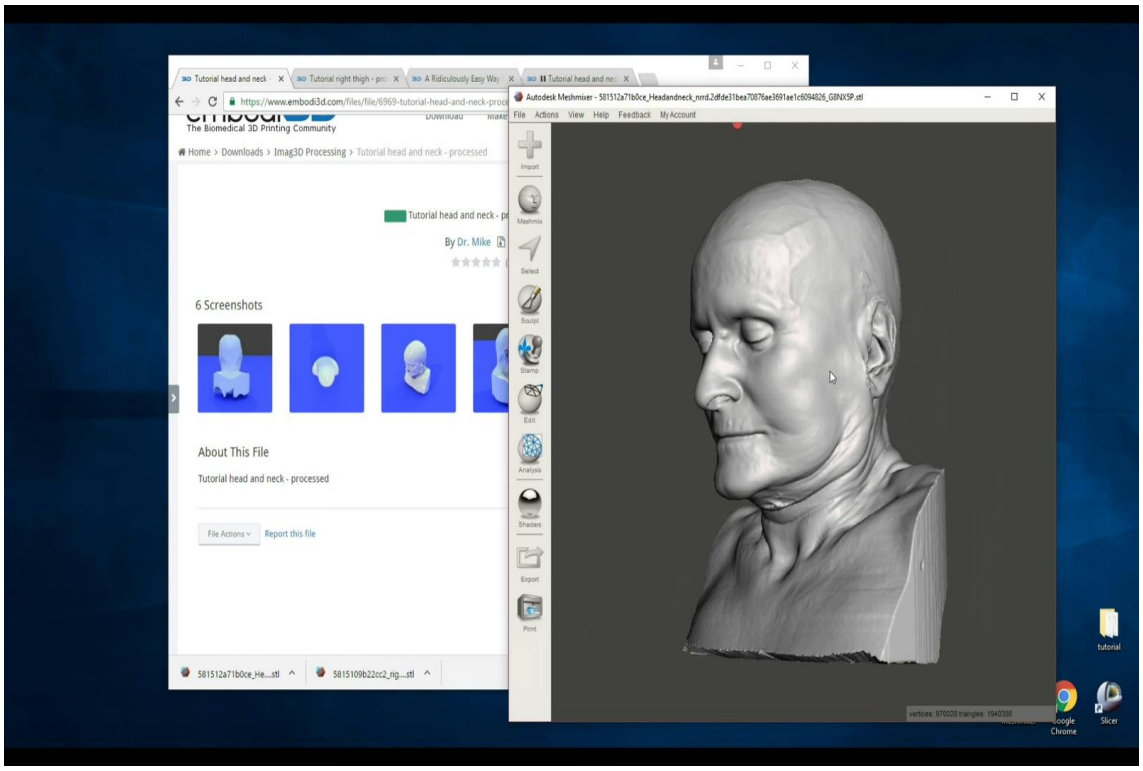

Figure 4: Opening the file in Meshmixer for quality control checks. The file is error free and incredibly lifelike. It is ready for 3D printing.

Appendix 3: Quality Control (QC) test

NHS Foundation Trust

Christie Medical Physics & Engineering
The Christie NHS Foundation Trust
Withington, Manchester
M20 4BX, UK

Diagnostic X-Ray Equipment Performance and Radiation Safety Report

Report No: 0077/SUSFU/19	Report Date: 4 February, 2019

Visit	
Establishment:	Salford University
Equipment location:	Mary Seacole Building, X-ray Room 1
Equipment summary:	Wolverson CPI Indico generator Konica AeroDR wireless DR detector Plate-1, s/n. A5DP-51165
Date of tests:	24/01/19
Performed by:	D Burke
Reason:	Routine equipment performance measurements
Report	
Sent to:	Andrew Tootell, Radiation Protection Supervisor Chris Beaumont, Radiation Protection Supervisor Claire Mercer, Director Christie Theodorakou, CMPE
Previous relevant reports:	0033/SUSFU/18

Areas needing attention	**Urgency**
Reprographic output reproducibility	**Low – next routine service.**
Detector uniformity	

Additional notes:

Follow-up	
Please report any action taken and outcome to the contact below	
Contact:	Daniel Burke on (0161) 446 3551 or e-mail daniel.burke@christie.nhs.uk

Diagnostic Radiology and Radiation Protection Group
BSI registered - certificate number: FS 37543

1 List of Measurements Performed

Measurement	Tolerance	Outcome		
		Pass	Fail	Ref
General Radiation Safety				
Operation of controls and warning devices	Functioning as expected	Pass		
X-Ray Tube				
Dose Area Product meter	Traceable value ±25%	Pass		
Generator				
kVp accuracy	Set kV ±5kV or ±5%	Pass		
Output reproducibility	Baseline ±20%		Fail	2.1.1
Output variation with kV, mA and time/mAs	Mean ±20%	Pass		
Automatic Exposure Control				
Receptor dose	1.5 µGy to 3.5µGy (DR)	Pass		2.2.1
Repeatability	Mean ±20%	Pass		
Chamber, absorber and kV dependence	Mean ±20%	Pass		
Digital Radiography (DR) System				
System response	As manufacturer's spec	Pass		
Dose Detector Indication, repeatability & reproducibility	Baseline ±20%	Pass		2.3.1
Uniformity	Mean ±5%		Fail	2.3.2
Contrast-detail imaging performance	IQF:baseline ±30%	Pass		
Dark Noise	As manufacturer's spec	Pass		
Limiting resolution	Baseline ±25%	Pass		
Blurring & stitching	No clinically significant artefacts	Pass		
Lag	<0.5%	Pass		
Measurement tool	Known distance ±2%	Pass		

2 Summary of Results and Recommendations

The results below are included for information or because there are recommendations concerning performance or safety. The results of all other measurements were satisfactory.

2.1 Generator

2.1.1 Radiographic Output Reproducibility

Output variation compared to the baseline exceeded the remedial level (baseline ±20%) at some settings. The following variations were recorded:

Focus	kV	mAs	% variation from the baseline (12/08/09)
Broad	60	20	**-27.1**
	80	20	**-21.8**
	100	20	-17.3
Fine	60	20	**-23.8**
	80	20	-18.4
	100	20	-13.6

As previously reported, output has decreased gradually from the baseline in 2009 and now exceeds the remedial level at some settings. This is only likely to be an immediate issue if the unit was to be used for patient studies. As this is not understood to be currently the case, it is recommended that this is drawn to the engineers attention for comment at its next routine service.

Appendix 4: Publication Arising from This Work

Paper 1

ELSEVIER

Journal of Medical Imaging and Radiation Sciences 51 (2020) 417-424

Journal of Medical Imaging and Radiation Sciences

Journal de l'imagerie médicale et des sciences de la radiation

www.elsevier.com/locate/jmir

Research

A Phantom-Based Method to Assess X-Ray Table Mattress Interface Pressures

Nadi Alresheedi, MSc*, Lucy Anne Walton, PhD, Andrew Tootell, PhD, Jo-Anne Webb, MSc and Peter Hogg, PhD

Department of Radiography, School of Health & Society, University of Salford, Salford, UK

ABSTRACT

Background: Pressure redistribution performance of x-ray table mattresses can influence the development of pressure ulcers in at-risk populations. Interface pressure analysis, with human participants, is a common method to assess mattresses. This approach has limitations that relate to the lack of standardisation between and within humans.

Aim: This study aimed to develop and validate an anthropomorphic phantom-based method to assess x-ray table mattress interface pressures as an index of mattress performance.

Methods: A three dimensional phantom simulating an adult's head, pelvis, and heels was printed from x-ray computed tomography image data and attached to a metal frame 175 cm in length. Dry sand was added to the phantom head, pelvis, and heels to represent a range of human weights. Pressure distribution was assessed using XSensor. Phantom validation was achieved by comparing phantom mattress interface pressure characteristics, for five human equivalent weights, against 27 sets of human mattress interface pressure data.

Results: Using the correlation coefficient R, phantom and human pressure data showed good correlation for the five phantom weights (R values: head = 0.993, pelvis = 0.997, and heels = 0.996).

Conclusion: A novel method to test x-ray mattresses for interface pressure was developed and validated. The method could have utility in the testing of x-ray mattresses that are in routine use and for new mattress development. Phantom interface pressure data could be provided by manufacturers to help inform procurement decisions when matching mattress characteristics to medical imaging demands and the underlying patient populations.

RÉSUMÉ

Contexte : Le rendement en redistribution de la pression des matelas de tables de radiographie peut avoir une incidence sur le développement des escarres dans les populations à risque. L'analyse de la pression d'interface, avec des participants humains, est une méthode commune d'évaluation des matelas. Cette approche a des limites qui ont trait au manque de standardisation chez et entre les êtres humains.

But : Développer et valider une méthode fondée sur un fantôme anthropométrique afin d'évaluer les pressions d'interface des matelas de table de radiographie sous la forme d'un indice de rendement de matelas.

Méthodologie : Un fantôme simulant la tête, le pelvis et les talons d'un être humain adulte a été produit par impression 3D à partir de données d'imagerie de tomodensitométrie et fixé à un cadre métallique de 175 cm de longueur. Du sable sec a été ajouté à la tête, au pelvis et aux talons du fantôme afin de représenter une plage de poids humains. La distribution de la pression a été évaluée à l'aide de XSensor. La validation du fantôme a été faite en comparant les caractéristiques de pression d'interface du fantôme avec le matelas à 27 ensembles de données humaines de pression d'interface avec le matelas.

Résultats : En utilisant le facteur de corrélation R, les données de pression humaines et du fantôme présentent une bonne corrélation pour les cinq poids du fantôme (valeurs de R: tête = 0,993, pelvis = 0,997 et talons = 0,996).

Conclusion : Une nouvelle méthode permettant de mesurer la pression d'interface des matelas de table de radiographie a été élaborée et validée. Cette méthode pourrait être utilisée pour tester les matelas couramment utilisés et pour le développement de nouveaux matelas.

Paper 2

ELSEVIER

Journal of Medical Imaging and Radiation Sciences xx (2020) 1-7

Journal of Medical Imaging and Radiation Sciences

Journal de l'imagerie médicale et des sciences de la radiation

www.elsevier.com/locate/jmir

Research Article

Pressure distribution analysis of X-Ray table mattresses

Nadi Alresheedi*, Lucy Anne Walton, Andrew Tootell, Jo-Anne Webb and Peter Hogg

School of Health and Society, University of Salford, Salford M5 4WT, United Kingdom

ABSTRACT

Background: There is a risk of developing pressure ulcers from lying on an X-ray table mattress, if the mattress pressure redistribution properties are poor.

Aim: To assess the pressure redistribution properties of 'new' and 'in current clinical use' X-ray table mattresses.

Methods and materials: Twenty one X-ray table mattresses, each of 2.5 cm thickness, were evaluated. An anthropomorphic human phantom of adult stature with five different weights (minimum, first quartile, mean, third quartile and maximum) was used to simulate human head, pelvis and heels (pressure ulcer jeopardy areas). Using Xsensor technology, peak pressure was measured and Interface Pressure Ratio was calculated for the three pressure ulcer jeopardy areas 'with' and 'without' an X-ray table mattress.

Results: For all mattresses, statistically significant differences ($p < 0.05$) were found between the peak pressure values with and without using an X-ray table mattress for the three pressure ulcer jeopardy areas; similarly, for all mattresses, statistically significant differences ($p < 0.05$) were found between the Interface Pressure Ratio values with and without using x-ray table mattress. The type and age of the mattress was observed to have an impact on peak pressure values and Interface Pressure Ratios, with older mattresses performing worse.

Conclusion: Peak pressure values and Interface Pressure Ratios are reduced significantly when using newer X-ray table mattresses. This could be because newer mattresses use more appropriate materials in their construction and/or older mattresses have lost their pressure redistribution properties. Radiology departments should consider assessing mattresses pressure redistribution properties, perhaps on an annual basis

RÉSUMÉ

Contexte : Il existe un risque de développer des escarres en s'allongeant sur un matelas de table à rayons X, si les propriétés de redistribution de la pression du matelas sont mauvaises.

Objectif : évaluer les propriétés de redistribution de la pression des matelas de table à rayons X « nouveaux » et « en usage clinique actuel ».

Méthodes et matériels : Vingt et un matelas de table à rayons X, d'une épaisseur de 2,5 cm chacun, ont été évalués. Un fantôme humain anthropomorphe de taille adulte avec cinq poids différents (minimum, premier quartile, moyenne, troisième quartile et maximum) a été utilisé pour simuler la tête, le pelvis et les talons (zones à risque d'escarres) d'un être humain. Grâce à la technologie Xsensor, la pression de pointe a été mesurée et le rapport de pression d'interface a été calculé pour les trois zones à risque d'escarres « avec » et « sans » matelas de table à rayons X.

Résultats : Pour tous les matelas, des différences statistiquement significatives ($p < 0,05$) ont été trouvées entre les valeurs de pression de pointe avec et sans l'utilisation d'un matelas de table à rayons X pour les trois zones à risque d'escarres; de même, pour tous les matelas, des différences statistiquement significatives ($p < 0,05$) ont été trouvées entre les valeurs du rapport de pression d'interface avec et sans l'utilisation d'un matelas de table à rayons X. On a observé que le type et l'âge du matelas avaient un impact sur les valeurs de pression de pointe et les rapports de pression d'interface, les matelas plus anciens ayant de moins bonnes performances.

Conclusion : Les valeurs de pression de pointe et les rapports de pression d'interface sont réduits de manière significative lors de l'utilisation de nouveaux matelas de table à rayons X. Cela pourrait être dû au fait que les nouveaux matelas utilisent des matériaux plus appropriés dans leur construction et/ou que les anciens matelas ont perdu leurs propriétés de redistribution de la pression. Les services de radiologie devraient envisager d'évaluer les propriétés de redistribution de la pression des matelas, peut-être sur une base annuelle.

Paper 3

ARTICLE IN PRESS

Radiography xxx (xxxx) xxx

Contents lists available at ScienceDirect

Radiography

journal homepage: www.elsevier.com/locate/radi

Evaluation of X-ray table mattresses for radiation attenuation and impact on image quality

N. Alresheedi, L. Walton, P. Hogg, J. Webb, A. Tootell*

School of Health and Society, University of Salford, UK

ARTICLE INFO

Article history:
Received 10 July 2020
Received in revised form
23 October 2020
Accepted 24 October 2020
Available online xxx

Keywords:
Radiography
Mattress
Attenuation
Image quality

ABSTRACT

Introduction: Mattresses in the radiology department tend to be an overlooked aspect of imaging equipment. This paper evaluates the radiation attenuation characteristics of mattresses and the effect they have on image quality.

Methods: Thirteen mattresses (from new to 20 years of age) were evaluated. Incident air kerma (IAK) was measured in two conditions, with and without mattress over a range of exposure factors using a digital dosimeter. Image quality was assessed by calculating the inverse image quality factor (IQF_{inv}) using a commercially available phantom (CDRAD) for the same exposure factors. The correlation of age and attenuation and image quality was calculated.

Results: Measured IAK and image quality was affected by the addition of a mattress with older mattresses having greater attenuation; there is a moderate/large correlation (0.38–0.51) between age and IAK. IQF_{inv} deteriorated with the addition of a mattress but there was no correlation with age (−0.41 to 0.16). Clinically, there is no impact of any mattress in the study as changes to the exposure factors to account for the attenuation are smaller than the increments in mAs available on X-ray equipment.

Conclusion: The results indicate that while the presence of a mattress does impact on transmitted radiation and the quality of the image, the clinical impact is insignificant. Attenuation correlates with age but with no clinical significance. There is no correlation between age and image quality.

Implications for practice: Quality control tests for attenuation and impact on image quality are not required in clinical practice. The method could be used by manufacturers to test new materials and mattresses and could provide users with specifications of new products.

Introduction

Mattresses used in radiology are arguably an overlooked aspect of ancillary imaging equipment. Their role is to facilitate patient comfort and compliance during imaging. In performing these roles, they should attenuate the primary beam minimally and ideally in turn this could require an increase in mAs to compensate for absorbed photons, thus increasing patient dose. The materials within the mattresses or their construction should not impact negatively on the diagnostic acceptability of the resulting radiographic image.

Any element of the imaging chain should undergo quality